TECHNISCHE UNIVERSITÄT MÜNCHEN

FAKULTÄT FÜR CHEMIE

LEHRSTUHL FÜR ANORGANISCHE UND METALLORGANISCHE CHEMIE

Hume-Rothery inspired Complexes and Clusters as Molecular Models for Intermediates in Heterogeneous Catalysis

JULIUS HORNUNG

Vollständiger Abdruck der von der Fakultät für Chemie der Technischen Universität München zur Erlangung des akademischen Grades eines

Doktors der Naturwissenschaften (Dr. rer. nat.)

genehmigten Dissertation.

Vorsitzender:	Prof. Dr. Johannes A. Lercher
Prüfer der Dissertation:	1. Prof. Dr. Roland Fischer
	2. Prof. Dr. Ulrich K. Heiz
	3. Prof. Dr. Jean-Yves Saillard

Die Dissertation wurde am 24.04.2019 bei der Technischen Universität München eingereicht und durch die Fakultät für Chemie am 20.05.2019 angenommen.

Hume-Rothery inspired Complexes and Clusters as Molecular Models for Intermediates in Heterogeneous Catalysis

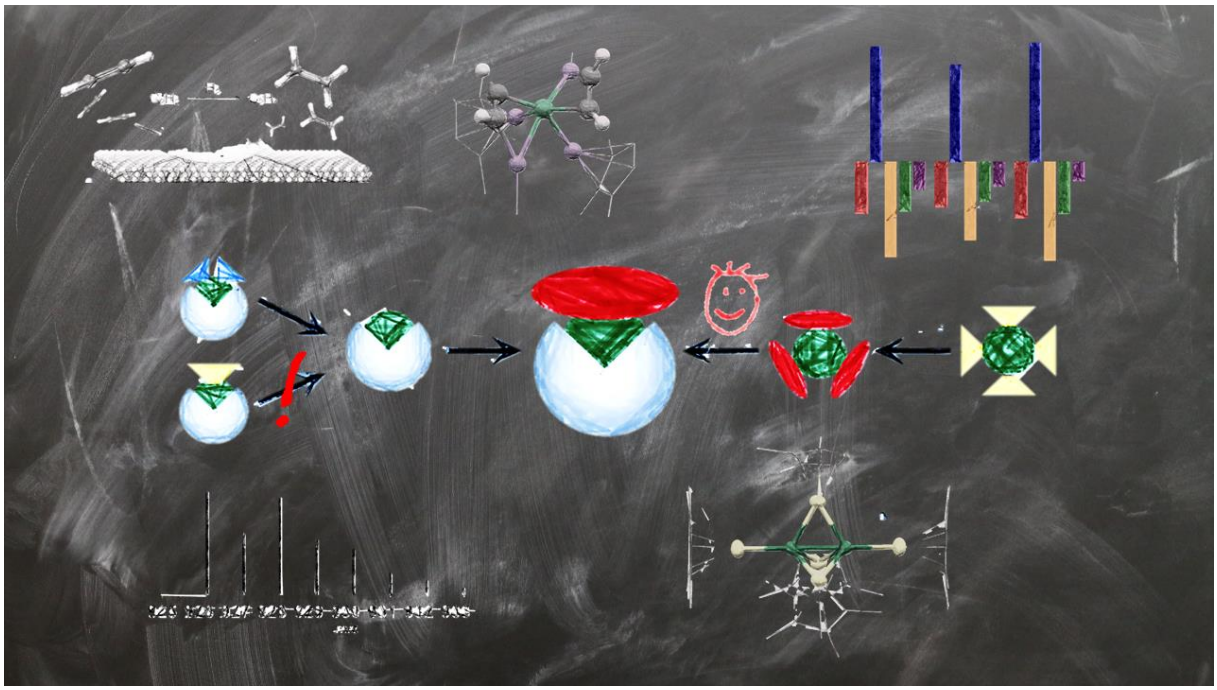

"The important thing in science is not so much to obtain new facts as to discover new ways of thinking about them"

Sir William Bragg (1862-1942)

Danksagung

Es gibt viele Menschen, die mich unterstützt und mir geholfen haben, die mit mir gelacht haben, die mich in meiner persönlichen und wissenschaftlichen Entwicklung weitergebracht haben oder die auf ihre jeweils ganz persönliche Art für mich da waren. Dafür möchte ich jedem einzelnen von ganzem Herzen danken. Ohne die vielen Einflüsse, Eindrücke und Hilfestellungen von euch hätten mein Leben und meine Promotion sicherlich einen ganz anderen Lauf genommen.

Zu aller erst möchte ich meinem Doktorvater **Prof. Dr. Roland A. Fischer** danken, dass er mich vor über drei Jahren in seiner Gruppe aufgenommen hat. Mit sehr großem Vertrauen haben Sie mir die Möglichkeit gegeben mich frei in meinem Thema zu entfalten und mich durch die Aufenthalte in Auckland und Rennes wissenschaftlich weiter zu entwickeln. Durch ausführliche und sehr hilfreiche Diskussionen haben Sie mir dabei geholfen mein Thema weiterzubringen und neue Wege einzuschlagen.

For my two stays in Rennes, the trip to Mont St. Michel and the very helpful discussions I want to specially thank **Prof. J.-Y. Saillard**! Furthermore, I am grateful that he agreed to be one of my examiners in my PhD. defence.

Mein Dank geht außerdem an meinen Drittprüfer **Prof. Dr. Ueli Heiz** und an **Prof. Dr. Johannes Lercher** für die Übernahme des Prüfungsvorsitzes.

Außerdem möchte ich **Dr. Christian Gemel** danken, der mir immer wieder beratend zur Seite stand und stehts ein offenes Ohr für meine wissenschaftlichen Probleme hatte.

Im Labor haben mir mit **Jana Weßing** und **Hung Banh** zwei erfahrene „Organometaller“ zur Seite gestanden und mir wertvolle praktische Tipps gegeben. Vielen Dank dafür!

Dr. Paul Jerabek und **Prof. Dr. Schwerdtfeger** danke ich für die nette und bereitwillige Aufnahme in Neuseeland und für die Unterstützung bei quantenchemischen Fragestellungen.

Für die tatkräftige Unterstützung bei NMR-Messungen, in der Zentralanalytik, oder bei der Elementaranalyse danke ich **Maria Mathews**, **Jürgen Kudermann**, **Ulrike Ammari**, **Petra Ankenbauer** und **Bircan Dilki**. Außerdem geht mein ausdrücklicher Dank an **Martin Schellerer** für die Hilfe bei so vielen organisatorischen Angelegenheiten.

Meinen Praktikanten **Xiaoyu Zhou**, **Carsten Aulenbacher**, **Patricia Heiß** und **Maximilian Muhr** und den Synthi-Studenten danke ich für die tatkräftige Unterstützung im Labor.

Patricia Heiß und **Maximilian Muhr** danke ich außerdem, dass Sie mir die Betreuung ihrer Masterarbeit anvertraut haben und wir gemeinsam viele spaßige und doch einige erfolgreiche Stunden im Labor verbringen konnten.

Außerdem danke ich **Pauline**, **Maxi**, **Patricia** und **Lorenz** fürs Korrigieren meiner Doktorarbeit.

Außerdem danke ich dem gesamten **AK Fischer** und **AK Kühn** für die vielen lustigen Stunden, die die Promotion um so viel bereichert haben.

Meinen Studienkollegen und **Freunden** sowohl in **Saarbrücken** als auch **Heidelberg**, danke ich für die Unterstützung beim Lernen und Feiern und die vielen Freundschaften, die sich trotz der Entfernung gehalten haben!

Meinem Labornachbarn und guten Freund **Konstantin Epp** danke ich für die persönliche sowie wissenschaftliche Unterstützung und die vielen Lacher, die Du mir beschert hast!

Mein ganz besonderer Dank gilt meiner Freundin **Pauline**, die mir auch abseits der Promotion immer zur Seite steht und mich unterstützt, auch wenn es manchmal nicht so einfach ist mit mir.

Danken möchte ich außerdem noch meiner ganzen Familie, meiner Mutter **Karin**, meinen Geschwistern **Annemarie** und **Jan-Moritz**, meinem Stiefvater **Heiko** und meinem Vater **Andreas**. Ihr wart immer da, wenn ich euch gebraucht habe, habt mich unterstützt und gefördert und mir bei jeder Entscheidung in meinem Leben zur Seite gestanden! Vielen Dank dafür!

Table of Contents

List of Abbreviations

Ar	aryl-ligand
AO	atomic orbital
ATR	attenuated total reflection
C_2H_x	x = 2: acetylene; x = 4: ethylene
cdt	*trans, trans, trans*-1,5,9-cyclododecatriene
cod	1,5-cyclooctadien
Cp	cyclopentadienyl
Cp*	1,2,3,4,5-pentamethylcyclopentadienyl
DDP	2-{(2,6-diisopropylphenyl)amino}-4-{(2,6-diisopropylphenyl)imino}-2-pentene
DFT	density functional theory
dvds	1,1,3,3-tetramethyl-1,3-divinyldisiloxane
EA	elemental analysis
EDA-NOCV	energy decomposition analysis with the natural orbital for chemical valence extension
E-R/E-Cp*	E = Al, Ga, In with organic ligand/Cp*
Et	ethyl
HMBC	heteronuclear multiple bond correlation
HOMO	highest occupied molecular orbital
HT	high temperature
IR	infrared (spectroscopy)
L	ligand
LIFDI	liquid injection field desorption ionization
LT	low temperature
LUMO	lowest unoccupied molecular orbital
MO	molecular orbital
M'-R	general abbreviation for Al/Ga/Zn ligands. The number of Zn ligands is usually two times the number of Al/Ga.
MS	mass spectrometry
NBO	natural bond orbitals
NMR	nuclear magnetic resonance

ppm	parts per million
QTAIM	quantum theory of atoms in molecules
R	organic residue, mostly R = Cp*/Me
r.t.	room temperature
TDDFT	time-dependent density functional theory
TM	transition metal
TOF	time of flight
UHC	unsaturated hydrocarbons
UV-Vis	ultraviolet – visible (light)
ve	valence electron
VT	variable temperature
XRD	X-ray diffraction

I Summary

Link between molecular [$TM_aM'_b$] clusters and solid-state TM/M' intermetallics. Following the conceptual link between molecular mixed-metal [$TM_aM'_b$][1] (TM = transition metal, M' = Al, Ga, Zn) complexes/clusters and solid-state TM/M' intermetallics[1-2], molecular [$Ni(M'R)_n(C_2H_x)_{4-n}$] (M' = Al, Ga, Zn_2; R = Cp*, Me; x = 2,4; n = 1-3) complexes are proposed as reasonable molecular models for substrate-surface interactions on intermetallic compounds with focus on the semi hydrogenation of alkynes. Initial theoretical investigations of [$Ni(L)_n(C_2H_x)_{4-n}$] (L = PEt_3, AlCp*, GaCp*, $(ZnR)_2$; R = Cp*, Me; x = 2,4; n = 1-3) at the DFT-level of theory (BP86-D3(BJ)/def2-TZVPP) presented in this thesis support the conceptual link between molecular mixed-metal compounds and solid-state intermetallics since M' coordination on the Ni-center has distinct effects on Ni-C_2H_x bonding. For instance, M'-free [$Ni(C_2H_2)_3$] and [$Ni(PEt_3)_2(C_2H_2)$] show the expected side-on coordination of C_2H_2 at Ni, whereas [$Ni(AlCp^*)_2(C_2H_2)_2$] and [$Ni(ZnR)_4(C_2H_2)_2$] feature Ni-M' bridged alkyne coordination modes. These metal-bridging substrate binding modes are reminiscent of the cooperative effects found for solid-state intermetallic catalysts applied in the catalytic semi hydrogenation. For instance, for the well-studied solid-state Pd/Ga intermetallic catalyst, theoretical and experimental investigations revealed Pd/Ga bridging alkyne coordination on Pd/Ga arrangements at the surface, which is rendered as a plausible explanation for the observed selectivity of this catalytic system.[3-5]

Experimental realization of [$Ni_a(M'R)_b(UHC)_c$]. Motivated by the theoretical results regarding [$Ni(M'R)_n(C_2H_x)_{4-n}$] the experimental access towards [$Ni_a(M'R)_b(UHC)_c$] (UHC = unsaturated hydrocarbons) complexes and clusters is investigated. The initial synthetic strategy was based on the formation of low-coordinated [$Ni(M'R)_n$] fragments with preformed Ni-M'R bonds either by PR_3 dissociation from [$Ni(M'R)_n(PEt_3)_{4-n}$] (n = 0-4) or by reductive elimination of H-$SiEt_3$ from [$(H)(SiEt_3)Ni(AlCp^*)_{3-n}(ZnR)_{2n}$] (n = 0-2) complexes. Investigations of the PEt_3 dissociation from [$Ni(M'R)_n(PEt_3)_{4-n}$] complexes revealed that the fast and extensive dissociation/association equilibrium of the Ni-PEt_3 bonds in [$Ni(PEt_3)_{4-n}$][6-7] is largely suppressed by M'R coordination. This phenomenon can be attributed to Ni-P bond polarization induced by M'R coordination. The newly established synthetic access of [$(H)(SiEt_3)Ni(AlCp^*)_{3-n}(ZnR)_{2n}$] (n = 0-2) together with the already reported [$(H)(SiEt_3)Ni(AlCp^*)_3$][8] could allow the synthesis of [$(UHC)Ni(AlCp^*)_{3-n}(ZnR)_{2n}$] (n = 0-2) compounds via the intermediate formation of low-coordinated [$Ni(AlCp^*)_{3-n}(ZnR)_{2n}$] species.

A more universal access to [$Ni_a(M'R)_b(UHC)_c$] compounds was achieved based on the "early-stage" incorporation of UHC's before M'R ligands are present. Promising results were obtained by initial

treatment of [Ni(cod)$_2$] with *3*-hexyne and subsequent addition of GaCp* yielding for instance the Ni_4Ga_4 cluster [Ni_4(GaCp*)$_4$(*3*-hexyne)$_2$] as evidenced by mass spectrometric analysis.

Increasing the knowledge of [(Ni$_a$E$_b$)Cp*$_c$] clusters. Furthermore, suitable reaction conditions for the formation of [(Ni$_a$E$_b$)Cp*$_c$] (E = Al, Ga) cluster were identified by mass-spectrometric studies, and differences in cluster formation for E = Al, Ga were revealed. For instance, treatment of [Ni_2(dvds)$_3$] with AlCp* results in the formation of mononuclear [Ni(AlCp*)$_4$] as the main product whereas the Ni_2 compound [Ni_2(AlCp*)$_5$] is only formed as a side product. The molecular structure of [Ni_2(AlCp*)$_5$] shows a very short Ni-Ni distance of only 2.2702(15) Å indicating Ni-Ni bonding interactions which is in accordance to theoretical analysis performed in collaboration with Prof. J.Y. Saillard. The interplay of Ni_2 and AlCp* results in a strengthening of the Ni-Ni interaction in [Ni_2(AlCp*)$_5$] which therefore serves as a model compound for higher nuclear [TM$_a$(ECp*)$_b$] clusters.

Treatment of [Ni_2(dvds)$_3$] with GaCp* however results in the formation of several high nuclear [Ni$_a$(GaCp*)$_b$(dvds)$_c$] clusters as e.g. [(Ni_4Ga_4)(Cp*)$_3$(dvds)$_2$]. The difference of AlCp*/GaCp* cluster growth processes can be attributed to dissociation/association processes for the Ni-GaCp* system which are not present for the kinetically inert and thermodynamically strong Ni-AlCp* bond. The molecular structure of [(Ni_4Ga_4)(Cp*)$_3$(dvds)$_2$] reveals a Cp* transmetallation from Ga to Ni. Therefore, the formula of this cluster should be written as [Ni_2(μ-GaCp*)(μ-GaNiCp*)$_2$(dvds)$_2$].

Critical Outlook. Even though the conceptual link of [Ni$_a$(M'R)$_b$(UHC)$_c$] compounds as potential molecular models for intermediates in heterogeneous semi hydrogenation could not be supported by experimental findings so far, the presented computational studies on [Ni(M'R)$_n$(C_2H_x)$_{4-n}$] complexes provides evidence for this relation. Furthermore, based on the presented experimental work and especially the development of a new synthetic strategy based on the "early-stage" incorporation of UHC's the isolation of the desired [Ni$_a$(M'R)$_b$(UHC)$_c$] should be possible in the future.

Ⅱ Introduction

Ⅱ.1. Semihydrogenation of Alkynes

On the way to inexpensive alternative catalysts

Heterogeneously catalyzed hydrogenation reactions of unsaturated hydrocarbons are long-known reactions and have been widely investigated. In 1874, de Wilde reported the full hydrogenation of acetylene to ethane applying a heterogeneous Pt catalyst.[9] Roughly 25 years later, Sabatier and Senderens reported the semihydrogenation of acetylene to ethylene using Pd or Ni catalysts.[10-11] In 1909, Paal discovered that the semihydrogenation of the sodium salt of 3-phenylpropiolic acid with a Pd catalyst affords Z-cinnamic acid.[12-13] This finding confirmed the *cis*-selectivity of heterogeneous hydrogenation reactions and thus, gave first insights into the mechanism of surface hydrogenation reactions.

Today, heterogeneous catalysts are widely used both in large scale industrial productions and small scale fine chemical synthesis. Especially the semihydrogenation of alkynes, selectively converting alkynes to alkenes, is of special importance. It is used for the purification of ethylene feedstocks, obtained by steam cracking of long chain hydrocarbons, from traces (usually about 1%[14]) of acetylene. Purified ethylene is used for the multi-ton scale production of polyethylene where even small traces of acetylene negatively affect the polymerization catalyst.[15] Therefore, a highly selective semihydrogenation catalyst is needed to avoid over-hydrogenation of acetylene to undesired ethane which would decrease the overall yield of polyethylene.

The most probable mechanism of heterogeneous hydrogenation reactions of acetylene can be described as follows. First gaseous acetylene and hydrogen adsorb exothermally on the catalyst surface. The catalyst-substrate interaction leads to an activation of H_2 by splitting into atomic hydrogen atoms on the catalytic surface. Hydrogen migrates to co-adsorbed C_2H_2 leading to a stepwise reduction to C_2H_4. The activation energy of the both hydrogenation step is well below the desorption energy for acetylene. Once ethylene is formed it can either desorb, giving free ethylene as the desired reaction product or it can be further hydrogenated to ethane.[16] A selective reaction is therefore achieved when the hydrogenation of acetylene to ethylene is thermodynamically and kinetically more feasible than the hydrogenation of ethylene to ethane. In summary, the alkene/alkane product ratio is determined by thermodynamic (heat of adsorption, hydrogen splitting, etc.) as well as kinetic parameters (activation energies, substrate mobility on the catalyst, etc.), which are directly related to the applied heterogeneous catalyst.

The semihydrogenation is industrially catalyzed by mixed metal Pd/Ag particles on alumina support.[17] Detailed investigations on the beneficial influence of Ag addition to Pd revealed that the enhanced selectivity compared to pure Pd is a result of electronic as well as geometric effects. The binding energy of both, C_2H_2 and C_2H_4, to the Pd/Ag surface is reduced compared to pure Pd. However, acetylene adsorption is still favored compared to ethylene adsorption.[18] Theoretical calculations by Studt *et al.* showed that the higher selectivity can be explained by a higher activation barrier for the second hydrogenation step which is significantly higher than the dissociation energy of C_2H_4 (see Figure 1).[16]

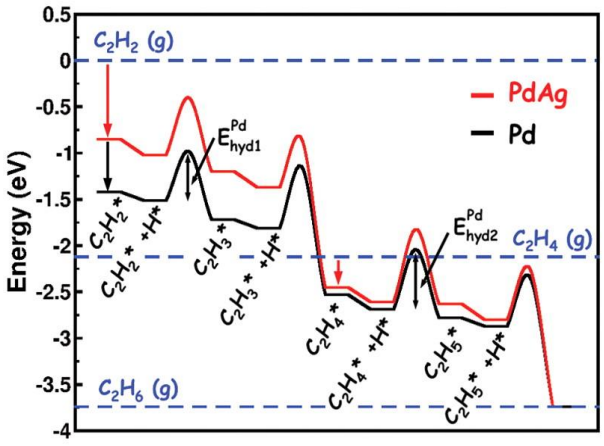

Figure 1: Estimated reaction mechanism of the semihydrogenation on the Pd(111) (black) and the Pd/Ag(111) (red) surface. Acetylene is adsorbed to the respective surface and hydrogenated twice giving adsorbed C_2H_4. The activation energy of the following hydrogenation step to intermediate C_2H_5 depends on the investigated surface. For Pd(111) the activation barrier is similar to the energy of desorption, which accounts for the low selectivity of the semihydrogenation. For the Pd/Ag(111) surface, the activation energy is higher than the desorption energy selectively yielding C_2H_4. Reprinted with permission from Studt *et al.*, Science **2008,** 320 (5881), 1320-1322. Copyright 2008 American Association for the Advancement of Science.

Recent investigations on industrially orientated semihydrogenation reactions are motivated by the aim to replace the noble metal based Pd/Ag catalyst by cheaper and more abundant alternatives. In this regard different TM/M' (TM = transition metal, M' = Al, Ga, Zn) intermetallic compounds belonging to Hume-Rothery solid-state phases like Pd/Ga[3, 5, 19], Ni/Ga[16] and ultimately Fe/Zn, Ni/Zn[16] or Fe/Al[20] have been shown to be highly selective catalysts for the semihydrogenation. The increase in selectivity is based on the bidirectional influence of both metals confined in an ordered intermetallic solid-state material.

An intermetallic solid state material as defined by Armbrüster *et al.* is a "chemical compound of two or more metallic elements adopting an ordered crystal structure that differs from that of the constituent metals".[19] In contrast, an alloy is a stochastic mixture of metals and can also be seen as a substitutional or interstitial "solid solution" containing the different metals randomly distributed.[21]

Intermetallic Pd/Ga represents a well-studied model system for an intermetallic heterogeneous catalyst for acetylene semihydrogenation. Structural investigations on stoichiometric PdGa reveal that bulk Pd atoms are uniformly "coordinated" by a shell of Ga leading to isolated Pd without significant

Pd-Pd interactions (d(Pd-Pd) > 3.016 Å). The rather short experimental Pd-Ga distances (2.543-2.712 Å) together with theoretical calculations indicate strong covalent Pd-Ga interactions. Ultra-high vacuum X-Ray photoelectron spectroscopy at the BESSY beam line indicates that Ga "coordination" considerably changes the electronic structure of the Pd atoms in PdGa with respect to metallic Pd.[19] Theoretical investigations showed that adsorbed acetylene is bound on local arrangements of Pd and Ga atoms on the surface. Acetylene adopts bridging positions between these atoms with strong covalent interactions to Pd and Ga. However, when being hydrogenated to ethylene, the bonding mode shifts to a π-bonded interaction with a single Pd atom.[4] This means that the Ga-rich environment does not only change the electronic properties of Pd, but plays an active role to bind and activate acetylene at the surface. On the other hand, Ga "coordination" leads to a distinct decrease in the Pd-ethylene bond strength facilitating the release of ethylene as the desired reaction product. As mentioned above, also the mobility of adsorbed intermediates and the trajectory of their approach (which depends on surface morphology, etc.) has been shown to have considerable effects on selectivity.[3-4] Furthermore, a combined experimental and theoretical investigation exposed that the Pd/Ga arrangements at the surface change with the investigated crystal plane[3] and with the stoichiometry of Pd/Ga[4]. For instance Pd/Ga single crystals[3] cooled to 5 K, were exposed to a low-pressure C_2H_2/C_2H_4 atmosphere before ultra-high vacuum conditions ($5x10^{-11}$ mbar) were applied. STM images of the cooled Pd/Ga single crystal at high vacuum conditions show that different binding sites for acetylene/ethylene are present at distinct Pd/Ga surfaces (see Figure 2).For instance, C_2H_2 prefers metal bridging positions whereas C_2H_4 solely coordinates to a single Pd atom.[3]

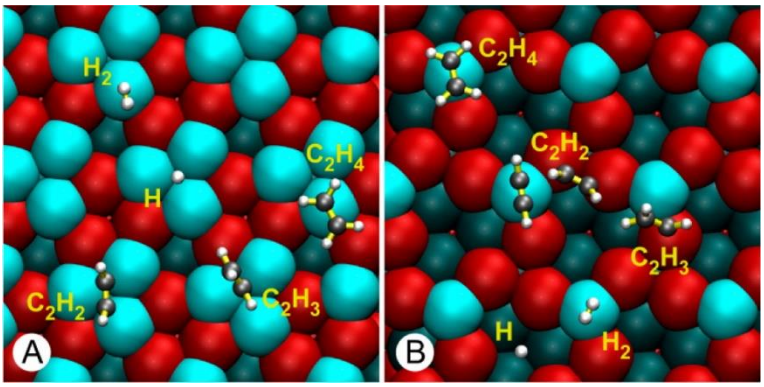

Figure 2: Calculated adsorption sites for the semihydrogenation of C_2H_2 to C_2H_4 on the PdGa:A(−1−1−1)Pd_3 (left) and the PdGa:A(111)Pd_1 surface (right). The atoms are colored as follows: Pd (blue), Ga (red), C (grey), H (white). On the Pd_3 surface (left), C_2H_2 is bound to a local arrangement of three Pd atoms whereas C_2H_4 is solely bound to one Pd atom in a side on fashion. For the Pd_1 surface, C_2H_2 can either bind to a single Pd atom or to two Ga atoms in the second atomic layer. C_2H_4 is again bound by a single Pd atom. Reprinted with permission from Prinz *et al.*, J. Am. Chem. Soc. **2014,** 136 (33), 11792-11798. Copyright 2014 American Chemical Society.

For Ni/Ga and Ni/Zn systems an increase of the element M' (Ga, Zn) has a beneficial influence on the semihydrogenation selectivity.[16, 22] In comparison to the Pd/Ga model system, intermetallic Ni/Zn

systems are only little investigated. The adsorption energy of ethylene is much weaker for NiZn. Furthermore, the activation barrier for further hydrogenation of ethylene to ethane is higher than the activation energy for the desorption of ethylene.[16] Therefore, Studt *et al.* concluded, that the selectivity results from changes of the electronic properties of the catalytically active Ni center by Zn "coordination" but no insights for substrate binding on the NiZn surface is given.[16] Therefore, the question arises whether different metal bridging C_2H_2/C_2H_4 coordination sites, as found for the Pd/Ga case, might also be present at Ni/Zn surfaces. This would potentially give an additional explanation for the increasing selectivity upon mixing of Zn with Ni.

Ⅱ.2 Molecular Solid-State Models

Breaking down complexity

Starting with the findings of Sabatier and Paal, heterogeneous semihydrogenation has substantially developed. A lot of research was devoted to a detailed understanding of the catalytic mechanisms, the influence of different metal combinations, and substrate binding to the surface. Heterogeneously catalyzed reactions are generally performed at elevated temperature and pressure which leads to substantial demands for experimental analysis. To circumvent this problem, the analysis is usually performed at milder conditions that are far off catalytic conditions. Therefore, a detailed description of surface processes is very challenging.

To circumvent these challenges but still permitting complementary insights for heterogeneous catalysis, simplified molecular compounds can be investigated as potential model compounds. Such surface models should “replicate” catalytically active sites, e.g. by showing similar “surface-substrate” interactions.[23] Therefore, a general alternative to the investigation of a surface reaction, is to break down complexity and study the reactivity of isolated atoms or small clusters towards catalytically relevant substrates. Helmut Schwarz substantiates this approach with his statement: ”An important aspect that supports the feasibility of using small systems as catalytic models derives from the fact that chemistry is a local event: bond breaking and bond making are confined to the catalytically active site(s)”.[24] Usually steps, edges or defects in the catalyst surface where reactive atoms with low coordination numbers are exposed at the surface are considered as the catalytically active centers.

Therefore, these active centers can be represented by bare atoms and small clusters. Applying the so-called matrix-isolation technique, the stabilization of such species in inert matrices allows their experimental analysis using isotopic labeling, IR, Raman or UV-Vis spectroscopy. Usually, the experimental investigations are accompanied by quantum chemical calculations leading to detailed insights into electronic properties and bonding situations of such compounds.[25-28] Furthermore, by doping of the inert matrix with catalytically relevant substrates (e.g. CO, H_2, CH_4, C_2H_4) the reactivity of the stabilized species towards these small molecules can be investigated.[29]

A further approach to investigate such small compounds is based on the deposition of size-selected metal clusters on a solid support followed by detailed experimental investigations of their electronic properties, geometrical structures or cluster-substrate interactions using analytical techniques like IR-[30], photoelectron spectroscopy[31] or structure-resolving 3D scanning transmission electron microscopy[32].

Furthermore, mass-selected metal clusters and their reactivity towards small molecules can be investigated in the gas-phase.[33] For instance, Schwarz *et al.* explored the effect of metal alloying in

small dimeric clusters on the reactivity towards C-N bond formation. This research is fundamental for the industrial Degussa process, producing HCN from methane and ammonia. Comparing the reactivity of $[Pt_2]^+$, $[PtAu]^+$ and $[Au_2]^+$, Schwarz *et al.* observed beneficial cooperative effects of $[PtAu]^+$ for the C-N bond forming reaction.[24, 34] The presented approaches usually require advanced technical setups and analytical techniques that impede a widespread application of such investigations.

Apart from these non-preparative techniques, there are several synthetic approaches to ligand stabilized metal clusters. These clusters can be investigated in terms of their physical and chemical properties as well as the underlying bonding principles. For instance ligand-protected Au clusters[35-37] represent an intensively studied field which has also been extended to mixed-metal clusters usually featuring similar metal atoms.[38] A further example can be seen in the work by Schnöckel *et al.* on the synthesis of several anionic metalloid $[Al_nR_m]^{x-}$ and $[Ga_nR_m]^{x-}$ clusters[39], like $[Al_{69}((NSiMe_3)_2)_{18}]^{3-}$, $[Al_{77}((NSiMe_3)_2)_{22}]^{2-}$ and $[Ga_{84}((NSiMe_3)_2)_{20}]^{4-}$.[40-42] Such monometallic clusters resemble molecular cut-outs of the respective element modifications and can therefore be seen as intermediates between organometallic molecular compounds and solid state elements.[43]

Heterogeneous catalytic systems usually consist of metal combinations and oxidic support materials which can form complex "mixtures" especially under conventional reaction conditions. Therefore, the formation of metal mixtures, like alloys or intermetallic compounds, under these reaction conditions cannot always be excluded[44] or is beneficial for catalysis[45].

Therefore, molecular mixed-metal compounds featuring catalytically relevant metal combinations are highly desirable. Fischer *et al.* synthesized a whole library of clusters with the general formula $[TM_a(M'R)_bL_c]$.[1, 46-47] For instance, a series of mixed Cu/Zn compounds including $[(CuZn_2)(Cp^*)_3]$[48], $[(Cu_4Zn_4)(CNtBu)_4(Cp^*)_4]$[49], $[(Cu_3Zn_4)(Cp^*)_5]$ and $[(Cu_2Zn_5)(Cp^*)_5]$[50] featuring distinct nuclearities and Cu/Zn ratios have been studied. The interpenetrated tetrahedra present in the core of

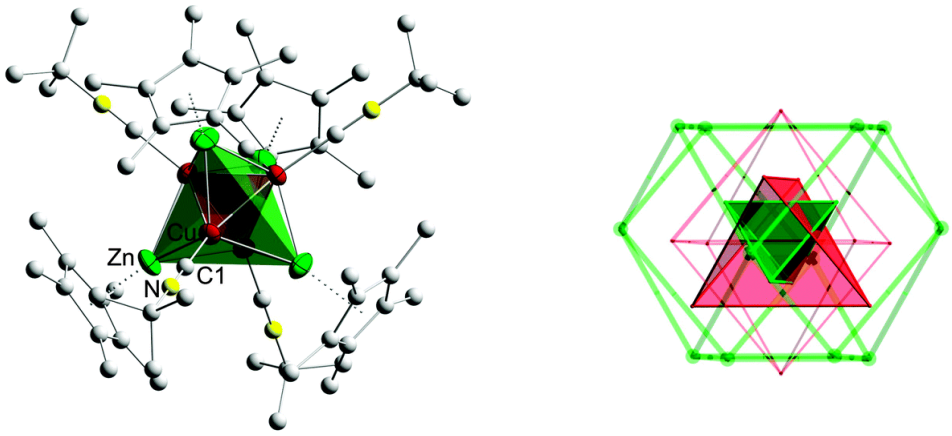

Figure 3: left: molecular structure of $[(Cu_4Zn_4)(CNtBu)_4(Cp^*)_4]$ showing the inner Cu_4 and outer Zn_4 tetrahedron. Right: solid state structure of γ-brass $Cu_{10}Zn_{16}$ with inner Zn_4 and outer Cu_4 tetrahedra. Reprinted with permission from Freitag *et al.*, Chem. Commun. **2014,** 50 (63), 8681-8684. Copyright 2014 Royal Society of Chemistry.

$[(Cu_4Zn_4)(CNtBu)_4(Cp^*)_4]$ are reminiscent of the solid state structure of $Cu_{10}Zn_{14}$ γ-brass (Figure 3). With respect to the heterogeneous CO_2 hydrogenation to methanol, the Cu/Zn combination has been intensively studied and debated.[44, 51-53] With respect to the ongoing research on the heterogeneous systems, the molecular Cu/Zn clusters represent interesting molecular models of a potential Cu/Zn intermetallic compound formed under catalytic conditions.

In addition to the structural relationship between Hume-Rothery inspired complexes and clusters and the solid state intermetallics, there is also a relationship in the reactivity as observed for the hydride containing $[(Cu_6Al_6)(Cp^*)_6(H)_4]$. It reacts with benzonitrile to afford the isolable cluster compound $[(Cu_6Al_6)(Cp^*)_6(H)_3(N{=}CHPh)]$ (Figure 4).[2] Therefore, this mixed-metal cluster represents the prototype to study the reactivity of TM/M' clusters towards catalytically relevant substrates on the molecular level. Such investigations might lead to complementary insights related to catalytic transformations on the surface of intermetallic solid-state materials.

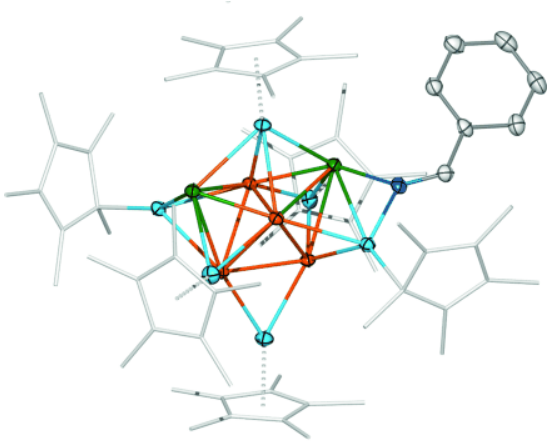

Figure 4: Molecular structure of $[(Cu_6Al_6)(Cp^*)_6(H)_3(N{=}CHPh)]$ as determined by single crystal X-Ray diffraction. The cluster core of the precursor $[(Cu_6Al_6)(Cp^*)_6(H)_4]$ remains intact and the benzonitrile intermediate is "attached" to the Cu_6Al_6 surface. Reprinted with permission from Ganesamoorthy *et* al., Angew. Chem. Int. Ed. **2014,** 53 (30), 7943-7947. Copyright 2014 John Wiley and Sons.

Ⅲ Motivation

Finding the right connection

Solid-state intermetallic compounds of the general composition TM/M' (TM = Pd, Fe, Co, Ni, Cu, M' = (Ag), Al, Ga, Zn) selectively catalyze the semihydrogenation of alkynes to alkenes. The combination of TM-M' was shown to be of major importance for the application of intermetallic compounds in catalysis.[3, 19] However, a detailed and fundamental understanding of the TM-M' interactions and the resulting surface-substrate interactions is hampered by the complexity of catalytic systems. A strategy to circumvent these problems is based on the investigation of well-defined molecular models to obtain a detailed understanding of metal-metal or metal-substrate interactions. Therefore, it is the goal of this research project to investigate the suitability of molecular $[TM_a(M'R)_b(UHC)_c]$ (UHC = unsaturated hydrocarbons) complexes and clusters as models for substrate-surface interactions with regard to the semihydrogenation of alkynes on intermetallic TM/M' catalysts. This approach is substantiated by the existence of e.g. $[Ni_2(ECp^*)_3(C_2H_4)_2]$[54], C-H activated $[W(AlCp^*)_6(C_2H_4)_2]$[55] and $[(C_2H_4)_3Ni_3(GaDDP)_2]$[56] featuring C_2H_4 linked to $[TM_a(ER)_b]$ cluster cores. Further examples of $[TM_a(M'R)_b(UHC)_c]$ will expand the structural relationship of molecular TM/M' clusters and TM/M' solid state materials to the level of comparable substrate-surface interactions or even substrate-surface reactivity (Figure 5).

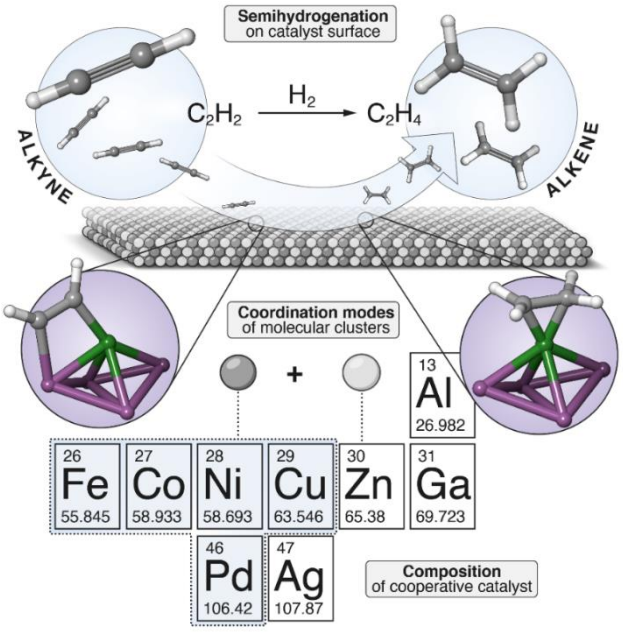

Figure 5: Schematic representation of heterogeneous semihydrogenation and molecular mixed-metal clusters highlighting the link between solid state intermetallics and Hume-Rothery inspired complexes and clusters.

Ⅳ Leading Research Questions

Hume-Rothery inspired coordination compounds of the general formula $[TM_a(M'R)_b(UHC)_c]$, featuring different ratios of TM/M' and direct TM-C_2H_x interactions, present reasonable research targets as molecular models. Following this conceptual approach, different research questions arise:

1. Do (selected) compounds with the general formula $[TM_a(M'R)_b(UHC)_c]$ present reasonable molecular models for substrate-surface interactions in intermetallic heterogeneous catalysts?

1.1. If yes, what is the effects of M'R ligands on TM and how does it influence TM-C_2H_x bonding?

2. How can $[TM_a(M'R)_b(UHC)_c]$ compounds be experimentally accessed?

3. What is the bonding situation of parent $[TM_a(M'R)_b]$ complexes/clusters. What can be learned for the TM-UHC interaction in $[TM_a(M'R)_b(UHC)_c]$?

These research questions are the signpost for this dissertation project. The respective theoretical/scientific background, especially for the synthetic chemistry of Hume-Rothery inspired complexes and clusters and the underlying bonding principles for the TM-M'R bonding will be given were necessary.

Ⅴ Results and Discussion

Ⅴ.1 All-Zinc Coordinated Nickel-Complexes as Molecular Mimics for NiZn Catalyst Surfaces, a Density Functional Theory Study

Parts of this chapter have been submitted to Chemical Science on March 5th, 2019.
J. Hornung, M. Muhr, C. Gemel, R. A. Fischer, submitted to Chem. Sci.

Ⅴ.1.1 Introduction to $[Ni(M'R)_n(UHC)_{4-n}]$

How to choose the right molecular models?

From the huge library of existing $[TM_a(M'R)_bL_c]$ complexes and clusters[1, 46-47], the propper compounds to represent suitable molecular models for substrate-surface interactions have to be identified. Thus, the following chapter will outline the reasons for the choice of model system to be investigated.

The theoretical and experimental investigations of solid-state intermetallics in the semihydrogenation of alkynes suggest NiZn catalysts as competing low-cost alternatives to industrially applied Pd/Ag.[16] The selectivity of NiZn originates from beneficial relative energies of alkyne/alkene adsorption and reaction barriers of alkyne/alkene hydrogenation. Acetylene is tightly bound to the NiZn surface (acetylene adsorption energy: ~1 eV) and hydrogenated to ethylene. The adsorption energy of ethylene on the NiZn surface, however is by far lower than acetylene adsorption energy (~ 0 eV). This results in the liberation of ethylene thus avoiding further hydrogenation to ethane (Figure 6).

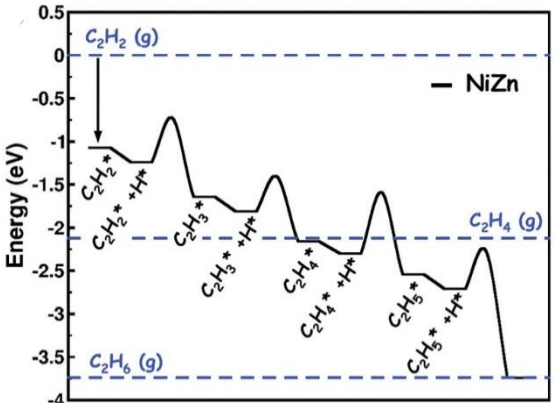

Figure 6: Calculated energy profile of the semihydrogenation of acetylene on the NiZn(111) surface. Reprinted with permission from Studt, F. et al., Science **2008,** 320 (5881), 1320-1322. Copyright 2008 American Association for the Advancement of Science.

Furthermore, it was experimentally found that the selectivity of the reaction mainly dependends on the NiZn ratio. For pure Ni only low selectivity was observed, whereas considerably increased selectivity could be achieved with higher Zn contend. The intermetallic compound with the

composition $NiZn_3$ was shown to be even more selective than the tested PdAg alloy.[16] Based on scaling relations the $NiZn_3$ was predicted to have a slightly lower turnover than the industrially applied PdAg catalyst, but no experimental data was presented in the original publication.[16]

As discussed in the introduction, the exact reason for the selectivity remains elusive, due to challenges associated with mechanistical investigations of surface reactions. In contrast to the Pd/Ga case, metal bridging adsorption sites of acetylene or ethylene on the Ni/Zn surface were not mentioned in the original publication.[16] Molecular models could help to give valuable insights whether metal bridging adsorption sites might be present at Ni/Zn surfaces as well. Idealized molecular models should feature a central Ni-center embedded in a Zn-rich environment (at the best with varying Ni/Zn ratios) and catalytically relevant UHC moieties near Ni.

With respect to these considerations, several interesting compounds can be found in the $[TM_a(M'R)_bL_c]$ library of the Fischer group, e.g. $[Ni(ZnCp^*)_4(ZnMe)_4]$.[57] This compound features a central Ni atom embraced in an all-Zn environment (Figure 7 left).

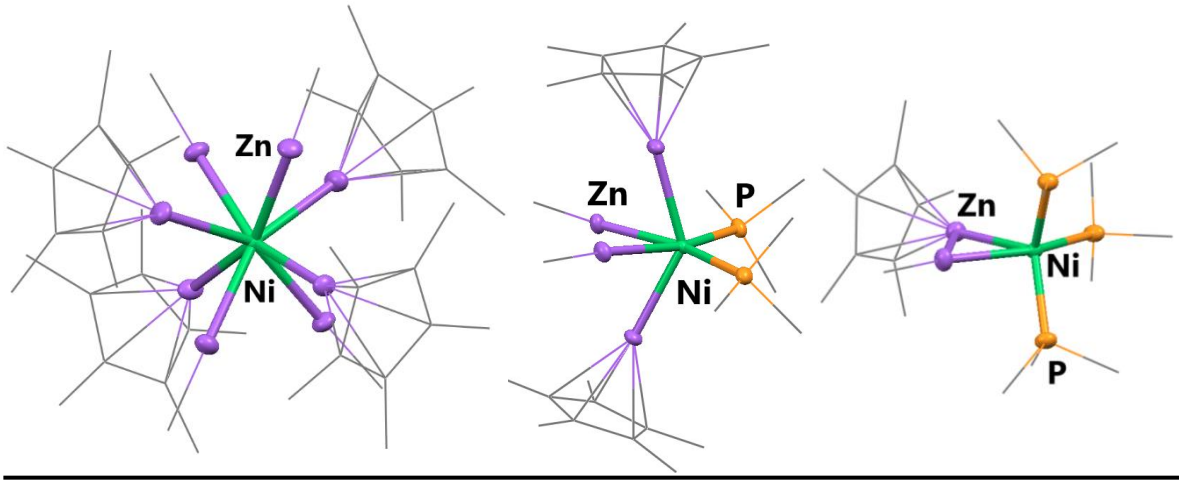

Figure 7: Left: molecular structure of $[Ni(ZnCp^*)_4(ZnMe)_4]$. d(Ni-Zn): 2.31-2.37 Å; d(Zn-Zn): 2.74-2.91 Å. Center: molecular structure of $[Ni(ZnCp^*)_2(ZnMe)_2(PMe_3)_2]$. d(Ni-Zn): 2.29-2.34 Å, d(Ni-P): 2.15, d(Zn-Zn): 2.71-2.80 Å. Right: molecular structure of $[Ni(ZnCp^*)(ZnMe)(PMe_3)_3]$. d(Ni-Zn): 2.30-2.35 Å, d(Ni-P): 2.14-2.16; d(Zn-Zn): 2.51 Å.

Therefore, the central Ni atom is shielded by eight ZnR ligands avoiding access of alkynes/alkenes to the Ni center. It is noteworthy that treating $[Ni(ZnCp^*)_4(ZnMe)_4]$ with an excess of the terminal alkyne $HC{\equiv}CSi(^iPr)_3$ results in selective replacement of the methyl groups by alkynyl coordination affording $[Ni(ZnCp^*)_4(ZnC{\equiv}CSi(^iPr)_3)_4]$.[58] In contrast to $[Ni(ZnCp^*)_4(ZnMe)_4]$, the Ni centers of $[Ni(ZnCp^*)_2(ZnMe)_2(PMe_3)_2]$ and $[Ni(ZnCp^*)(ZnMe)(PMe_3)_3]$ are not as sterically crowded with ZnR ligands.[59] Furthermore, PR''_3 ligands can potentially undergo ligand exchange reactions if treated with alkynes/alkenes to access $[TM_a(M'R)_b(UHC)_c]$ compounds. In principle, $[Ni(ZnCp^*)_3(ZnMe)_3(PMe_3)]$ should exist as well, however due to synthetic problems the respective precursor, is still missing (for more detail see chapter V.2.1.1 Introduction to heteroleptic $[Ni(M'R)_n(PEt_3)_{4-n}]$ complexes).

Based on these heteroleptic Ni-Zn-PR_3 compounds, Ni-Zn-UHC surface models are envisioned. Formal replacement of PMe_3 ligands with catalytically relevant C_2H_2 or C_2H_4 gives $[Ni(ZnR)_{2n}(C_2H_x)_{3-n}]$ (R = Cp*/CH_3 in 1:1 ratio; n = 1, 2, 3; x = 2, 4). These compounds allow the examination of the interaction of C_2H_2 and C_2H_4 with distinct $NiZn_{2n}$ "coordination sites". Since Al and Ga containing intermetallics are considered as potential alternatives for the industrial Pd/Ag catalyst (and the respective $[Ni(ECp^*)_n(PR''_3)_{4-n}]$[60] compounds are accessible), molecular $[Ni(ECp^*)_n(C_2H_x)_{4-n}]$ compounds shall be investigated as well. For comparison parent $[Ni(C_2H_x)_3]$ and M'R free $[Ni(PEt_3)_n(C_2H_x)_{4-n}]$ are considered as reference compounds in this study.

Ⅴ.1.2 Geometry optimization of $[Ni(L)_n(UHC)_{4-n}]$

Prior to the synthetic approaches towards $[Ni(M'R)_n(C_2H_x)_{4-n}]$, computational screening of the molecular structures at the DFT level of theory shall help to substantiate the idea of $[Ni(M'R)_n(C_2H_x)_{4-n}]$ as relevant molecular models for substrate-surface interactions on solid-state intermetallics.

Based on the experimental structures of $[Ni(M'R)_n(PR'_3)_{4-n}]$[59-61] the respective model compounds $[Ni(M'R)_n(C_2H_x)_{4-n}]$ were derived. The structures of $[Ni(C_2H_x)_3]$, $[Ni(PEt_3)_n(C_2H_x)_{4-n}]$, $[Ni(ZnR)_{2n}(C_2H_x)_{4-n}]$, $[Ni(GaCp^*)_n(C_2H_x)_{4-n}]$ and $[Ni(AlCp^*)_n(C_2H_x)_{4-n}]$ (denoted as $[NiL_n(C_2H_x)_{4-n}]$) were optimized at the BP86-D3/def2-TZVPP level of theory and the existence of local minima was verified by frequency calculations (for computational details see chapter Ⅶ Experimental Section). This combination of functional and basis set has been shown to give reasonable agreement between experimental and theoretical structures and was used to determine bonding properties in related complexes and clusters by energy decomposition analysis (EDA).[50, 57, 59, 61] Selected structural parameters are given in Table 1.

Table 1: Overview of selected structural parameters of $[NiL_n(C_2H_x)_{4-n}]$ (L = PEt_3, $(ZnR)_2$, AlCp*, n = 1-3, x = 2, 4) compounds. Distances are given in Å.

		d(C-C)			d(Ni-L)			d(L-C)		
	L =	PEt_3	$(ZnR)_2$	AlCp*	PEt_3	$(ZnR)_2$	AlCp*	PEt_3	$(ZnR)_2$	AlCp*
$[NiL_1(C_2H_x)_3]$	x = 2	1.25	1.25	1.28-1.47	2.21	2.41	2.48	>3.15	>2.76	1.98
	x = 4	1.39	1.40	1.39-1.40	2.21	2.40	2.25	>3.16	>2.41	>2.97
$[NiL_2(C_2H_x)_2]$	x = 2	1.26	1.34	1.27-1.37	2.21	2.30-2.43	2.45-2.60	>3.11	2.03	2.04-2.18
	x = 4	1.40	1.40	1.41	2.17	2.35-2.36	2.21	>3.09	>2.95	>3.01
$[NiL_3(C_2H_x)_1]$	x = 2	1.27	1.28	1.27	2.15-2.24	2.31-2.39	2.22-2.27	>3.02	>2.55	>3.24
	x = 4	1.40	1.42	1.41	2.15-2.19	2.33-2.38	2.20-2.23	>3.06	>2.57	>3.18

For a full comparison of the calculated $[Ni(M'R)_n(PR'_3)_{4-n}]$ structures please see Ⅸ Appendix. The series of PEt_3 complexes $[Ni(PEt_3)_n(C_2H_x)_{4-n}]$ was included in the calculations as reference for "regular" changes in Ni-C_2H_x bonding associated with the coordination of a typical σ-donating ligand[62] for TM centers within the classic Dewar-Chatt-Duncanson model for TM-alkene/alkyne bonding.[63-64] Introduction of ancillary ligands at the Ni center such as M'R rather than PR''$_3$ is expected to result in distinct changes in the electronic properties of the central Ni atom thus affecting Ni-C_2H_x bonding.

The structural parameters of the calculated $[Ni(C_2H_x)_3]$ complexes are close to reported values. Whereas $[Ni(C_2H_4)_3]$ was described as having a perfect D_{3h} symmetry featuring coplanar side-on coordinated ethylene[26, 65], the acetylene ligands in $[Ni(C_2H_2)_3]$ slightly deviate from coplanarity due to interligand H-H repulsions.[65-66] The CC bond lengths of 1.25 Å for $[Ni(C_2H_2)_3]$ and 1.39 Å for $[Ni(C_2H_4)_3]$) and the Ni-C bond lengths are also well in line with published data.[26, 66]

For the pseudo-tetrahedral $[Ni(PEt_3)_n(C_2H_x)_{4-n}]$ compounds, the Ni-P bond lengths (2.15-2.24 Å) are in the range of related compounds and underline covalent interactions between the central Ni atom and

the surrounding ligands.[59, 61] The distances between the P ligator atom and the carbon atoms of C_2H_x are larger than 3.02 Å in all cases, indicating negligible P-C interactions. The C_2H_x side-on coordination does not change with variation of the number of coordinated PEt_3. The Ni-Zn bonds in $[Ni(ZnR)_{2n}(C_2H_x)_{4-n}]$ (2.30-2.43 Å) (Figure 9) are in accordance to published data for thermodynamically stable and isolable cluster compounds. [57, 59, 67] This result stands in contrast to the Ni-Ga and Ni-Al series where some members exhibit long Ni-Ga and Ni-Al distances which exceed usual bond lengths for covalent interactions. This phenomenon is most pronounced for the $[Ni(GaCp^*)_n(C_2H_2)_{4-n}]$ model series where a maximum Ni-Ga distance of 3.21 Å was found for $[Ni(GaCp^*)_1(C_2H_2)_3]$ (see Figure S 6).[61, 68] In most of the theoretical complexes $[Ni(M'R)_n(C_2H_x)_{4-n}]$, the C_2H_x ligands coordinate to the central Ni atom in the typical side-on fashion as found for the parent complexes $[Ni(C_2H_x)_3]$ and $[Ni(PEt_3)_n(C_2H_x)_{4-n})]$, well matching with experimental observations for such compounds.[26, 69, 70, 71]

In contrast, the Ni-C_2H_2 coordination is different in $[Ni(AlCp^*)_1(C_2H_2)_3]$, $[Ni(AlCp^*)_2(C_2H_2)_2]$ and $[Ni(ZnR)_4(C_2H_2)_2]$. For $[Ni(AlCp^*)_1(C_2H_2)_3]$ (Figure S 5), structure optimization leads to a C_2H_2 dimerization product with C_4H_4-Ni and C_4H_4-Al interactions and elongated Ni-Al distances (2.48 Å). For $[Ni(AlCp^*)_2(C_2H_2)_2]$ (Figure 8) one C_2H_2 ligand is bridging between the central Ni and the two adjacent Al atoms leading to elongated Ni-Al distances (2.45 and 2.60 Å) and shortened Al-Al interaction (2.50 Å). This C_2H_2 coordination to a $NiAl_2$ trimer site in the theoretical $[Ni(AlCp^*)_2(C_2H_2)_2]$ complex mimics C_2H_2 coordination to a trinuclear $PdGa_2$ site as determined for the solid state PdGa catalyst.[3]

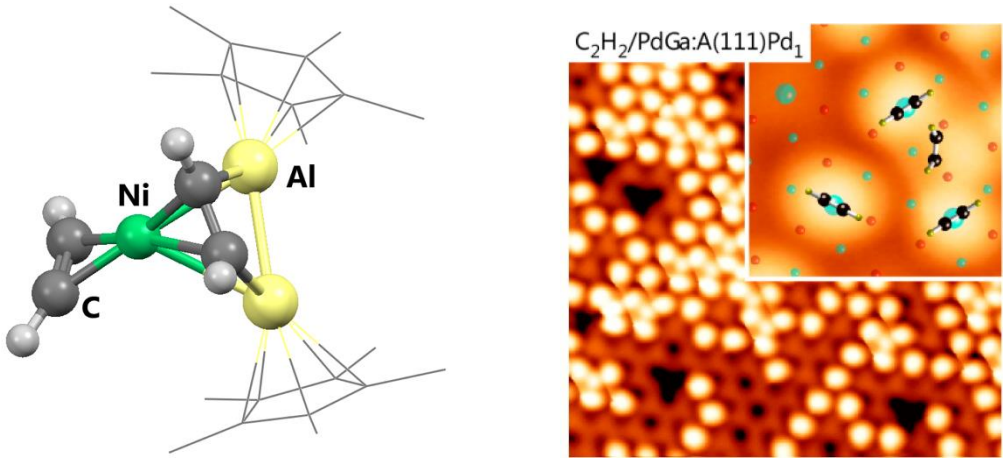

Figure 8: left: Calculated structure of $[Ni(AlCp^*)_2(C_2H_2)_2]$ showing the coordination of C_2H_2 on top of a $NiAl_2$-trimer site. The Cp* and Me groups are shown as wireframes for clarity. Distances are given in [Å]: Ni-Al: 2.45-2.63, Al-Al: 2.51, Ni-$C_{bridging}$: 1.92-2.24, Ni-$C_{nonbridging}$: 1.89. C-C distance: 1.37 Å. right: STM images (10x10 nm) of C_2H_2 adsorbed at T = 5 K on a the PdGa (111) surface. The adsorbates have a round shape which is attributed to a fast rotation or hopping of the adsorbate on the surface. For the (111) surface, two different almost isoenergetic adsorption sites were found for C_2H_2. C2H2 either adsorbes on a Pd atom or on a $PdGa_2$ triangle. For the later, the CC bond distance were calculated to be 1.35 Å. The inset shows the calculated adsorption sites for C_2H_2 on this surface. Reprinted with permission from Prinz *et al.*, J. Am. Chem. Soc. **2014,** 136 (33), 11792-11798. Copyright 2014 American Chemical Society.

For $[Ni(ZnR)_4(C_2H_2)_2]$, the C_2H_2 ligands adopt bridging positions between the central Ni atom and a coordinated Zn moiety (Figure 9 left). Ni-Zn bond critical points and bond paths can be found for the C_2H_2 bridged Ni-Zn interaction, as a good indication for a Ni-Zn covalent bond (see Figure S 7). In the related $[Ni(ZnR)_4(C_2H_4)_2]$ the C_2H_4 coordination is unaltered by the ZnR ligands. C_2H_4 coordinates in a side-on fashion to the central Ni atom (Figure 9 right).

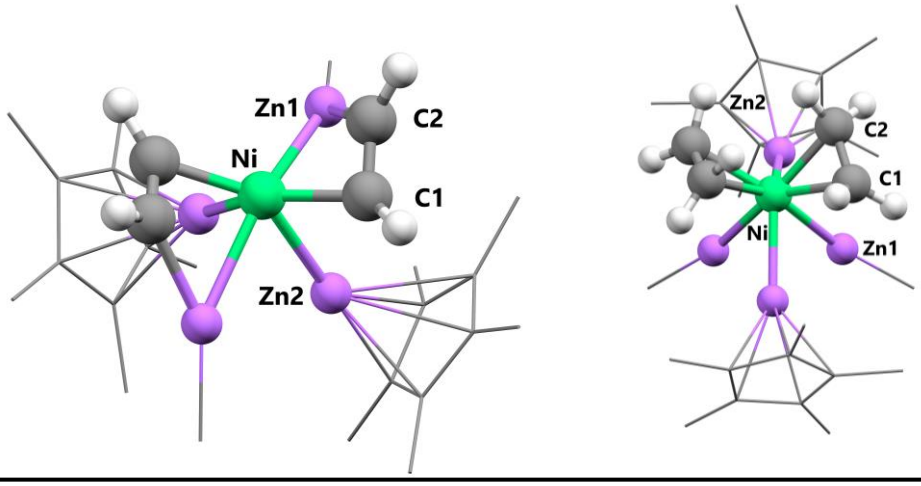

Figure 9: Calculated structures of $[Ni(ZnR)_4(C_2H_x)_2]$ showing the Ni-Zn bridging coordination mode of C_2H_2 vs. side-on C_2H_4. The Cp* and Me groups are shown as wireframes for clarity reasons. Left: $[Ni(ZnR)_4(C_2H_2)_2]$, distances in [Å]: Ni-C1: 1.89, Ni-C2: 2.23, Ni-Zn1: 2.44, Ni-Zn2: 2.31, Zn1-C2: 2.03, Zn2-C1: 2.53, C1-C2: 1.34, Zn-Zn: 3.02-3.31. Right: $[Ni(ZnR)_4(C_2H_4)_2]$, distances in [Å]: Ni-C1: 2.10, Ni-C2: 2.08, Ni-Zn1: 2.35, Ni-Zn2: 2.36, Zn1-C1: 2.96,Zn2-C2: 3.14, C1-C2: 1.40, Zn-Zn: 2.62-2.80.

To evaluate the significance of the obtained bridging/non-bridging structures, the C_2H_2 coordination mode at the $[Ni(ZnR)_{2n}]$ fragments was evaluated. Therefore, the Ni-Zn bridging C_2H_2 moiety of the $[Ni(ZnR)_4(C_2H_2)_2]$ was shifted to the regular side-on coordination to the central Ni atom. Geometry optimization leads to the already discussed structure featuring Ni-Zn bridging C_2H_2 moieties. Furthermore, geometry optimization of a Ni-Zn-bridging C_2H_2 input structure for $[Ni(ZnR)_6(C_2H_2)]$, non-bridging, side-on coordinated C_2H_2 at the Ni centre is obtained. For $[Ni(ZnR)_2(C_2H_2)_3]$ this approach results in a new minimum structure featuring three bridging C_2H_2-moieties(see Figure S 4). This finding clearly underlines an additional link to solid-state TM/E catalysts. In the solid state as well on the molecular level, the TM/E ratio has a significant influence on C_2H_x bonding. The existence of different minimum structures suggests flat potential energy surfaces of such systems. Thus, the possibility to obtain versatile $[TM_aE_b(C_2H_x)_c]$ compounds depending on reaction conditions, choice of substituents, steric bulk, solvent etc. was deduced. It is thus expected that some members of the $[Ni(M'R)_n(C_2H_x)_{4-n}]$ complexes are not stable under experimental conditions and might be difficult to isolate and characterize, especially for E = Al/Ga.

V.1.3 Bonding in $[Ni(L)_n(UHC)_{4-n}]$ complexes

Considering the distinct coordination modes of C_2H_2 to different $[NiL_n]$ (L = PEt_3, AlCp*, GaCp*, $(ZnR)_2$; n = 1-3) fragments the Ni-L bonding in parent $[NiL_4]$ will be shortly reviewed. Further, the Ni-UHC bonding in $[Ni(L)_n(UHC)_{4-n}]$ will be investigated. All $[NiL_4]$ complexes are 18 valence electron complexes. Within a simplified picture, Ni^0 offers ten d-electrons and each PEt_3, Al^ICp^* or Ga^ICp^* ligand donates two additional electrons by σ-donation of their lone-pairs. However, the TM-L interactions in different $[(CO)_xTM(L)]$ compounds (L = PR''_3, AlR, GaR) are better described as polar covalent bonds with huge contributions of electrostatic interactions and only a small orbital share.[72] This situation is more complicated for the one-electron donating Zn^IR ligands. In principle, since having eight ZnR ligands, the Ni center formally fulfills the 18 valence electron rules which is in line with the stability of $[Ni(ZnCp^*)_4(ZnMe)_4]$ under experimental conditions.[57] For the related model compound $[Pd(ZnH)_8]$ the Pd-Zn bonding was described as follows. The radial Pd-Zn interactions can be described as direct Pd-Zn bonds based on a quantum theory of atoms in molecules (QTAIM) analysis. However tangential, or "cage" Zn-Zn interactions are only weak interactions and no bond paths or bond critical points can be found. These weak interactions however are very important and help to stabilize this highly-coordinated and sterically crowded compound. Energy decomposition analysis (EDA) of the interaction of the "interstitial" Pd atom to the $(ZnH)_8$ "cage" indicates that this Pd-$(ZnH)_8$ interaction mainly derives from electrostatic interactions (78%) whereas only 22% are based on orbital interactions.[57] The bonding in related $[Mo(ZnCp^*)_3(ZnMe)_9]$[73] was also described as being related to the bonding in "hypervalent" molecules, e.g. SF_6[74]. The sd^5-hybridized Mo-orbitals would engage in six two-electrons-three center Mo-Zn bonds and the remaining six electrons are used for highly delocalized Zn-Zn bonding in the Zn_{12} cage.[57, 73]

To further elucidate the Ni-L bonding in parent $[NiL_4]$ compounds theoretical investigations were performed. After geometry optimization and insurance of a local minimum geometry, NBO charges (NBO: natural bond orbital) were calculated for these compounds. The results are summarized in Table ***2***.

Table 2: Overview of the calculated NBO charges for $[NiL_4]$ (L = PEt_3, GaCp*, AlCp*, $(ZnR)_2$) (BP86-D3/def2-TZVPP).

NBO charge	Ni	ligator atom (P, Ga, Al, Zn)
$[Ni(PEt_3)_4]$	-1.3	1.1
$[Ni(GaCp^*)_4]$	-2.1	1.0
$[Ni(AlCp^*)_4]$	-3.2	1.5
$[Ni(ZnCp^*)_4(ZnMe)_4]$	-3.7	0.9-1.0

This analysis shows that the central Ni atom is always negatively charged whereas the ligator atoms (P, Al, Ga, Zn) are positively charged underlining the finding of polar TM-E bonds for comparable compounds.[57, 72] The negative charge increases from L = PEt_3 < GaCp* < AlCp* < $(ZnR)_2$. The overall polarization between Ni and L is comparable for L = AlCp*, $(ZnR)_2$.

The polar TM-L bond was also verified by EDA for the Ni-L bond in homoleptic [$Ni(PEt_3)_4$], [$Ni(GaCp^*)_4$] and [$Ni(AlCp^*)_4$] (Figure 10). The Ni-Zn bond in [$Ni(ZnCp^*)_4(ZnMe)_4$] could not be investigated in the same manner, since the ZnR ligands are not "separated" ligands (see also chapter V.2.1.6 Ni-Zn bonding in [$Ni(ZnR)_{2n}(L)_{4-n}$] compounds).

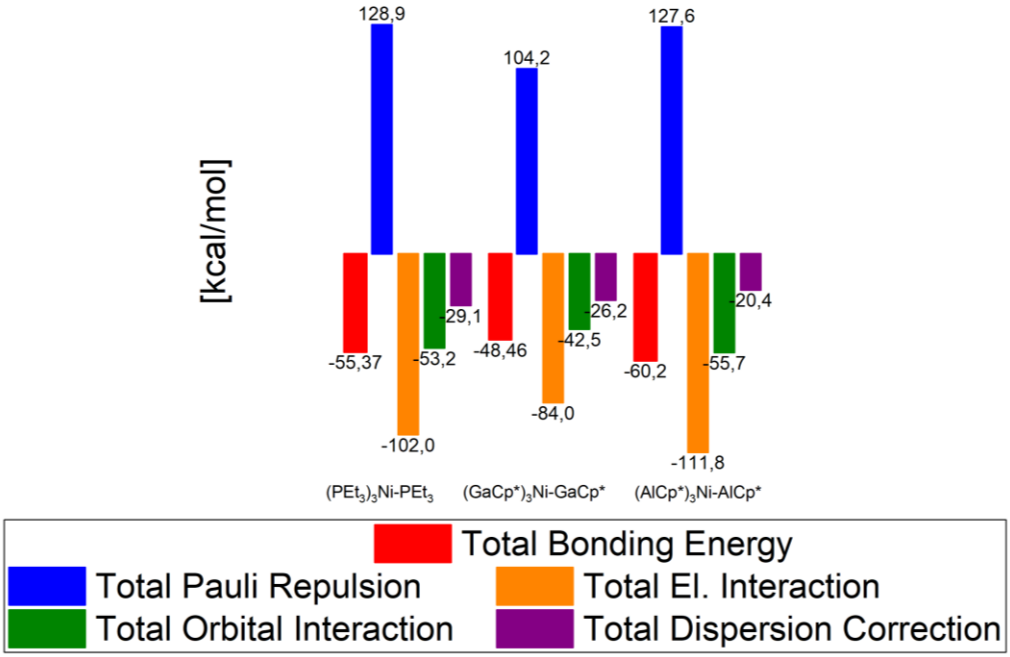

Figure 10: EDA-NOCV analysis of the Ni-L bond in [$Ni(PEt_3)_4$], [$Ni(GaCp^*)_4$] and [$Ni(AlCp^*)_4$], showing that the electrostatic contributions dominate over orbital contributions for the investigated Ni-L bonds.

From this result it becomes evident that the Ni-L bonds are dominated by electrostatic interactions (always about 66% of the attractive contributions including electrostatic as well as orbital interactions).[72] For the TM-ECp* bond the electrostatic interactions are shown to derive from attractive interactions between the positively charged TM nucleus and the negative charge of the lone-pair at ECp*.[72, 75] In a comparable approach the Ni-{(MeZnZnCp*)} bond in heteroleptic [$Ni(ZnCp^*)(ZnMe)(PMe_3)_3$] featuring a "side-on" bonded (ZnR_2) moiety (for comparison see Figure 7), was described as being slightly more polarized with a electrostatic contribution of about 72%.[59] Furthermore, it has to be noted that the Ni-AlCp* bond (total bonding energy = -60.2 kcal/mol] is predicted to be stronger than the Ni-GaCp* bond (total bonding energy = -48.5 kcal/mol), in accordance to previous results for comparable compounds.[75] This finding is important for later

experimental results (see chapter V .4.5 Synthesis and characterization of [Ni2(μ-GaCp*)(μ-GaNiCp*)$_2$(dvds)$_2$]).

After the discussion of the bonding in parent NiL$_4$ complexes, the following section will focus on a more detailed bonding analysis of [Ni(ZnR)$_{2n}$(C$_2$H$_2$)$_{4-n}$] in comparison to the PEt$_3$ analogs to investigate the influence of PEt$_3$/ZnR coordination on Ni-C$_2$H$_x$ bonding. At selected parts of the discussion, the values for L = GaCp*, AlCp* will be discussed as well. For the PEt$_3$/(ZnR)$_2$ series, higher PEt$_3$ or ZnR coordination numbers lead to a slight elongation of the CC bonds of side-on coordinated C$_2$H$_x$. Qualitatively, this observation can be explained by a more negatively charged Ni-center receiving electron density from the coordinating ligands PEt$_3$ or ZnR. The calculated more negative NBO charges for the central Ni atoms support this assumption. The NBO charge of the Ni atom was also shown to be strongly dependent on the number of coordinated L (and in turn C$_2$H$_x$) getting more negative with higher numbers of L (Figure 11).

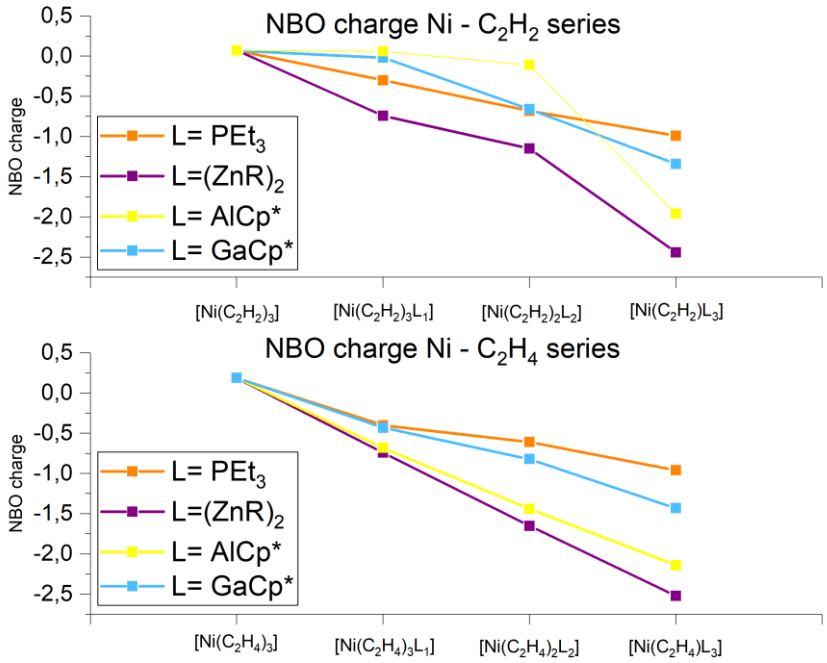

Figure 11: NBO charges calculated for Ni in [Ni(L)$_n$(C$_2$H$_x$)$_{4-n}$] (L = PEt$_3$, AlCp*; GaCp*, (ZnR)$_2$) complexes. With increasing numbers of L, the Ni-center is more negatively charged. For the series of C$_2$H$_4$ compounds, where no Ni-L bridiging coordinations are found, the NBO charge follows the general trend of the parent NiL$_4$ compounds.

Further, the nature of L has a decisive influence on the NBO charge. Even though, PR$_3$ ligands are known to be good donor ligands in transition metal complexes[62], ZnR coordination leads to a more negatively polarized Ni centre. However, the charge of the Ni center seems to be less sensitive to alkyne/alkene coordination.

For side-on coordinated C$_2$H$_x$, the Wiberg bond indices (WBI) of the CC bonds gradually decrease with rising coordination numbers of L. Interestingly, [Ni(ZnR)$_4$(C$_2$H$_2$)$_2$] deviates from this general trend. Here,

the C_2H_2 ligands adopt bridging positions between the central Ni atom and the Zn atom of one of the ZnR groups. The Ni-C and Zn-C distances of 1.90-2.25 and 2.03 Å respectively, indicate significant M-C interactions. The CC distance is elongated to 1.34 Å which is in the range of coordinated alkenes indicating significant bond activation. The low WBI of 1.93 for the CC bond points at significant bond activation as well. For comparison the CC distance in the reference complex $[Ni(PEt_3)_2(C_2H_2)_2]$ is 1.26 Å (WBI = 2.43). It has to be noted that the Zn-Zn distances in $[Ni(ZnR)_4(C_2H_x)_2]$ increase from 2.62-2.82 Å in the alkene to 3.02-3.31 Å in the alkyne complex. This finding will be further investigated in chapter V.2.1.6 Ni-Zn bonding in $[Ni(ZnR)_{2n}(L)_{4-n}]$ compounds. One could assume that the increased steric demand in the Ni-Zn series with more ZnR ligands, might solely enforce additional alkyne-zinc

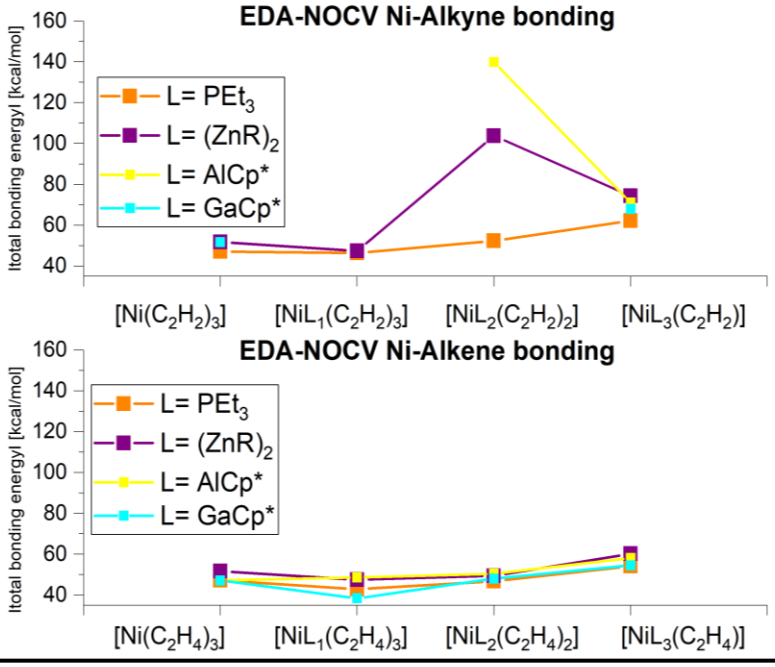

Figure 12: Total bonding energies of the Ni-C_2H_x bonding depending on the nature of L. It can be seen, that the total bonding energy of Ni-C_2H_4 are independent of the number and nature of L. However especially for $[Ni(AlCp^*)_2(C_2H_2)_2]$ and $[Ni(ZnR)_4(C_2H_2)_2]$ the total bonding energy is very high due to additional C_2H_2-Al/Zn interactions. $[Ni(AlCp^*)_1(C_2H_2)_3]$ is not considered since it shows alkyne dimerization upon structure optimization. The Ni-Ga distance in $[Ni(GaCp^*)_n(C_2H_2)_{4-n}](n = 1, 2)$ exceds standard Ni-Ga bond lengths and thus only $[Ni(GaCp^*)_3(C_2H_2)_1]$ is shown.

interactions. However, this assumption is rescind by the optimized structures of $[Ni(ZnR)_6(C_2H_x)]$ and the alkene complex $[Ni(ZnR)_4(C_2H_4)_2]$ featuring side-on coordinated C_2H_x without significant C_2H_x-Zn interactions.

Table 3: Overview of EDA-NOCV results for $[NiL_2(C_2H_x)_2]$ (L = PEt_3, AlCp*, $(ZnR)_2$) and the respective WBI values of the CC bonds showing distinct C_2H_x bonding on NiL_2 fragments.

	$[NiL_2(C_2H_4)_2]$			**$[NiL_2(C_2H_2)_2]$**		
L=	PEt_3	$(ZnR)_2$	AlCp*	PEt_3	$(ZnR)_2$	AlCp*
ΔE_{int}	-46.8	-49.4	-50.5	-52.4	-103.8	-139.9
ΔE_{Pauli}	171.4	177.0	169.3	181.2	348.3	379.7
$\Delta E_{electrostat}$	-122.5	-123.6	-121.4	-126.9	-215.7	-235.3
ΔE_{orb}	-85.7	-89.5	-89.6	-97.9	-225.0	-275.4
π-type interaction	-54.9	-48.8	-55.8	-63.6		
σ-type interaction	-20.8	-27.6	-23.3	-23.1		
ΔE_{Disp}	-9.9	-13.4	-8.8	-8.8	-11.22	-8.8
WBI (CC)	1.51	1.48	1.45	2.43	1.93	1.76

Investigation of Ni-C_2H_x bonding using energy decomposition analysis yields (Figure 12 and Table 3) the total interaction energy ΔE_{int} as a result of attractive and repulsive forces (see Ⅷ Experimental Section).

From $[Ni(C_2H_x)_3]$ to $[Ni(PEt_3)_n(C_2H_x)_{4-n}]$ without P-C_2H_x interaction, ΔE_{int} marginally decreases for $[Ni(PEt_3)_1(C_2H_x)_3]$ before it increases with higher numbers of coordinated PEt_3. As expected, ΔE_{int} is slightly higher for the alkyne series compared to the alkene series, due to higher Ni→C_2H_x π-back and C_2H_x→Ni σ contributions in the orbital share. The general trend in the Ni-C_2H_x total interaction energy is independent of L, i.e. ZnR vs. PEt_3. $(ZnR)_{2n}$ coordination leads to a slightly higher value of ΔE_{int} compared to PEt_3 coordination attributed to higher electrostatic and covalent contributions. Again, the $NiZn_4$ acetylene complex $[Ni(ZnR)_4(C_2H_2)_2]$ is a special case. Here, ΔE_{int} is by far higher than for any other member of the series. When taking a closer look at the electrostatic and covalent contributions to ΔE_{int}, a significant feature becomes evident for the $NiZn_4$ environment. In the side-on coordinated C_2H_x in $[Ni(PEt_3)_n(C_2H_x)_{4-n}]$ and $[Ni(ZnR)_{2n}(C_2H_x)_{4-n}]$ (except $[Ni(ZnR)_4(C_2H_2)_2]$) the Ni-C_2H_x bond is dominated by electrostatic interactions. This situation changes for $[Ni(ZnR)_4(C_2H_2)_2]$. Here the covalent contribution slightly exceeds electrostatic interaction.

This underlines the higher covalent character between C_2H_2 and the NiZn containing fragment. Speaking in terms of surface science it can be concluded that C_2H_x is "physisorbed" in most cases, whereas for $[Ni(ZnR)_4(C_2H_2)_2]$ acetylene is "chemisorbed" to the cluster "surface". This can be explained by the Ni-Zn bridging coordination mode of C_2H_2 increasing ΔE_{int} by roughly 50 kcal/mol for the C_2H_2 coordination in comparison to the ethylene compound $[Ni(ZnR)_4(C_2H_4)_2]$. The same applies for $[Ni(AlCp^*)_2(C_2H_x)_2]$. The bridging coordination, or "chemisorption", of C_2H_2 leads to a stabilization of about 90 kcal/mol when compared to the unbridged C_2H_4 congener.

V.1.4 Summary of $[Ni(M'R)_n(C_2H_x)_{4-n}]$ as potential surface model compounds

The presented computational studies of the series of theoretical complexes $[Ni(M'R)_n(C_2H_x)_{4-n}]$ reveal that such species can indeed be seen as molecular models of intermediates in hydrogenation reactions on intermetallic surfaces. The molecular complexes mimic acetylene and ethylene surface binding modes at TM/M'_n sites. Remarkably, some members as e.g. $[Ni(AlCp^*)_2(C_2H_2)_2]$ and $[Ni(ZnR)_4(C_2H_2)_2]$ show unique Ni-E bridging coordination modes for C_2H_2 in contrast to C_2H_4. This result is conceptualized from the viewpoint of heterogeneous semihydrogenation: acetylene is strongly "chemisorbed" to and highly activated by the unique structure of the "$NiZn_4$ surface" which involves cooperative Ni/Zn interactions with C_2H_2. Hydrogenation to ethylene results in weaker interactions to the "surface" (physisorption) which would suppress over-hydrogenation to C_2H_6, by C_2H_4 desorption (i.e. dissociation in case of molecular complexes). Therefore, it can be concluded that the computational results on the simple model systems support the proposed link between intermetallic catalysts for semihydrogenation and the related Hume-Rothery inspired complexes and clusters. Certainly, the stability of $[Ni(M'R)_n(C_2H_x)_{4-n}]$ cannot be estimated based on the presented theoretical study. Nevertheless, the results suggest that among the synthetic targets of the general formula $[TM_a(M'R)_b(UHC)_d]$ some examples may indeed resemble interesting molecular model intermediates of the semihydrogenation process on related intermetallic surfaces. Thus, it is valid to seek for such compounds applying different experimental strategies and methods.

V.2 Research Strategies for the Synthetic Access to $[Ni_a(M'R)_b(UHC)_c]$

The computational results presented above suggest that selected $[TM_a(M'R)_b(UHC)_c]$ complexes and clusters could serve as molecular models for surface hydrogenation reactions, featuring unsaturated hydrocarbon moieties. In this regard the series of $[Ni(ZnR)_2(C_2H_x)_{4-n}]$ complexes represent very interesting research targets. As discussed, such compounds cannot be accessed from sterically crowded all-Zn coordinated $[Ni(ZnCp^*)_4(ZnMe)_4]$ since treatment of the latter with alkynes and alkenes mostly results in unwanted decomposition of the complexes.[76] Solely for the terminal alkyne $HC{\equiv}CSi(^iPr)_3$, featuring a sterically demanding $Si(^iPr)_3$-moitey a $CH_3/C{\equiv}CSi(^iPr)_3$ exchange was reported yielding $[Ni(ZnCp^*)_4(ZnC{\equiv}CSi(^iPr)_3)_4]$ after 30 days.[58] In addition to ZnR-containing compounds, nteresting Ni-Al-bridiging C_2H_2 coordination modes were observed for $[Ni(AlCp^*)_2(C_2H_2)_2]$ as well. However, the parent $[Ni(AlCp^*)_4]$ is kinetically inert and cannot undergo ligand exchange reactions.[8] Interesting reactivities were found for low-coordinated $[Ni(AlCp^*)_3]$, present as an intermediate during the synthesis of $[Ni(AlCp^*)_4]$. Treatment of the organometallic precursor $[Ni(cod)_2]$ with $[AlCp^*]_4$ in hexane at elevated temperatures of 70°C selectively yields $[Ni(AlCp^*)_4]$. Performing the reaction under the same conditions but in benzene as solvent gives $[(AlCp^*)_3Ni(\mu\text{-}H)(Al(C_6H_5)Cp^*)]$ revealing a C-H activated C_6H_5 moiety. Changing the solvent to $H\text{-}SiEt_3$ leads to H-Si bond activation yielding $[(H)(SiEt_3)Ni(AlCp^*)_3]$ as a clean reaction product in good yields (Figure 13).

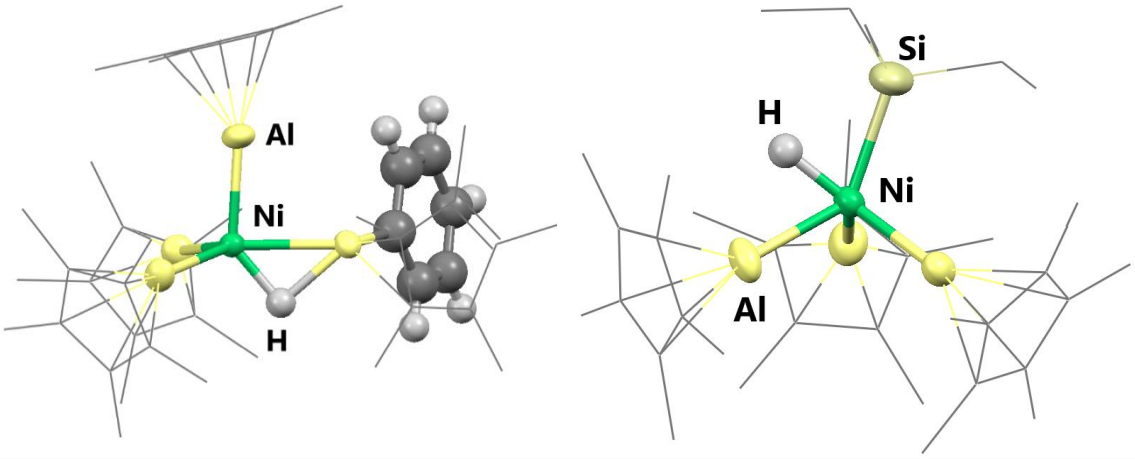

Figure 13: Left: Molecular structure of $[(AlCp^*)_3Ni(\mu\text{-}H)(Al(C_6H_5)Cp^*)]$ showing C-H bond activation of C_6H_6 and a Ni-Al-bridging hydride. Right: Molecular structure of $[(H)(SiEt_3)Ni(AlCp^*)_3]$ showing the Si-H bond activation reaction at the intermediate $Ni(AlCp^*)_3$-fragment.

Interestingly, $[(H)(SiEt_3)Ni(AlCp^*)_3]$ is not kinetically inert and can undergo reductive elimination of $H\text{-}SiEt_3$ liberating a highly reactive $[Ni(AlCp^*)_3]$ fragment. Treatment with additional $[AlCp^*]_4$ in n-hexane selectively yields $[Ni(AlCp^*)_4]$ whereas in benzene partial decomposition occurs but also $[(AlCp^*)_3Ni(\mu\text{-}H)(Al(C_6H_5)Cp^*)]$ is formed. Therefore, $[(H)(SiEt_3)Ni(AlCp^*)_3]$ is considered to be a reasonable starting

point for the synthetic access to [(UHC)Ni(AlCp*)$_3$] by formation of intermediate low-coordinated [Ni(AlCp*)$_3$] and subsequent association of a UHC moiety (Figure 14). This strategy would however only allow the synthesis of a single potential surface model compound [Ni(AlCp*)$_3$(UHC)]. As presented for the heterogeneous semihydrogenation of alkynes and also for molecular [Ni(M'R)$_n$(UHC)$_{4-n}$], the TM/M' ratio is crucial for TM-UHC bonding. Therefore, a more universal access to various [TM$_a$(M'R)$_b$(UHC)$_c$] compounds is highly desirable.

In general, low-coordinated transition metal centers can not only be obtained by reductive elimination but also by ligand dissociation from saturated complexes. In homogeneous catalysis, phosphines are often used as labile ligands to afford the catalytically active species featuring open-coordination sites.[62, 77] As presented above, the library of Hume-Rothery inspired complexes and clusters also contains [Ni(M'R)$_n$(PR''$_3$)$_{4-n}$] (M' = Al, Ga, Zn; R'' = Me, Ph, cyclo-hexyl) were selected examples have already been synthesized in the group of Prof. Fischer.[59-60] However, for none of the metals M' a complete series with variation of the Ni/M' ratio has been established, nor has the dissociation of the phosphine ligands been investigated so far. The series of [Ni(M'R)$_n$(PR''$_3$)$_{4-n}$] for M' = Al, Ga, Zn would potentially allow access to [Ni(M'R)$_n$(UHC)$_{4-n}$] by ligand displacement reactions.

In Figure 14, the two strategies for the access of low-coordinated [Ni(M'R)$_n$] fragments, as intermediates on the way to the envisioned molecular surface models, are depicted schematically. In contrast to the reductive elimination from [(H)(SiEt$_3$)Ni(AlCp*)$_3$] phosphine dissociation from [Ni(M'R)$_n$(PR''$_3$)$_3$] would potentially allow a wider range of [Ni(M'R)$_n$] fragments. Therefore, the next chapter will deal with the synthesis of the complete series of [Ni(M'R)$_n$(PR''$_3$)$_{4-n}$] and the investigation of PR''$_3$-ligand dissociation.

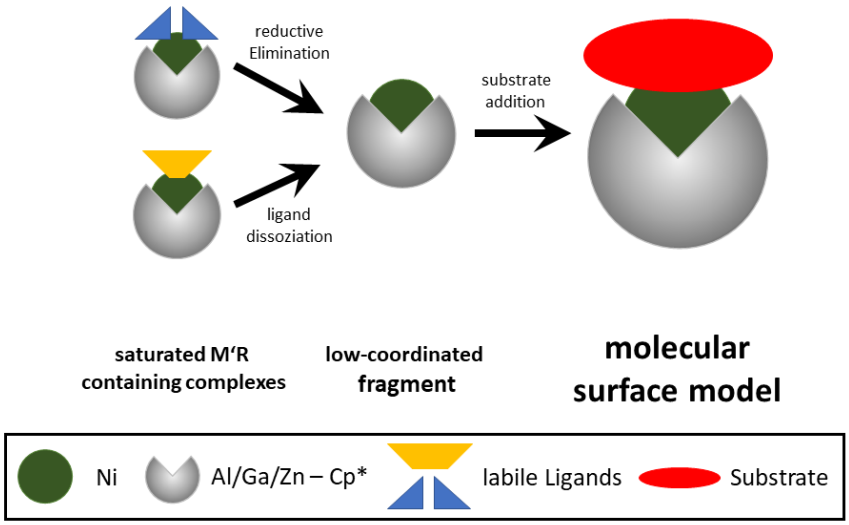

Figure 14: Schematic representation of experimental strategies to [Ni$_a$(M'R)$_b$(C$_2$H$_x$)$_c$] compounds (right structure). The approach is based on the generation of low-coordinated Ni-fragments with preformed Ni-M'R bonds. This would allow the addition of suitable "substrates" like alkynes or alkenes. In general, low-coordinated transition metal fragments can either be achieved by reductive elimination (left top) or ligand dissociation (left bottom).

V.2.1 Functionalized $[Ni(M'R)_nL_m]$ complexes

V.2.1.1 Introduction to heteroleptic $[Ni(M'R)_n(PEt_3)_{4-n}]$ complexes

The following chapters summarize the work on $[Ni(ECp^*)_n(PEt_3)_{4-n}]$ published in

J. Hornung, J. Weßing, P. Jerabek, C. Gemel, A. Pöthig, G. Frenking and R. A. Fischer, *Inorg. Chem.*, 2018, **57**, 12657-12664

and the Master thesis of Patricia Heiß dealing with the investigation of $[Ni(ZnR)_{2n}(PEt_3)_{4-n}]$. The master thesis by P. Heiß was supervised by the author of this dissertation.

Phosphines are generally applied as ligands for transition metal based catalysts since they possess a huge tendency for dissociation.[62] Nickel-PR_3 chemistry was studied by Tolman *et al.*[6, 62]using competing ligand exchange reactions and VT-UV/Vis spectroscopy to determine the ability of ligand dissociation/ligand exchange reactions of several phosphine ligands. Finally, this area of research led to the growing awareness of the importance of the ligand's steric effects on TM-L bonding.[6] Based on VT-UV-Vis studies on several $[Ni(PR_3)_n]$ Tolman established a relation between the steric and electronic properties of the phosphines and their ligand exchange/dissociation behavior. Three phosphine ligands, namely PEt_3, PPh^3, and $PMePh_2$ were described as exhibiting fast exchange behavior and an extensive dissociation from Ni-complexes.[7] Furthermore, the exchange of Ni-coordinated P-donor ligands by alkenes leading to $[Ni(alkene)_n(PR''_3)_m]$ was reported, indicating that similar reactions could lead to heteroleptic $[Ni(M'R)_{4-n}(alkene)_n]$ complexes starting from heteroleptic $[Ni(M'R)_n(PR''_3)_{4-n}]$.[78-79] With respect to the phosphine chemistry of Hume-Rothery inspired complexes and clusters PR''_3 ligands were shown to be compatible co-ligands in heteroleptic $[Ni(ECp^*)_{4-n}(PR''_3)_n]$ (E = Al, Ga, n = 0-4, R'' = Me, Ph, cyclohexyl) complexes. Such compounds can be synthesized by treatment of $[Ni(cod)_2]$ with suitable equivalents of ECp^*/PR''_3. However, the ECp^*/PR''_3 ratio in the final compounds, does not only depend on the applied stoichiometry but also on the steric demand of the PR''_3 ligands. For example, the compounds $[Ni(ECp^*)_3(PR''_3)]$ can only be accessed for sterically demanding PPh_3 and PCy_3. In contrast, the usage of the smaller PMe_3 results in the formation of $[Ni(ECp^*)(PMe_3)_3]$. $[Ni(ECp^*)_2(PR''_3)_2]$, can be obtained independent of the steric demand of the phosphines.[60]

In summary, the criteria of a suitable phosphine ligand for a homologue series of $[Ni(ECp^*)_n(PR''_3)_{4-n}]$ include: i) an intermediate steric demand, enabling the access to the entire homologue series of ECp* complexes. ii) a vast tendency for dissociation, allowing ligand dissociation. Indeed, the cone angle, as a measure of the steric demand, of PEt_3 (132°) is right in between the values for PMe_3 (118°) and PPh_3 (145°).[62] Therefore the PEt_3 ligand suits to the aforementioned criteria.

Starting from the series of $[Ni(ECp^*)_n(PEt_3)_{4-n}]$, the access of $[Ni(ZnR)_{2n}(PR_3)_{4-n}]$ complexes should be feasible. The general approach to Zn-rich transition metal complexes and clusters is based on fascinating redox-reactions.[47, 80] For example $[Ni(ZnCp^*)_2(ZnMe)_2(PMe_3)_2]$ was synthesized by treatment of $[Ni(GaCp^*)_2(PEt_3)_2]$ with $Zn^{II}Me_2$. This reaction includes the oxidation of $Ga^{I}Cp^*$ to $Ga^{III}R_3$, the reduction of $Zn^{II}Me_2$ to $Zn^{I}R$ as well as Cp*/Me transfer reactions. It has to be noted that one two electron ECp* ligand is replaced by two one-electron ZnR ligands. This reactivity is not only restricted to Ni/ECp* but allows the synthesis of a variety of different $[(TM_aZn_b)R_cL_d]$ complexes and clusters.[80] Sub-stoichiometric addition of $ZnMe_2$ can also lead to partially E/Zn exchanged products, e.g. $[(MoZn_4Ga_4)(Cp^*)_4(Me_4)]$ and $[(MoZn_8Ga_2)(Cp^*)_4(Me)_6]$ which were formed as 'intermediates" on the way from $[Mo(GaCp^*)_6]$ to the dodeca-coordinated $[Mo(ZnCp^*)_3(ZnMe)_9]$.[73]

$[Ni(ECp^*)_n(PEt_3)_{4-n}]$ represent promising starting materials for E/Zn exchange reactions. So far, this reaction was only successfully applied for the sterically less demanding PMe_3 ligand. Substitution of one ECp* ligand by two ZnR seems to be very sensitive towards the steric access around the central transition metal. Therefore, only $[Ni(ZnCp^*)(ZnMe)(PMe_3)_3]$ and $[Ni(ZnCp^*)_2(ZnMe)_2(PMe_3)_2]$ have been synthesized so far. For example treatment of $[Ni(GaCp^*)_3(PPh_3)]$ with $ZnMe_2$, featuring PPh_3 with a higher steric demand compared to PMe_3, does not lead to the desired $[Ni(ZnR)_6(PPh)_3]$ but unselective decomposition is observed instead. The necessary precursor $[Ni(ECp^*)_3(PR''_3)]$, bearing three ECp* ligands and a PR''_3 ligand with lower steric demand is however not accessible so far.[59]

From the potential $[Ni(ECp^*)_n(PEt_3)_{4-n}]$ series, E/Zn exchange reaction shall be tested for the sterically intermediate PEt_3 ligand, which would afford the whole $[Ni(M'R)_n(PEt_3)_{4-n}]$ series. With the knowledge that Ni-PEt_3 complexes show a vast dissociation potential, the access of low-coordinated

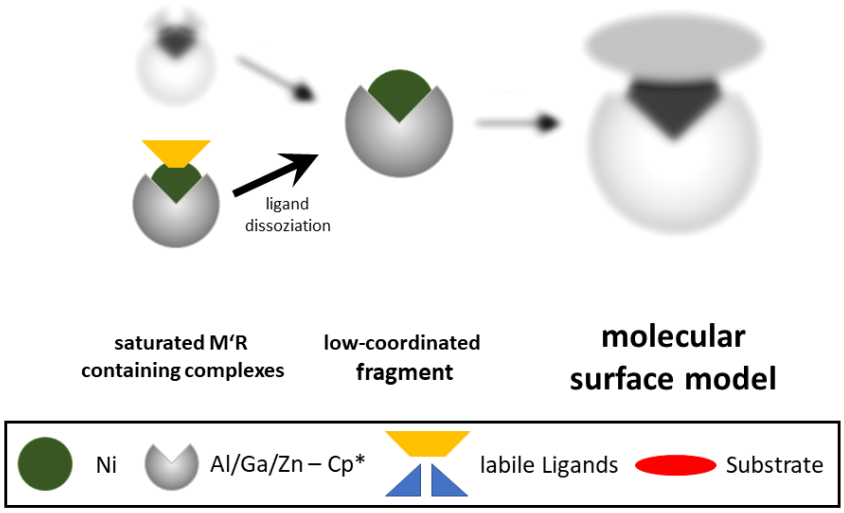

Figure 15: Schematic representation of the experimental access to low-coordinated [Ni(M'R)n] fragments by ligand dissociation of PR''_3 ligands.

$[Ni(M'R)_n(PEt_3)_{3-n}]$, as a prerequisite to react with UHC's, will then be tested by experimental as well as theoretical means (Figure 15).

The nomenclature of these compounds will be given as summarized in Table 4.

Table 4: Nomenclature of $[Ni(M'R)_n(PEt_3)_{3-n}]$ (M' = Al, Ga, Zn; R = Cp*, (Me); n = 0-4). It has to be noted, that for M' = Zn, two Zn ligands are present, due to the replacement of one ECp* ligand by two ZnR ligands. For the cases presented here, the residues on Zn are always represented by one Cp* and one Me group.

		number	**formula**		
		5	$[Ni(PEt_3)_4]$		
1a	$[Ni(AlCp^*)(PEt_3)_3]$	**1b**	$[Ni(GaCp^*)(PEt_3)_3]$	**1c**	$[Ni(ZnCp^*)(ZnMe)(PEt_3)_3]$
2a	$[Ni(AlCp^*)_2(PEt_3)_2]$	**2b**	$[Ni(GaCp^*)_2(PEt_3)_2]$	**2c**	$[Ni(ZnCp^*)_2(ZnMe)_2(PEt_3)_2]$
3a	$[Ni(AlCp^*)_3(PEt_3)]$	**3b**	$[Ni(GaCp^*)_3(PEt_3)]$	**3c**	$[Ni(ZnCp^*)_3(ZnMe)_3(PEt_3)]$
4a	$[Ni(AlCp^*)_4]$	**4b**	$[Ni(GaCp^*)_4]$	**4c**	$[Ni(ZnCp^*)_4(ZnMe)_4]$

V.2.1.2 Synthesis and characterization of $[Ni(M'R)_n(PEt_3)_{4-n}]$ complexes

To investigate the potential access of low-coordinated compounds via dissociation from suitable precursors, the series of heteroleptic Ni-Al/Ga/Zn phosphine compounds, was synthesized. To support experimental investigations, the compounds were also optimized at the DFT-level of theory (BP86-D3/def2-TZVPP). In general, the geometrical parameters compare well between experimental molecular structures and calculated values (Table 6). Therefore, also the theoretical results are included in the discussion where useful. For the $[Ni(M'R)_n(PEt_3)_{4-n}]$, the ^{31}P-NMR signal is a reliable probe to determine the formed species in the respective reaction solutions. The detailed characterization of $[Ni(ECp^*)_n(PEt_3)_{4-n}]$ has already been discussed in the publication. For a detailed discussion I refer to the publication and the supplementary information.[61] Therefore, focus herein will be set on the characterization of so far unpublished $[Ni(ZnR)_{2n}(PEt_3)_{4-n}]$ and a comparison between the $[Ni(M'R)_n(PEt_3)_{4-n}]$ series.

Experimentally, the $[Ni(ECp^*)_n(PEt_3)_{4-n}]$ are accessed by treatment of $[Ni(cod)_2]$ with suitable equivalents of PEt_3/ECp* leading to the selective formation of heteroleptic **1a**, **1b**, **2a**, **2b**, and homoleptic **4a**[8], **4b**[81] and **5**[82] (Scheme 1). This is in accordance to earlier results for PMe_3 ligands.[60] Unfortunately, the $[Ni(ECp^*)_3]$ members **3a**/**3b** cannot be synthesized under these reaction conditions due to the formation of product mixtures with different ECp*/PEt_3 ratios.

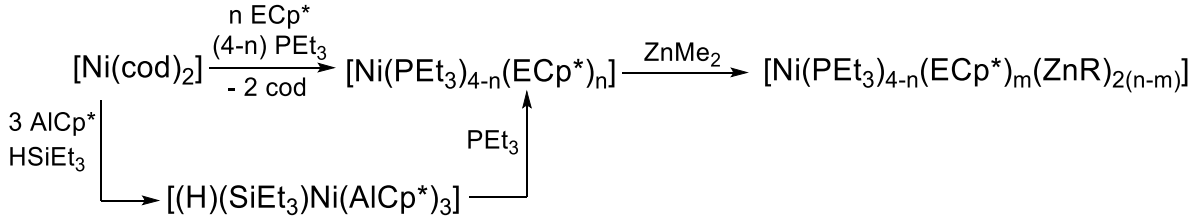

Scheme 1. Synthesis of $[Ni(ECp^*)_n(PEt_3)_{4-n}]$ by ligand replacement from $Ni(cod)_2$ and subsequent treatment with $ZnMe_2$ yielding $[Ni(PEt_3)_{4-n}(ECp^*)_n(ZnR)_{2(n-m)}]$.

However, **3a** can be isolated by treatment of $[(H)(SiEt_3)Ni(AlCp^*)_3]$[8] with excess PEt_3 at elevated temperatures. This reactivity implies that reductive elimination of H-$SiEt_3$ and subsequent coordination of PEt_3 takes place as already discussed in the original publication.[8] Therefore, the temporary formation of a low-coordinate $[Ni(AlCp^*)_3]$ species can be assumed. Applying the route starting from $[(H)(SiEt_3)Ni(AlCp^*)_3]$ with a preformed $[Ni(AlCp^*)_3]$ fragment, the homologous series of $[Ni(AlCp^*)_n(PEt_3)_{4-n}]$ together with $[Ni(GaCp^*)_n(PEt_3)_{4-n}]$ (n = 1, 2, 4) was synthesized. Starting from these compounds E/Zn exchange reactions shall now be tested to obtain the series of $[Ni(ZnR)_{2n}(PEt_3)_{4-n}]$ complexes.

During the studies on E/Zn exchange reactions unexpected experimental results were obtained which will be presented in the following paragraph prior to the discussion of the synthesis of $[Ni(ZnR)_{2n}(PEt_3)_{4-n}]$. The following paragraph presents a set of unfinalized results that show a) the Ni-GaCp* bond is not kinetically inert and b) ECp* ligands change the dissociation behavior of PEt_3 ligands in $[Ni(ECp^*)_n(PEt_3)_{4-n}]$ complexes. Unsuccessful attempts to synthesize $[Ni(ZnCp^*)(ZnMe)(PEt_3)_3]$ were first performed starting from $[Ni(GaCp^*)(PEt_3)_3]$ and addition of $ZnMe_2$. Surprisingly, this reaction did not mainly afford **1c** as the predicted product but **2c**, featuring four ZnR ligands. The formation of **2c** is only possible from precursors that contain two ECp* ligands due to the redox-reaction that is required for the reduction of $Zn^{II}Me_2$ to afford $Zn^{I}R$. It has to be noted, that in contrast to $[Ni(AlCp^*)_2(PEt_3)_2]$, the GaCp* congener $[Ni(GaCp^*)_2(PEt_3)_2]$ was shown to be kinetically active. Treatment of a C_6D_6 solution of $[Ni(GaCp^*)_2(PEt_3)_2]$ with either GaCp* or PEt_3 led to different observations. If **2b** is treated with GaCp* no reaction can be observed. However, if treated with PEt_3, GaCp* is released affording $[Ni(GaCp^*)_1(PEt_3)_3]$.[61] Based on this observation it can be concluded that the formation of **2c** starting from **1b** is a result of a delicate equilibrium reaction which leads to the formation of $[Ni(GaCp^*)_2(PEt_3)_2]$ and $[Ni(PEt_3)_4]$ from $[Ni(GaCp^*)_1(PEt_3)_3]$ (Figure 16).

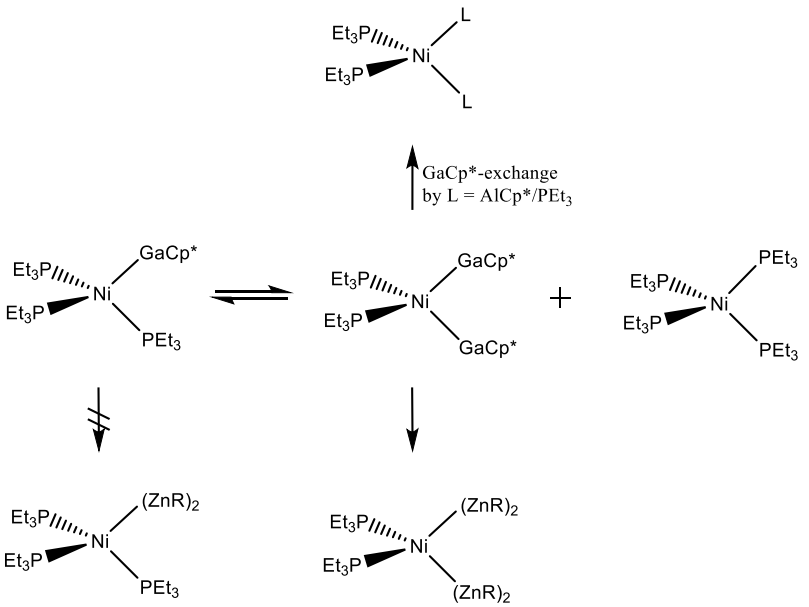

Figure 16: Proposed equilibrium of $[Ni(GaCp^*)(PEt_3)_3]$ resulting in $[Ni(GaCp^*)_2(PEt_3)_2]$ and $[Ni(PEt_3)_4]$ as a potential explanation for the formation of $[Ni(ZnR)_4(PEt_3)_2]$ in the reaction of $[Ni(GaCp^*)(PEt_3)_3]$ with $ZnMe_2$. Isolated $[Ni(GaCp^*)_2(PEt_3)_2]$ reacts with AlCp* or PEt_3 resulting in GaCp* exchange affording the respective $[Ni(PEt_3)_2(L)_2]$ complexes.

This reactivity is not a result of PEt_3 dissociation but of Ni-GaCp* dissociation, which is an unexpected result based on the usually vast dissociation potential of TM-PR_3 complexes. Furthermore, this reactivity represents a special case for Hume-Rothery inspired complexes since TM-ECp* bonds were generally considered as being kinetically inert.[8] In agreement to the calculations for the ΔE_{int} value in

[Ni(ECp*)$_4$] compounds (see chapter V.1.3 Bonding in [Ni(L)$_n$(UHC)$_{4-n}$] complexes) the Ni-GaCp* bond is predicted to be much weaker than the Ni-AlCp* bond. Here it should also be noted that **2b** can be selectively transferred to **2a**, but no other [Ni(ECp*)$_n$] compound is formed. Taking these results together, the cause for the problematic synthesis of **1c** starting from **1b** originates from Ni-GaCp* dissociation. On the other hand, PEt_3 was shown not to be replaceable by GaCp*, as a first indication for a distinct dissociation behavior of Ni-PEt_3 when ECp* ligands are present in the complex. These findings on Ni-GaCp* bond dissociation are be the basis for chapter V.4.5 Synthesis and characterization of [Ni2(μ-GaCp*)(μ-GaNiCp*)$_2$(dvds)$_2$].

Coming back to the series of [Ni(ZnR)$_{2n}$(PEt_3)$_{4-n}$] complexes, **1c** can be synthesized starting from [Ni(AlCp*)$_1$(PEt_3)$_3$], since the TM-AlCp* bond is stronger than the TM-GaCp*[75] and therefore AlCp* dissociation might be hampered. In agreement to this reasoning, treatment of **1a** with 8 eq. $ZnMe_2$ at room temperature affords **1c**. The ^{1}H-NMR shifts appear at 2.30 (ZnCp*), 1.44 and 0.97 (protons of the PEt_3 ligand) and 0.03 ppm (ZnMe) in the correct integration ratio of 15:18:27:3 (Figure 17). The isolation of a pure sample of this compound is still in progress.

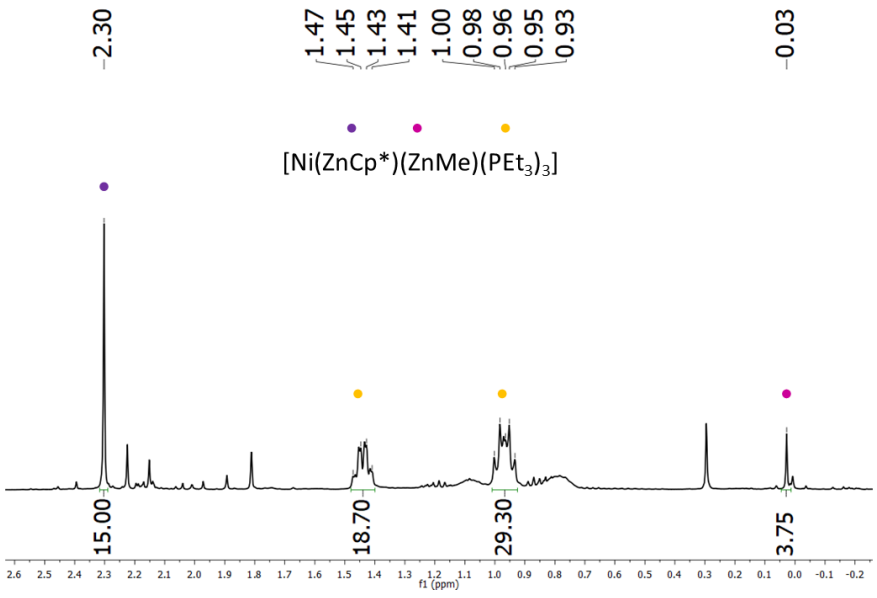

Figure 17: ^{1}H-NMR spectrum of [Ni(ZnCp*)(ZnMe)(PEt_3)$_3$] in C_6D_6.

Treatment of a toluene solution of **2b** at -30°C with 4 eq. $ZnMe_2$ for 2h yields the partially Ga/Zn exchanged [Ni(ZnMe)(ZnCp*)(GaCp*)(PEt_3)$_2$], where one GaCp* is replaced by two ZnR moieties. Application of 10 eq. $ZnMe_2$ at 0°C and 2h reaction time affords fully substituted **2c**. The ^{1}H-NMR signal of GaCp* in **2b** at 2.05 ppm disappears for the intermediate [Ni(ZnMe)(ZnCp*)(GaCp*)(PEt_3)$_2$]. Two new signals appear at 2.29 ppm and 2.01 ppm with an integration ratio of 15:15. The signal at 2.29 ppm can be assigned to the newly formed ZnCp* whereas the signal at 2.01 ppm is assigned to

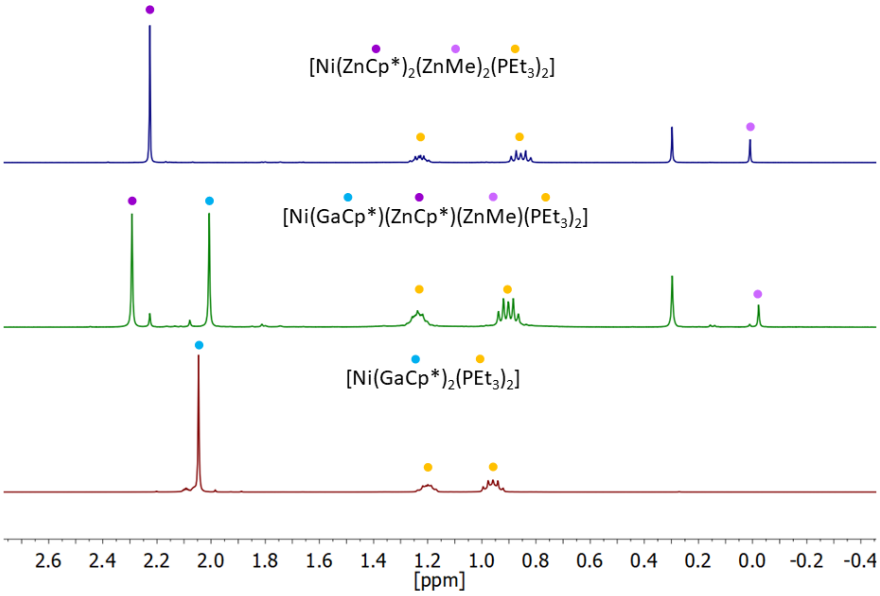

Figure 18: Comparison of the ^{1}H-NMR spectra of $[Ni(GaCp^*)_2(PEt_3)_2]$, $Ni(GaCp^*)(ZnCp^*)(ZnMe)(PEt_3)_2]$ and $[Ni(ZnCp^*)_2(ZnMe)_2(PEt_3)_2]$ in C_6D_6.

remaining GaCp* and is only slightly upfield compared to the signal of **2b**. The ZnMe protons (integration 3) appear at -0.02 ppm. For **2c** only one signal appears in the Cp* proton region at 2.23 ppm. The chemical shift of the ^{1}H-NMR signals of the PEt_3 groups remain basically unchanged for the three compounds (Figure 18).

Since $[Ni(GaCp^*)_3(PEt_3)]$ could not be isolated in pure form[61], the synthesis of **3c** was achieved starting from $[Ni(AlCp^*)_3(PEt_3)]$ at room temperature. The ^{1}H-NMR signals of the so far missing hepta-

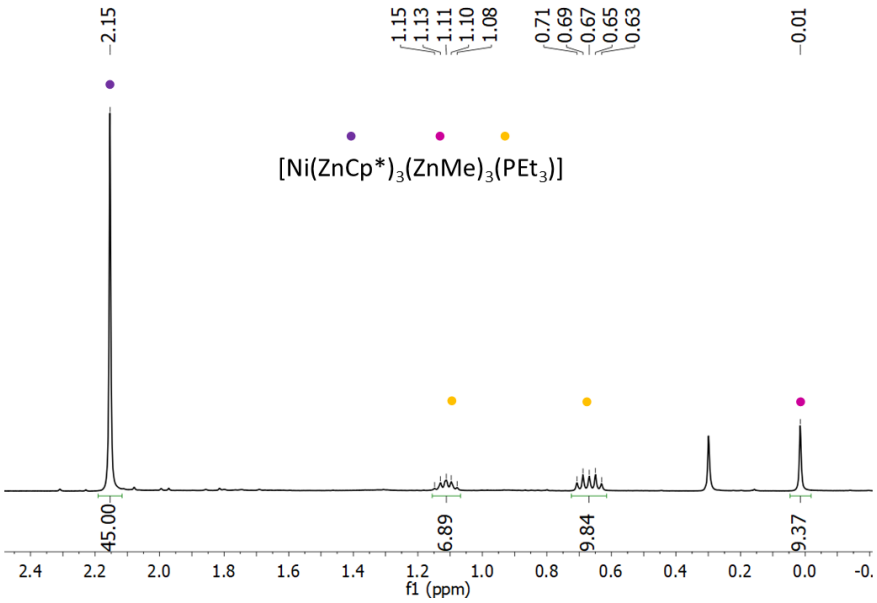

Figure 19: ^{1}H-NMR spectrum of $[Ni(ZnCp^*)_3(ZnMe)_3(PEt_3)]$ in C_6D_6.

coordinated [Ni(ZnCp*)$_3$(ZnMe)$_3$(PEt$_3$)$_3$] appear at 2.15 (ZnCp*), 1.11 and 0.67 (PEt$_3$) and -0.01 ppm (ZnMe) with an integration ratio of 45:6:9:9 as expected for this compound (Figure 19).

Preliminary results by Patricia Heiß indicate fluxional processes of the ZnR ligands in this compound. Upon cooling of a toluene-d$_8$ solution of **3c** to -90°C a decoalescence of the ZnMe signals can be observed affording two signals at 0.19 and -0.06 ppm with a ratio 2:1 (see Figure S 14).

Table 5: Comparison of the ^{31}P chemical shifts of the compounds **5** and **1a**-**3c**. The ^{31}P-signal of **3b** was observed in reaction mixtures but a clear assignment is not possible since **3b** was never isolated in pure form.

compound	^{31}P-signal [ppm]	compound	^{31}P-Signal [ppm]	compound	^{31}P-Signal [ppm]
		5	17.8		
1a	19.5	**1b**	16.6	**1c**	12.7
2a	39.4	**2b**	31.2	**2c**	27.8
3a	61.9	**3b**	45.7	**3c**	29.5

As stated above, the ^{31}P-NMR signal of the respective products is a reliable probe for a fast identification of the reaction outcome. In general, within the three series of compounds, (theoretical) replacement of PEt$_3$ groups by ECp* or (ZnR)$_2$ leads to distinct changes in the ^{31}P-NMR signal of the respective compounds (Table 5). With higher numbers of replaced PEt$_3$ groups, the remaining phosphine signal experiences an upfield shift which is most pronounced in **3a**. In comparison to [Ni(PEt$_3$)$_4$] (17.8 ppm), the signal of **3a** is shifted to 61.9 ppm. This drastic shift can be explained by the deshielding of the phosphorous nuclei as a result of ECp* coordination. For GaCp* and (ZnR)$_2$, this effect is not as significant. For **1b** and **1c**, the phosphine signal experiences a small downfield shift with respect to **5**.

Having the two homologous series of AlCp* (**1a**-**3a**) and ZnR (**1c**-**3c**) containing compounds as well as two GaCp* representatives (**1b**, **2b**) in hand for the first time, a systematic study on their properties, depending on the number of coordinated ECp*/ZnR ligands, was performed. Single crystals suitable for X-ray diffraction studies were obtained by slow cooling of saturated solutions to -30°C (usually hexane or toluene). For **2a**, **2b** and **3a**, a distorted tetrahedral coordination around the central nickel atom can be observed (Figure 20 and Figure 21). In **2a** and **2b**, the P-Ni-P angle (118-121°) is considerably larger than the E-Ni-E angle (99°) which is most probably an effect of the higher steric demand of PEt$_3$ with respect to ECp*. This reasoning is in line with the respective structural data of the literature known compound [Ni(PMe$_3$)$_2$(GaCp*)$_2$] in which the Ga-Ni-Ga angle is larger than the P-Ni-P angle (120.8 vs. 106.9 °), presumably due to the lower steric demand of the PMe$_3$ ligand.[60]

Replacement of the two GaCp* units of **2b** by four ZnR ligands, results in a decrease in the P-Ni-P angle to about 107° in **2c** (Figure 20).In the related compound $[Ni(ZnCp^*)_2(ZnMe)_2(PMe_3)_2]$, the P-Ni-P angle differs only marginally with roughly 106 °.[59]

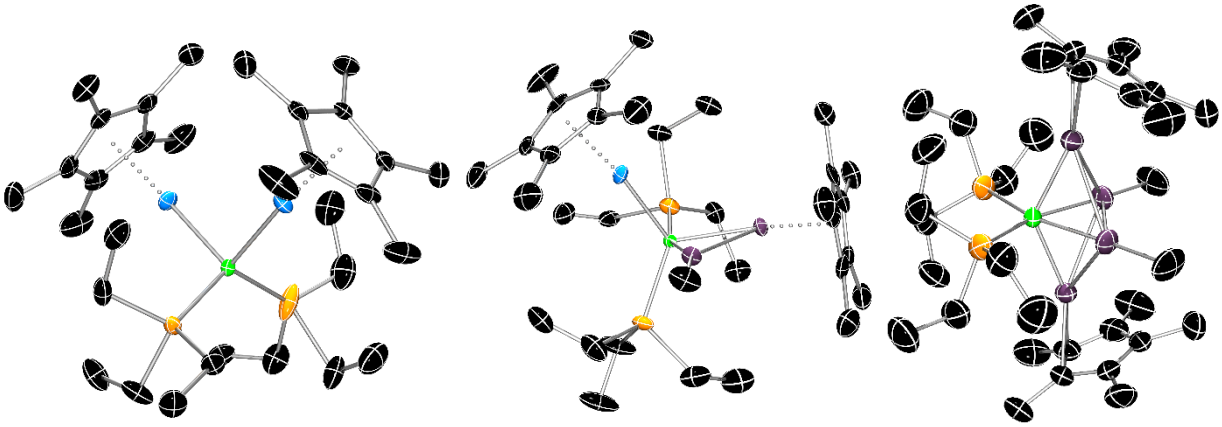

Figure 20: Molecular solid state structures of $[Ni(GaCp^*)_2(PEt_3)_2]$ (**2b**) (left) and $[Ni(GaCp^*)(ZnCp^*)(ZnMe)(PEt_3)_2]$ (middle) and $[Ni(ZnCp^*)_2(ZnMe_2)(PEt_3)_2]$ (**2c**) (right). Hydrogen atoms and disorders are omitted for clarity. For **2b** only one of the two independent molecules of the asymmetric unit is depicted. The displacement ellipsoids are shown at the 50 % probability level. Selected interatomic distances (Å) and angles (°): **2b**: Ni-P: 2.1361(14) – 2.1401(14), Ni-Ga: 2.2375(11) – 2.2462(10), P-Ni-P: 119.85(4) – 122.43(4) Ga-Ni-Ga: 98.80(4) – 98.92(4); $[Ni(GaCp^*)(ZnCp^*)(ZnMe)(PEt_3)_2]$: Ni-P: 2.15326(17) – 2.1649(17) , Ni-Ga: 2.252(17)- 2.27(3), Ni-ZnCp*: 2.329(19) – 2.32(3), Ni-ZnMe: 2.292(5) – 2.337(3), Zn-Zn: 2.529(18) - 2.53(2), Ga-Zn: 2.890(16)-2.89(2) , P-Ni-P: 113.78(7); **2c**: Ni-P: 2.177(11)-2.193(5), Ni-ZnMe: 2.3108(9), Ni-ZnCp*: 2.3753(7), Zn-Zn: 2.7341(10)-2.7379(9), P-Ni-P: 106.6(3)-107.9(6), Ni-Zn-Me: 173.8(3).

Taking these results into account, it becomes obvious that the coordination environment of the central Ni atom is flexible with respect to the steric demand of the ligands. Furthermore, the Ni-P distance successively increases from **2b** to **2c** with increasing number of ZnR ligands from 2.14 to 2.18 Å, which might also be a result of the higher steric demand when more ligands are coordinated to the central Ni atom as in **2c**. The short Zn-Zn distance in $[Ni(GaCp^*)(ZnCp^*)(ZnMe)(PEt_3)_2]$ of only 2.53 Å has already been described for other $[L_3Ni(ZnCp^*(ZnMe)]$ compounds.[59] It is only slightly elongated compared to the Zn-Zn distance in [Cp*ZnZnCp*] of 2.31 Å.[83] Furthermore, the short Ga-Zn contact in $[Ni(GaCp^*)(ZnCp^*)(ZnMe)(PEt_3)_2]$ of only 2.89 Å might stabilize this “intermediate” and is a reasonable explanation for the selective synthesis of this compound without further Ga/Zn exchange. Comparing $[Ni(GaCp^*)(ZnCp^*)(ZnMe)(PEt_3)_2]$ with **2c**, the Zn-Zn distances increase to 2.74 Å.[59] A more detailed analysis of the Zn-Zn distances will be given in chapter Ⅴ.2.1.6 Ni-Zn bonding in $[Ni(_{ZnR})2n(_L)4\text{-}n]$ compounds.

Since investigation of potential Ni-PEt_3 dissociation from $[Ni(M'R)_n(PEt_3)_{4-n}]$ complexes was intended, the influence of M'R coordination on Ni-PEt_3 bonding will be discussed in the following. Within the series of heteroleptic Ni-ECp* phosphine complexes, the (average) Ni-P distances decrease significantly from 2.212 Å in **5** [84] to 2.133 Å in **2a** (2.138 in **2b**) and even to 2.1170(1) Å in **3a** (Figure 21, Table 6). These changes in the Ni-PEt_3 bond lengths are nicely reproduced by DFT (BP86-D3/TZVPP) calculations showing that successive introduction of ECp* is reflected by a stepwise Ni-P-bond shortening. For the Zn containing complexes, the shortening of the Ni-P distance is not as pronounced, most probably due to the higher steric demand of the Zn_{2n} units. The Ni-P distance is shortened to 2.177(11) Å in **2c** and 2.16 Å for calculated $[Ni(ZnCp^*)_3(ZnMe)_3(PEt_3)]$.

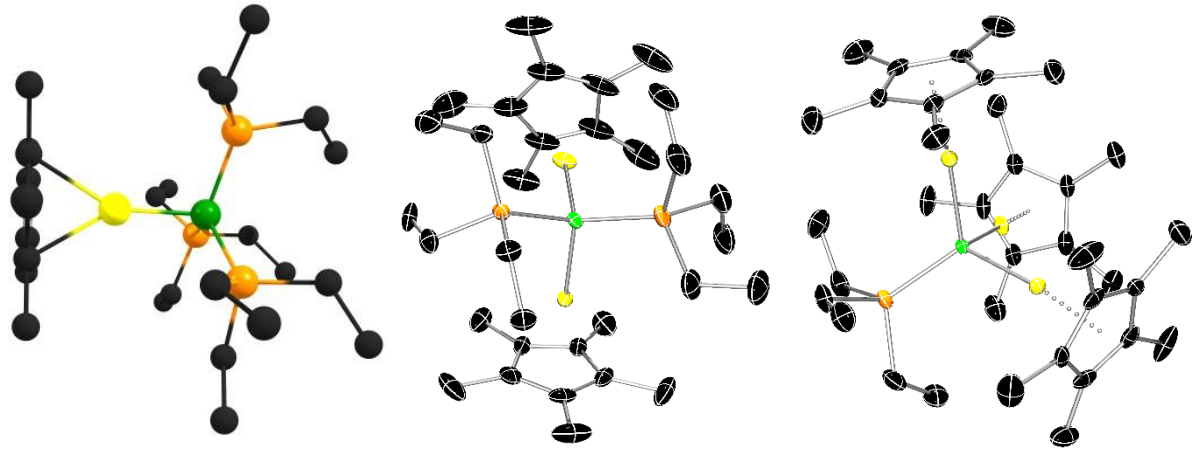

Figure 21: Left: Calculated structure of $[Ni(AlCp^*)(PEt_3)_3]$ (**1a**) (BP86-D3/def2-TZVPP). Middle and right: Molecular structure of $[Ni(AlCp^*)_2(PEt_3)_2]$ (**2a**) and $[Ni(AlCp^*)_3(PEt_3)]$ (**3a**) in the solid state. For clarity, hydrogen atoms and disorders are omitted. The displacement ellipsoids are shown at the 50 % probability level. Selected interatomic distances (Å) and angles (°):**1a**: Ni-P:2.15, Ni-Al: 2.21, P-Ni-P: 112-118; **2a**: Ni-P: 2.1305(7)-2.1353(7), Ni-Al: 2.2040(7), P-Ni-P:118.00(3) **3a**: Ni-P: 2.1170(1), Ni-Al: 2.18451(1)– 2.1863(1), Al-Ni-Al: 102.047(2) - 104.714(2). The series of $[Ni(AlCp^*)_n(PEt_3)_{4-n}]$ shows the shortening of the Ni-P bond upon AlCp* coordination.

In general, the optimized gas phase structures of **1**-**5** are in good agreement (Table 6) with the experimentally determined structures from single-crystal X-ray diffraction data, which was also shown for other $[TM_x(ECp^*)_y(L)_z]$ compounds using the BP86 functional.[48, 57, 59] For example, the calculated Ni-PEt_3 bonds in **2b, 3a** and **5** nicely reproduce the experimental results with a maximum deviation of 0.02 Å for **5** (for **2b** and **3a** only 0.01 Å). The Ni-ECp* bonds are calculated to be about 0.03 Å longer in **2b** as compared to the X-ray structures.

In summary, the successful synthesis of the three series of $[Ni(M'R)_n(PEt_3)_{4-n}]$ was presented. For some members, molecular structures could be determined using single crystal X-Ray-diffraction. For the series of $[Ni(AlCp^*)_n(PEt_3)_{4-n}]$ compounds a significant shortening of the Ni-P distances is observed with higher numbers of AlCp* coordination. For $[Ni(GaCp^*)_n(PEt_3)_{4-n}]$, unexpectedly Ni-GaCp* dissociation was observed which is a valuable insight for further studies. Ligand displacement reactions starting from $[Ni(GaCp^*)_2(PEt_3)_2]$ always led to the replacement of GaCp* ligands, but no indication for PEt_3

replacement was found. As already observed for other $[Ni(ZnR)_{2n}(PR''_3)_{4-n}]$ compounds, the intramolecular Zn-Zn distance change with the number of ZnR ligands attached to Ni.

Table 6: Comparison of selected structural parameters of heteroleptic Ni-Al/Ga/Zn phosphine complexes. Experimental bond lengths are given in Å, bond angles in °. If applicable, average values are given for bond distances and angles. Calculated values (BP86-D3(BJ)/def2-TZVPP) are added in brackets below for comparison. For comparison, the assignment of the complexes is given below the table.

	5[84]	**1a**	**1b**	**1c**	**2a**	**2b**	**2c**	**3a**	**3b**	**3c**	**4a**[85]	**4b**[81]	**4c**[57]
d(Ni-P)	2.212				2.133	2.138	2.18	2.1170					
	(2.23)	(2.15)	(2.16)	(2.17)	(2.14)	(2.15)	(2.17)	(2.12)	(2.13)	(2.16)			
d(Ni-M)					2.2040	2.242	2.31-2.38	2.185			2.1727	2.2188	2.31-2.37
		(2.21)	(2.28)	(2.35)	(2.20)	(2.27)	(2.32-2.36)	(2.19)	(2.26)	(2.31-2.36)	(2.18)	(2.25)	(2.31-2.38)
d(M-Cp*$_{centroid}$)					1.955	2.052		1.942			1.933	2.00	
		(1.97)	(2.10)	(2.15)	(1.96)	(2.09)	(2.02)	(1.95)	(2.08)	(1.96-2.17)	(1.93)	(2.07)	(1.93-2.13)
d(M-M)					3.36		2.73						2.75-2.91
				(2.49)	(3.34)	(3.43)	(2.72)	(3.43)	(< 3.43)	(< 2.65)	(< 3.53)	(< 3.50)	(2.68-3.02)
∢(P-Ni-P)	107.0				118.0	121.1	107						
	(110.2)	(115.7)	(116.7)	(104-117)	(126.0)	(125.0)	(113.0)						
∢(M-Ni-M)					99.31	98.9		103.4			109.4	109.5	
				(64)	(99.0)	(98.1)	(71)	(103)	(102)	(69-73)	(108-112)	(102-113)	(73-80)

number	**formula**		
5	$[Ni(PEt_3)_4]$		
1a	$[Ni(AlCp^*)(PEt_3)_3]$	**1b**	$[Ni(GaCp^*)(PEt_3)_3]$	**1c**	$[Ni(ZnCp^*)(ZnMe)(PEt_3)_3]$
2a	$[Ni(AlCp^*)_2(PEt_3)_2]$	**2b**	$[Ni(GaCp^*)_2(PEt_3)_2]$	**2c**	$[Ni(ZnCp^*)_2(ZnMe)_2(PEt_3)_2]$
3a	$[Ni(AlCp^*)_3(PEt_3)]$	**3b**	$[Ni(GaCp^*)_3(PEt_3)]$	**3c**	$[Ni(ZnCp^*)_3(ZnMe)_3(PEt_3)]$
4a	$[Ni(AlCp^*)_4]$	**4b**	$[Ni(GaCp^*)_4]$	**4c**	$[Ni(ZnCp^*)_4(ZnMe)_4]$

V.2.1.3 Ligand dissociation from $[Ni(M'R)_n(PEt_3)_{4-n}]$ studied by UV-Vis spectroscopy

In this chapter, the dissociation behavior of the series of heteroleptic $[Ni(AlCp^*)_n(PEt_3)_{4-n}]$ is investigated and compared to $[Ni(PEt_3)_4]$ as reference. Suitable comparisons to $[Ni(GaCp^*)_n(PEt_3)_{4-n}]$ and $[Ni(ZnR)_{2n}(PEt3)_{4-n}]$ are drawn when possible. As indicated by the previous results, $[Ni(GaCp^*)_n(PEt_3)_{4-n}]$ complexes show Ni-GaCp* dissociation reactions but not the desired Ni-PEt_3 dissociation reaction. However, EDA calculations in chapter V.1.3 Bonding in $[Ni(L)_n(UHC)_{4-n}]$ complexes showed that the Ni-AlCp* bond is stronger in comparison to the Ni-GaCp* bond. Thus, the question arises if at all ligand dissociation occurs from $[Ni(AlCp^*)_n(PEt_3)_{4-n}]$, and if yes, what is the dissociating species (Scheme 2).

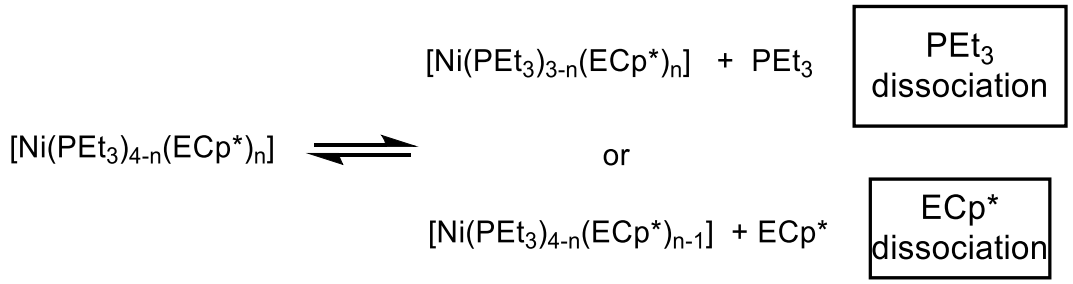

Scheme 2. Two concurring ligand dissociation pathways for the heteroleptic complexes $[Ni(PEt_3)_{4-n}(ECp^*)_n]$ (**1-5**).

Classic studies by Tolman *et al*. investigating the dissociation of $[Ni(PR_3)_n]$ were performed applying variable temperature (VT) UV-Vis spectroscopy. For $[Ni(PEt_3)_4]$, the most intensive absorption band was found at λ_{max} = 290 nm. However, variations in temperature revealed extensive PEt_3 dissociation by the appearance of a band at λ_{max} = 502 nm which was attributed to the electronically unsaturated 16 valence electron species $[Ni(PEt_3)_3]$.[7] Therefore, VT UV-Vis spectroscopy of the Al-series $[Ni(AlCp^*)_n(PEt_3)_{4-n}]$ (**1a-4a**) was performed to investigate the dissociation behavior of either PEt_3 or AlCp*. Qualitatively, this approach was verified by time-dependent (TD) DFT calculations giving the first 50 electronic transitions for the species $[Ni(AlCp^*)_n(PEt_3)_{4-n}]$ in comparison to low-coordinated $[Ni(AlCp^*)_a(PEt_3)_b]$. Figure 22 shows the experimental absorption spectrum (blue line graph, top diagram) in comparison to the calculated TDDFT spectrum (red line graph, top diagram) of $[Ni(AlCp^*)_2(PEt_3)_2]$. The bottom two diagrams, show the calculated TDDFT spectra of the two potential dissociation products $[Ni(AlCp^*)_1(PEt_3)_2]$ and $[Ni(AlCp^*)_2(PEt_3)_1]$, indicating that ligand dissociation of either ligand would lead to the appearance of new absorptions at higher wave lengths.

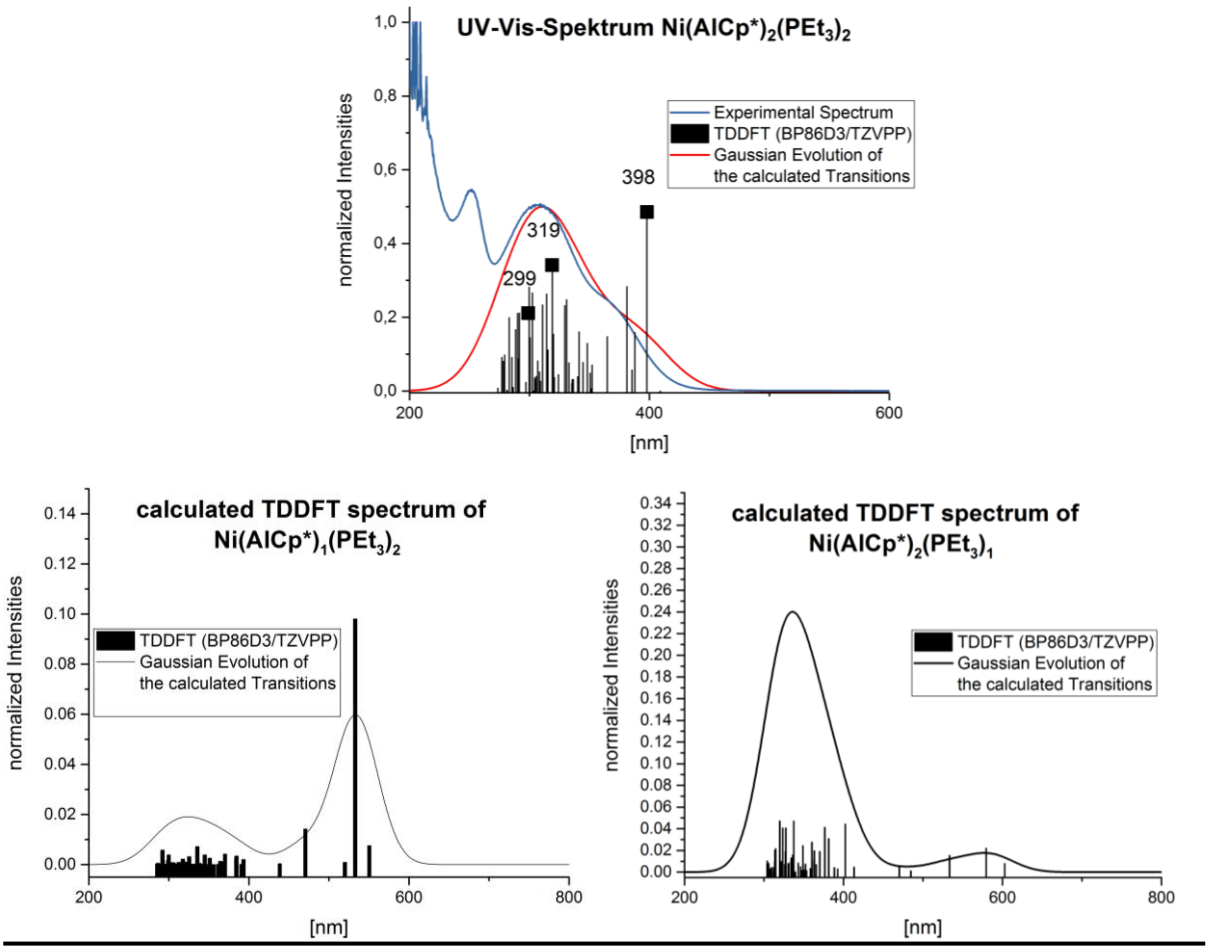

Figure 22: Top: Overlay of the measured UV-Vis spectrum of $[Ni(AlCp^*)_2(PEt_3)_2]$ (**2a**) in hexane with the calculated TDDFT spectrum (BP86/def2-TZVPP, 50 transitions). Bottom: Calculated TDDFT spectra of two low-coordinated $[Ni(AlCp^*)_a(PEt_3)_b]$ compounds. Both can be derived from $[Ni(AlCp^*)_n(PEt_3)_{4-n}]$ either by Ni-AlCp* or Ni-PEt_3 dissociation.

The room temperature UV-Vis spectrum of **2a** in n-hexane exhibits three different features, two bands at 260 and 302 nm and a small shoulder at around 380 nm. TDDFT calculations of **2a** show that the experimental spectrum can be reproduced and thus the shoulder at 380 nm is an intrinsic feature in the absorption spectrum of **2a** (Figure 22). Stepwise heating of the solution of **2a** from 25°C to 61 °C (Figure 23 right) however, does not lead to significant changes in the UV-Vis spectra. Together, these investigations confirm that **2a**, even at low concentrations (roughly $5*10^{-5}$ mol/L) and moderately elevated temperatures, shows no sign of any ligand dissociation. Thus **2a** is kinetically inert under usual conditions. This is also the case for **3a** and **4a** which show absorption bands at 305 and 315 nm respectively, but no signs of dissociation are visible even at elevated temperatures (see Figure S 15).

The room temperature UV-Vis spectrum of **1a** shows an intensive band at 320 nm and a weak absorption at 500 nm. Upon heating, the absorption intensity at 500 nm increases whereas the band at 320 nm decreases (Figure 23 left).

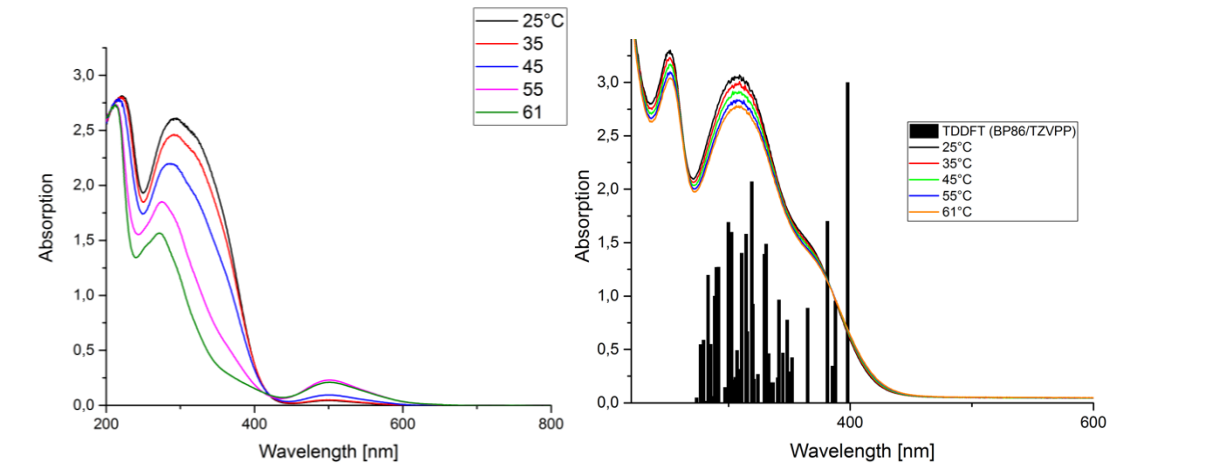

Figure 23: left: VT-UV-Vis spectra of [Ni(AlCp*)(PEt_3)$_3$] (**1a**) right: VT-UV-Vis spectra of [Ni(AlCp*)$_2$(PEt_3)$_2$] (**2a**) (line diagram with absorption bands at 260, 302 and 380 nm compared with the calculated absorptions (black bars) of [Ni(AlCp*)$_2$(PEt_3)$_2$] on the TDDFT (BP86/TZVPP) level of theory.

In accordance to the experimental UV-Vis spectra of **5**, the increase of the band located at 500 nm can be attributed to dissociation processes. However, under the experimental conditions this unsaturated species seems to be quite unstable or too reactive as small traces of moisture or oxygen cannot be rigorously excluded for the UV-Vis spectroscopic measurements. Thus, a thermodynamic analysis of a fully reversible dissociation process was not possible. The absorption band at 500 nm is assigned to PEt_3 dissociation from **1a** yielding [Ni(AlCp*)$_1$(PEt_3)$_2$] based on the high purity of the employed sample as evidenced by elemental analysis and ^{31}P-NMR spectrum of this batch which rules out the presence of traces of **5**. These results indicate, that there is a significant difference in the dissociation behavior of [Ni(AlCp*)$_1$(PEt_3)$_3$] and [Ni(AlCp*)$_2$(PEt_3)$_2$]. In contrast to the latter which seems to be kinetically inert, [Ni(AlCp*)$_1$(PEt_3)$_3$] undergoes PEt_3 dissociation.

These findings can be further supported by synthetic results from ligand exchange reactions (monitored by ^{1}H and ^{31}P-NMR). Treatment of kinetically labile [Ni(PEt_3)$_4$] with one equivalent AlCp* leads to the selective formation of **1a**, the addition of four equivalents AlCp* does not yield the fully substituted product **4a**. However, the formation of **2a** is observed (Figure 24), which again underlines that phosphine dissociation is largely hampered in **2a**. The distinct dissociation behavior of **1a** in contrast to **2a** can also be seen if both compounds are treated with bromobenzene BrC_6H_5. BrC_6H_5 is a common substrate for oxidative addition reactions which usually occur at open coordination sites. The finding that, treatment of **1a** and **2a** with BrC_6H_5 leads to the full consumption of **1a** whereas **2a** shows no reaction towards BrC_6H_5, underlines the formation of open coordination sites of **1a** due to ligand dissociation. So far, no clear characterization of the reaction product was obtained.

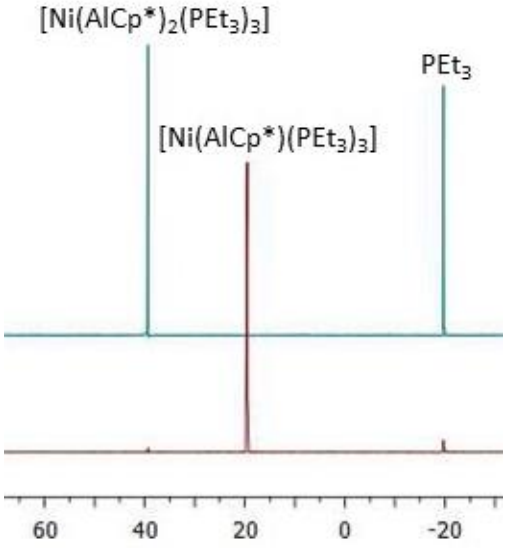

Figure 24: ^{31}P-NMR spectra of the reaction of Ni(cod)$_2$ with 1 eq. AlCp* selectively yielding [Ni(AlCp*)$_1$(PEt$_3$)$_3$] (brown spectrum) as well as the reaction of Ni(cod)$_2$ with 4 eq. of AlCp* selectively yielding [Ni(AlCp*)$_2$(PEt$_3$)$_2$] (blue spectrum).

In accordance to this observation, phosphine replacement is also not possible for [Ni(GaCp*)$_2$ (PEt$_3$)$_2$] as treatment with excess GaCp* does not result in reaction to **3b** or **4b** (Scheme 3) but [Ni(GaCp*)$_2$(PEt$_3$)$_2$] remains unchanged. If [Ni(GaCp*)$_2$(PEt$_3$)$_2$] is treated with AlCp* which is known to give stronger Ni-AlCp* bonds, the phosphine ligands also remain in the complex, but GaCp* is replaced by AlCp* giving [Ni(AlCp*)$_2$(PEt$_3$)$_2$] (as discussed in the previous chapter). The VT-UV-Vis analysis together with the ligand exchange reactions thus show that ECp* coordination indeed changes Ni-PEt$_3$ bonding hampering phosphine dissociation processes.

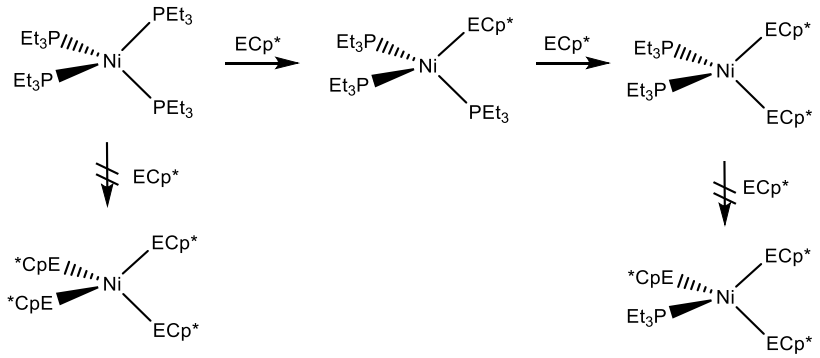

Scheme 3: Reaction scheme showing the phosphine replacement which is possible for [Ni(PEt$_3$)$_4$] and [Ni(PEt$_3$)$_3$(AlCp*)$_1$]. However, after introduction of two ECp* ligands a further phosphine replacement is suppressed.

VT-UV-Vis studies of $[Ni(ZnCp^*)_2(ZnMe)_2(PEt_3)_2]$ as the representative of the Ni-Zn series $[Ni(ZnR)_{2n}(PEt_3)_{4-n}]$, show that no phosphine dissociation is observed also in this case as well. The room temperature UV-Vis spectrum (Figure 25 left) exhibits absorptions bands at about 300 and 400 nm. The experimental spectrum can be reproduced by TDDFT (BP86/def2-TZVPP) calculations. Higher temperatures do not change the appearance of the spectrum. As it was the case for $[Ni(ECp^*)_n(PEt_3)_{4-n}]$, phosphine dissociation would result in new absorptions at higher wavenumbers. TDDFT calculations of $[Ni(ZnCp^*)_2(ZnMe_2)(PEt_3)]$ (Figure 25 right) reveal additional absorptions in the range between 500 and 600 nm, which however are not observed in the VT-UV-Vis spectrum. Further studies for **1c** and **3c** are currently performed by Patricia Heiß.

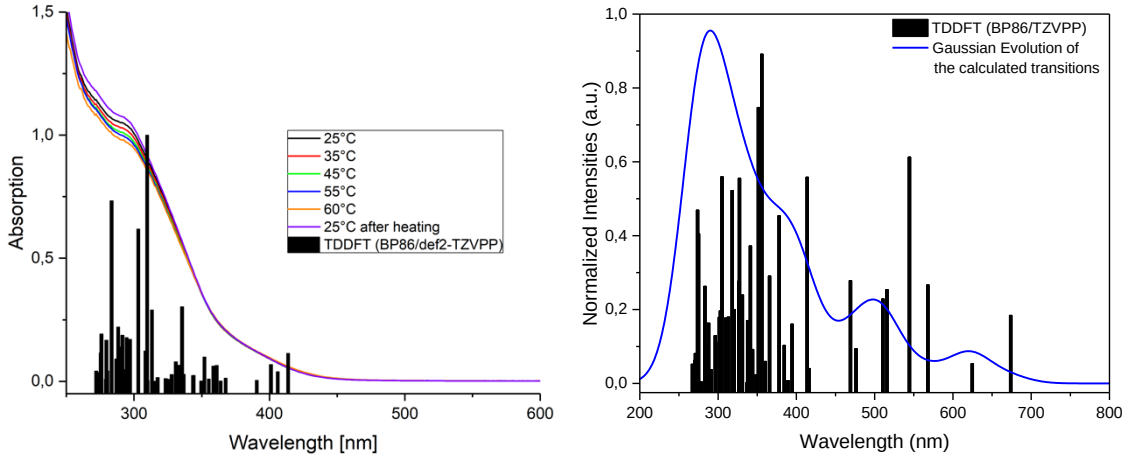

Figure 25: Left: VT-UV-Vis spectra (line diagram) of **2c** in n-hexane with absorption bands at 300 and 400 nm compared to the calculated absorptions (black bars) of $[Ni(ZnCp^*)_2(ZnMe)_2(PEt_3)_2]$ on the TDDFT (BP86/TZVPP) level of theory. Right: TDDFT calculated absorption spectrum of the potential dissociation product $[Ni(ZnCp^*)_2(ZnMe)_2(PEt_3)]$.

Therefore, it can be summarized that the extensive dissociation of parent $[Ni(PEt_3)_4]$ is surprisingly suppressed by coordination of M'R. The compounds $[Ni(M'R)_n(PEt_3)_{4-n}]$ (with except of $[Ni(AlCp^*)(PEt_3)_3]$) do not undergo PEt_3 displacement reactions.

As discussed in the previous chapter, the coordination of M'R results in a shortening of the respective Ni-PEt_3 bond as evidenced by single crystal X-ray structures as well as DFT calculations. Both results could be interpreted as an M'R induced Ni-PEt_3 bond strengthening. However, for $[Ni(ZnR)_n(PEt_3)_{4-n}]$ further experimental studies are currently performed to underline this assumption.

V.2.1.4 Theoretical Investigations for the influence of L on Ni-PEt_3 bonding in $[Ni(L)_n(PEt_3)_{4-n}]$

The significant effect on the Ni-PEt_3 bond upon coordination of the strong σ-donor ligands ECp* was the starting point to perform further theoretical analyses in order to get deeper insight into the character of the Ni-L (L = Al, Ga, $(ZnR)_2$, PEt_3) bonds in $[Ni(M'R)_n(PEt_3)_{4-n}]$. Applying the qualitative σ-type donation/π-type back-donation concept, one could argue that the electron-donating effect of the M'R ligands[75] increases the electron density at the central Ni atom which in turn would lead to stronger Ni→P back donation into low-lying P-C σ*-bonds.[62] However, previous investigations revealed that M-M'R and M-PR_3 bonds are governed by electrostatic interactions and the covalent orbital-based bonding picture described above may not be applicable.[57, 72]

Based on the DFT optimized structures (BP86-D3/def2-TZVPP) of **1**-**5**, which are generally in good agreement to the experimental structural parameters obtained by X-Ray analysis (see Table 6), NBO charges were calculated (Figure 26).

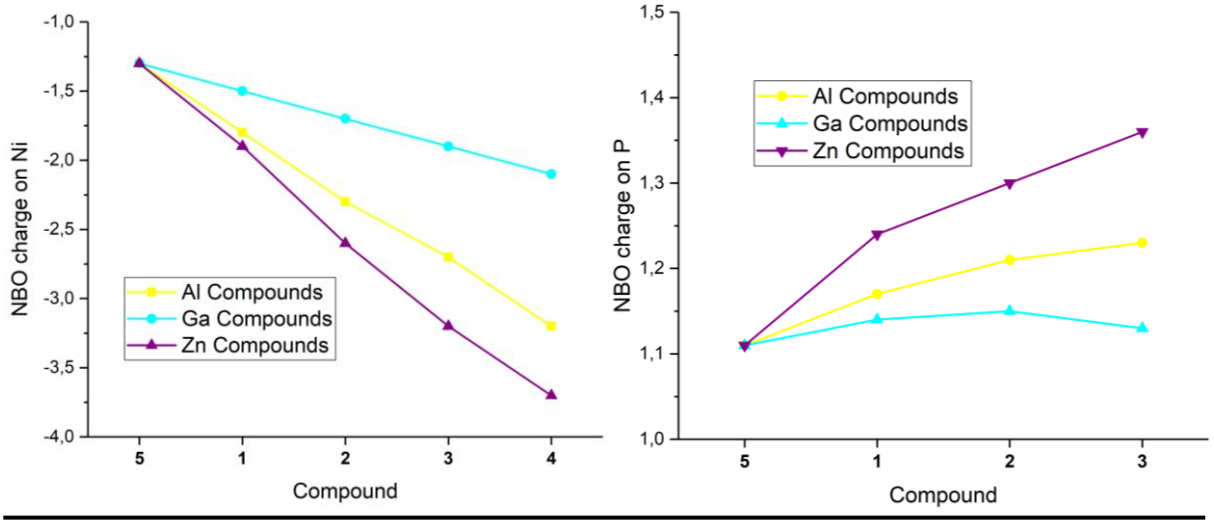

Figure 26: NBO charges on Ni (left) and P (right) for compounds **1**-**5** calculated on the BP86/def2-TZVPP level of theory. Using NBO3.1 as implemented in Gaussian09.

From the NBO charges it can be concluded, that: i) higher numbers of M'R gives a more negative Ni center which is most pronounced for $(ZnR)_2$ addition. ii) With increasing AlCp*/$(ZnR)_2$, P is getting more positively charged. For GaCp*, the charge on P does not change considerably. The smaller overall polarization of the Ni-Ga and Ni-P bonds in $[Ni(GaCp^*)_n(PEt_3)_{4-n}]$ in comparison to the Al/Zn analogous might represent a potential explanation for the observed dissociation behavior of $[Ni(GaCp^*)_n(PEt_3)_{4-n}]$. Further bonding analysis of **1a**-**5** was performed employing EDA with the "Natural Orbitals for Chemical Valence" extension (EDA-NOCV).[86-87] Therefore, complexes **1**-**5** were fragmented into $[Ni(M'R)_n(PEt_3)_{3-n}]$ and PEt_3 (to investigate the Ni-PEt_3 donor-acceptor bond) or into

$[Ni(ECp^*)_{n-1}(PEt_3)_{4-n}]$ and ECp* (to investigate the Ni-ECp* donor-acceptor bond), respectively. The investigations on the Ni-ZnR bonds will be discussed in chapter V.2.1.6 Ni-Zn bonding in $[Ni(ZnR)_{2n}(L)_{4-n}]$ compounds.

The bonding in the homoleptic complexes $[NiL_4]$ has already been described in chapter V.1.3 Bonding in $[Ni(L)_n(UHC)_{4-n}]$ complexes. A more detailed analysis will be given in the following. For $[Ni(PEt_3)_4]$ (**5**), the interaction energy of the Ni-PEt_3 bond is calculated to about -55 kcal/mol. This energy consists of Pauli repulsion (129 kcal/mol), electrostatic interaction (-102 kcal/mol), orbital interaction (-53 kcal/mol) and dispersive attractions (-29 kcal/mol). The attractive interaction of the Ni-PEt_3 bond of **5** derives quite substantially from electrostatic contributions (55%), which is in line with results from Frenking *et al.*[72] Analysis of the orbital interaction term shows contributions from σ-type donation (-18 kcal/mol), π-type back donation (2x -10 kcal/mol) and σ-type back donation (-6 kcal/mol). Comparison of the Ni-ECp* bonds in the homoleptic complexes **4a**/**4b** reveals that the intrinsic Ni-AlCp* bond energy (around -60 kcal/mol) is significantly higher than for the Ni-GaCp* bond (-48 kcal/mol) (see Figure S 17 and Figure S 18). Orbital interactions of the Ni-ECp* bonds in **4a/4b** closely resemble the orbital contributions to the Ni-PEt_3 bond in **5**.

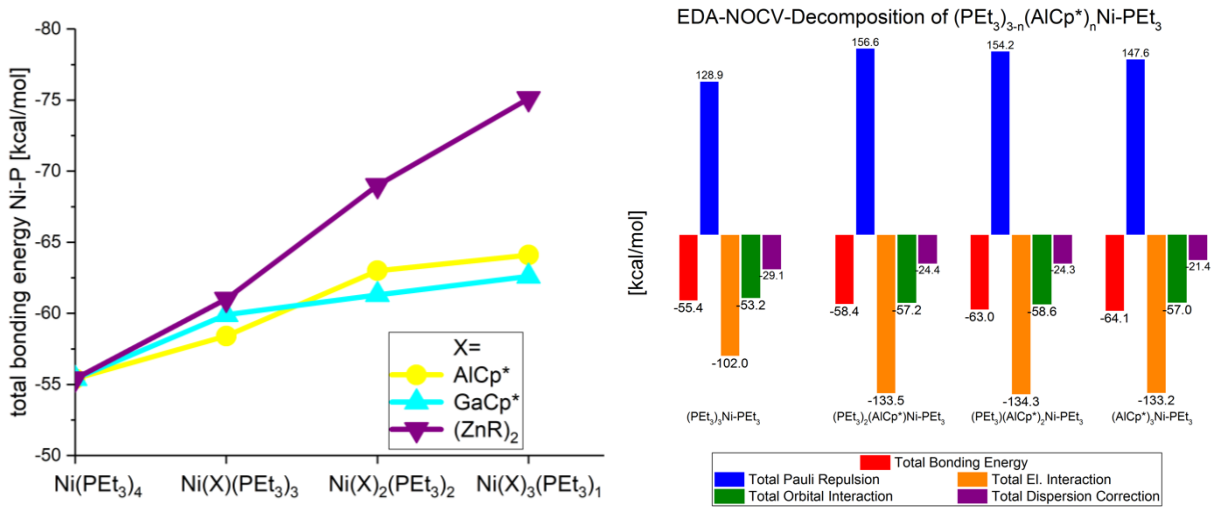

Figure 27: left: Total bonding energy for the Ni-P bonds obtained by EDA-NOCV-decomposition for $[Ni(M'R)_n(PEt_3)_{4-n}]$. right: detailed results of the EDA-NOCV decomposition of the Ni-P bond in $[Ni(AlCp^*)_n(PEt_3)_{4-n}]$. The total bonding energy steadily increases with higher number of AlCp* ligands. Incorporation of AlCp* ligands leads to an increase in Pauli repulsion as well as in the attractive electrostatic interaction.

After having discussed the bonding situation in the homoleptic systems, the following will focus on the heteroleptic complexes. Stepwise introduction of M'R in the series **5** to **3a**/**3b**/**3c** results in a steady strengthening of the Ni-PEt_3 bond (Figure 27, Table 7) from -55.4 kcal/mol up to –75.1 kcal/mol in **3c**. For AlCp*, the biggest increase in the Ni-PEt_3 bond strength is observed when a second PEt_3-ligand is replaced by AlCp* to yield $[Ni(PEt_3)_2(AlCp^*)_2]$ (**2a**), which correlates to the experimentally observed

differences between **1a** and **2a** in their dissociation behavior. Another intriguing feature is the sharp rise in Pauli repulsion (+27.7 kcal/mol) and attractive electrostatic interactions (-31.5 kcal/mol) when one AlCp* is introduced (from **5** to **1a**). Further replacement of PEt_3 by AlCp* leads to a slight decrease of the Pauli repulsion but the electrostatic interactions remain constantly high. The dispersive forces as well as the orbital interactions vary only slightly with minor changes in the σ/π-bonding ratio. In general, the contributions from dispersion interactions cannot be neglected for the sterically demanding (hydrocarbon) ligands M'R (R = Me and Cp*) and PEt_3.

Since no changes in the values of the covalent σ/π bonding contributions for the Ni-P bonds in **1a**-**5** could be determined these theoretical results conclusively suggest that the introduction of M'R ligands leads to polarization of the Ni-PEt_3 bond which in turn rises the electrostatic interaction and thus strengthens the Ni-PEt_3 bond, irrespective of the nature of M'R. This polarization is probably the result of the higher electrophilicity of the ligating atoms M'R with respect to P. This assumption is well in line with the experimentally determined ^{31}P-NMR shifts caused by the successive introduction of of M'R ligands resulting in a significant upfield shift of the respective ^{31}P signals, induced by the polarizing effects of the M'R ligands.

Table 7: EDA-NOCV-Decomposition of the Ni-P-bonds for the different complexes **1**-**5** $[Ni(M'R)_n(PEt_3)_{4-n}]$ (n = 0-4, M'R = AlCp*: **a**, GaCp*: **b**, $(ZnR)_2$: **c**). For an easier assignment Table 4 is reproduced below Table 7.

	5	**1a**	**1b**	**1c**	**2a**	**2b**	**2c**	**3a**	**3b**	**3c**
Total Bonding Energy	-55.4	-58.4	-59.9	-61.0	-63.0	-61.3	-69.0	-64.1	-62.6	-75.1
Total Pauli Repulsion	128.9	156.6	156.6	152.9	154.2	148.9	179.2	147.6	147.3	195.7
Total Electrostatic Interaction	-102.0	-133.5	-133.0	-124.6	-134.3	-131.5	-143.0	-133.2	-134.0	-155.4
Total Orbital Interaction	-53.2	-57.2	-57.3	-61.6	-58.6	-55.5	-69.4	-57.0	-54.8	-76.3
Total Dispersion Correction	-29.1	-24.4	-26.5	-27.7	-24.3	-23.2	-35.8	-21.4	-21.1	-39.2
Orbital/ (Orbital+Electrostatic)	0.34	0.30	0.30	0.33	0.30	0.30	0.33	0.30	0.29	0.33

		number	**formula**		
		5	$[Ni(PEt_3)_4]$		
1a	$[Ni(AlCp^*)(PEt_3)_3]$	**1b**	$[Ni(GaCp^*)(PEt_3)_3]$	**1c**	$[Ni(ZnCp^*)(ZnMe)(PEt_3)_3]$
2a	$[Ni(AlCp^*)_2(PEt_3)_2]$	**2b**	$[Ni(GaCp^*)_2(PEt_3)_2]$	**2c**	$[Ni(ZnCp^*)_2(ZnMe)_2(PEt_3)_2]$
3a	$[Ni(AlCp^*)_3(PEt_3)]$	**3b**	$[Ni(GaCp^*)_3(PEt_3)]$	**3c**	$[Ni(ZnCp^*)_3(ZnMe)_3(PEt_3)]$
4a	$[Ni(AlCp^*)_4]$	**4b**	$[Ni(GaCp^*)_4]$	**4c**	$[Ni(ZnCp^*)_4(ZnMe)_4]$

V.2.1.5 Summary of heteroleptic $[Ni(M'R)_n(PEt_3)_{4-n}]$ complexes

In summary, phosphine dissociation, which is known for $[Ni(PR_3)_4]$[7] and is very important for reactive transformations, is strongly suppressed by introduction of M'R in the series of compounds $[Ni(M'R)_n(PEt_3)_{4-n}]$ (n = 1 – 3, M = Al, Ga, Zn). This was revealed by variable temperature UV-Vis measurements and as well as PEt_3/ECp* ligand displacement reactions monitored by ^{31}P-NMR spectroscopy. All compounds of the investigated homologous series $[Ni(M'R)_n(PEt_3)_{4-n}]$ with $n \geq 2$ are kinetically inert, only $[Ni(AlCp^*)(PEt_3)_3]$ shows PEt_3 dissociation. The initial idea of deriving electron rich, however coordinatively unsaturated and reactive fragments $[Ni(M'R)_n]$ by pre-dissociation of PR''_3 is therefore not feasible. These experimental observations are supported by theoretical analysis of the donor-acceptor bonding situation using EDA-NOCV. A successive strengthening of the Ni-PEt_3 bond was found with increasing number of M'R ligands. For M'R = AlCp*, the biggest increase in the bond strength was found progressing from $[Ni(AlCp^*)_1(PEt_3)_3]$ (**1a**) to $[Ni(AlCp^*)_2(PEt_3)_2]$ (**2a**)**,** which is in accordance with experimental findings. The strongest Ni-PEt_3 bond was found for the Zn-rich compound **3c**. In contrast to the covalent σ/π donor-acceptor orbital bonding picture which is often used to rationalize effects on M-L bond strengths, it was found that electrostatic interactions are the dominant contribution to the Ni-PEt_3/Ni-M'R bonds also in the heteroleptic compounds and these effects govern the ligand dissociation behavior in the studied complexes. This finding is in accordance to previous results of EDA-NOCV bonding analysis for homoleptic M-PR''_3 and M-M'R compounds.[72] Therefore, it can be concluded that M'R ligands cause a significant Ni-P bond polarization as the main reason for bond strengthening leading to the kinetic inertness of most of the heteroleptic compounds. Phosphine dissociation from $[Ni(M'R)_n(PEt_3)_{4-n}]$ precursors can therefore not be applied as a general approach to access $[Ni(M'R)_n(UHC)_{4-n}]$ compounds.

V.2.1.6 Ni-Zn bonding in $[Ni(ZnR)_{2n}(L)_{4-n}]$ compounds

A complementary way of thinking about Ni-Zn and Zn-Zn Interactions

After investigation of the $[Ni(ZnR)_{2n}(PEt_3)_{4-n}]$ series, the Ni-Zn bonding and the peculiar intramolecular Zn-Zn interaction will be analyzed in more detail. Since up to date, molecular structure determination has not been achieved for **3c**, the following (qualitative) discussion will be based on theoretically predicted structures (Figure 28) which generally exhibit good agreement to the experimental structures (see chapter above).

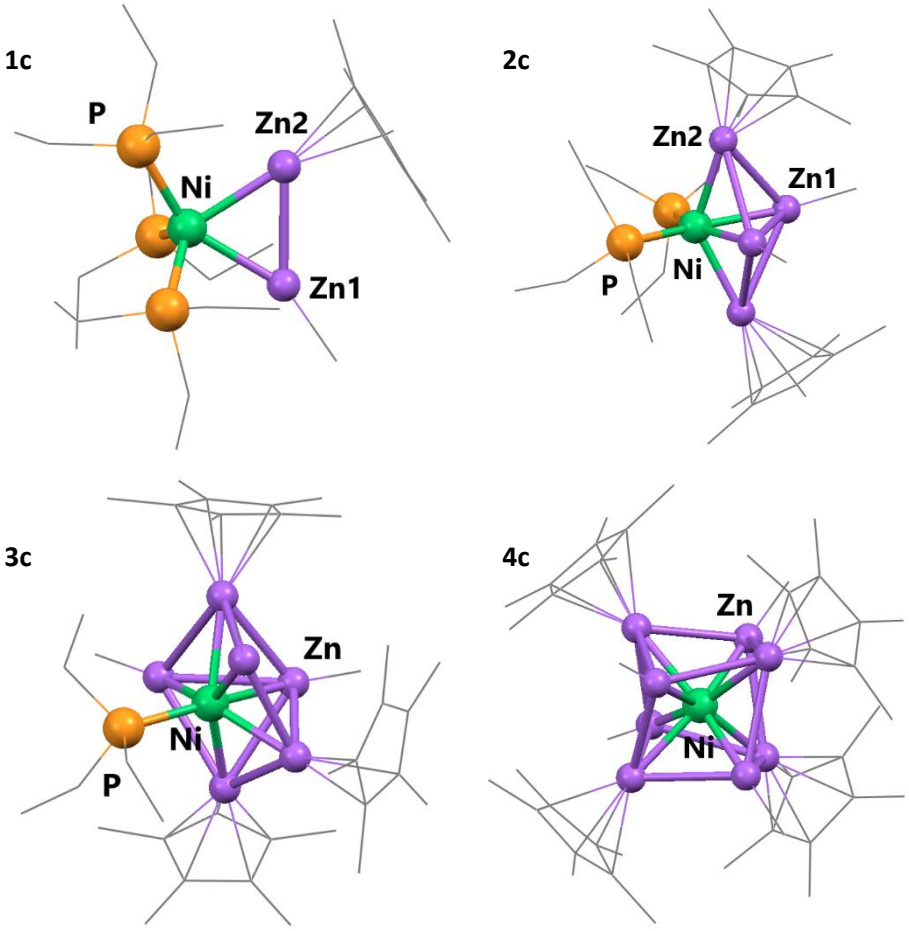

Figure 28: Theoretically predicted structures of the series of $[Ni(ZnR)_{2n}(PEt_3)_{4-n}]$ (**1c** - **4c**) compounds at the BP86-D3/def2-TZVPP level of theory. The Zn-Zn bonding "sticks" are arbitrary and should not be interpreted as "regular" Zn-Zn bonds. A discussion of the Zn-Zn interactions will be presented in the main text. Selected bond distances in Å: $[Ni(ZnCp^*)(ZnMe)(PEt_3)_3]$: Ni-Zn1: 2.35, Ni-Zn2: 2.36, Zn1-Zn2: 2.49, $[Ni(ZnCp^*)_2(ZnMe)_2(PEt_3)_2]$: Ni-Zn1: 2.33, Ni-Zn2: 2.36, Zn1-Zn2: 2.71, Zn1-Zn1': 2.72 $[Ni(ZnCp^*)_3(ZnMe)_3(PEt_3)_2]$: Ni-ZnCp*: 2.32-2.35, Ni-ZnMe: 2.31-2.35, range of Zn-Zn distances: 2.68-2.95 $[Ni(ZnCp^*)_4(ZnMe)_4]$: Ni-ZnCp*: 2.33, Ni-ZnMe: 2.33, range of Zn-Zn distances: 2.72-2.77.

The description of Ni-Zn bonding in $[Ni(ZnR)_2(PMe_3)_3]$[59] and $[Ni(ZnR)_8]$[57] have been introduced separately in previous studies. For $[Ni(ZnR)_8]$ it can be concluded that the strong radial TM-ZnR bonds are further stabilized by tangential, but very weak Zn-Zn interactions.[57] For $[Ni(ZnR)_2(PMe_3)_3]$, featuring

a $NiZn_2$ triangular motif with direct Zn-Zn bonds (Zn-Zn distance only 2.525(1) Å), the Ni-Zn interaction was described as being dominated by Ni→ $(ZnR)_2$ back-donation. It has to be noted, that the Zn-Zn distance in $[Ni(ZnR)_2(PMe_3)_3]$ is only roughly 9% longer compared to the Zn-Zn distance in [Cp*Zn-ZnCp*] (2.305(3) Å)[83]. This feature of the short Zn-Zn distance is however not present in $[Ni(ZnR)_4(PMe_3)_2]$ where the Zn-Zn distances are elongated to 2.716(1) Å. A more detailed study, lead to the conclusion of different bonding modes of the ZnR ligands in $[Ni(ZnR)_2(PMe_3)_3]$ and $[Ni(ZnR)_4(PMe_3)_2]$ (Figure 29). The Ni-Zn bond in $[Ni(ZnR)_4(PMe_3)_2]$, was described as being mainly determined by RZn→Ni σ-donation. The distinct Zn-Zn interactions in these two compounds was explained to be highly dependent on the co-ligands.[59]

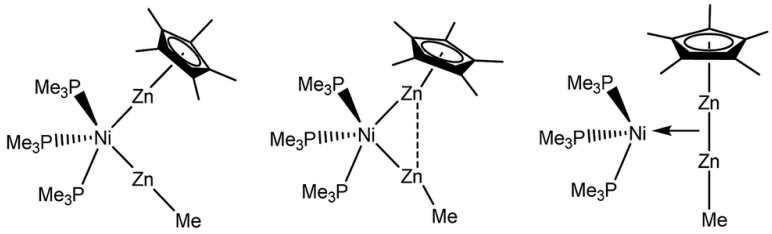

Figure 29: Schematic representation of different bonding modes of $(ZnR)_2$ units to Ni. Left: no Zn-Zn interactions but RZn→Ni sigma bonds, middle: weak Zn-Zn interactions, right: side on bonded $(ZnR)_2$ unit with significant Zn-Zn interaction. In the original publication the middle bonding motif was assigned to $[Ni(ZnR)_2(PMe_3)_3]$, whereas the left bonding motif of separated ZnR ligands was assigned to $[Ni(ZnR)_4(PMe_3)_2]$. Reprinted with permission from [K. Freitag *et al.*, Chem. Sci., 2016, **7**, 6413-6421.] - Published by The Royal Society of Chemistry.

The experimental and theoretical results presented here, applying the more sterically demanding PEt_3 co-ligand (Tolman angle PEt_3: 132 °, PMe_3: 118 °), show that the Zn-Zn interactions are still comparable to the PMe_3 results. For $[Ni(ZnR)_2(PEt_3)_3]$ (2.49 Å) and $[Ni(ZnR)_4(PEt_3)_2]$ (2.71 Å), the Zn-Zn distances remain basically unchanged compared to $[Ni(ZnR)_2(PMe_3)_3]$ and $[Ni(ZnR)_4(PMe_3)_2]$. Even for the bulky PPh_3 ligands (Tolman angle PPh_3: 145 °), the Zn-Zn distance in $[Ni(ZnR)_2(PPh_3)_3]$ (2.48 Å) does not considerably change (Figure S 21). Therefore, it can be concluded that the Zn-Zn distance is rather insensitive to the steric demand of the co-ligands. As found in the study by Freitag *et al.*[59] Zn-Zn bond critical points can be found for $[Ni(ZnR)_2(PR''_3)_3]$ whereas no Zn-Zn bond critical points or bond paths can be found for $[Ni(ZnR)_4(PR''_3)_2]$. Calculations on $[Ni(ZnR)_2(L)_3]$ complexes featuring different ligands L (L = C_2H_4, CO Figure S 21) also did not change the Zn-Zn distances (2.46 Å and 2.49 Å, respectively). This shows that also changes in the electronic properties of the co-ligands do not effect on Zn-Zn bonding significantly. The Zn-Zn distances of about 2.53 Å found in the experimental structure of $[Ni(GaCp^*)(ZnCp^*)(ZnMe)(PEt_3)_2]$ (Figure 20) further underlines this finding. Therefore, it can be concluded that the differences in the Zn-Zn distances are an intrinsic feature of the $(ZnR)_n$ unit and a more unified bonding model for $[Ni(ZnR)_{2n}L_{4-n}]$ compounds is necessary.

In a strictly formal assignment, the bonding in the series of $[Ni(ZnR)_{2n}(PEt_3)_{4-n}]$ (in principle every member is a 18 valence electron complex) can be depicted as follows: In the tetrahedral 18 valence electron complex $[Ni(PEt_3)_4]$, Ni has 10 d electrons plus 4x2 electrons from the σ-donation of PEt_3. Formally replacing one vertex of the tetrahedron by a [Cp*Zn-ZnMe] unit gives the following situation. The Zn_2 unit keeps its electron pair from the Zn-Zn sigma bond[83] whereas Ni donates one electron pair for a three center two electron (3c2e) Ni-(Zn_2) bonding interaction. Since the Zn_2 unit can also be regarded to be "isolobal" to H-H, also an oxidative addition of Zn_2 at the Ni center can be considered.[59] Such an oxidative addition of (Cp*Zn-ZnCp*) to Pd has been observed in the reaction with $[(Pd(CN^tBu)_2)_3]$ yielding $[Pd(CN^tBu)_2(ZnCp^*)_4]$ with isolated ZnCp* ligands.[59] Increasing the Zn content in the series $[Ni(ZnR)_{2n}(PEt_3)_{4-n}]$ from the P_4 to the Zn_8 environment, Ni remains with one "lone-pair", 4x 3c2e Ni-(Zn_2) bonding and 4x (Zn_2) bonding electron pairs (Table 8).

Table 8: Formal assignments of electrons in $[Ni(ZnR)_{2n}(PEt_3)_{4-n}]$ and the resulting formal "bond order" of the respective Zn-Zn interactions.

	Ni- "lone-pairs"	Ni-P bonds	3c2e Ni(Zn_2) bonding	Zn-Zn electron pairs	Edges of the Zn polyhedra	Formal Zn-Zn "bond order"
$Ni(PEt_3)_4$	5	4	0	0	0	0
$Ni(ZnR)_2(PEt_3)_3$	4	3	1	1	1	1
$Ni(ZnR)_4(PEt_3)_2$	3	2	2	2	5	2/5 = 0.4
$Ni(ZnR)_6(PEt_3)$	2	1	3	3	10	3/10 = 0.3
$Ni(ZnR)_8$	1	0	4	4	20	4/20 = 0.2

Following this line of thought, $[Ni(ZnR)_2(PR''_3)_3]$ is related to the σ-aromatic triangular compounds $[Zn_3](Cp^*)_3^+$ and $[Zn_2Cu](Cp^*)_3$.[48] Indeed, the $[Ni(PR''_3)_3]$ fragment featuring 16 valence electrons is isoelectronic to the [CuCp*] and $[ZnCp^*]^+$ fragments, further supporting the view of delocalized Ni-Zn and Zn-Zn bonding.

The mismatch of the Zn-Zn bond distances in $[Ni(ZnCp^*)(ZnMe)(PMe_3)_3]$ (2.51 Å) and Cp*ZnZnCp* (2.31 Å) can be explained if the Zn-Zn bonding electrons pairs are also delocalized over the Ni-Zn bonds in a 3c4e bonding situation over the $NiZn_2$ triangle. In this respect it has to be noted, that in contrast to $[Zn_3](Cp^*)_3^+$ and $[Zn_2Cu](Cp^*)_3$[48], the triangular $NiZn_2$ sites in $[Ni(ZnCp^*)(ZnMe)(PMe_3)_3]$ do not have similar distances. Within this entire framework, this would suggest that the highly delocalized 3c4e bond situation in $[Zn_3](Cp^*)_3^+$ and $[Zn_2Cu](Cp^*)_3$ is more localized in the Ni-Zn bonds of $[Ni(ZnCp^*)(ZnMe)(PMe_3)_3]$.

Extending this concept to $[Ni(ZnCp^*)_4(ZnMe)_4]$, the Zn-Zn and Ni-Zn bonding electron pairs are delocalized over the metal bonds of $NiZn_8$, leading to a pronounced elongation of the Zn-Zn distances

in $[Ni(ZnCp^*)_4(ZnMe)_4]$ when compared to $[Ni(ZnCp^*)(ZnMe)(PMe_3)_3]$. Therefore, this formal bonding assignment represents a uniform bonding model for the series of $[Ni(ZnR)_{2n}(PR''_3)_{4-n}]$ compounds.

With the mentioned findings in mind, the question arises whether this formal assignments of electrons can be applied in order to explain a certain property of $[Ni(ZnR)_n]$ compounds. Indeed, it can be used to explain the "in-silico reactivity" of $[Ni(ZnR)_n]$ compounds towards C_2H_x substrates. Whereas $[Ni(ZnR)_2]$ and $[Ni(ZnR)_4]$ were shown to undergo Zn-C bond forming reactions giving Ni-Zn bridging coordination modes of C_2H_2, $[Ni(ZnR)_6]$ does not show an analog "reactivity". In the first compounds $[Ni(ZnR)_2(C_2H_2)_3]$ and $[Ni(ZnR)_4(C_2H_2)_2]$, the formal Zn-Zn bonding electrons pairs are involved in Zn-C bonding resulting in a formal reduction of C_2H_2 whereas this is not the case for the more delocalized Zn-Zn bonding electron pairs in $[Ni(ZnR)_6(C_2H_2)]$. The "loss" of the Zn-Zn bonding electron pairs to form Zn-C bonds is the reason for the increase in Zn-Zn distances as found e.g. in $[Ni(ZnR)_4(C_2H_2)_2]$ (range of Zn-Zn distances: 2.72-3.17 Å) compared to "unreacted" $[Ni(ZnR)_4(C_2H_4)_2]$ (range of Zn-Zn distances: 2.62-2.80 Å) (see Figure 9). Furthermore, the fluxional processes of the ZnR ligands as observed for $[Ni(ZnCp^*)_3(ZnMe)_3(PEt_3)]$ could also be explained by the described formal approach. The delocalized NiZn and Zn-Zn bonding interactions lead to a flat energy surface with respect to the Ni-Zn and Zn-Zn distances which potentially allows ligand rearrangements even down to very low temperatures.

Interestingly, the described approach might also apply for TM-ECp* bonds. For $[Ni(AlCp^*)_2(C_2H_2)_2]$ a Ni-Al bridging C_2H_2 coordination similar to $[Ni(ZnR)_4(C_2H_2)_2]$ was observed. The Al-Al distance in the acetylene complex $[Ni(AlCp^*)_2(C_2H_2)_2]$ (2.50 Å) is considerably shortened compared to the ethylene complex $[Ni(AlCp^*)_2(C_2H_4)_2]$ (3.12 Å). In line with the approach presented above, one could argue that Al_2 contributes two electrons to the Al-C bond, leaving the two Al centers "isoelectronic" to a ZnR fragment. Within this picture, the $NiAl_2$ triangle would exhibit a similar bonding situation as the $NiZn_2$ triangle. Interestingly, this assignment of a formal two electron oxidation of the $NiAl_2$ triangle is supported by the theoretically predicted structure of $[Ni(AlCp^*)_2(PEt_3)_2]^{2+}$ (BP86-D3/def2-SVP see Figure S 22). In $[Ni(AlCp^*)_2(PEt_3)_2]^{2+}$ The Al-Al distance of 2.70 Å is considerably shortened compared to $[Ni(AlCp^*)_2(PEt_3)_2]$ (3.34 Å). Furthermore, the compounds $[W(AlCp^*)_6(C_2H_4)_2]$[55] and $[(AlCp^*)_3Ni(\mu\text{-}H)(Al(C_6H_5)Cp^*)]$[88] show that AlCp* ligands are indeed oxidized in reactive transformations. In $[W(AlCp^*)_6(C_2H_4)_2]$, featuring metal bridging C-H activated C_2H_x moieties, this leads to a shortening of the Al-Al distances to 2.84 Å.

In summary, the Ni-Zn and Zn-Zn bonding in $[Ni(ZnR)_{2n}(PEt_3)_{4-n}]$ can be visualized by the three structures shown in Figure 29, if these are considered as mesomeric formula which together represent the "real" bonding description. From the viewpoint of "reactivity" $(ZnR)_n$ ligands can be seen as electron reservoirs that can potentially donate electrons for "small molecule activation reactions"

comparable to redox non-innocent ligands. In combination with early transition metals such ligands "allow" two-electron-oxidative addition reactions that are uncommon for 3d transition metals like Fe.[89] There might also be a connection between the formal electron assignment for $[Ni(ZnR)_{2n}(PEt_3)_{4-n}]$ and TM-ECp* bonds as discussed in several cases for $[TM(AlCp^*)_n]$ compounds. Therefore, interesting and potentially new reactivities can be assumed for $[TM(ZnR)_n]$ compounds as already evidenced in-silico for $[Ni(ZnR)_4(C_2H_2)_2]$. To proof the described concept, further experimental evidence of the reactivity of $[TM(ZnR)_n]$ compounds as well as new experimental approaches to $[TM(ZnR)_n(UHC)_m]$ are needed. Furthermore, a more detailed theoretical analysis could substantiate the formal assignment of delocalized bonding over $Ni(ZnR)_n$, as e.g. the nucleus independent chemical shift (NICS)[90], the anisotropy of the induced current density (ACID)[91] and the delocalization index $\delta(M^1,M^2)$ (M^1/M^2: different metal atoms)[92-93].

V.2.1.7 Introduction to $[(H)(SiEt_3)Ni(M'R)_n]$ complexes

Phosphine dissociation from $[Ni(M'R)_n(PEt_3)_{4-n}]$ complexes was shown to be hampered by M'R coordination. Therefore, $[Ni(M'R)_n(PEt_3)_{4-n}]$ complexes cannot be used to obtain low-coordinated $[Ni(M'R)_n]$ fragments as intermediates on the way to $[Ni(M'R)_n(UHC)_{4-n}]$ compounds. Thus, an alternative approach to low-coordinated $[Ni(M'R)_n]$ fragments based on reductive elimination from $[(X)(Y)TM(M'R)_n]$ shall be tested (Figure 30).

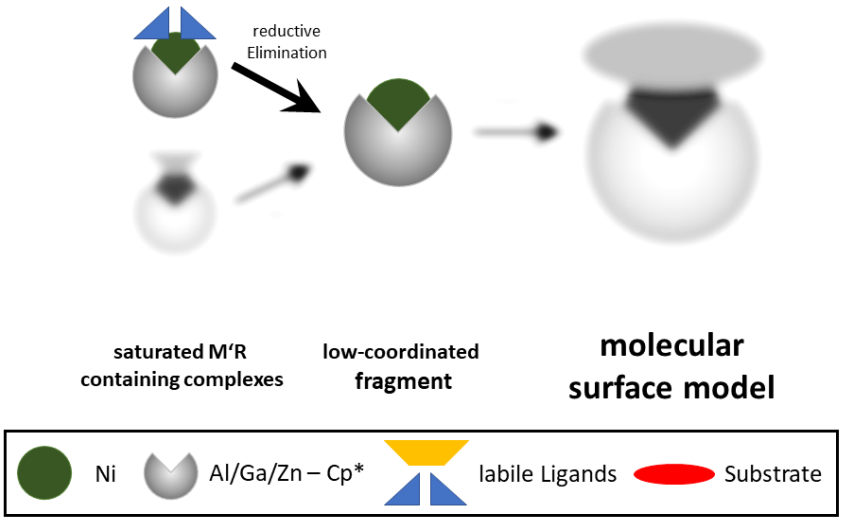

Figure 30: Schematic representation of the experimental access to low-coordinated $[Ni(M'R)_n]$ fragments by reductive elimination of X-Y ligands as e.g. H-$SiEt_3$.

From the original publication and the chapter above, it is known that $[(H)(SiEt_3)Ni(AlCp^*)_3]$ is a reasonable precursor for open coordination sites, liberating a very reactive $[Ni(AlCp^*)_3]$ fragment.[8] This hypothetical intermediate shows interesting Si-H and C-H activation reactions. However, no GaR or ZnR analogue to this compound is known, which impedes the access of several low-coordinated $[Ni(M'R)_n]$ species by reductive elimination. The access of the GaR analogue was tested in the original publication however without success. Al/Zn exchange reactions starting from $[(H)(SiEt_3)Ni(AlCp^*)_3]$ would possibly yield $[(H)(SiEt_3)Ni(AlCp^*)_{3-n}(ZnR)_{2n}]$ compounds, that might still have the potential to eliminate H-$SiEt_3$. However, the $(H)(SiEt_3)$ moiety might be to reactive to tolerate the conditions of the Al/Zn exchange reactions involving redox processes from $Zn^{II}R_2$ to $Zn^{I}R$ and $Al^{I}Cp^*$ to $Al^{III}R_3$.[47] Therefore, the abstraction of H or $SiEt_3$ moieties and the formation of H-M'R or Et_3Si-M'R compounds could be a reasonable (side) reaction, potentially impeding selective E/Zn exchange reactions. So far, three hydride containing precursors of the general formula $[Ru(PR''_3)_2(ECp^*)_a(H)_b)]$ have been subjected to E/Zn exchange conditions. In two products, the hydride moieties remained whereas one product was isolated without hydrides.[94] This reactivity indicated that when applying suitable conditions during

E/Zn exchange reactions and work-up, the transformation of $[(H)(SiEt_3)Ni(AlCp^*)_3]$ to $[(H)(SiEt_3)Ni(AlCp^*)_{3-n}(ZnR)_{2n}]$ could be successful.

Ⅴ.2.1.8 Synthesis and Characterization of $[(H)(SiEt_3)Ni(M'R)_a]$ complexes

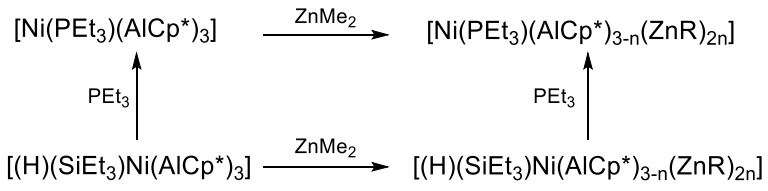

Scheme 4: Synthesis of $[(H)(SiEt_3)Ni(AlCp^*)_{3-n}(ZnR)_{2n}]$ by Al/Zn exchange from $[(H)(SiEt_3)Ni(AlCp^*)_3]$. $[(H)(SiEt_3)Ni(AlCp^*)_3]$ and $[(H)(SiEt_3)Ni(AlCp^*)(ZnCp^*)_2(ZnMe)_2]$ were shown to undergo $HSiEt_3/PEt_3$ exchange reactions as a good indication for the intermediate formation of open coordination sites at the respective $[Ni(AlCp^*)_{3-n}(ZnR)_{2n}]$ fragment.

The ^{31}P-NMR signal served as a reliable probe for an efficient screening of $[Ni(M'R)_n(PEt_3)_{4-n}]$ species in solution. In contrast, for $[(H)(SiEt_3)Ni(AlCp^*)_{3-n}(ZnR)_{2n}]$, the ^{1}H-NMR hydride signal proofed to be a reliable source of information of the product distribution in reaction mixtures. For published $[(H)(SiEt_3)Ni(AlCp^*)_3]$ this hydride signal appears at -12.81 ppm being well separated from any other ^{1}H signals. Upon heating, $(H)(SiEt_3)$ can be replaced by AlCp*, C-H activated C_6H_6 or PEt_3 resulting in the disappearance of the hydride signal and the formation of the respective compound.[8] $[(H)(SiEt_3)Ni(AlCp^*)_3]$ was further treated with BrC_6H_5 to test oxidative addition reactions or with 3-hexyne potentially yielding the desired $[(EtC{\equiv}CEt)Ni(AlCp^*)_3]$. For both reactions, the hydride signals disappear but the isolation or characterization of a reaction product based on NMR studies was so far unsuccessful. Therefore, the reactivity of $[(H)(SiEt_3)Ni(AlCp^*)_3]$ towards UHC compounds should be systematically studied using liquid injection field desorption ionization mass spectrometry (LIFDI-MS) as the standard analytical technique (see chapter Ⅴ.3.1 Introduction to $[Ni_a(M'R)_b(UHC)_c]$).

Furthermore, the access of $[(H)(SiEt_3)Ni(ZnR)_6]$ was investigated (Scheme 4). Starting from $[Ni(ZnCp^*)_4(ZnMe)_4]$ a $(ZnR)_2$/H-$SiEt_3$ ligand substitution reaction was tested. Therefore, $[Ni(ZnCp^*)_4(ZnMe)_4]$ was heated to 100°C in pure H-$SiEt_3$ but ^{1}H-NMR analysis did not indicate the appearance of a hydride containing species and the starting material $[Ni(ZnCp^*)_4(ZnMe)_4]$ is retained. In a second approach, $[(H)(SiEt_3)Ni(AlCp^*)_3]$ was treated with $ZnMe_2$ to initiate the Al/Zn exchange reaction. Due to the expected reactivity of the $(H)(SiEt_3)$ moiety, this reaction was performed carefully at very low temperatures. In a NMR-scale reaction, $ZnMe_2$ was added to a solution of $[(H)(SiEt_3)Ni(AlCp^*)_3]$ in toluene-d_8 at -60°C. ^{1}H-NMR analysis of the crude reaction mixture reveals that the signals of the starting material have disappeared. The new signals can be assigned to the partially Al/Zn exchanged species $[(H)(SiEt_3)Ni(AlCp^*)_2(ZnCp^*)(ZnMe)]$. They appear at 2.14 (ZnCp*, 15H), 1.85 (AlCp*, 30H), 1.22 ($SiCH_2\mathit{CH_3}$, 9H), 0.83 ($Si\mathit{CH_2}CH_3$, 6H), -0.05 (ZnMe, 3H) and -11.92 (Ni-H) ppm (Figure 31).

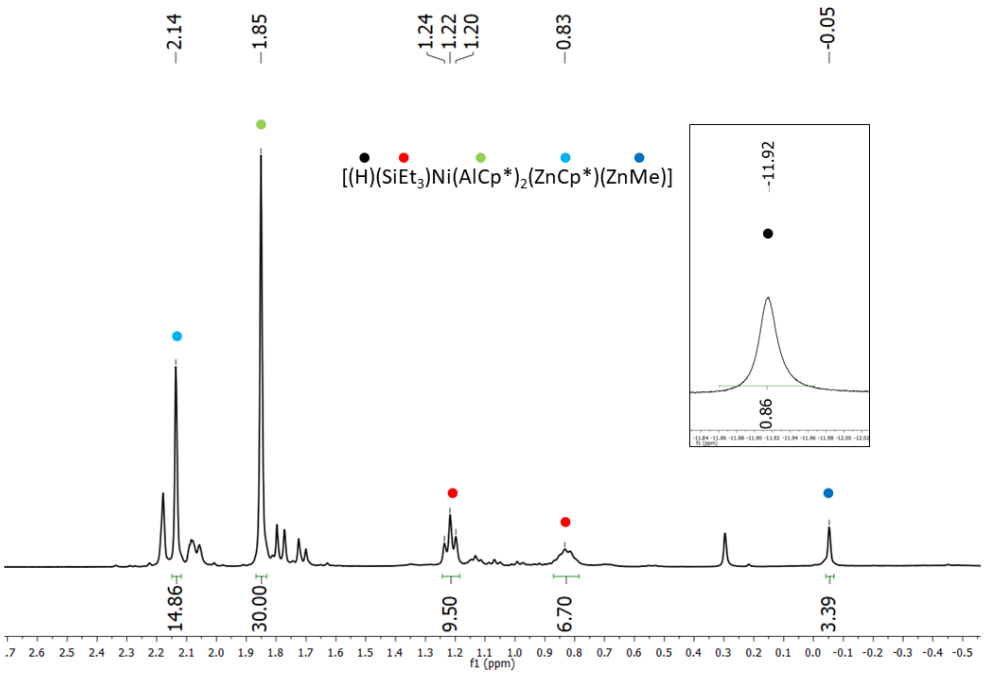

Figure 31: ^{1}H-NMR spectrum of the crude reaction mixture containing [(H)(SiEt$_3$)Ni(AlCp*)$_2$(ZnCp*)(ZnMe)] in toluene-d$_8$. The signal at 0.3 ppm can be assigned to impurities from silicon grease, whereas the additional signals in the M-Cp* region can be assigned to [Ni(ZnCp*)$_4$(ZnMe)$_4$] and [(H)(SiEt$_3$)Ni(AlCp*)$_{3-n}$(ZnCp*)$_n$(ZnMe)$_n$] species. The latter is in accordance to the additional SiEt$_3$ signals between 1.3 and 0.8 ppm.

Due to this promising result of a selective Al/Zn exchange reaction without affecting the (H)(SiEt$_3$) moiety, the reaction was performed on preparative scale. To a toluene solution of [(H)(SiEt$_3$)Ni(AlCp*)$_3$] cooled to -50°C, a ZnMe$_2$ solution (8 eq.) in toluene was added. The reaction mixture was allowed to reach -5°C after 5h reaction time. The solvent was removed in vacuo. ^{1}H-NMR analysis of this reaction mixture shows distinct signals in the Ni-H range at -10.65 and 12.00 ppm indicating the formation of different hydride containing reaction products. In addition, also the signals for free H-SiEt$_3$ are found at 3.90 (Si-H, 1H), 0.97 (SiCH$_2$*CH$_3$*, 9H) and 0.86 ppm (Si*CH$_2$*CH$_3$, 6H). Furthermore, the signals at 2.06 (ZnCp* species, 15H) and 0.00 (ZnMe species, 3H) ppm hint to the formation of literature known [Ni(ZnCp*)$_4$(ZnMe)$_4$] (^{1}H-NMR signals in C$_6$D$_6$: 2.08 (60H), 0.00 ppm (12H)).[57] Indeed, LIFDI-MS analysis of this reaction mixture is in agreement to this observation showing the formation of [Ni(ZnCp*)$_4$(ZnMe)$_4$]. Taken together, these results suggest the release of H-SiEt$_3$ from an intermediate [(H)(SiEt$_3$)Ni(AlCp*)$_{3-n}$(ZnR)$_{2n}$] species during the reaction. From the crowded ^{1}H-NMR spectrum and the MS measurements, no indication for the formation of the desired [(H)(SiEt$_3$)Ni(ZnCp*)$_3$(ZnMe)$_3$] (calculated for NiSiZn$_6$CH: 1018.05 m/z) can be deduced.

Further adjustment of the reaction conditions finally lead to the isolation of pure [(H)(SiEt$_3$)Ni(AlCp*)(ZnCp*)$_2$(ZnMe)$_2$] (Figure 32). To a toluene solution of [(H)(SiEt$_3$)Ni(AlCp*)$_3$] cooled to -50°C, a ZnMe$_2$ solution (5.3 eq) in toluene precooled to -50°C was added over the course of 15 min. After 3 h at -50°C the reaction mixture was concentrated to about 50 % at this temperature. The cooling bath was removed while further concentrating the reaction solution to obtain a dark green residue. ^{1}H-NMR measurements show a Ni-H hydride signal at -12.00 ppm in accordance to the observed signal above. The remaining signals appear at 2.18 (ZnCp*, 30H), 1.76 (AlCp*, 15H), 1.07 (SiCH$_2$*CH$_3$*, 9H), 0.71 (Si*CH$_2$*CH$_3$, 6H) and -0.09 (ZnMe, 6H) ppm.

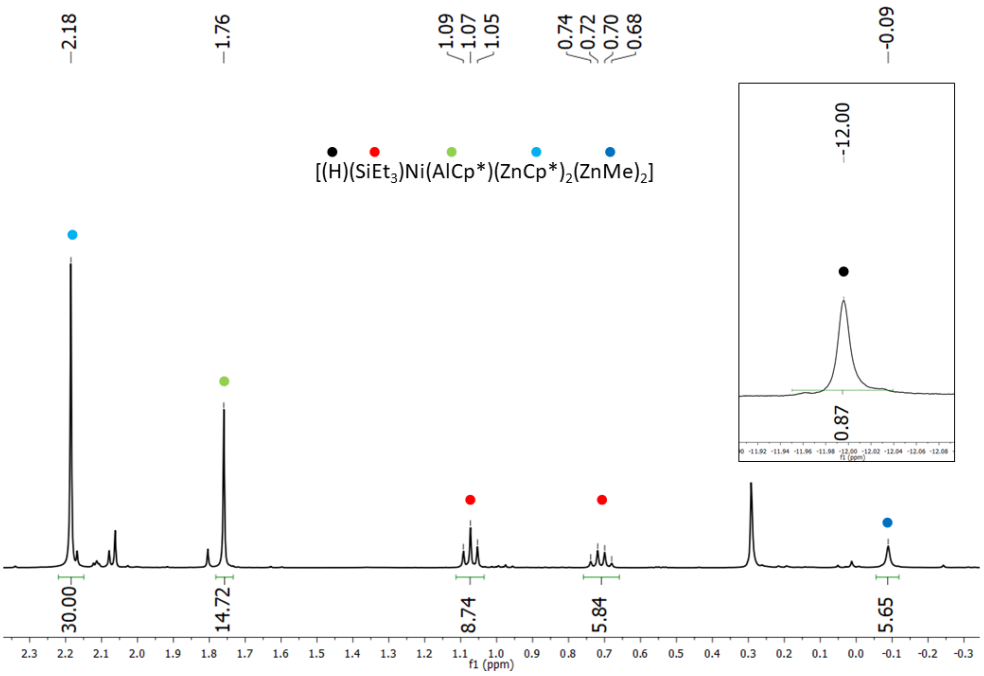

Figure 32: ^{1}H-NMR spectrum of [(H)(SiEt$_3$)Ni(AlCp*)(ZnCp*)$_2$(ZnMe)$_2$] in C$_6$D$_6$. The signal at 0.3 ppm can be assigned to silcon grease.

LIFDI-MS analysis of this batch exhibits the molecular ion peak of the desired species at 899.57 m/z (calculated for NiSiZn$_4$AlC$_{28}$H$_{67}$: 898.13 m/z) with the right isotopic pattern (Figure 33). The discrepancy of the calculated and measured mass is due to initial calibration problems of the LIFDI which can now be circumvented by additional external calibration using polystyrene (see chapter Ⅶ Experimental Section). Therefore, the LIFDI measurement for this compound should be repeated in a subsequent thesis work. Nevertheless, the ^{1}H-NMR signals together with the matching isotopic pattern obtained by LIFDI-MS are in agreement to the formation of [(H)(SiEt$_3$)Ni(AlCp*)(ZnCp*)$_2$(ZnMe)$_2$].

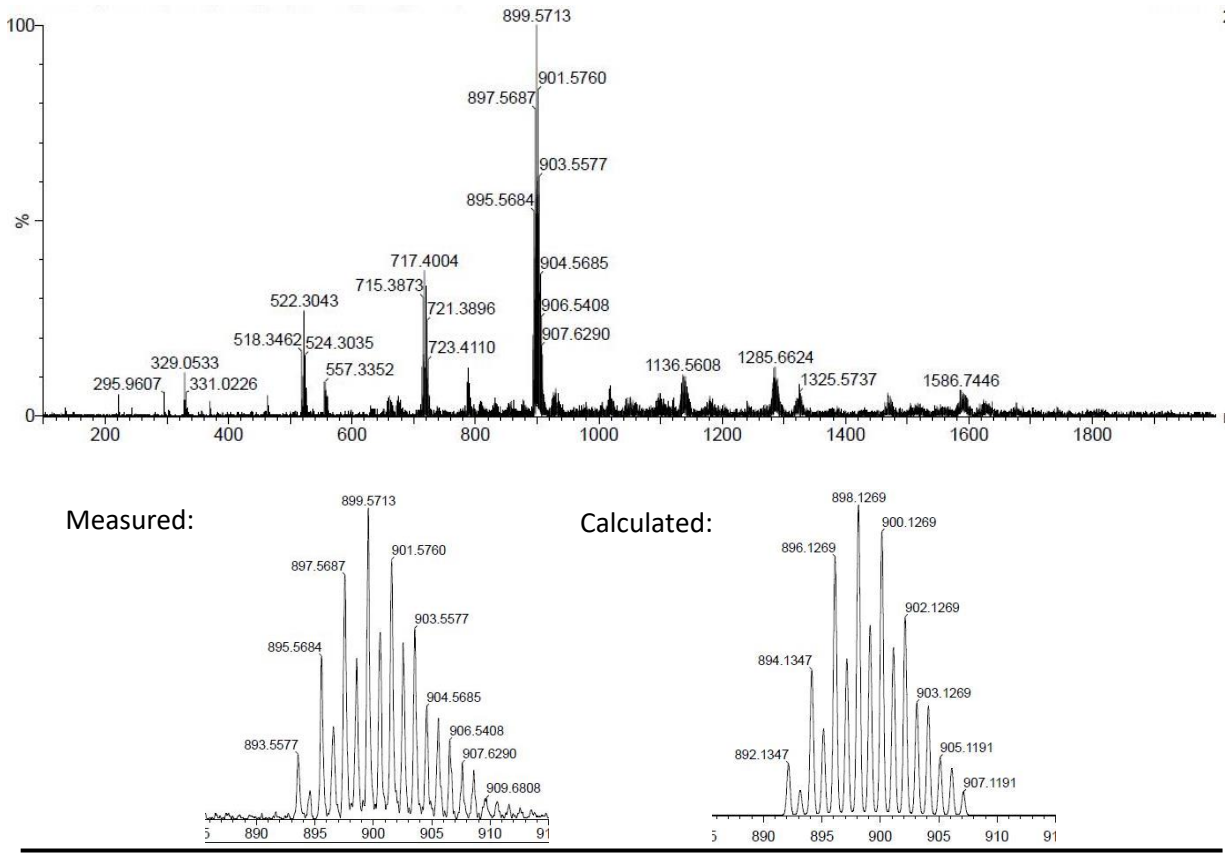

Figure 33: LIFDI-MS spectrum of [(H)($SiEt_3$)(Ni($AlCp^*$)($ZnCp^*$)$_2$($ZnMe$)$_2$] and a comparison of the calculated and measured isotopic patterns. The LIFDI-MS spectrum shows impurities that still need to be identified, especially at higher masses.

The Ni-H signals of [(H)($SiEt_3$)Ni($AlCp^*$)$_3$] (-12.81 ppm), [(H)($SiEt_3$)Ni($AlCp^*$)$_2$($ZnCp^*$)($ZnMe$)] (-11.92 ppm) and [(H)($SiEt_3$)Ni($AlCp^*$)($ZnCp^*$)$_2$($ZnMe$)$_2$] (-12.00 ppm) are reliable probes for the indication of these compounds. In the second reaction described above an additional signal in the range for Ni-H species was detected at -10.65 ppm, which could potentially be an indication for the formation of fully Al/Zn exchanged [(H)($SiEt_3$)Ni(ZnR)$_6$]. However, no indications for such species (or for any [Ni(ZnR)$_6$ fragments] could be found in LIFDI-MS spectra. A plausible explanation could be the "isoelectronic" replacement of H-$SiEt_3$ by (ZnR)$_2$ either from [(H)($SiEt_3$)Ni($AlCp^*$)($ZnCp^*$)$_2$($ZnMe$)$_2$] or from an elusive [(H)($SiEt_3$)Ni(ZnR)$_6$] species. Due to the existence of the unassigned Ni-H signal at -10.65 ppm, the intermediate formation of [(H)($SiEt_3$)Ni($ZnCp^*$)$_3$($ZnMe$)$_3$] can be assumed, which is however unstable under the applied reactions conditions leading to the observed formation of [Ni($ZnCp^*$)$_4$($ZnMe$)$_4$]. In accordance to the observations for [(H)($SiEt_3$)Ni($AlCp^*$)$_3$], treatment of [(H)($SiEt_3$)Ni($AlCp^*$)($ZnCp^*$)$_2$($ZnMe$)$_2$] with PEt_3 at elevated temperatures in an NMR-scale reaction, results in the replacement of H-$SiEt_3$ and the formation of [(PEt_3)Ni($AlCp^*$)($ZnCp^*$)$_2$($ZnMe$)$_2$] can be assumed, based on $^1H/^{31}P$-NMR investigations (Figure S 19, Figure S 20). This reactivity shows that reductive elimination from Zn-rich Ni complexes is still possible.

V.2.1.9 Summary [(H)($SiEt_3$)Ni(M'R)$_a$] complexes

In addition to [(H)($SiEt_3$)Ni($AlCp^*)_3$], that is known to liberate a highly reactive [Ni($AlCp^*)_3$] fragment, the synthetical access of [(H)($SiEt_3$)Ni($AlCp^*)_{3-n}(ZnR)_{2n}$] (n = 1, 2) was demonstrated. The appearance of an unassigned Ni-H signal in the ^{1}H NMR spectra of different reaction solutions is an indication for the (intermediate) formation of [(H)($SiEt_3$)Ni($ZnCp^*)_3(ZnMe)_3$]. Further, fine-tuning of the reaction conditions or adjustment of the functional group (X-Y) (other silanes H-SiR_3, H-BR_2, H_2, …) could potentially result in the selective formation of [(X)(Y)Ni$(ZnR)_6$] compound.

Reductive elimination of H-$SiEt_3$ was also possible for the partly Al/Zn exchanged [(H)($SiEt_3$)Ni($AlCp^*$)($ZnCp^*)_2(ZnMe)_2$] as demonstrated by the reactivity towards PEt_3. Therefore, the reactivity of [(H)($SiEt_3$)Ni($AlCp^*)_{3-n}(ZnR)_{2n}$] with suitable UHCs should be further investigated to potentially achieve ternary [(UHC)Ni($AlCp^*)_{3-n}(ZnR)_{2n}$] compounds. Since reductive elimination will only lead to selected [Ni(M'R)$_n$] low-coordinated fragments, this pathway does not present a general access to [Ni$_a$(M'R)$_b$(UHC)$_c$] compounds. Therefore, alternative approaches will be necessary to enable a general access to a broad library of [Ni$_a$(M'R)$_b$(UHC)$_c$] complexes and clusters.

V.3 An alternative approach to $[Ni_a(M'R)_b(UHC)_c]$

V.3.1 Introduction to $[Ni_a(M'R)_b(UHC)_c]$

So far the strategy to access $[Ni(M'R)_{4-n}(UHC)_n]$ compounds was based on ligand displacement reactions from precursors featuring preformed Ni-M'R bonds as for example in $[Ni(M'R)_n(PEt_3)_{4-n}]$ or $[(H)(SiEt)_3Ni(AlCp^*)_{3-n}(ZnR)_{2n}]$. However, neither phosphine displacement reactions from $[Ni(M'R)_n(PEt_3)_{4-n}]$ nor reductive elimination from $[(H)(SiEt)_3Ni(AlCp^*)_{3-n}(ZnR)_{2n}]$ proofed to be a general method to access low-coordinated $[Ni(M'R)_n]$ fragments. Therefore, a more universal synthetic access to $[Ni(M'R)_n(UHC)_{4-n}]$ compounds, as potential molecular surface models, has so far not been achieved. An alternative approach is not based on the "late-stage" functionalization with UHC's by ligand exchange of $[Ni(M'R)_n(L)]$ but would make use of "early-stage" incorporation of UHC's before M'R ligands are present. Therefore, the synthetic strategy involves treatment of organometallic Ni^0 precursors with UHC moieties and subsequent treatment with ECp*. Interestingly, for the presented cases, this approach does not lead to the formation of (envisioned) mononuclear $[Ni(M'R)_n(UHC)_{4-n}]$, but polynuclear $[Ni_a(M'R)_b(UHC)_c]$ clusters are accessed (Figure 34).

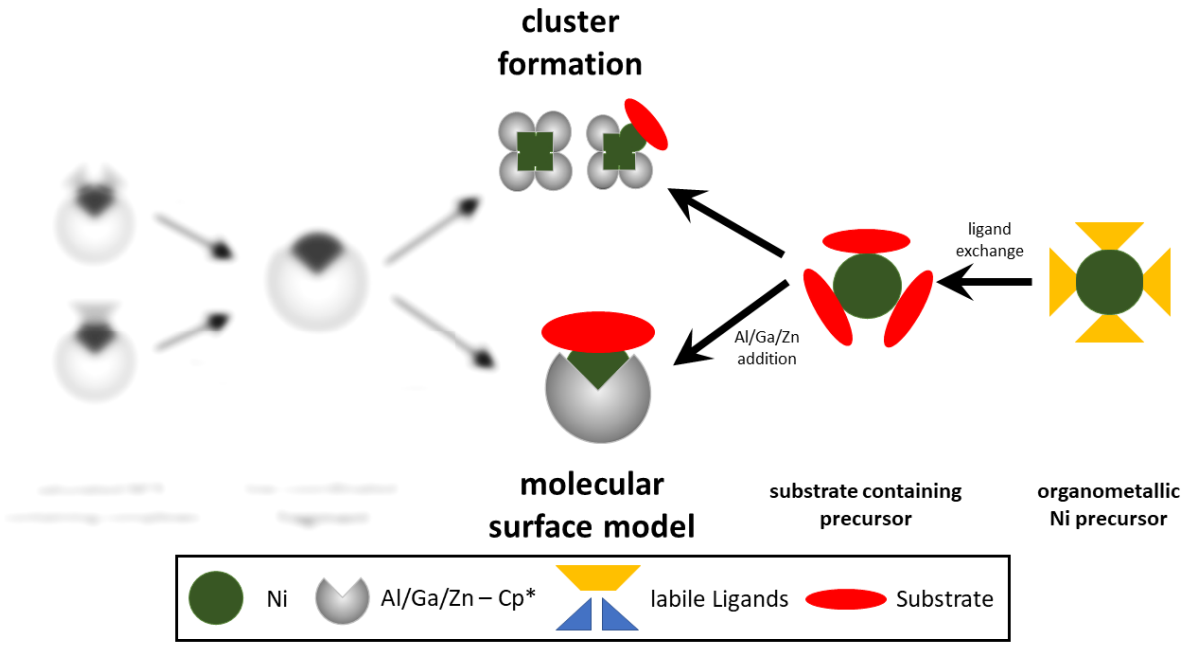

Figure 34: New research strategy to access $[Ni_a(M'R)_b(UHC)_c]$ by the "early-stage" incorporation of UHC moieties and subsequent introduction of M'R ligands. So far this approach does not yield mononuclear $[Ni(M'R)_{4-n}(UHC)_n]$ but polynuclear $[Ni_a(M'R)_b(UHC)_c]$ clusters.

Therefore, common Ni^0 precursors like $[Ni(cod)_2]$, $[Ni_2(dvds)_3]$ and [Ni(cdt)] were treated with 3-hexyne in different stoichiometries yielding different $[Ni_a(EtCCEt)_c(L)_d]$ compounds. The application of internal

3-hexyne, shall prevent (unwanted) C-H activation of terminal olefinic/ (as for $[W(AlCp^*)_6(C_2H_4)_2]$[55] and $[Ni_3(GaDDP)_2(C_2H_4)_3]$[56]). Such reactions are indeed very interesting and could potentially lead to the discovery of new reactivities. However, additional reactive channels make the analysis more complicated and therefore this shall be avoided in the initial state by applying 3-hexyne. Promising reaction mixtures containing $[Ni_a(EtCCEt)_cL_d]$ shall subsequently be treated with ECp* to access compounds of the general formula $[Ni_a(ECp^*)_b(EtCCEt)_cL_d]$ (Scheme 5). The reaction mixtures will be analyzed by mass spectrometry using the liquid injection field desorption ionization (LIFDI) method.

$$[NiL_n] \xrightarrow{x\ EtCCEt} [Ni_a(EtCCEt)_cL_d] \xrightarrow[T]{y\ ECp^*} [Ni_a(ECp^*)_b(EtCCEt)_cL_d]$$

Scheme 5: Synthesis scheme for the experimental access to $[Ni_a(ECp^*)_b(EtCCEt)_c(cod)_d]$.

The new analytical approach applying LIFDI-MS has several advantageous compared to "conventional" analysis based on $^1H/^{13}C$ NMR and single crystal XRD. First of all, the phosphine ligands in $[Ni(M'R)_{2n}(PEt_3)_{4-n}]$ complexes were reliable probes for the proper identification of the respective species in reaction mixtures. The same applies for the hydride moieties in $[(H)(SiEt)_3Ni(AlCp^*)_{3-n}(ZnR)_{2n}]$. However, in $[Ni_a(ECp^*)_b(EtCCEt)_c]$, with narrow ranges for the ^1H signals of the Cp*-methyl protons and overlapping signals for the hexyne ligands, NMR analysis is not very conclusive. Furthermore, the number of Ni/E-atoms in a cluster core cannot be determined by NMR spectroscopy (especially for NMR silent nuclei). Analysis based on single crystal XRD, requires large single crystals of suitable quality, for adequate structure determinations. Moreover, the crystalized species might only represent a cut-out of the existing species in solution. However, mass spectrometric measurements of reaction solutions give valuable insights into the composition of diverse reaction mixtures. The LIFDI method was shown to mainly result in the formation of the molecular ion $[M]^+$ for $[TM_a(M'R)_bL_c]$ complexes and clusters.[49, 67] Usually only little fragmentation of these compounds is observed which allows the determination of the molecular cluster species based on their mass but also by the isotopic pattern. This enables the proper assignment of the elemental composition of reaction products in diverse reaction mixtures. However, it has to be noted, that the calibration of the LIFDI-spectrometer was not properly achieved during the course of the presented studies. Therefore, the masses usually deviate by 1-1.7 m/z depending on the mass range. The assignments of signals to respective species was therefore carefully performed based on the isotopic pattern. In addition, for MS-measurements less quantities of the reactants are necessary and faster screening to fine-tune proper reaction conditions is possible. However, a major problem of LIFDI-measurement is the lack of information about the relative quantity of different species in the reaction mixture. Only rough

estimations about the ratio of different compounds in a reaction mixture can be drawn, if comparable ionizability is assumed for different species.

V.3.2 Synthesis of $[Ni_4(GaCp^*)_4(EtCCEt)_2]$

The starting point for the synthetic access of $[Ni_a(GaCp^*)_b(EtCCEt)_c]$ was $[Ni(cod)_2]$ which was treated with different equivalents of 3-hexyne usually in toluene or benzene. Independent of the applied stoichiometry (1 eq, 3 eq, 5 eq, 10 eq of 3-hexyne), only two reaction products could be analyzed in the red solutions, namely $[Ni_2(cod)_2(hexyne)]$ (m/z: 415.21, calculated: 414.13 m/z) and $[Ni_3(cod)_2(hexyne)_2]$ (557.41 m/z, calculated: 556.74 m/z) besides the starting material $[Ni(cod)_2]$ (Figure 35).

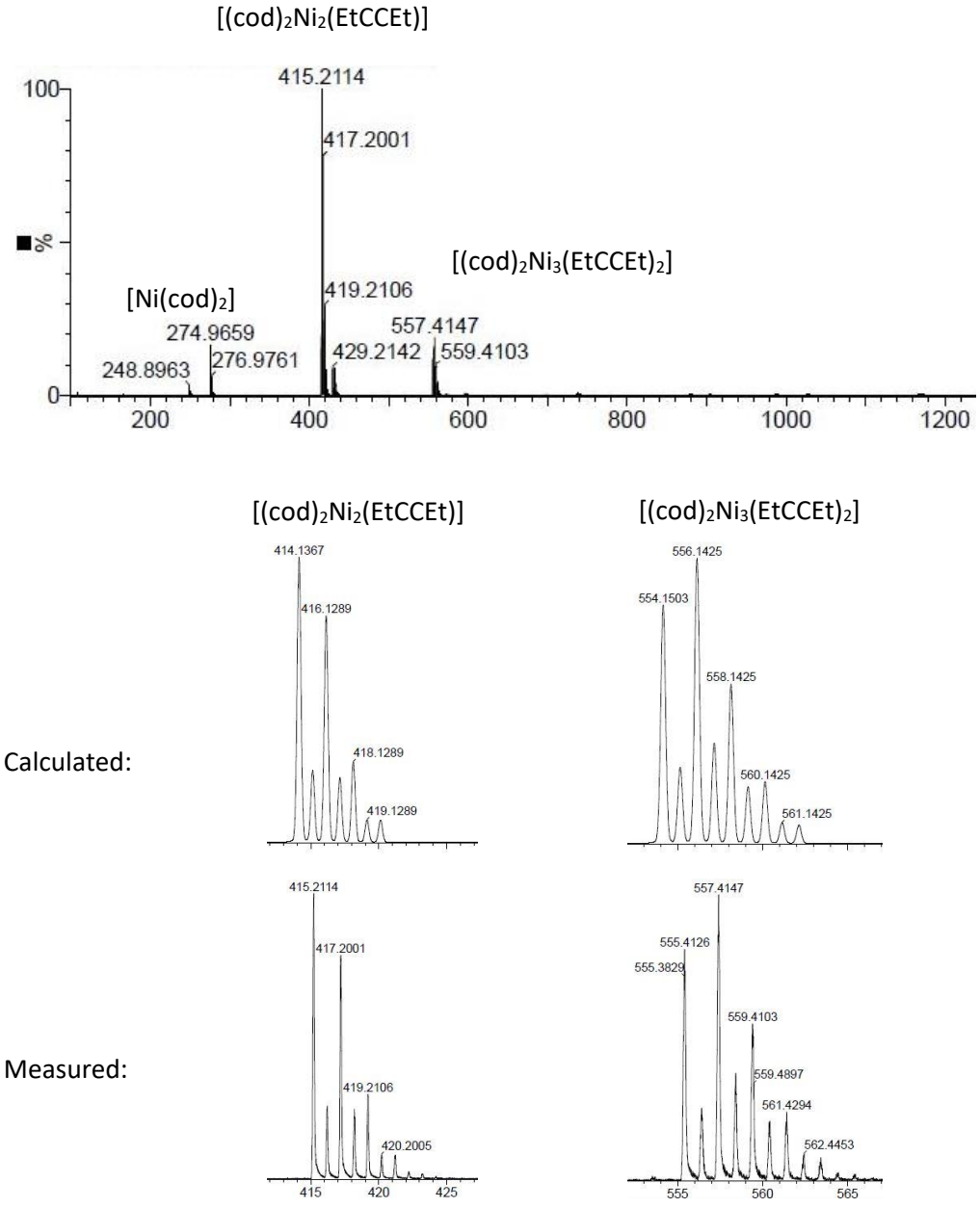

Figure 35: LIFDI-MS spectrum of the reaction of $[Ni(cod)_2]$ with 3 eq. 3-hexyne in toluene. In the reaction mixture, the signal patterns of $[Ni(cod)_2]$, $[(cod)_2Ni(EtCCEt)]$ and $[(cod)_2Ni_3(EtCCEt)_2]$ are present.

The ratio of the two reaction products in all reaction mixtures seemed to be independent of the applied equivalents, however as discussed above no reliable conclusions about product ratios can be drawn from LIFDI-MS measurements. Using pure 3-hexyne as "solvent" for $[Ni(cod)_2]$, dark reaction mixtures are obtained however no product species can be determined, indicating unselective decomposition. At a first glance, the Ni atoms in $[Ni_x(cod)_2(EtCCEt)_y]$ do not possess a saturated coordination environment, independent of the exact molecular structure. This might allow the formation of higher aggregates or further coordination of different ligands. DFT calculations reveal a central hexyne in a bridging coordination between two Ni(cod) moieties for $[Ni_2(cod)_2(EtCCEt)]$. The same structural motif was experimentally determined in $[Ni_2(cod)_2(PhCCPh)]$.[95] For $[Ni_3(cod)_2(EtCCEt)_2]$ a central $Ni(EtCCEt)_2$ with two coordinating Ni(cod) fragments was found to be a local minimum (Figure 36).

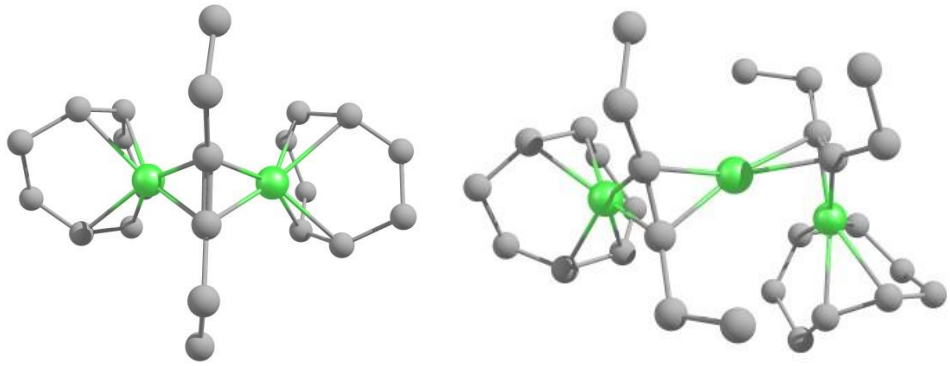

Figure 36: Calculated structures [BP86-D3/def2-TZVPP) of $[Ni_2(cod)_2(hexyne)]$ and $[Ni_3(cod)_2(hexyne)_2]$.

Treatment of reaction mixtures containing $[Ni_2(cod)_2(EtCCEt)]$ and $[Ni_3(cod)_2(EtCCEt)_2]$ with GaCp* results in the formation of different compounds, in dependence of the applied equivalents, reaction time and temperature (see Table 9).

Table 9: Summary of the reaction conditions and preliminary assignment of the observed species in the reaction solutions. As observed in chapter V.4.5. Cp* transmetallation from GaCp* to Ni may occur in $[Ni_aGa_b]$ clusters and should therefore also be considered in future studies on these compounds. The term "Ni8Ga6" will be explained in chapter V.4.5.

X [eq. EtCCEt]	Y [eq. GaCp*]	T [°C]	Observed species
3	1	20	923.78 ($[Ni_2(GaCp^*)_3(cod)(EtCCEt)]$, calc.: 922.17) 1219.94 ($[Ni_4(GaCp^*)_4(EtCCEt)_2]$, calc.: 1218.06)
3	5	20	879.83 ($[Ni(GaCp^*)_4]$, calc.: 878.11) 923.78 ($[Ni_2(GaCp^*)_3(cod)(EtCCEt)]$, calc.: 922.17) 1019.60 ($[Ni_2(GaCp^*)_4(EtCCEt)]$, calc.: 1018.12) 1219.66 ($[Ni_4(GaCp^*)_4(EtCCEt)_2]$, calc.: 1218.06)
3	5	110 5 min	879.83 ($[Ni(GaCp^*)_4]$, calc.: 878.11) 1019.60 ($[Ni_2(GaCp^*)_4(EtCCEt)]$, calc.: 1018.12) 1219.66 ($[Ni_4(GaCp^*)_4(EtCCEt)_2]$, calc.: 1218.06) 1650-1710 "Ni_8Ga_6"
1	1	20	819.55 (not identified) 879.83 ($[Ni(GaCp^*)_4]$, calc.: 878.11) 923.78 ($[Ni_2(GaCp^*)_3(cod)(EtCCEt)]$, calc.: 922.17) 1019.60 ($[Ni_2(GaCp^*)_4(EtCCEt)]$, calc.: 1018.12) 1137.67 (not identified) 1219.66 ($[Ni_4(GaCp^*)_4(EtCCEt)_2]$, calc.: 1218.06) 1401.86 (not identified) 1650-1710 "Ni_8Ga_6"

Figure 37 exemplarily shows the LIFDI-MS spectrum recorded after reaction of 5 eq. GaCp* (with respect to $[Ni(cod)_2]$) with $[Ni_2(cod)_2(EtCCEt)]$/$[Ni_3(cod)_2(EtCCEt)_2]$ after heating to 110°C for 5 min. The signals at 879.46 and 1219.66 m/z are most prominent in this spectrum. Based on their isotopic patterns, they can be assigned to $[Ni(GaCp^*)_4]$ (calc.: 878.10 m/z) and $[Ni_4(GaCp^*)_4(EtCCEt)_2]$ (calc.: 1218.06 m/z). The formation of literature known $[Ni(GaCp^*)_4]$[96] in reaction mixtures containing $[NiL_n]$ and GaCp* is not surprising. The formation of tetranuclear $[Ni_4(GaCp^*)_4(EtCCEt)_2]$ was at first sight unexpected. However, this compound can be seen as "dimeric" $[(cod)_2Ni_2(EtCCEt)]$, where the cod ligands are replaced by two GaCp* ligands that have a Ni-Ni bridging coordination between the two "monomers". Structure optimization (BP86-D3/def2-TZVPP) support the structural suggestion (Figure 38). Structural parameters are given below the calculated structure, but are not discussed in detail, due to the uncertainty of the structural suggestion (see also chapter V.4.6 Summary of $[Ni_2(\mu\text{-}GaCp^*)(\mu\text{-}GaNiCp^*)_2(dvds)_2]$.

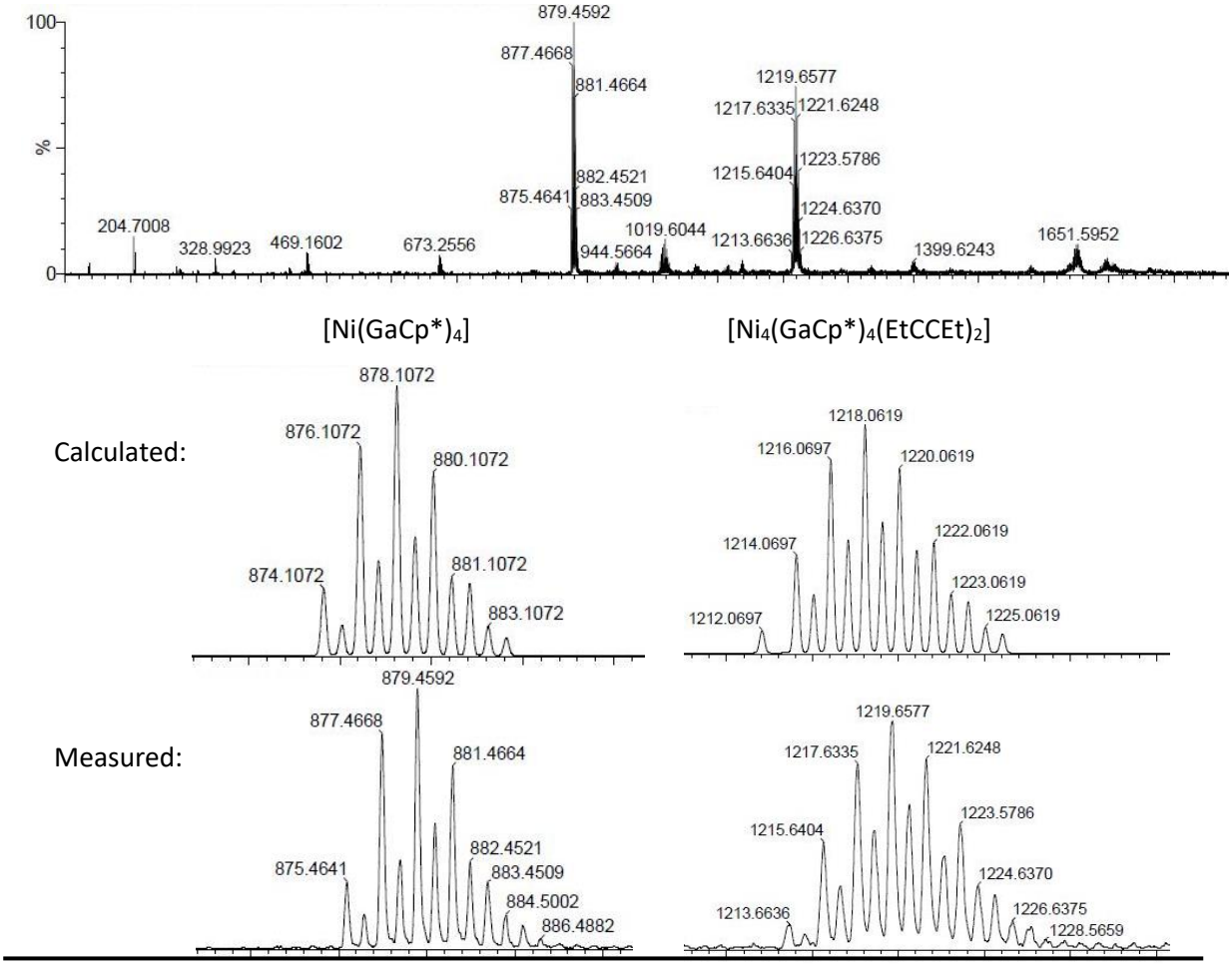

Figure 37: LIFDI-MS spectrum of the reaction mixture of $[Ni(cod)_2]$ treated with 3 eq. 3-hexyne at r.t. prior to the addition of 5 eq. GaCp*. The mixture was heated to 110°C for 5 min. The isotopic patterns of the two most intense signals are given below with the calculated isotopic patterns of $[Ni(GaCp^*)_4]$ and $[Ni_4(GaCp^*)_4(EtCCEt)_2]$ as comparison.

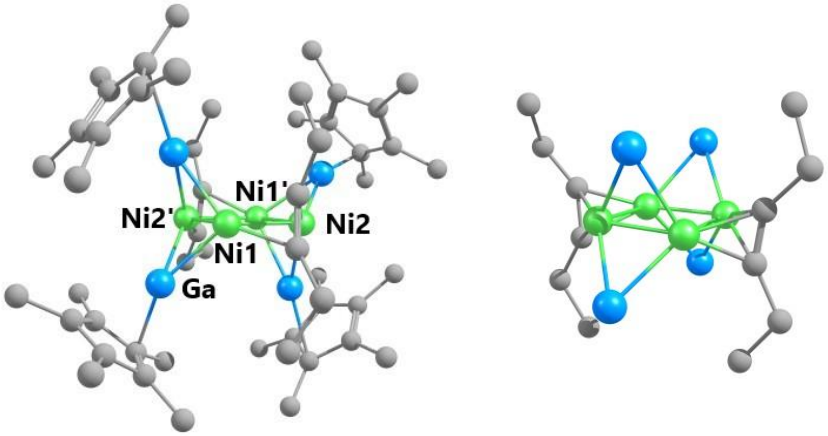

Figure 38: Calculated structure of $[Ni_4(GaCp^*)_4(EtCCEt)_2]$. This structure was confirmed to be a local minimum at the BP86-D3/def2-SVP level of theory. For a better visibility, the Cp* ligands were removed in the right structure. The possibility of a Cp* transmetallation from Ga to Ni observed for $[Ni_2(\mu\text{-}GaCp^*)(\mu\text{-}GaNiCp^*)_2(dvds)_2]$, has to be considered for subsequent investigations of $[Ni_4(GaCp^*)_4(EtCCEt)_2]$ as well. The depicted structure was optimized at BP86-D3/def2-TZVPP, but no frequency calculation could be performed at this level of theory. Bond distances [Å]: Ni1-Ni2: 2.40, Ni1-Ni2': 2.29, Ni-Ga: 2.34-2.41**,** Ni-$C_{C\equiv C}$: 1.93-2.00, C≡C: 1.34.

TM_2 bridging GaCp* motifs have already been described for other $[TM_a(ER)_b(L)_c]$ (TM = Ni, Pd, Pt; R = Cp*, DDP, L = PMe_3, CO, C_2H_4) compounds.[85, 97-98] The only precedence of a Ni_2 bridging GaR ligand is found in $[Ni_3(H)(C_2H_4)_2(C_2H_3)(GaDDP)_2]$ (DDP = 2-{(2,6-diisopropyl-phenyl)amino}-4-{(2,6-diisopropylphenyl)imino}-2-pentene). In addition to $[Ni_4(GaCp^*)_4(EtCCEt)_2]$, the reaction mixtures contain other $[Ni_a(GaCp^*)_bL_c]$ compounds of high nuclearity.

These preliminary results of only a few experiments reveal a divers chemistry of the Ni/Ga clusters and already indicate the formation of various $[Ni_a(M'R)_b(UHC)_c]$. These compounds are of special interest with regard to molecular models for semihydrogenation reactions. Furthermore, LIFDI-MS analysis together with quantum chemical calculations proofed to be very valuable for a fast screening of diverse reaction mixtures. This approach will help in future work to identify promising $[Ni_a(M'R)_b(UHC)_c]$ compounds. Furthermore, LIFDI-MS allows fast screening of reaction conditions leading to a selective synthesis of $[Ni_a(M'R)_b(UHC)_c]$ compounds. As shown above, the Ni/Ga ratio in compounds with low overall nuclearity can be assigned based on the isotopic patterns. Preliminary results by Patricia Heiß suggest, that especially for higher Ni amounts, the isotopic patterns do not significantly differ for close Ni/Ga ratios. Therefore, also the assignment of $[Ni_4(GaCp^*)_4(EtCCEt)_2]$ should be critically verified in future. Furthermore, the results in V .4.5 Synthesis and characterization of $[Ni_2(\mu\text{-}GaCp^*)(\mu\text{-}GaNiCp^*)_2(dvds)_2]$ proofed that Cp* transfer reactions should be considered for any Ni/Ga compound. The molecular ion peak generally observed in LIFDI-spectra however, do not contain any structural information. The new LIFDI-MS setup featuring a collision chamber with controllable N_2 pressure, might help to overcome this problem. Variations in the collision conditions could give the molecular ion peak at low N_2 pressure, whereas at elevated pressures the collisions lead to fragments which can

help to obtain structural information of the parent molecule. A definite assignment will only be possible for isolated and well characterized compounds using different analytical techniques including single crystal X-ray diffraction.

Ⅴ.3.3 Additional results for $[Ni_a(M'R)_b(UHC)_c]$ complexes

In addition to $[Ni(cod)_2]$ which was shown to be a promising starting material for the synthesis of $[Ni_a(M'R)_b(UHC)_c]$ compounds, also $[Ni_2(dvds)_3]$ and [Ni(cdt)] were subjected to reactions with 3-hexyne. Treatment of $[Ni_2(dvds)_3]$ with 0.5 eq. 3-hexyne and subsequent analysis with LIFDI-MS reveals only signals of the starting material $[Ni_2(dvds)_3]$. This observation can be explained by the flexibility of the dvds ligand in comparison to the more rigid cod ligand which leads to a thermodynamic stabilization of Ni-dvds bonding (see also chapter Ⅴ.4 Polynuclear $[Nia(M'R)_b]$ clusters for flexibility of dvds). However, the access of $[Ni_a(UHC)_c(dvds)_d]$ compounds should be tested in the future using more equivalents of 3-hexyne and or higher temperatures.

In the series of olefinic ligands dvds > cod > cdt, the cdt ligand is by far the least flexible ligand. Therefore, also [Ni(cdt)] is subjected to reactions with 3-hexyne. Indeed, treatment of [Ni(cdt)] with 1 eq. 3-hexyne in toluene solution and subsequent analysis by LIFDI-MS reveals a fascinating reaction mixture (Figure 39).

The observed peaks cannot be assigned so far. However, some preliminary ideas should be mentioned here:

The reaction mixture only contains Ni (M = 58.69 g/mol), cdt ($C_{12}H_{18}$, M = 182.28 g/mol), toluene (C_7H_8, M = 92.14 g/mol) and 3-hexyne (C_6H_{10}, M = 82.15 g/mol). If no bond activation takes place, the observed masses should fit to the molecular mass of a compound belonging to the general formula $[Ni_a(C_{12}H_{18})_b(C_7H_8)_c(C_6H_{10})_d]$ (with a possible uncertainty of ± 3 a.m.u, due to the unsolved calibration problem at the time of the measurement). The molecular formulas summarized in Table 10 would therefore fit to the signal with the highest intensity at 1010.2 a.m.u.

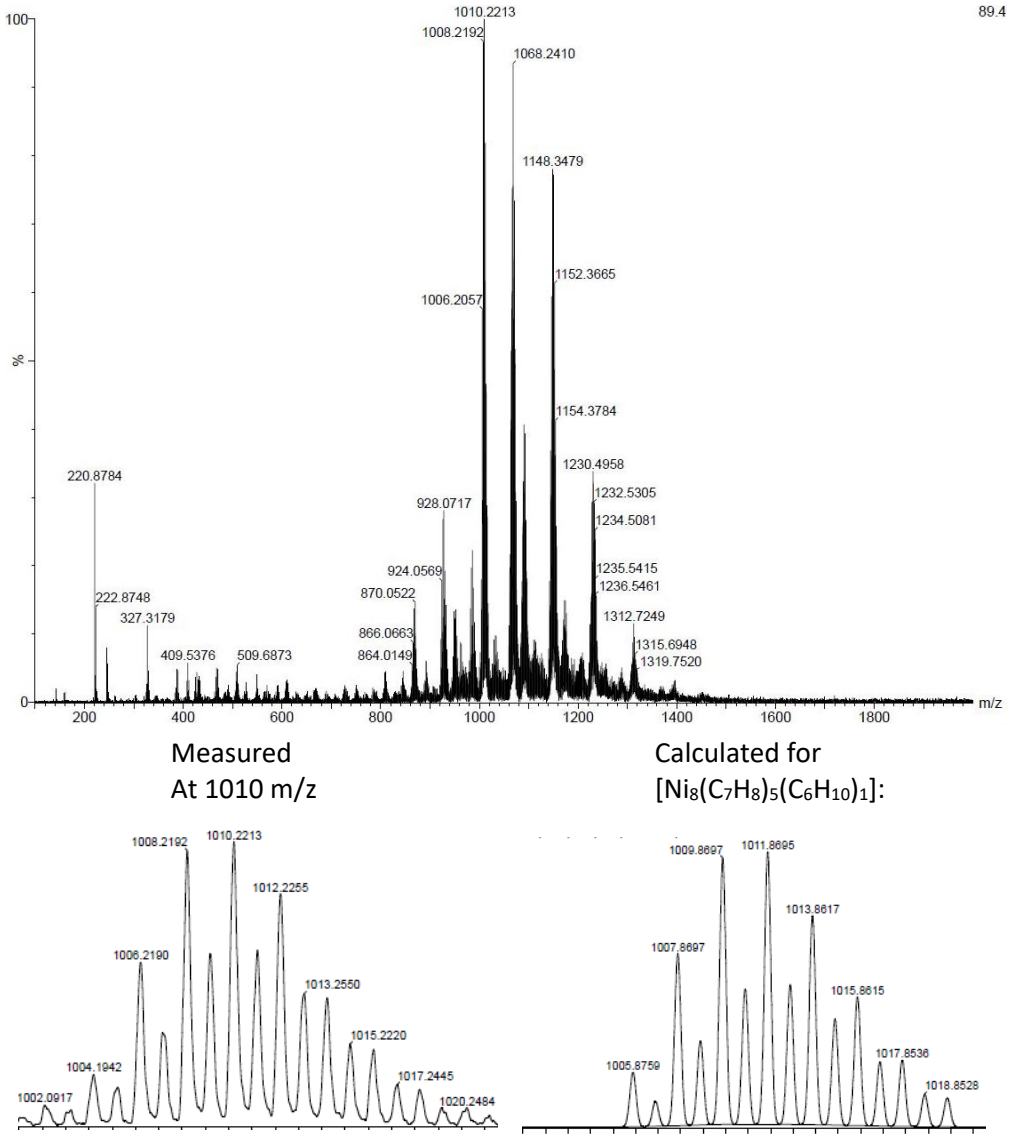

Figure 39: LIFDI-MS spectrum of the reaction of [Ni(cdt)] with 1 eq. 3-hexyne in toluene. A concluding assignment of the reaction products has not been achieved so far. The inset shows the isotopic pattern of the signal at 1010 m/z compared to the calculated isotopic pattern of $[Ni_8(C_7H_8)_5(C_6H_{10})_1]$.

Table 10: Compounds that fit to the general formula $[Ni_a(C_{12}H_{18})_b(C_7H_8)_c(C_6H_{10})_d]$ within the molecular mass range 1010 ± 3 g/mol.

Compound $[Ni_a(C_{12}H_{18})_b(C_7H_8)_c(C_6H_{10})_d]$	Molecular mass [g/mol]
$[Ni_6(C_{12}H_{18})_1(C_6H_{10})_6]$	1007.3
$[Ni_3(C_7H_8)_1(C_6H_{10})_9]$	1007.5
$[Ni_5(C_{12}H_{18})_5(C_6H_{10})_1]$	1008.9
$[Ni_6(C_6H_{10})_8]$	1009.3
$[Ni_2(C_{12}H_{18})_5(C_6H_{10})_1]$	1010.9
$[Ni_3(C_{12}H_{18})_3(C_7H_8)_2(C_6H_{10})_2]$	1011.5
$[Ni_4(C_{12}H_{18})_1(C_7H_8)_4(C_6H_{10})_3]$	1012.1
$[Ni_8(C_7H_8)_5(C_6H_{10})_1]$	1012.4
$[Ni_6(C_{12}H_{18})_3(C_7H_8)_1(C_6H_{10})_1]$	1013.3

A simple guess would render $[Ni_6(C_6H_{10})_8]$ as the most suitable compound. However, the observed isotopic pattern does not match to the calculated pattern of a Ni_6 species. It has to be mentioned, that the isotopic pattern is largely determined by the amount of Ni atoms but is rather unaffected by changes in the C/H ratio. Only the Ni_8 cluster $[Ni_8(C_7H_8)_5(C_6H_{10})_1]$ reproduces the measured isotopic pattern quite well (Figure 39 inset). Therefore, the signal with the highest intensity should be assigned to a Ni_8 species. However, the estimated 5 toluene ligands are in contrasts with chemical intuition. First, [Ni(cdt)] is reasonably stable in toluene solution and second the Ni-toluene bond is believed to be rather unstable. As mentioned a definite assignment of a molecular formula is not possible based on the performed experiment. However, the assumption of a Ni_8 cluster seems to be valid. This is also supported by the signal at 1068 m/z. It is separated from the signal at 1010 m/z by the mass of one Ni atom. Indeed, the isotopic pattern at 1068 would also fit to the assumption of a Ni_9 cluster. The signal at 1148 is separated by 80 g/mol from the Ni_9, which is about the mass of a hexyne moiety ($M(C_6H_{10})$ = 82.15 g/mol). However, the isotopic pattern does not fit to a Ni_9 species but to a Ni_{10} species of the approximate sum formula $[Ni_{10}(C_{42}H_{59})]$. The signal at 1230 m/z most probably represents a Ni_{12} cluster of the approximate sum formula $[Ni_{12}(C_{39}H_{59})]$.

Of course, the uncertainty of the calibration hampers a reliable proposition of the observed species in solution. The assumption of several Ni_a $[Ni_aC_xH_y]$ species seems to be valid based on the differences in the isotopic patterns. Further experiments applying different reaction conditions (equivalents, concentration, temperature, etc.) could help to shed more light on the elusive species formed in

solution. To address the questions weather toluene ligands are present in the Ni_a clusters, the reaction should be repeated in toluene-d_8 or n-hexane. Furthermore, changing 3-hexyne to 2-pentyne could also lead to further indications about the species in solution. Furthermore, also the possibility of bond activation reactions should be considered. In this regard only recently a Ni_5 cluster was shown to split olefinic C=C double bonds leading to the incorporation of a carbon atom into the cluster core.[99]

At this stage of knowledge of the $[Ni_aC_xH_y]$, quantum chemical calculations are only of limited since no suitable starting geometry can be deduced from the experimental results. However, if the assignment of the nuclearity Ni_a and the number and nature of the organic ligands can be definitely assigned, quantum chemical calculations can be a helpful tool for ongoing investigations.

V.3.4 Summary and outlook for $Ni_a(M'R)_b(UHC)_c]$

It can be concluded that early-stage functionalization of common Ni precursors with 3-hexyne leads to several promising compounds. $[Ni_a(cod)_2(EtCCEt)_c]$ are viable precursors for the formation of $[Ni_a(M'R)_b(EtCCEt)_c]$compounds like e.g. $[Ni_4(GaCp^*)_4(EtCCEt)_2]$. Variation of reaction parameters (time, equivalents, temperature) and the use of AlCp* or other UHC's will lead to a diverse library of $[Ni_a(ECp^*)_b(UHC)_c]$ compounds. Respective ZnR containing compounds could be accessed by treatment of $[Ni_a(ECp^*)_b(UHC)_c]$ with $ZnMe_2$, expanding the library to $[Ni_a(ZnR)_b(UHC)_c]$ compounds. Based on these results, a universal synthetic access to a diverse library of $[Ni_a(M'R)_b(UHC)_c]$ can be envisioned. Polynuclear $[Ni_aC_xH_y]$ clusters obtained by treatment of [Ni(cdt)] with 3-hexyne would be very interesting compounds. They exhibit quite large Ni_a cluster cores that are only stabilized by weakly coordinating ligands (only cdt, 3-hexyne and toluene are present in the reaction mixture). Therefore, those compounds are of special interest for further treatment with ECp* ligands. Due to a recent publication presenting the unprecedented splitting of C=C double bonds by a Ni_5 cluster (Figure 40) also C-H or CC bond activation reactions should be considered.[99]

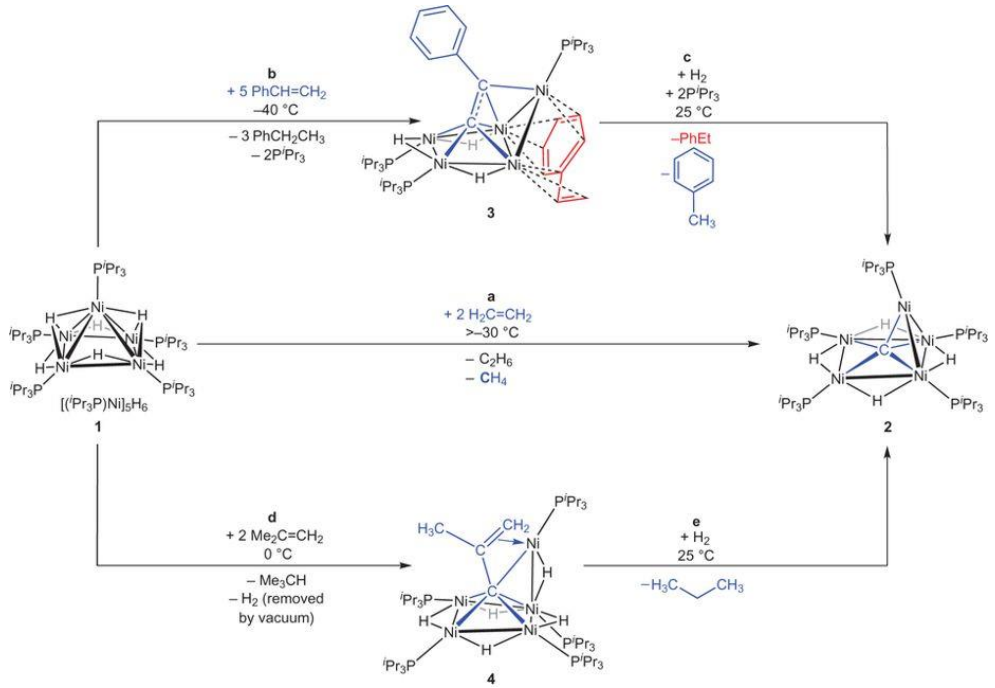

Figure 40: C=C double bond activation by a Ni_5 cluster leading to the incorporation of a single C atom into the Ni_5 cluster core. Similar cooperative C-C or C-H activation reactions could potentially explain the nature of the $[Ni_aC_xH_y]$ clusters obtained by treatment of [Ni(cdt)] with 3-hexyne. To proof this assumption a detailed experimental and quantum chemical investigation has to be performed. Reprinted with permission from Shoshani *et al.*, Nat. Chem. **2018,** 9, 1282. Copyright 2018 Springer Nature.

Furthermore, LIFDI-MS analysis proofed to be a reliable analytical tool to get profound insights into diverse product mixtures in solution, without the need of laborious purification processes. Of course,

the bad calibration so far has hampered the definite assignment of signals. The new calibration method which at least allows the calibration of a specific mass range, but especially the new LIFDI-MS setup that will be used in our group in the future will be very helpful to conquer this problem. Starting from these results, the number of observed $[Ni_a(M'R)_b(UHC)_c]$ compounds can be easily increased by variation of the reaction parameters (time, equivalents, temperature) and of course also by the nature of ECp* and UHC. The future LIFDI-MS analysis work should also include isotopic labeling experiments (toluene vs. toluene-d_8) and the use of similar UHC compounds (3-hexyne, vs. 2-pentyne) to get a deeper insight into doubtable product compositions as observed for example for the $[Ni_aC_xH_y]$ clusters. Due to the valid expectation of diverse reaction pathways occurring in such reaction solutions (ligand replacement, bond activation reactions, Cp* transfer reaction, see V .4.5 Synthesis and characterization of $[Ni_2(\mu\text{-}GaCp^*)(\mu\text{-}GaNiCp^*)_2(dvds)_2]$, etc) future LIFDI-MS studies will also face puzzling experimental results at first sight. However, unpredictable reactivities could lead to fascinating findings in future work. The combination of experimental LIFDI-MS and theoretical calculations on the DFT-level of theory has shown to give complementary insights into diverse reaction solutions. However, the choice of a reasonable starting geometry for the calculation of $[Ni_a(ECp^*)_b(UHC)_c]$ has to be based on profound structural knowledge of similar $[Ni_a(ECp^*)_b(UHC)_c]$ and $[Ni_a(ECp^*)_b]$ compounds, especially with regard to unexpected reactions. Furthermore, detailed studies of the interaction of UHC moieties with $[Ni_a(ECp^*)_b]$ fragments requires an elaborate understanding of the bonding principles of high nuclear $[Ni_a(ECp^*)_b]$ clusters. Therefore, the isolation, complete characterization and bonding analysis of selected $[Ni_a(ECp^*)_b(EtCCEt)_c]$, $[Ni_a(ECp^*)_b]$ and $[TM_a(ECp^*)_b(UHC)_c]$ in general will still be necessary in the future.

Ⅴ.4 Polynuclear $[Ni_a(M'R)_b]$ clusters

Ⅴ.4.1 Introduction to $[Ni_a(M'R)_b]$ clusters

Structural prototypes for $[Ni_a(M'R)_b(EtCCEt)_c]$

Experimental studies on polynuclear $[Ni_a(M'R)_b(UHC)_c]$ and concomitant investigations of the underlying bonding principles of $[Ni_a(M'R)_b]$-(UHC) interactions require detailed knowledge of structural motifs and bonding properties of similar polynuclear $[Ni_a(M'R)_b]$ clusters. A diverse library of $[TM_a(M'R)_b(L)_c]$ clusters proofs that ECp* and ZnR represent viable ligands to stabilize higher nuclear $[TM_a]$ clusters. The ECp* and ZnR ligands can adopt terminal or bridging coordination efficiently stabilizing the $[TM_a]$ core, by TM-M interactions and effective kinetic shielding due to the bulky Cp* ligands.[1, 47, 49, 68, 100-102] However, there is only limited precedence of $[Ni_a(M'R)_b(UHC)_c]$ and $[Ni_a(M'R)_b]$ compounds. These include $[Ni_2(C_2H_4)_x(GaDDP)]$ (x = 3, 4), $[Ni_2(GaDDP)(cod)(PhCCPh)_2]$ and $[Ni_3(C_2H_4)_3(GaDDP)_2]$. The latter compounds feature GaDDP ligands in bridging coordination to a Ni_2-dimer, and side-on as well as Ni_2-bridging UHC moieties.[56] Furthermore, in the dissertation of Tobias Steinke the synthetic access of $[Ni_2(ECp^*)_3(C_2H_4)_2]$[54] was described, however up to date no publishable molecular structure determination was possible, due to bad crystal quality. From preliminary structure determination, the ECp* ligands are estimated to adopt bridging positions on the $[(C_2H_4)Ni$-$Ni(C_2H_4)]$dimer. Treatment of $[Ni_2(ECp^*)_3(C_2H_4)_2]$ with $ZnMe_2$ lead to the formation of $[(\eta_5\text{-}Cp^*)$-$Ni_2(ZnMe)_6(ZnCp^*)(ZnCp^*)]$. Besides the loss of weakly bound C_2H_4, this reaction involves E/Zn exchange and Cp* transfer from M'Cp* to Ni. In this compound, the Ni_2 dimer is bridged by four ZnMe ligands.[67] The assignment of Ni_2 bridging ECp* ligands in $[Ni_2(ECp^*)_3(C_2H_4)_2]$ is supported by the molecular structures of $[TM_2(ECp^*)_3L_2]$ and $[TM_2(ECp^*)_5]$ (TM = Pd, Pt, L = CO, PPh_3, CN^tBu).[98] However, the homologous compounds $[Ni_2(ECp^*)_5]$, have not been described so far. In general, $[TM_2(ECp^*)_5]$ clusters are of special interest for two reasons. In contrast to the respective $[TM(ECp^*)_4]$ homologues, the ECp* ligands in $[Pd/Pt_2(ECp^*)_5]$ were shown to be kinetically labile and involved in fluxional processes allowing ligand replacement reactions at the transition metal centers.[98] Furthermore $[TM_2(ECp^*)_5]$ form the simplest members in the series of high nuclear $[TM_a(ECp^*)_b]$ clusters. Therefore, the TM-TM and TM-E interactions in these compounds can be seen as the "prototypes" for bonding interactions in polynuclear $[TM_a(ECp^*)_b]$. An early quantum chemical study on $[Pt_2(GaCp^*)_5]$ (d(Pt-Pt): 2.58 Å, twofold covalent radius for Pt: 2.76 Å) described the Pt-Pt interaction as resulting from weak d^{10}-d^{10} interactions based on NBO and QTAIM analysis.[103] In contrast to this finding, iso-structural and iso-valence-electronic $[Ni_2(CO)_5]$ was described as featuring a Ni-Ni triple bond. R. Bruce King *et al.*

theoretically analyzed (on the DFT level, BP86/DZP) the Ni-Ni bonding in the $[Ni_2(CO)_x]$ series (x = 7: formal Ni-Ni single bond, x = 6 formal Ni-Ni double bond, x = 5 formal Ni-Ni triple bond).[104] It was found that $[Ni_2(CO)_5]$ would be surprisingly stable with respect to dissociation (in contrast to x = 6, 7). The calculated short Ni-Ni distance of 2.19 Å in $[Ni_2(CO)_5]$ would be well below the twofold covalent radius of Ni (2.48 Å). In a different approach Pyykkö *et al.* determined the single bond covalent radius for the elements 1-118. The Ni-Ni single bond radius was determined to 2.20 Å- the calculated Ni-Ni distance in $[Ni_2(CO)_5]$. Despite the largely studied field of Ni carbonyl clusters[105], no experimental indications for $[Ni_2(CO)_5]$ are present in literature.[106-107] Interestingly $[Ni_2(CO)_5]$ is not only iso-valence-electronic (30 valence electrons) to the isolated $[M_2(ECp^*)_5]$ compounds but it is also predicted to be isostructural to $[TM_2(ECp^*)_5]$ with three bridging and two terminal ligands. Therefore, some questions arise that we want to address: Despite the existence of $[Ni(CO)_4]$, $[Ni(ECp^*)_4]$[8] and $[M_2(ECp^*)_5]$[97-98, 103], no dimeric $[Ni_2L_5]$ compound has been obtained so far. i) Can $[Ni_2(ECp^*)_5]$ be synthesized and what would be its structure? ii) How can the Ni-Ni bonding be described? What is the effect of the CO and ECp* ligands on TM-TM bonding? iii) What can be learned regarding the bonding in higher nuclear clusters?

The syntheses of the related compounds $[Pd_2(ECp^*)_5]$ and $[Pt_2(ECp^*)_5]$ were accomplished by different strategies (Figure 41).[97-98, 103, 108] Ligand substitution starting from organometallic precursors like $[Pd_2(dvds)_3]$ or $[Pt(C_2H_4)_3]$ with GaCp* followed by dimerization processes is the most feasible synthetic route. Additionally, treatment of higher nuclear clusters like $[Pd_3(GaCp^{*Ph})_4(dvds)]$ with $GaCp^{*Ph}$ results in selective cluster "decomposition" yielding $[Pd_2(GaCp^{*Ph})_5]$. Another interesting access represents the dimerization of $[Pd(cod)_2]$ and $[Pd(GaCp^*)_4]$.

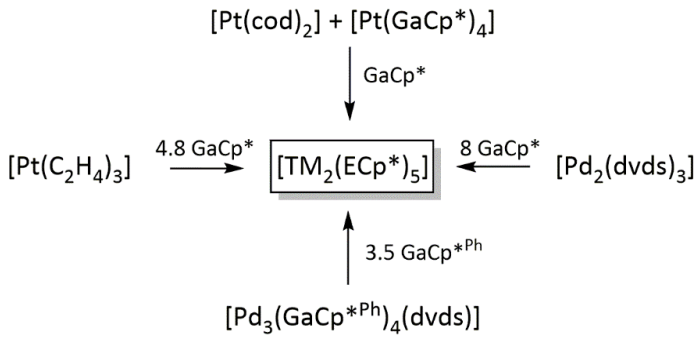

Figure 41: Established syntheses of $[TM_2(ECp^*)_5]$ (TM = Pd, Pt).

V.4.2 Synthesis and characterization of $[Ni_2(AlCp^*)_5]$

The first $[Ni_2L_5]$ compound

A journal manuscript dealing with $[Ni_2(AlCp^*)_5]$ is currently under preparation. The theoretical bonding analysis was performed in close collaboration with the group of Prof. J.-Y. Saillard, Rennes, France.

Synthesis of $[Ni_2(ECp^*)_5]$ was not possible via the reaction of $[Ni(GaCp^*)_4]$ and $[Ni(cod)_2]$. Therefore, the access was tested via literature known $[Ni_2(dvds)_3]$.[109] Cooling of a concentrated hexane solution to -30°C affords single crystals suitable for X-ray analysis (Figure 42).

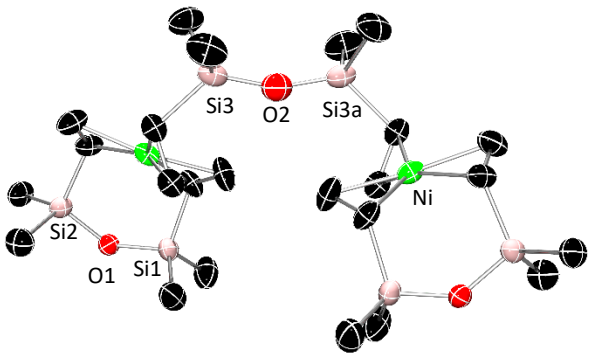

Figure 42: Molecular structure of $[Ni_2(dvds)_3]$ (displacement ellipsoids shown on the 50% probability level, hydrogen atoms omitted for clarity). Selected interatomic distances (Å) and angles (deg): Ni – C: 2.021(12) – 2.107(10), Si – O: 1.6150(9) - 1.6424(15), Si1 – O1 – Si2: 129.33(9), Si3 – O2 – Si3a: 159.77(19).

The analysis of the long orange needles proves the dimeric structure with one bridging dvds ligand as also found for $[Pt_2(dvds)_3]$.[110] The dvds ligand offers huge coordination flexibility, due to the conformational freedom of the alkene moieties and the flexibility of the Si-O-Si backbone (range of Si-O-Si angles (129.33(9) – 159.77(19)°).

Treatment of a toluene solution of $[Ni_2(dvds)_3]$ with 3 eq. AlCp* at 70°C results in the formation of different $[Ni_a(ECp^*)_b(dvds)_c]$ compounds as evidenced by LIFDI measurements of the reaction solutions (see Figure S 23) Treatment of the same reaction solution with additional 3 eq. AlCp*, LIFDI-MS analysis shows the formation of $[Ni(AlCp^*)_4]$ (707.60 m/z, calculated for $NiAl_4C_{40}H_{60}$: 707.54 m/z) and $[Ni_2(AlCp^*)_5]$ (926.23 m/z, calculated for $Ni_2Al_5C_{50}H_{75}$: 928.44 m/z) (see Figure S 25). This reaction indicates the "decomposition" of higher nuclear Ni_x clusters by treatment with additional AlCp* as also described above for $[Pd_3(GaCp^{*Ph})_4(dvds)]$.[108]

Using 6 eq. AlCp* and heating to 75°C for 15 min, the reaction mixture turns from orange to deep red. Recrystallisation from n-hexane affords $[Ni_2(AlCp^*)_5]$ in pure form. The ^{1}H-NMR of the isolated product in C_6D_6 exhibits two signals in the expected range for Ni-AlCp* protons[8, 60-61, 68] at 2.01 and 1.97 ppm with a signal ratio of 2:3 indicating the existence of two distinct AlCp* groups (see Figure S 24). Measurements at elevated temperatures (90°C in toluene-d_8) does not lead to a coalescence of these signals. The ^{13}C-NMR signals are in accordance to the ^{1}H-NMR showing two sets of signals for the distinct AlCp* groups (see Figure S 26). LIFDI-MS measurement of the isolated compound confirms the crystallization of $[Ni_2(AlCp^*)_5]$, showing the $[M]^+$ ion peak at m/z = 926.2 with the expected isotopic pattern (Figure 43 a). Here, the calculated and measured LIFDI-MS signals match quite well, since the spectrometer was externally calibrated to a polystyrene signal at the specific mass range of $[Ni_2(AlCp^*)_5]$. Single crystal X-Ray measurement unambiguously verifies the isolation of $[Ni_2(AlCp^*)_5]$ (Figure 43 b).

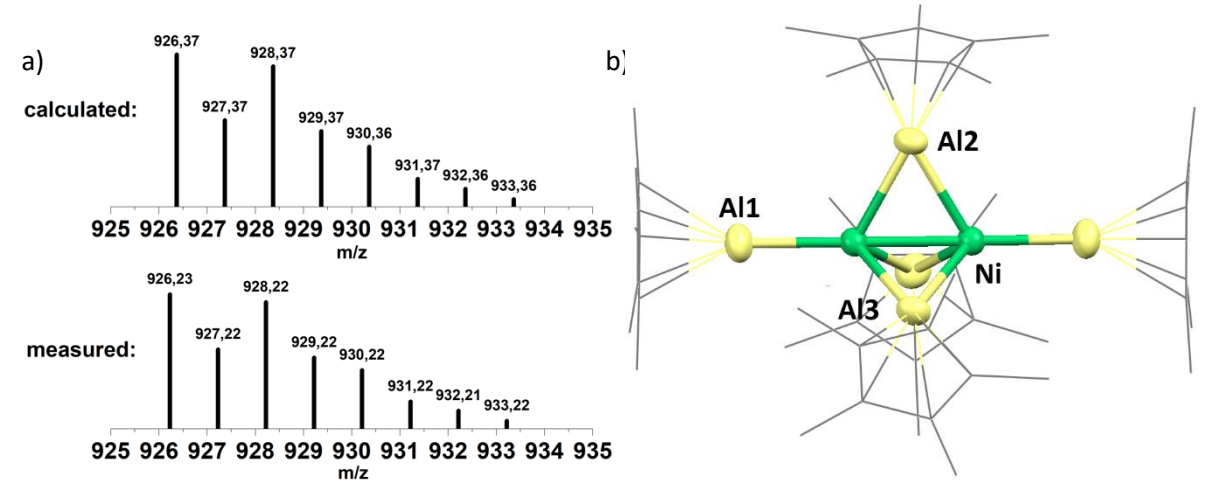

Figure 43: a) Comparison of the calculated isotopic pattern of $[Ni_2(AlC_{10}H_{15})_5]$ (top) to the measured LIFDI- MS spectrum of the isolated solid showing $[M]^+$ = 926 m/z (bottom).
b) Molecular structure of $[Ni_2(AlCp^*)_5]$. Ellipsoids are shown at the 50% probability level. H atoms and disorders are omitted for clarity. Bond lengths [Å] and angles [°]: Ni-Ni = 2.2702(15), Ni-Al1 = 2.2309(16), Ni-Al2 = 2.3088(12), Ni-Al3 = 2.3209(16), Al1-Cp*$_{Centroid}$ = 1.946, Al2-Cp*$_{Centroid}$ = 1.940, Al3–Cp*$_{Centroid}$ = 1.940, Al1-Ni-Ni = 179.13(2), Al1-Ni-Al2 = 118.90(4), Al1-Ni-Al3 = 120.11(3).

Indeed, $[Ni_2(AlCp^*)_5]$ is isostructural to the already known $[TM_2(ECp^*)_5]$[98] compounds and the calculated $[Ni_2(CO)_5]$[104], having three bridging and two terminal ligands at the central Ni-dimer. The Ni-Ni distance of 2.2702(15) Å is considerably shorter (about 8%) than twice the covalent radius of Ni (2.48 Å) and only slightly longer than the predicted Ni-Ni distance in $[Ni_2(CO)_5]$ (2.20 Å), hinting to the presence of Ni-Ni interactions. The Ni-AlCp*$_{terminal}$ distances of 2.2309(16) Å are in the range of other Ni-AlCp* distances[85], whereas the Ni-AlCp*$_{bridging}$ distance is slightly longer with 2.31 Å (average). The Al-Cp*$_{centroid}$ distances are independent of the bonding mode of the AlCp* ligands and with about 1.94

Å comparable to literature known values.[85, 98] Following the structural discussion, the nature of the short Ni-Ni contact should be discussed. Considering the closely related $[Ni_2(CO)_n]$ (n = 7, Ni-Ni: 2.73 Å; n = 6, Ni-Ni: 2.56 Å; n = 5, Ni-Ni: 2.19 Å;), the shortening of the Ni-Ni distance is most pronounced going from n = 6 to n = 5. In $[Ni_2(CO)_5]$, the Ni-Ni distance of 2.19 Å is about 12% shorter compared to the covalent radius.[104] One could argue that this is an effect of the increasing number of bridging CO ligands. In $[Fe_2(\mu_2\text{-}CO)_3(CO)_6]$, (34 valence electrons, formal Fe-Fe single bond), the Fe-Fe distance of 2.531(1) Å[111] is only about 4% shorter compared to the twofold covalent radius of Fe (2.64 Å) despite the three bridging CO ligands. Also for $[\{Ni(CNtBu)_2(\mu_2\text{-}ZnCp^*)(\mu_2\text{-}ZnMe)\}_2]$ featuring four bridging ZnR ligands, the Ni-Ni is with 2.572(1) Å well above the Ni-Ni covalent interaction.[59] Therefore, the short Ni-Ni distance in $[Ni_2L_5]$ could be based on a delicate balance of several effects including the bridging ECp* as well as Ni-Ni bonding interactions. In addition, for the large ECp* ligands, also steric contributions and dispersion forces should be considered.

V.4.3 Theoretical investigation on the Ni-Ni bonding in $[Ni_2(AlCp^*)_5]$ and $[Ni_2(CO)_5]$

The following paragraph is based on a manuscript which was in part written by J.Y. Saillard.

To shed more light on the bonding situation of these $[TM_2L_5]$ compounds, an extensive theoretical investigation was performed. $[Ni_2(AlCp^*)_5]$ (HOMO-LUMO gap: 2.13 eV) was optimized at the DFT-level of theory (BP86-D3(BJ)/TZ2P). The structural parameters compare reasonably well between experiment and theory. For example, the Ni-Ni distance in $[Ni_2(AlCp^*)_5]$ was calculated to 2.347 Å which is slightly longer than the experimental value of 2.2702(15) Å. This deviation could be a result of a shallow potential energy surface of with regard to the Ni-Ni distance (see Figure S 27). The predicted Ni-AlCp*$_{terminal}$ and Ni-AlCp*$_{bridging}$ values are with 2.23 Å and 2.32 Å (average) in accordance to experimental values. For comparison, $[Ni_2(CO)_5]$ was recalculated using the same level of theory. The D_3h structure with three bridging and two terminal CO ligands was confirmed to be a local minimum with a Ni-Ni distance of 2.232 Å, slightly longer than the value of 2.20 Å obtained by King *et. al*.[104]
NBO analysis of $[Ni_2(AlCp^*)_5]$ reveals that the Ni atoms are negatively charged (-0.42 e) whereas the Ni atoms are positively charged (0.33 e) in $[Ni_2(CO)_5]$. This can be explained by the better π-accepting properties of CO compared to AlCp* leading to a significant charge relocation to the CO ligands. For both compounds $[Ni_2(AlCp^*)_5]$ and $[Ni_2(CO)_5]$ QTAIM analysis reveals bond critical points and bond paths for the Ni-Ni interaction (Figure 44).

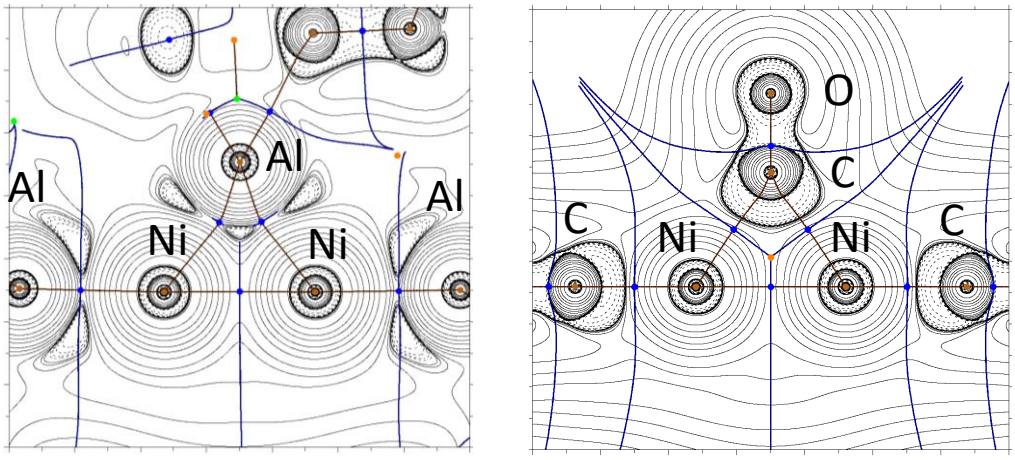

Figure 44: Plots of the Laplacian of electron density of $[Ni_2(AlCp^*)_5]$ and $[Ni_2(CO)_5]$. Solid lines indicate areas of charge concentration and dotted lines indicate areas of charge depletion. The solid brown lines connecting atoms are bond paths and the blue points resemble bond critical points. The orange dots indicate (-3;+1) ring critical points.

Comparing the curvature of the bond path between the Ni_2 dimer and the briging ligand L a significant difference becomes obvious. The Ni-AlCp* bond path is inwardly curved in agreement to the estimation of a large Al→Ni_2 σ-contribution. In contrast, the Ni-CO bond path is oudwartly curved

which suggests higher contributions of $Ni_2 \rightarrow CO$ π* donation.[26] The Ni-Ni Wiberg bond indices for both compounds $[Ni_2(AlCp^*)_5]$ and $[Ni_2(CO)_5]$ were predicted to 0.1.

The short Ni-Ni distance and the existence of BCP's suggest significant Ni-Ni interactions for $[Ni_2(AlCp^*)_5]$ and $[Ni_2(CO)_5]$. However, no formal bond description can be derived from these results. In the following a simplified molecular orbital-based approach for the bonding in $[Ni_2(CO)_5]$ shall be developed. Subsequently the changes upon incorporation of AlCp* instead of CO will be highlighted. The bonding description of $[Ni_2(CO)_5]$ can be developed starting from the crude MO diagram illustrating the interaction between (CO)-Ni…Ni-(CO) and the bridging $(\mu\text{-CO})_3$ fragment (Figure 45).

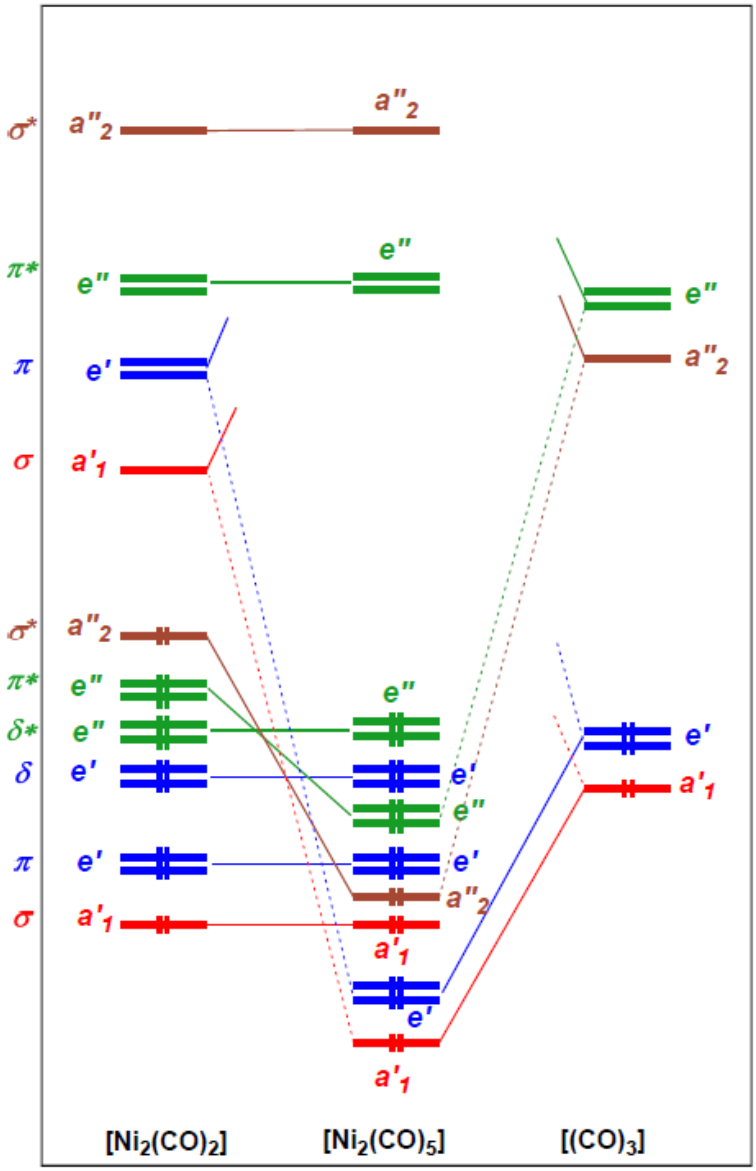

Figure 45: Simplified interaction MO diagram for $Ni_2(CO)_5$. Only the 2-orbital/2-electron bonding interactions are considered. The energy scale is arbitrary.

Figure 45 only represents the 2-orbital/2-electron stabilizing interactions, which are principally associated with the bonding between the two fragments. For the sake of simplicity, secondary interactions associated with intermixing between several orbitals of same symmetry are neglected in this first step. The (CO)-Ni…Ni-(CO) frontier orbitals are the in-phase and out-of-phase combinations of the five 3d(Ni) AOs as well as the vacant $4p_\pi$(Ni) AOs and sp(Ni) hybrids. The frontier orbitals of the $(\mu\text{-CO})_3$ fragment are the combinations of the three σ-lone pairs ($a'_1 + e'$) and the three π^*(CO) orbitals which are parallel to the Ni-Ni vector. The three other π^*(CO) orbitals, perpendicular to the Ni-Ni vector, are involved in C=O bonding and thus not considered at this stage of the analysis. The carbonyl $a'_1 + e'$ lone pairs interact in a bonding way with the vacant sp(Ni) and $4p_\pi$ combinations of the same symmetry. The vacant $a''_2 + e''$ π^*(CO) combinations interact in a bonding way with the occupied 3d(Ni) combinations of δ^* and σ^* nature. As a result, six occupied metal-ligand bonding MOs are built ($a'_1 + e' + a''_2 + e''$), to which the corresponding six antibonding vacant counterparts exist. These six bonding electron pairs are associated with the six Ni-(μ-CO) bonds. The other occupied MOs of $[Ni_2(CO)_5]$ are non-bonding with respect to metal-ligand interactions, but with respect to Ni-Ni interactions they are of σ, π, δ and π^* character. Whereas the occupation of both π and π^* cancels π bonding (four ($e' + e''$) π lone pairs), one may wonder about σ and δ bonding. Within a localized 2-center 2-electron scheme one σ and two δ bonds would require the existence of vacant σ^* and δ^* MOs, associated with their occupied bonding components. It turns out that this is not the case since the σ^* and δ^* counterparts are formally occupied and participate in metal-ligand bonding. Thus, the electrons occupying the 3d-type levels of σ and δ character should rather be considered as metal lone pairs. From the strict point of view of a localized 2-center 2-electron bonding description, the MO diagram depicted in Figure 45 corresponds to a $[Ni_2(CO)_5]$ Lewis structure without Ni-Ni bond.

It could be argued that the vacant e" and $a"_2$ MOs are in fact the "missing" σ^* and π^* counterparts of the occupied σ and π levels, thus completing the MO panel for a localized triple bond. However, a look at the participation of the 4s(Ni) and 4p(Ni) AOs to the occupied orbitals of the (CO)Ni…Ni(CO) fragment indicates minor involvement in metal-metal bonding.

Substantial through-bond Ni-Ni interactions are however present. They occur from the mixing of the σ^* and δ^* orbitals with their ligand counterparts. This mixing leads to partial depopulation of these metal-metal antibonding levels, thus creating Ni-Ni bonding. A similar effect is induced by mixing of the vacant a'_1 and e' levels with CO lone-pair combinations, significantly populating these Ni-Ni bonding orbitals. Introduction of intermixing between several orbitals of same symmetry (in particular the non-negligible π/δ and π^*/δ^* mixings), yields supplementary stabilization. Moreover, the e' combinations of the three π^*(CO) orbitals which are associated to C=O bonding (perpendicular to the

Ni-Ni vector, not represented in Figure 45), are also somewhat participating to bonding interactions with occupied 3d levels. The occupation of all the fragment orbitals discussed above are summarized in Table 11.

Table 11: Occupation of the frontier orbitals of the L-Ni…Ni-L and $(\mu\text{-L})_3$ fragments in $[Ni_2(L)_5]$ (L = CO, AlCp) in D_3h symmetry. Due to the overall higher symmetry, here $[Ni_2(AlCp)_5]$ was calculated.

	$[Ni_2(CO)_5]$	$[Ni_2(AlCp)_5]$
σ(*sp)	0.03	0.01
π*(4p)	0.02	0.05
π(4p)	0.90	0.96
σ(sp)	0.66	1.20
σ*(3d)	1.54	1.60
π*/δ*(3d)	7.62	7.75
π/δ(3d)	7.31	7.30
σ(3d)	1.89	1.72
e' (π*-ligand)	0.47	0.34
e" (π*-ligand)	0.30	0.15
a''_2 (π*-ligand)	0.46	0.48
e' (ligand lone pairs)	3.28	2.98
a'_1 (ligand lone pairs)	1.43	1.27

It appears from these values that the occupation of the Ni-Ni bonding orbitals of the metallic fragment largely overpasses those of the antibonding ones. In particular, substantial bonding is induced by occupation of diffuse σ(sp) and π(4p) levels. The data corresponding to the isoelectronic $[Ni_2(AlCp)_5]$ complex is also provided in Table 11 assuming D_{3h} pseudo-symmetry. These values are a bit more approximate because of the actual lowest symmetry (C_s) of the molecule. First of all, one may wonder about the existence and capabilities of vacant accepting orbitals of the AlCp* fragments, which would play the same role as the π*(CO) orbitals. It turns out that the vacant Al-Cp* antibonding orbitals have similar shape, localization and energy as the π*(CO) orbitals (see Figure S 28). The values given in Table 11 indicate that with respect to nickel, AlCp* is only slightly less π-acceptor than CO. On the other hand, it is a better σ donor. The values associated with the occupation of the metallic fragment orbitals are similar to those obtained for $[Ni_2(CO)_5]$, with exception of the σ(sp) frontier orbital which is doubled, indicating even more Ni-Ni bonding interaction.

V.4.4 Summary of $[Ni_2(AlCp^*)_5]$

In summary the successful synthesis of $[Ni_2(AlCp^*)_5]$ as the first isolable congener of the experimentally unknown $[Ni_2(CO)_5]$ was presented. The compounds $[Ni_2L_5]$ (L = CO, ECp*) are the smallest clusters in the homologue series of $[Ni_xL_y]$ clusters and therefore allow the investigation of fundamental metal-metal interactions in regard to high nuclear clusters. X-Ray crystallography of $[Ni_2(AlCp^*)_5]$ reveals a very short Ni-Ni distance of only 2.2702(15) Å, in accordance to the short Ni-Ni distance in $[Ni_2(CO)_5]$. Together with theoretical results, this hints to a Ni-Ni bond. Detailed theoretical investigations reveal that the Ni-Ni bond is a result of mixing of Ni_2 and L_5 based ligands. The synthetic success of the $[Ni_2(AlCp^*)_5]$ synthesis in contrast to the experimentally unknown $[Ni_2(CO)_5]$, can be explained by effective shielding of the Ni_2 core by the sterically demanding but still flexible AlCp* ligands. The steric shielding has already been shown to stabilize high nuclear clusters, like $[Cu_6(AlCp^*)_6(H_4)]^2$ and even the open-shell cluster $[Cu_{43}(AlCp^*)_{12}]$[112-113]. In addition, the strong σ donating and weak π accepting properties of AlCp* in contrast to CO strengthens the Ni-Ni interactions, potentially enabling the formation of higher nuclear ECp* protected Ni^0 clusters. The fact that most of the isolated Ni carbonyl clusters possess negative charge further substantiates this assumption.[105] We showed that the Ni-Ni bonding interactions is stabilized by interactions with AlCp* potentially being the basis for higher nuclear $[Ni_n(ECp^*)_m]$ clusters. Furthermore, detailed understanding of the bonding in transition metal dimers as the "simplest" compounds featuring direct TM-TM interactions will help to access and understand higher nuclear $[TM_x(L)_y]$ clusters in future. Furthermore, $[Ni_2(AlCp^*)_5]$ is an additional representative for the Ni_2-bridging ECp* motif, that was also predicted for $[Ni_4(GaCp^*)_4(EtCCEt)_2]$. Furthermore, the shortest Ni-Ni distance in $[Ni_4(GaCp^*)_4(EtCCEt)_2]$, which is bridged by two GaCp* ligands, was calculated to 2.28 Å in accordance to the experimentally observed Ni-Ni distance in $[Ni_2(AlCp^*)_5]$. This substantiates the structural relationship of dimeric $[TM_2(ECp^*)_5]$ compounds with higher nuclear $[TM_a(ECp^*)_b]$ as well as $[TM_a(ECp^*)_b(UHC)_c]$.

V.4.5 Synthesis and characterization of $[Ni_2(\mu\text{-}GaCp^*)(\mu\text{-}GaNiCp^*)_2(dvds)_2]$

Unexpected Cp transfer from Ga to Ni*

The results in this chapter were obtained by Maximilian Muhr during his master thesis. A journal manuscript dealing with the results of this chapter is currently under preparation. The master thesis by M. Muhr was supervised by the author of this dissertation.

Reaction of $[Ni_2(dvds)_3]$ with AlCp* results in the formation of $[Ni(AlCp^*)_4]$ and $[Ni_2(AlCp^*)_5]$ as side product. For the $[Ni(ECp^*)_n(PEt_3)_{4-n}]$ complexes, a decisive difference in Ni-ECp* bonding was observed. In contrast to the kinetically inert Ni-AlCp* bond, the Ni-GaCp* bond was shown to be labile allowing ligand displacement reactions. Furthermore, the $[TM_2(GaCp^*)_5]$ compounds (TM = Pd, Pt) undergo ligand exchange reactions when treated with CO, PPh_3 and AlCp*.[98] In addition trinuclear $[Pd_3(GaCp^{*Ph})_4(dvds)]$[108] as well as tetranuclear $[Ni_4(GaCp^*)_3(CNtBu)_7]$ and $[Pd_4(GaCp^*)_4(CNPh)_4]$[68] $[TM_a(ECp^*)_bL_c]$ compounds can be synthesized. Furthermore, there is experimental evidence for a M_{14} $[(Ni_aGa_b)(Cp^*)_6]$ (a+b = 14) cluster. A unambiguous determination of the elemental composition and assignment by single crystal X-ray diffraction was hampered by bad crystal quality, the low solubility of this compound and the similar X-ray scattering factors of Ga and Ni.[114]

The number of different Ni_aGa_y clusters in contrast to the few examples of Ni_aAl_b underlines the diversity of $[TM_aGa_b]$ cluster. Therefore, the access of $[Ni_aGa_b]$ clusters shall be tested starting from the promising precursor $[Ni_2(dvds)_3]$.

Treatment of $[Ni_2(dvds)_3]$ with 7 eq. GaCp* and subsequent analysis of the reaction mixture by LIFDI-MS shows the formation of several $[Ni_a(GaCp^*)_b(dvds)_c]$ species. This finding is in contrast to the

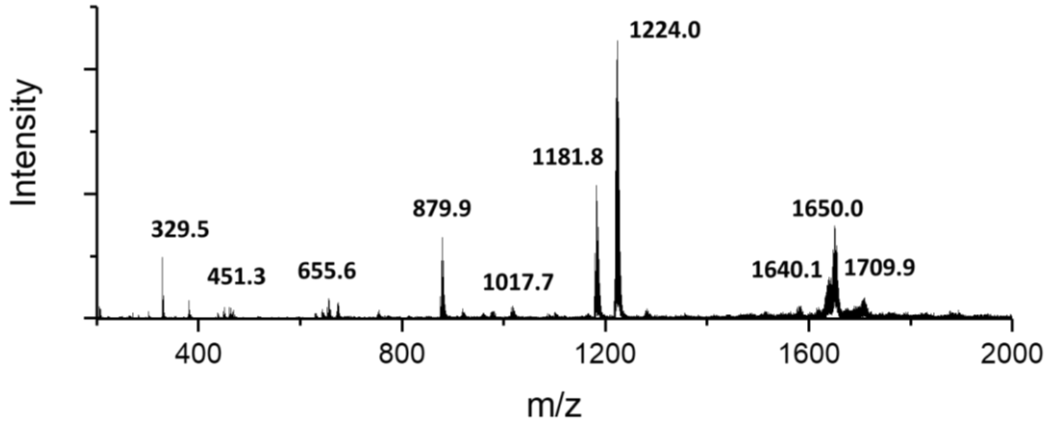

Figure 46: LIFDI-MS spectrum of the reaction of $[Ni_2(dvds)_3]$ with 7 eq. GaCp* at room temperature. The assignment of the different signals is ummarized in the following table.

comparable reaction using AlCp*, where the addition of 6 eq. AlCp* solely results in the formation of $[Ni(AlCp^*)_4]$ and small quantities of $[Ni_2(AlCp^*)_5]$.

Table 12: Preliminary assignments of the observed mass signals to $[Ni_a(GaCp^*)_b(dvds)_c]$ compounds. The term "Ni8Ga6" will be explained in chapter and 5.5.6.

Observed mass (m/z)	Proposed compound
451.3	[Ni(GaCp*)(dvds)] (450.05 g/mol)
879.9	$[Ni(GaCp^*)_4]$ (878.51 g/mol)
1017.7	$[Ni_4(GaCp^*)_2(dvds)_2]$ (1017.48 g/mol)
1181.8	$[Ni_3(GaCp^*)_4(dvds)]$ (1182.29 g/mol)
1224.0	$[Ni_4(GaCp^*)_3(dvds)_2]$ (1222.43 g/mol)
1640 – 1710	"Ni_8Ga_6"

After adjusting the reaction conditions the isolation of [Ni(GaCp*)(dvds)] could be achieved. This compound can be accessed by treatment of $[Ni_2(dvds)_3]$ with two eq. GaCp* at -30°C in toluene. At this low-temperature pure [Ni(GaCp*)(dvds)] crystalizes from the reaction solution as orange crystalline solid. The solid material, as well as its solutions have to be handled at low temperatures as it decomposes over time at ambient temperatures.

The ^1H NMR spectrum of freshly prepared solutions of [Ni(GaCp*)(dvds)] shows three doublets of doublets between 2.69 and 3.01 (olefinic H, 6H), a singlet at 1.84 (GaCp*, 15H) and two singlets at 0.57 and -0.05 ppm (SiMe groups, 12H). The ^{13}C NMR spectrum fits to the observed signals of the ^1H-NMR. The signal for the ring carbon atoms and the adjacent CH_3 groups are found at 113.8 and 9.2 ppm respectively, in accordance to other Ni-GaCp* compounds. [60-61, 96] The signals of the dvds ligands at 55.2, 47.5, 1.9 and -0.4 ppm are only slightly shifted compared to $[Ni_2(dvds)_3]$.[109]

Single crystals suitable for X-ray analysis were obtained from cooled toluene solutions at -30°C after several days (Figure 47).

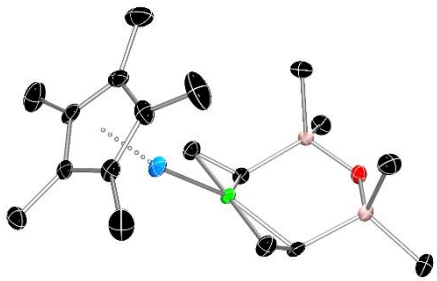

Figure 47: Molecular structure of [Ni(GaCp*)(dvds)]. Hydrogen atoms are omitted for clarity. The displacement ellipsoids are shown at the 50 % probability level. Selected interatomic distances (Å) and angles (°): Ni-Ga: 2.2527(3), Ni-C(dvds): 2.00 (average), Ga-$Cp^*_{centroid}$: 1.941, Si-O-Si: 129.08(1).

The Ni-GaCp* distance of 2.2527(3) Å is in the range of other Ni-GaCp* distances but slightly elongated compared to [Ni(GaCp*)$_4$] (2.2188(5) Å). The Ga-Cp* centroid distance of 1.941 Å is slightly shorter than in [Ni(GaCp*)$_4$] (2.003(4) Å). [96] The dvds ligand adopts a terminal coordination mode as it was also found in [Ni$_2$(dvds)$_3$]. [Ni(GaCp*)(dvds)] featuring only 16 valence electrons at the central Ni atom is a very promising candidate for further reactions. In addition to the low-coordinated central Ni atom, it features a weakly bound dvds ligand and a potentially weak Ni-GaCp* bond.

Addition of different equivalents GaCp* to a freshly prepared solution of [Ni(GaCp*)(dvds)] and analysis via ^{1}H-NMR revealed a fast exchange process between ligated and free GaCp* ligands. The ^{1}H-NMR of free GaCp* (1.93 ppm) and [Ni(GaCp*)(dvds)] (1.84 ppm) show a single coalesced signal (see Figure S 29). The chemical shift of this signal depends on the applied equivalents of free GaCp*. Using 1 eq. GaCp*, the coalesced signal shows no sign of splitting upon cooling to -95°C (see Figure S 30). This observation hints to a very low activation barrier for the GaCp* exchange. DFT calculations (BP86-D3/def2-TZVPP) for the reaction of [Ni(GaCp*)(dvds)] with free GaCp* to [Ni(GaCp*)$_2$(dvds)], representing a plausible intermediate in the GaCp* exchange, indicate that the reaction energy is rather balanced with [Ni(GaCp*)$_2$(dvds)] being favored by only 5kcal/mol compared to [Ni(GaCp*)(dvds)] and free GaCp*. In addition, treatment of [Ni(GaCp*)(dvds)] with PEt$_3$ results in the formation of [Ni(PEt$_3$)(dvds)] (calculated: 363.3 m/z) as evidenced by the signal at 362.9 m/z obtained by LIFDI-MS measurements of the reaction solution. Taken together, this underlines a readily dissociating GaCp* ligand in [Ni(GaCp*)(dvds)] which might be beneficial for the formation of higher nuclear clusters.

Time-dependent ex-situ LIFDI-MS measurements of a heated toluene solution of [Ni(GaCp*)(dvds)] indicate the initial formation of a species with the molecular mass 1219.7 m/z. This species seems to be unstable under the applied reaction conditions and new species form in the mass range between 1640 and 1720 m/z. The former species can be selectively synthesized upon heating of solid [Ni(GaCp*)(dvds)] to 110°C *in vacuo*. LIFDI-MS measurements of a toluene solution of the remaining brown residue shows the selective formation of [(Ni$_4$Ga$_3$)(Cp*)$_3$(dvds)$_2$] (calculated 1222.4 m/z) as the intermediate species. Single crystals suitable for X-ray crystallography were obtained by cooling of a concentrated hexane solution to -30°C. The single crystal structure unambiguously reveals a transmetallation of Cp* from Ga to Ni. Therefore the overall molecular formula of this compound should be written as [Ni$_2$(μ-GaCp*)(μ-GaNiCp*)$_2$(dvds)$_2$] (Figure 48).

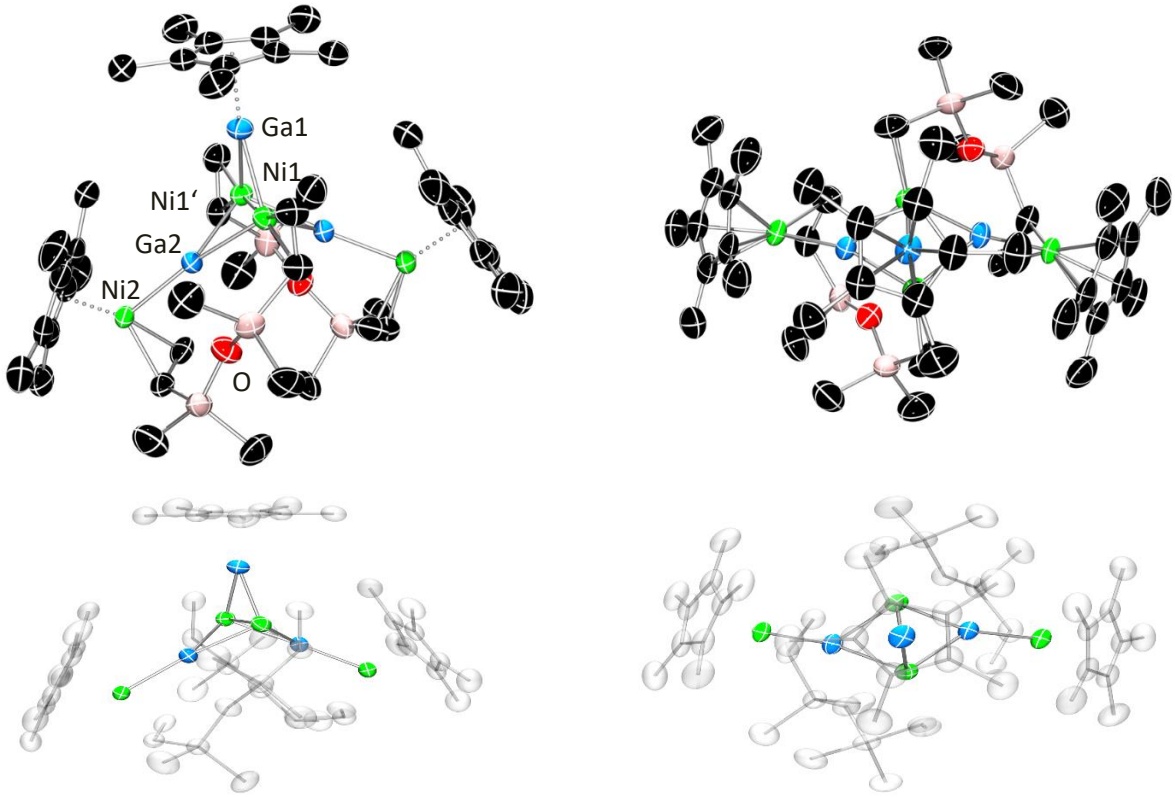

Figure 48: Molecular structure of $[Ni_2(\mu\text{-}GaCp^*)(\mu\text{-}GaNiCp^*)_2(dvds)_2]$. Hydrogen atoms and disorders are omitted for clarity. The displacement ellipsoids are shown at the 50 % probability level. In the bottom representations, the organic ligand shell is faded for a better visibility of the metallic cluster core. Selected interatomic distances (Å) and angles (°): Ni1-Ni1': 2.339(2), Ni1-Ga1: 2.39 (average), Ni1-Ga2: 2.362(3), Ga2-Ni3: 2.33 (average), Ni3-$Cp^*_{centroid}$: 1.80 (average), Ga1-$Cp^*_{centroid}$: 2.008, Ni1-olefinic C: 1.92-2.08, Ni2-olefinic C: 2.00-2.02 , Ga-O: 2.80-2.89, Si-O-Si: 140.0-142.0.

The arrangement of the inner M_5 atoms is reminiscent of the structure of $[TM_2(ECp^*)_5]$ (TM = Ni, Pd, Pt; E = Al, Ga). In these compounds the central TM_2 unit is bridged by three ECp* ligands and each TM atom is coordinated by terminal ECp*. In $[Ni_2(\mu\text{-}GaCp^*)(\mu\text{-}GaNiCp^*)_2(dvds)_2]$, the central Ni_2-dimer is coordinated by one GaCp* ligand and two bare formally Ga^0 atoms. Each Ga atom is bound to an additional $Ni^{I}Cp^*$ unit. The metal core structure is further stabilized by two dvds ligands arranged in a bridging coordination between Ni1 and Ni3. Moreover, the coordination mode of the dvds ligand to the Ni_2 unit is disordered, showing two preferred orientations. Therefore, the alkene unit either coordinates in parallel or perpendicular to the Ni1-Ni1'-Ga1 plane, giving two different isomers The Ga2-O distance of only 2.80 Å suggest a stabilizing Ga-O interaction. Therefore, in addition to its flexible coordination mode, dvds helps to stabilize the bare Ga^0 atom. Compared to $[Ni_2(AlCp^*)_5]$ (Ni-Ni distance: 2.2702(15) Å), the distance of the central Ni_2 dimer is slightly elongated to 2.339(2) Å. The remaining intermetallic distances, including the unprecedented Cp^*Ni^{I}-Ga^0 distance are in the range for other Ni-Ga interactions.[60, 68] An additional observation that supports the metal assignment is based on the M-$Cp^*_{centroid}$ distances. The Ga-$Cp^*_{centroid}$ and Ni-$Cp^*_{centroid}$ distances differ by about 0.2 Å. The

Ga-Cp*centroid distance of 2.008 Å is in the range found for other Ga-Cp*centroid distances as, e.g. [Ni(GaCp*)$_4$] (2.003(4) Å)[81] and [Ni(GaCp*)(dvds)] (1.941 Å). In contrast the Ni-Cp*centroid distance of about 1.80 Å relates well to Ni-Cp centroid distances found in [(η_5-Cp)Ni[(iPr$_3$P)Ni]$_4$(μ_2-H)$_2$(μ_4-Tl)] (1.788 Å) [115] and [(η_5-Cp*)Ni$_2$(ZnMe)$_6$(ZnCp*)(GaCp*)] (1.752 Å)[67] DFT calculations further support the metal assignments. Only the metal assignment presented above reproduces the experimental crystal structure. At the BP86-D3/def2-TZVPP level of theory, e.g. the Ni-Ni in the Ni$_2$ unit was calculated to 2.36 Å, only slightly longer when compared with the experimental distance.

Based on the experimental crystal structure a definite assignment of the NMR-data (Figure 49) was possible. The unprecedented Cp* transmetallation from Ga to Ni as well as the two possible isomers resulting from the different coordination modes of the dvds ligand lead to rather complicated NMR spectra.

The ^{1}H NMR shows several signals for the SiMe (0.43-0.12 ppm) and olefinic protons (3.75-2.55) of the dvds ligand. The large number of signals and their broad range is in accordance to the observed disorder of the dvds ligand and the coordination of the alkene-moieties to distinct Ni^0/Ni^I-sites. The observation of different isomers is further supported by the ^{13}C NMR signals of the dvds ligand. The Si-Me groups lead to two sets of signals between 3.0 and -1.0 ppm. One set of signals gives eight peaks for eight distinct SiMe groups. The other signal set only consists of four signals of twofold intensity compared to the aforementioned signals referring to an isomer of higher symmetry. The same applies to the olefinic carbon atoms which are found in the range between 46 and 62 ppm. Furthermore, five signals appear in the ^{1}H-NMR in the range of the M-Cp* protons at 2.06, 1.90, 1.88 and two overlapping signals at 1.84 and 1.83 ppm with an integration ratio of 15:6:3:15:6. An unambiguous assignment to NiCp*/GaCp solely based on the ^{1}H chemical shifts of the Cp* protons is not possible, since GaCp* protons can span quite a large range between 2.2 and 1.8 ppm.[60, 68, 81] However, ^{13}C NMR and ^{1}H/^{13}C 2D HMBC (heteronuclear multiple bond correlation) NMR support the assignment of the GaCp*/NiCp* signals (see Figure S 32). In the 2D experiment, the ^{1}H NMR signal at 2.06 ppm is coupled to the ^{13}C signal at 114.3 ppm, whereas the signals between 1.90 and 1.83 are coupled to the ^{13}C signals at 98 and 97 ppm. This is in accordance to literature data for the ^{13}C chemical shifts of GaCp* (120-110 ppm)[60, 68, 81] and Ni^{I}Cp* (reference: 93 ppm[115]). The observed splitting of the Ni-Cp* signals can be attributed to the existence of the two different isomers. In one isomer, the Cp* ligand can freely rotate around the Ni-Cp* axis whereas in the other one rotation is suppressed. Therefore, the signal with an integration ratio of 15 can be assigned to the first isomer and the signals with integration ratio 6:3:6 can be attributed to the latter isomer.

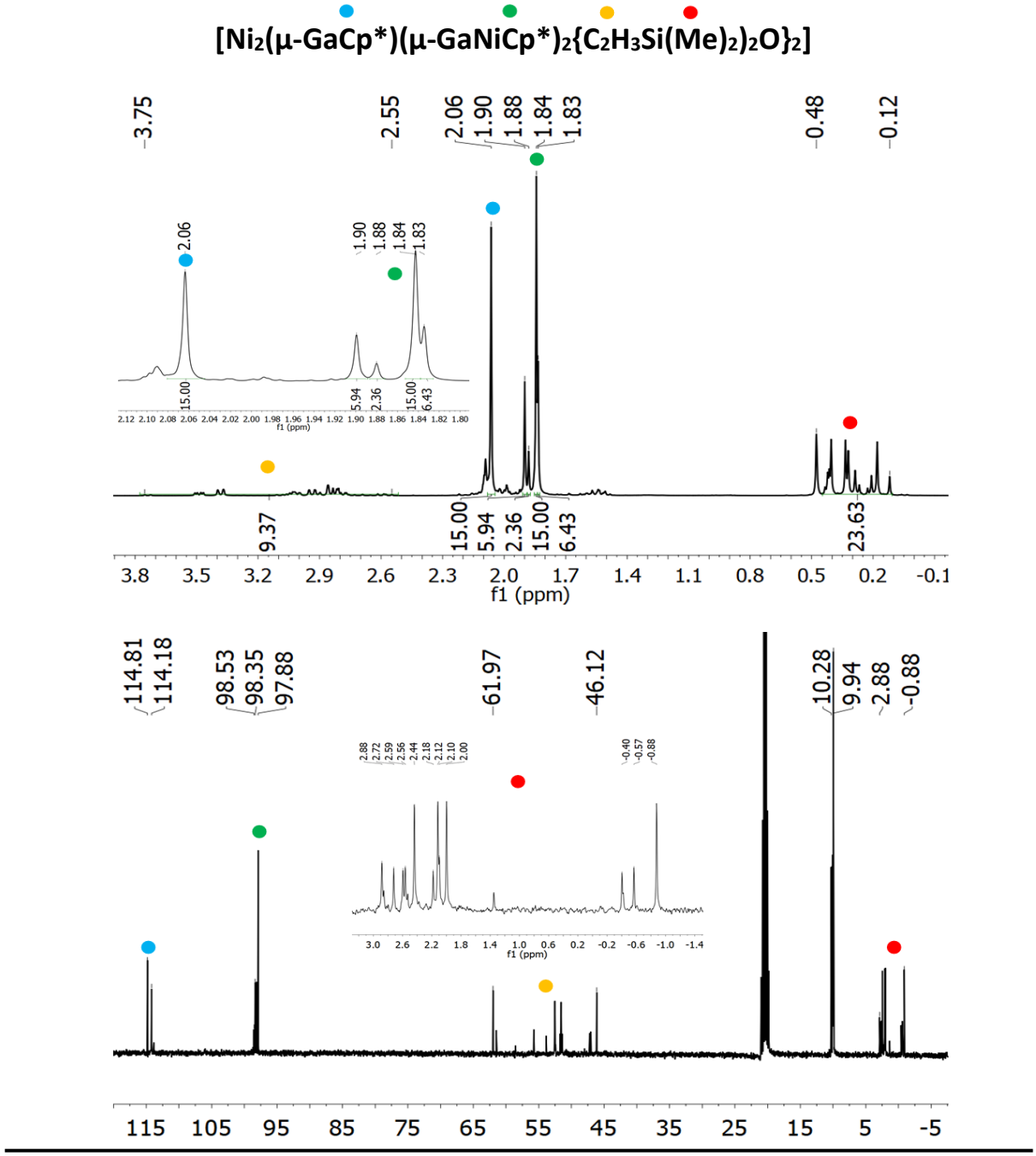

Figure 49: ^{1}H (top) and ^{13}C (bottom) NMR spectrum of $[Ni_2(\mu\text{-}GaCp^*)(\mu\text{-}GaNiCp^*)_2(dvds)_2]$. The insets show the ^{1}H-NMR range for the MCp* protons and the ^{13}C-NMR range for the SiMe groups respectively.

The Cp* bound to Ga can rotate freely around the Ga-Cp*centroid axis for both isomers even when lowering temperature to -90°C. However, a splitting of the GaCp* signals due to the two isomers is obtained upon cooling to -20°C (Figure S 31). The reason for the observed splitting of the NiCp* signals has so far not been understood. A potential explanation for this observation could be based on unexpectedly strong H H interactions from dvds to NiCp* which would be supported by short H-H

contacts found in the experimental crystalstructure (lowes (Ni-Cp*)H-H(dvds-Ni) distance 2.05 Å). A further explanation could be based on a C-H activation of the Cp* ligand (e.g. by Ga^0), whereas no tilting of the NiCp* ligand towards Ga can be observed. Therefore, both explanations seem to be rather unlikely and further investigations have to be performed. For instance, NMR studies at higher temperatures, or the detection of potential M-H signals could give helpful insights into this puzzling observation. Furthermore, the mechanism of the solid-state reaction leading to the formation of $[Ni_2(\mu\text{-}GaCp^*)(\mu\text{-}GaNiCp^*)_2(dvds)_2]$ should be investigated. Preliminary results have already been obtained by Maximilian Muhr during his master and PhD thesis.

V.4.6 Summary of $[Ni_2(\mu\text{-}GaCp^*)(\mu\text{-}GaNiCp^*)_2(dvds)_2]$ and the implications on the debated $[Ni_8(GaCp^*)_6]$

Comparing the reactivity of AlCp* and GaCp* towards $[Ni_2(dvds)_3]$ significant differences were observed. First of all, the main product afforded by reaction with AlCp* is the long-known $[Ni(AlCp^*)_4]$[8] whereas the Ni_2-dimer $[Ni_2(AlCp^*)_5]$ is obtained as a side-product. Only when applying 1-3 eq. AlCp* higher nuclear Ni_xAl_y species can be observed as well. This result is in stark contrast to the reactivity of GaCp*. Even treatment of $[Ni_2(dvds)_3]$ with 7 eq. GaCp* results in the formation of a huge set of Ni_xGa_y compounds. The difference can be explained by the stronger Ni-AlCp* bond compared to the Ni-GaCp*, favoring the formation of the 18 valence electron complex $[Ni(AlCp^*)_4]$.[75] In addition, the Ni-GaCp* bond was shown to be kinetically active and can undergo ligand exchange reactions. This was observed for the Ni-GaCp* interactions in $[Ni(GaCp^*)_n(PEt_3)_{4-n}]$. These findings are in contradiction to published literature, where the TM-ECp* bond was proposed to be kinetically inert.[8] Due to the lower Ni-Ga bond strength together with its kinetic lability, the formation of unsaturated Ni/Ga species is favored compared to the corresponding Ni-Al species. These low-coordinated Ni-Ga species are involved in diverse reactions in solution finally resulting in the formation of higher nuclear $[Ni_aGa_b]$ clusters.

Therefore, [Ni(GaCp*)(dvds)] represents a very interesting compound. The 16 valence electron Ni center features a free coordination site, a labile Ni-GaCp* interaction and the dvds ligand which can be replaced during reactions. This was shown to be beneficial for the formation of the Ni_4Ga_3 cluster $[Ni_2(\mu\text{-}GaCp^*)(\mu\text{-}GaNiCp^*)_2(dvds)_2]$. The latter compound revealed a new fascinating structural motif. During the formation of $[Ni_2(\mu\text{-}GaCp^*)(\mu\text{-}GaNiCp^*)_2(dvds)_2]$, the transmetallation of Cp* from Ga to Ni takes place resulting in the formation of a $Ni^{I}Cp^*$ moiety. Therefore, $[Ni_2(\mu\text{-}GaCp^*)(\mu\text{-}GaNiCp^*)_2(dvds)_2]$ can be seen as a nano-alloy featuring a zerovalent Ni_2Ga_2 core structure. Mechanistic studies on the formation process of this compound are currently under investigation by Maximilian Muhr. The observed Cp* transmetallation from Ga to Ni, is an additional difference between GaCp* and AlCp*, since for the latter such a reactivity has not been observed so far. This transmetallation might also be a reason for the access of different $[Ni_aGa_b]$ clusters in contrast to the few $[Ni_aAl_b]$ examples.

The observed transmetallation has significant impact on a reoccurring scientific question of the Fischer group that has been unsolved for years dealing with a high nuclear Ni_xGa_y cluster. For instance, in the LIFDI MS spectra of the reaction mixtures containing $[Ni_4(GaCp^*)_4(EtCCEt)_2]$ (1218.1 g/mol) or $[Ni_2(\mu\text{-}GaCp^*)(\mu\text{-}GaNiCp^*)_2(dvds)_2]$ (1222.4 g/mol) signals at higher mases (1640-1710 m/z) have been

observed and attributed to the Ni_xGa_y cluster. These signals are also obtained by treatment of different NiL_n precursors with GaCp*, like [Ni(cod)$_2$], [Ni(cdt)] or [Ni_2(dvds)$_3$]. Based on the low solubility of the unassigned Ni_xGa_y cluster, the single crystals obtained directly from reaction solutions were usually of very low quality showing a huge degree of disorder, which together with the similar scattering factors of Ni and Ga impedes a clear-cut structural characterization. From the crystal structure, a M_{14} cluster core featuring an octahedrally coordinated Cp^*_6 shell is clearly visible. Based on elemental analysis, the molecular composition [Ni_8(GaCp*)$_6$] was proposed for the Ni_xGa_y cluster.[114] However, preliminary results from Maximilian Muhr, Max Schütz, Lena Staiger and of this dissertation lead to a more conclusive picture. This "compound" actually represents a mixture of at least three co-crystalized clusters of the sum formula [(Ni_7Ga_6)Cp^*_6] (M = 1640.6 g/mol), [(Ni_6Ga_7)Cp^*_6] (M = 1651.6 g/mol) and [(Ni_7Ga_7)Cp^*_6] (M = 1710.3 g/mol). Depending mainly on the Ni-precursor, different ratios of these cluster are obtained in reaction solutions. All clusters feature an octahedral Cp* shell and similar molecular dimension which results in their co-crystallization, explaining the huge degree of disorder present in the crystal structure determination. The present results obtained from the precursor [Ni_2(dvds)$_3$], which allows stabilization of the intermediate-sized cluster [Ni_2(μ-GaCp*)(μ-GaNiCp*)$_2$(dvds)$_2$] substantiates the occurrence of NiCp* moieties in these compounds as well. For a more detailed description of these compounds, I refer to the ongoing work of Muhr, Schütz and Staiger.

Besides the structural implications on "[Ni_8(GaCp*)$_6$]", the occurring Cp* transmetallation from Ga to Ni might also occur in the reaction of [(cod)Ni(EtCCEt)Ni(cod)] with GaCp* yielding [Ni_4(GaCp*)$_4$(EtCCEt)$_2$] as presented in chapter Ⅴ.3.2 Synthesis of [Ni4(GaCp*)$_4$(EtCCEt)$_2$]. Therefore, future investigations of [Ni_4(GaCp*)$_4$(EtCCEt)$_2$] aplyying ^{1}H, ^{13}C and 2D ^{1}H/^{13}C HMBC NMR shall give valuable information about a potential Cp* transmetallation in this case. However, a concluding structural description will only be possible based on molecular structure determination by single crystal X-Ray diffraction. To access further [Ni_aGa_b(UHC)$_c$(Cp*)$_d$] complexes, which shall increase the structural knowledge of such compounds, [Ni(GaCp*)(dvds)] as well as [Ni_2(μ-GaCp*)(μ-GaNiCp*)$_2$(dvds)$_2$] shall be treated with different UHCs. For both compounds, featuring potentially labile dvds ligands, the formation of interesting [Ni_aGa_b(UHC)$_c$(Cp*)$_d$] compounds is expected.

Ⅵ Conclusion and Outlook

Based on a computational study, molecular $[Ni(M'R)_n(UHC)_{4-n}]$ (M' = Al, Ga, Zn, R = Me, Cp*, UHC = unsaturated hydrocarbons, e.g. C_2H_2 and C_2H_4 n = 1-3) compounds where shown to exhibit coordination modes of unsaturated hydrocarbons that are reminiscent of substrate-surface interactions found on solid state intermetallic TM/M' (TM = Pd, Fe, Co, Ni, Cu, M' = (Ag), Al, Ga, Zn) semihydrogenation catalysts.[3] Therefore, a conceptual link between molecular $[TM_a(M'R)_b(UHC)_c]$ compounds and intermetallic solid state TM/M' catalysts for semihydrogenation is proposed. In analogy to the solid state TM/M' intermetallics, the M' coordination in molecular $[Ni(M'R)_n(UHC)_{4-n}]$ complexes was shown to have a pronounced influence on Ni-UHC bonding in molecular $[Ni_a(M'R)_b(UHC)_c]$ as well. The computational study reveals unique Ni-M' bridging coordination modes for C_2H_2 in $[Ni(AlCp^*)_2(C_2H_2)_2]$ and $[Ni(ZnR)_4(C_2H_2)_2]$. This bridging coordination mode was however not observed for the ethylene compounds $[Ni(AlCp^*)_2(C_2H_4)_2]$ and $[Ni(ZnR)_4(C_2H_4)_2]$ where ethylene solely coordinates to the central Ni atom. The Ni-M' bridging C_2H_2 coordination mimics PdGa bridging C_2H_2 coordination to a trinuclear $PdGa_2$ site as determined for the solid state PdGa catalyst.[3] Relating the results presented for the $[Ni(M'R)_n(UHC)_{4-n}]$ to the catalytic semihydrogenation on heterogeneous TM/M' intermetallics, the molecular compounds indicate that acetylene is strongly chemisorbed to and highly activated by the Ni-M' bridging coordination mode which would facilitate alkyne hydrogenation. However, the weaker Ni-C_2H_4 physisorption would suppress over-hydrogenation to C_2H_6, by C_2H_4 desorption (i.e. dissociation in case of molecular complexes).

The initial synthetic strategy to access $[Ni(M'R)_n(UHC)_{4-n}]$ complexes by late-stage introduction of UHCs was based on ligand exchange reactions from $[Ni(M'R)_n(PEt_3)_{4-n}]$ (n = 1-3) precursors featuring preformed Ni-M'R bonds. However, a combined experimental and theoretical study revealed that phosphine dissociation, which is commonly known for $[Ni(PR_3)_4]$[7], is strongly suppressed by introduction of M'R in the series of $[Ni(M'R)_n(PEt_3)_{4-n}]$ compounds. The M'R ligands cause a significant Ni-P bond polarization as a plausible explanation for the Ni-P bond strengthening.[61]

The reported reductive elimination of H-$SiEt_3$ from $[(H)(SiEt_3)Ni(AlCp^*)_3]$ to access the low-coordinated and highly reactive $[Ni(AlCp^*)_3]$ fragment[8] was used as a motivation for the experimental access of $[(H)(SiEt_3)Ni(AlCp^*)_{3-n}(ZnR)_{2n}]$ (n = 0-3) compounds. However only the complexes with n = 1 $[(H)(SiEt_3)Ni(AlCp^*)_2(ZnCp^*)(ZnMe)]$ and n = 2 $[(H)(SiEt_3)Ni(AlCp^*)(ZnCp^*)_2(ZnMe)_2]$ can be accessed. From $[(H)(SiEt_3)Ni(AlCp^*)(ZnCp^*)_2(ZnMe)_2]$, H-$SiEt_3$ can be replaced by PEt_3 yielding $[(PEt_3)Ni(AlCp^*)(ZnCp^*)_2(ZnMe)_2]$ which is a good indication for the intermediate formation of a low-coordinated $[Ni(AlCp^*)(ZnCp^*)_2(ZnMe)_2]$ species. Therefore, the $[(H)(SiEt_3)Ni(AlCp^*)_{3-n}(ZnR)_{2n}]$ (n = 0-

2) precursors could potentially allow the synthesis of $[(UHC)Ni(AlCp^*)_{3-n}(ZnR)_{2n}]$ (n = 0-2) compounds which should be tested in subsequent studies.

A new synthetic strategy based on the early-stage functionalization of common Ni precursors with UHCs and subsequent introduction of M' was developed and could be shown to be a promising and universal access to $[Ni(M'R)_n(UHC)_{4-n}]$ compounds. Reaction of $[Ni(cod)_2]$ with the internal alkyne 3-hexyne and subsequent treatment with GaCp* affords different $[Ni_a(GaCp^*)_b(EtCCEt)_c]$ compounds like e.g. $[Ni_4(GaCp^*)_4(EtCCEt)_2]$. The unexpected kinetic lability[8] of the Ni-GaCp* bond as observed for $[Ni(GaCp^*)_n(PEt_3)_{4-n}]$ and [Ni(GaCp*)dvds] is the main cause for the synthetic access of diverse NiGa clusters and was shown to be beneficial for the formation of the Ni_4Ga_3 cluster $[Ni_2(\mu\text{-}GaCp^*)(\mu\text{-}GaNiCp^*)_2(dvds)_2]$. The latter compound revealed a new fascinating structural motif. During its formation, the transmetallation of Cp* from Ga to Ni takes place resulting in the formation of a Ni^ICp^* moiety. Therefore, $[Ni_2(\mu\text{-}GaCp^*)(\mu\text{-}GaNiCp^*)_2(dvds)_2]$ can be seen as a nano-alloy featuring a mixed NiGa core structure. It has to be noted, that the transmetallation has so far not been observed for related $[Pd_aGa_b]$ and $[Pt_aGa_b]$ clusters.[97-98, 108] The observed transmetallation has significant impact on the current research on other NiGa clusters. For instance, based on this observation the debated $[Ni_8(GaCp^*)_6]$ cluster could be identified as a mixture of $[(Ni_xGa_y)Cp^*_6]$[114] (x = 6,7; y = 6,7) clusters featuring NiCp* moieties. Furthermore, for the presented $[Ni_4(GaCp^*)_4(EtCCEt)_2]$ Cp* transmetallation should be considered as well. For the Ni/Ga system the lability of the Ni-GaCp* bond and the unexpected Cp* transmetallation from Ga to Ni favors the formation of high nuclear $[Ni_aGa_b]$ clusters. This contrasts with the Ni/Al system, where the kinetically stable and thermodynamically strong Ni-AlCp* largely suppresses cluster growth reactions. Only the isolation of dimeric $[Ni_2(AlCp^*)_5]$ was successful so far. For $[Ni_2(AlCp^*)_5]$ the short Ni-Ni distance of 2.2702(15) Å together with the results of quantum chemical calculations at the DFT level of theory support the assignment of a Ni-Ni bonding that is stabilized by the interaction with the surrounding AlCp* ligands. Expanding this result, the ECp* ligands seem to have a beneficial influence on TM-TM bonding potentially being the basis for the large number of $[TM_n(ECp^*)_m]$ clusters.[46-47] In addition, such clusters are kinetically stabilized by the steric shielding of the bulky Cp*. This interplay of electronic and kinetic stabilization allows the isolation of highly reactive cluster species as recently achieved for the open shell $[(Cu_{43}Al_{12})Cp^*_{12}]$ cluster.[102, 113]

Screening of suitable reaction conditions to access particular $[Ni_a(GaCp^*)_b(L)_c]$ compounds, as e.g. $[Ni_4(GaCp^*)_4(EtCCEt)_2]$ and $[Ni_2(\mu\text{-}GaCp^*)(\mu\text{-}GaNiCp^*)_2(dvds)_2]$, necessitates the establishment of new analytical techniques. For instance, the assignment of $[Ni(M'R)_n(PEt_3)_{4-n}]$ compounds in reaction mixtures is usually possible based on the chemical shift of the ^{31}P NMR signal. However, as discussed for $[Ni_2(\mu\text{-}GaCp^*)(\mu\text{-}GaNiCp^*)_2(dvds)_2]$, the assignment of the $^1H/^{13}C$ NMR signals is not

straightforward. Furthermore, NMR signals do not give the number and ratio of TM/M' in the cluster core. The mild ionization of the liquid injection field desorption ionization mass spectrometry (LIFDI-MS) technique largely suppresses fragmentation processes usually allowing the characterization of the molecular ion peak $[M]^+$ of different product species in solution. Therefore, LIFDI-MS represents an efficient strategy for rapid screening of reaction conditions resulting in different product distributions for the investigation of other TMM' systems. However, the method should be further improved to reveal the products obtained from treatment of [Ni(cdt)] with 3-hexyne in toluene. The measured LIFDI-MS spectra of this reaction solutions suggest the formation of different Ni_a clusters $[Ni_aC_xH_y]$ (a = 8, 9, 10, 12) based on the respective isotopic patterns. Based on a recent publication, C-H or CC bond activation reactions should be considered during the formation of high nuclear $[Ni_aC_xH_y]$ clusters.[99] Furthermore, those compounds are of special interest with respect to their reactivity towards GaCp* since the formation of high nuclear Ni/Ga clusters can be envisioned.

Based on the promising theoretical results for $[Ni(M'R)_n(UHC)_{4-n}]$, especially for M' = Al, Zn, the experimental access to $[TM_a(M'R)_b(UHC)_c]$ should be investigated in the future. The access to $[Ni_a(AlCp^*)_b(UHC)_c]$ could be achieved applying similar reactions conditions as for the formation of $[Ni_4(GaCp^*)_4(EtCCEt)_2]$ or $[Ni_2(\mu\text{-}GaCp^*)(\mu\text{-}GaNiCp^*)_2(dvds)_2]$. The so far unobserved Cp* transmetallation from AlCp* to Ni could be beneficial for the formation of $[Ni_a(AlCp^*)_b]$ "core-shell" clusters. However, the formation of kinetically inert $[Ni(AlCp^*)_4]$ has to be suppressed potentially by addition of low amounts of AlCp*. Furthermore, the synthetic target could be changed to Pd/Al or Pd/Ga clusters. For both systems, the Pd-E bond were calculated to be weaker than the Ni-E bonds[116] which might be beneficial for the formation of higher nuclear clusters by Pd-E dissociation/association processes. In addition, no Cp* transmetallation from ECp* to Pd has been reported so far even though quite a large number of $[Pd_a(ECp^*)_b]$ cluster has already been reported.[97-98, 108] LIFDI-MS based screening of Pd/Al and Pd/Ga reaction solutions might also be beneficial for the identification of further $[Pd_a(ECp^*)_b]$ cluster. For the access of $[TM_a(ZnR)_b(UHC)_c]$ compounds, the reaction of $[TM_a(ECp^*)_b(UHC)_c]$ towards $ZnMe_2$ shall be investigated. Due to the high polarity of the Ni-Al and Ni-Zn bond, interesting $[Ni_a(M'R)_b(UHC)_c]$ compounds are expected which will most likely exhibit new structural features, like Ni-M' bridging UHC coordination.

In conclusion, this thesis supports the close relationship of molecular Hume-Rothery inspired TM/M' complexes and clusters with solid state TM/M' intermetallics which are currently investigated as promising semihydrogenation catalysts. For solid state materials, the elemental combinations TM/M' are not restricted to Ni/Al, Ni/Ga and Ni/Zn but for example also the Fe/Al system represents a very promising catalytic system for semi hydrogenation.[20] Furthermore, TM/M' intermetallics are also

considered as catalysts for other relevant transformations, as e.g. CO_2 reduction to methanol (applying NiZn[45] or Cu/Zn[52-53]). Therefore, a huge playground for the investigation of diverse TM/M'-substrate interactions has opened for the organometallic chemistry of Hume-Rothery inspired complexes and clusters.

Ⅶ Experimental Section

General Remarks: All manipulations were carried out under inert atmospheres using standard Schlenk techniques or in the glovebox with water and oxygen contents below 0.1 ppm. All glassware was treated with boiling 1,1,1,3,3,3-hexamethyldisilazan under static vacuum prior to usage. Excess 1,1,1,3,3,3-hexamethyldisilazan was removed *in vacuo*. Solvents were dried with a *MBraun* Solvent Purification System. The final H_2O content of all solvents was checked by Karl Fischer titration and was below 5 ppm.

The literature known compounds:
$[Ni(cod)_2]$[117], GaCp*[96], AlCp*[118], $[Ni(PEt_3)_4]$[82], $[Ni(GaCp^*)_4]$[81], $[Ni(AlCp^*)_4]$[8], $[(H)(SiEt_3)Ni(AlCp^*)_3]$[8], $[Ni_2(dvds)_3]$[109], [Ni(cdt)][119]
were synthesized according to the respective literature procedures.

Elemental analysis (EA): EA-measurements were performed in the microanalytical laboratory at the Technical University Munich or in the microanalytical laboratory Kolbe at the Fraunhofer Institut Oberhausen.

NMR-spectroscopy: NMR-spectra were recorded on a *Bruker* AV 400 US spectrometer or a *Bruker* DRX 400 (^{1}H 400 MHz; ^{13}C 101 MHz, ^{27}Al 104 MHz, ^{31}P 162 MHz) in C_6D_6 or toluene-d_8. The solutions were prepared inside a glove box with water and oxygen contents below 0.1 ppm and transferred into gas-tight *J. Young* NMR tubes. Chemical shifts (δ) are given in ppm relative to tetramethylsilane (TMS) and referenced to the residual solvent resonances as internal standards.[120] The NMR signals stated beneath were obtained at room temperature. VT-NMR measurements were performed by Maria Mathews on a *Bruker* DRX 400 spectrometer usually in toluene-d_8.

LIFDI-MS measurements: The LIFDI-MS spectra were recorded on a *Waters* LCT Classic orthogonal acceleration reflectron-TOF (time of flight) mass spectrometer using a liquid injection field desorption ionization (LIFDI) source from the *Linden* CMS GmbH. The samples were dissolved in dry toluene and transferred to a tightly-sealed GC-MS vial equipped with a rubber septum after filtration with a syringe filter in the glove box. The solution inside the vial was transferred to the LIFDI-emitter via a quartz cannula permanently connected to the spectrometer. Due to calibration problems, external calibration was performed using polystyrene as reference. Therefore, the respective sample was measured and the mass of the species which should be calibrated was noted. Subsequently a toluene solution of polystyrene was measured and the $[C_8H_8]_n^+$ signal closest to the sample species was used as a

reference. However, this calibration method was only established at the end of this dissertation project. Therefore, it was not commonly applied for all the measurements.

IR-spectroscopy: Infrared spectra were measured in a glovebox on an Alpha FT-IR from *Bruker* equipped with an ATR device using a platinum diamond. The interferometer range was 450 to 4000 cm^{-1}. The compounds were measured as dried powder under inert atmosphere in a glovebox.

Single crystal X-ray: Measurements were performed by Dr. Christian Jandl or Dr. Jana Weßing. X-ray diffraction intensities were collected on a *Bruker* D8-Venture diffractometer equipped with a CMOS detector (*Bruker* Photon-100), an IMS microfocus with Mo K_α radiation (λ = 0.71073 Å) and a Helios mirror optic or on a *Bruker* D8-Venture system equipped with a Helios optic monochromator and a Mo XTS rotating anode. Suitable crystals were coated in perfluoropolyether and mounted on a microsampler in the cooled nitrogen stream (100 K) of the respective diffractometer. Diffraction data was processed with APEX III[121] and the implemented SAINT and SADABS programs.[122] Molecular structures were solved and refined within APEX III using SHELXT[123] and refined with SHELXL-2017[124] in conjunction with SHELXLE[125]. CCDC 1852316 (**2b**) and 1852315 (**3a**) contain the supplementary data for the already published crystal structures. This data can be obtained free of charge from the Cambridge Crystallographic Data Centre via http://www.ccdc.cam.ac.uk/data_request/cif.

Computational details: Structures of the calculated molecules were optimized using the ORCA4.0[126] software package and Becke's exchange functional[127] with Perdew's correlation functional[128] (BP86). Grimme's dispersion correction including Becke-Johnson damping (D3BJ)[129-130] was used. After preoptimization and analytical calculation of the Hessian using Ahlrich's def2-SVP basis set, the respective structures were further optimized using the def2-TZVPP basis sets.[131] The resolution of identity approximation (RI) was applied to speed up the calculations.[132] Time-dependent density functional theory (TDDFT) calculations were performed to compute the UV-Vis spectra including the lowest 50 eigenvalues. Wiberg indices and NBO charges were computed using the NBO 3.1[133] program as implemented in Gaussian 09[134] program package with single point calculations (BP86/def2-TZVPP). Calculations within the Quantum Theory of Atom in Molecules (QTAIM) were performed applying the MULTIWFN package[135], using Gaussian 09 .wfx files (BP86/def2-TZVPP). Energy decomposition analyses with the natural orbital for chemical valence extension (EDA-NOCV)[87, 136-137] were carried out using the ADF (2013.01) program package[138] at the BP86/TZ2P+ level of theory where the previously optimized uncontracted Slater-type orbitals (STOs) were employed as basis functions in self-consistent field (SCF) calculations.[139] Triple-zeta quality basis sets were used which were augmented by two sets of polarization functions (p and d functions for H, d and f functions for other atoms). An auxiliary set

of s, p, d, f and g STOs was used to fit the molecular densities and to represent the coulomb and exchange potentials accurately in each SCF cycle. Scalar relativistic effects were considered using the zero-order regular approximation (ZORA).[140, 141, 142-144] The bond formation between the interacting fragments is divided into three steps within the EDA calculations. In the first step, the fragments (in the frozen geometry of the whole molecule) are superimposed without electronic relaxation yielding the quasi classical electrostatic attraction ΔE_{elstat}. The second step involves anti-symmetrization and normalization of the product wave function which gives the repulsive term ΔE_{Pauli}. In the final step, the molecular orbitals are allowed to relax which gives the stabilizing orbital interaction ΔE_{orb}. This orbital term can be further divided into contributions of different symmetry, representing different bonding situations (σ, π, etc.). Dispersion forces are accounted for using Grimme's D3 dispersion corrections. These contributions sum up to the total interaction energy ΔE_{int} :

$$\Delta E_{int} = \Delta E_{elstat} + \Delta E_{Pauli} + \Delta E_{orb} + \Delta E_{disp}$$

The computational results presented for $[Ni_2(AlCp^*)_5]$, $[Ni_2(AlCp)_5]$ and $[Ni_2(CO)_5]$ were calculated by Samia Kahlal and Prof. Dr. J.-Y. Saillard using the ADF 2017 version[1] and NBO 6.0[2] program. The BP86 functional[127-128]with the standard STO-TZ2P basis set together with Grimme-D3 dispersion[129-130] were used.

Synthetic protocols:

The following reactions were performed by Julius Hornung or lab course students ("Forschungspraktikanten"). The heteroleptic $[Ni(PEt_3)_{4-n}(M'R)_n]$ complexes were synthesized on the basis of previously published results for $[Ni(M'R)_n(PR_3)_{4-n}]$[59-60].

$[Ni(PEt_3)_3(AlCp^*)]$ (1a): $[Ni(cod)_2]$ (200 mg, 0.73 mmol, 1 eq.) was suspended in toluene (5.5 mL) and subsequently AlCp* (118 mg, 0.73 mmol, 1 eq.) and PEt_3 (0.32 mL, 2.19 mmol, 3 eq.) were added. The yellow suspension was stirred at 60 °C for 1 h. After cooling to r.t., all volatile components were removed *in vacuo* yielding a yellow solid, which was washed with cold *n*-hexane (3x 1 mL) and dried *in vacuo*. Yield: 225 mg (0.34 mmol, 47%). ^{1}H NMR (400.1 MHz, C_6D_6): δ = 2.04 (s, 15H), 1.43 (m, 18H), 1.07 (m, 27H) ppm; ^{13}C NMR (100.6 MHz, C_6D_6): δ = 113.5 (s, C_5Me_5), 25.9 (d, CH_2), 10.7 (s, C_5Me_5), 9.1 (s, CH_3) ppm; ^{27}Al NMR (104 MHz, C_6D_6): δ = -71.2 (s) ppm; ^{31}P NMR (162.0 MHz, C_6D_6): δ = 19.5 (s) ppm; IR (cm^{-1}): 2956, 2925, 2902, 2871, 2816, 1452, 1424, 1370, 1260, 1095, 1021, 799, 759, 722, 685, 662,

[1] SCM, ADF2017, Theoretical Chemistry, Vrije Universiteit, Amsterdam, The Netherlands

[2] E. D. Glendening, J. K. Badenhoop, A. E. Reed, J. E. Carpenter, J. M. Bohmann and F. Weinhold, Theoretical Chemistry Institute, University of Wisconsin, Madison, WI, (http://nbo6.chem.wisc.edu/).

640, 601, 408. Elemental anal. calcd for $C_{28}H_{60}AlNiP_3$: C, 58.41; H, 10.51; Al, 4.69; P, 16.15; Ni, 10.20, found: C, 58.68; H, 10.73; Al, 4.7; P, 15.73; Ni, 10.3.

[Ni(PEt$_3$)$_2$(AlCp*)$_2$] (2a): To a suspension of[Ni(cod)$_2$] (200 mg, 0.73 mmol, 1 eq.) and AlCp* (236 mg, 1.45 mmol, 2 eq.) in *n*-hexane (5 mL) a solution of PEt_3 (0.21 mL, 1.45 mmol, 2 eq.) in *n*-hexane (5 mL) was added. The yellow suspension was stirred at 60 °C for 1.5 h. After cooling to room temperature, all volatile components were removed *in vacuo* resulting in a yellow solid, which was recrystallized, from cold *n*-hexane (2 mL). The solvent was removed with a cannula and the yellow crystalline solid was dried in vacuo. Yield: 230 mg (0.37 mmol, 51%). ^{1}H NMR (400.1 MHz, C_6D_6): δ = 2.01 (s, 30H), 1.26 (m, 12H), 1.03 (m, 18H) ppm; ^{13}C NMR (100.6 MHz, C_6D_6): δ = 113.3 (s, C_5Me_5), 28.4 (d, CH_2), 10.7 (s, C_5Me_5), 9.7 (s, CH_3) ppm; ^{27}Al NMR (104 MHz, C_6D_6): δ = -61.3 (s) ppm; ^{31}P NMR (162.0 MHz, C_6D_6): δ = 39.4 (s) ppm;IR (cm^{-1}): 2951, 2910, 2863, 1450, 1426, 1413, 1375, 1243, 1023, 999, 800, 760, 746, 721, 666, 646, 608, 587, 460, 435. Elemental anal. calcd for $C_{32}H_{60}Al_2NiP_2$: C, 62.05; H, 9.76; Al, 8.71; P, 10.00; Ni, 9.48; found: C, 61.37; H, 9.84; Al, 8.5; P, 9.92; Ni, 9.4;

[Ni(PEt$_3$)(AlCp*)$_3$] (3a): [(H)(SiEt$_3$)Ni(AlCp*)$_3$] (200 mg, 0.30 mmol, 1 eq.) was suspended in *n*-hexane (5 mL) and PEt_3 (0.087 mL, 0.60 mmol, 2 eq.) was added. The yellow suspension was stirred at 60 °C for 1.5 h. After cooling to room temperature, all volatile components were removed *in vacuo* resulting in a yellow solid, which was re-crystallized, from cold *n*-hexane (2 mL). The solvent was removed with a cannula, the remaining yellow crystalline solid was dried in vacuo. Yield: 133 mg (0.20 mmol, 65%). ^{1}H NMR (400.1 MHz, C_6D_6): δ = 1.98 (s, 45H), 1.05 (m, 6H), 0.99 (m, 9H) ppm; ^{13}C NMR (100.6 MHz, C_6D_6): δ = 112.8 (s, C_5Me_5), 29.0 (d, ^2J = 17.7 Hz, CH_2), 10.4 (d, ^3J = 4.9 Hz, CH_3) 10.3 (s, C_5Me_5) ppm; ^{27}Al NMR (104.6 MHz, C_6D_6): δ = -53.1(s) ppm; ^{31}P NMR (162.0 MHz, C_6D_6): δ = 61.9 (s) ppm; IR (cm^{-1}): 2949, 2911, 2860, 1451, 1426, 1375, 1258, 1023, 800, 762, 722, 662, 620, 584, 560, 599, 453, 440. Elemental anal. calcd for $C_{36}H_{60}$Al3NiP: C, 65.17; H, 9.12; Al, 12.20; P, 4.67; Ni, 8.85, found: C, 64.75; H, 9,01; Al, 12.0; P, 4.41; Ni, 8.3.

[Ni(PEt$_3$)$_3$(GaCp*)$_1$] (1b): [Ni(cod)$_2$] (200 mg, 0.72 mmol, 1 eq.) and GaCp* (150 mg, 0.73 mmol, 1 eq.) were suspended in *n*-hexane (5 mL) and 0.32 mL of a 1 M solution of PEt_3 solution (2.19 mmol, 4 eq.) in *n*-hexane (5 mL) was added. The yellow suspension was stirred at 60 °C for 1 h. After cooling to room temperature, all volatile components were removed *in vacuo* resulting in a yellow solid, which was recrystallized from cold *n*-hexane (2 mL). The solvent was removed with a cannula and the yellow crystalline solid was dried. When applying this procedure, the product still contained trace amounts of **2b** and free PEt_3. Yield: 65 mg (0.11 mmol, 15%). ^{1}H NMR (400.1 MHz, C_6D_6): δ = 2.14 (s, 15H), 1.36 (m, 18H), 1.03 (m, 27H) ppm; ^{13}C NMR (100.6 MHz, C_6D_6): δ = 113.0 (s, C_5Me_5), 23.1 (s, CH_2), 10.8 (s, C_5Me_5),

8.9 (s, *C*H_3) ppm; ^{31}P NMR (162.0 MHz, C_6D_6): δ = 16.6 (s) ppm; IR (cm^{-1}): 2955, 2900, 2872, 1451, 1422, 1372, 1244, 1024, 990, 798, 760, 747, 723, 687, 665, 645, 605, 424.

[Ni(PEt$_3$)$_2$(GaCp*)$_2$] (2b): [Ni(cod)$_2$] (350 mg, 1.28 mmol, 1 eq.) and GaCp* (522 mg, 2.55 mmol, 2 eq.) were suspended in *n*-hexane (5 mL)and PEt_3 (0.374 mL, 2.55 mmol, 2 eq.) dissolved in *n*-hexane (2.5 mL) was added. The yellow suspension was stirred at r.t. for 2 h. All volatile components were removed *in vacuo* resulting in a yellow solid, which was washed with cold *n*-hexane (2x1 mL) and dried. Yield: 680 mg (0.97 mmol, 76%). ^{1}H NMR (400.1 MHz, C_6D_6): δ = 2.07 (s, 30H), 1.22 (m, 12H), 0.97 (m, 18H) ppm; ^{13}C NMR (100.6 MHz, C_6D_6): δ = 112.9 (s, *C*$_5$Me$_5$), 26.4 (d, *C*H_2), 10.4 (s, C$_5$*Me*$_5$), 9.4 (s, *C*H_3) ppm; ^{31}P NMR (162.0 MHz, C_6D_6): δ = 29.4 (s) ppm; IR (cm^{-1}): 2956, 2926, 2899, 2872, 1451, 1422, 1370, 1259, 1244, 1096, 1022, 994, 798, 759, 745, 722, 687, 664, 643, 603, 422, 411. Elemental Anal. calcd for $C_{32}H_{60}Ga_2NiP_2$: C, 54.52; H, 8.58; Ga, 19.78; P, 8.79; Ni, 8.33; found: C, 55.63; H, 8.75; Ga, 18.6; P, 8.25; Ni, 8.6.

[Ni(PEt$_3$)$_2$(GaCp*)(ZnCp*)(ZnMe)]: [Ni(PEt$_3$)$_2$(GaCp*)$_2$] (100 mg, 0.14 mmol, 1.0 eq.) was dissolved in toluene (1.5 mL) and cooled to -30 °C. Subsequently, a 1 M solution of $ZnMe_2$ in toluene (54.4 mg, 0.57 mmol, 4.0 eq.) was added resulting in an orange solution. The reaction mixture was stirred for 2 h at -20 °C. The solvent was removed while the cooling bath was allowed to reach r.t. The crude product was dissolved in *n*-hexane (5 mL) and filtrated via cannula to remove the dark/black residue. Single crystals were obtained by storing the concentrated filtrate at -30 °C overnight. ^{1}H NMR (400 MHz, C_6D_6): δ = 2.29 (s, 15H, H_{GaCp*}), 2.01 (s, 15H, H_{ZnCp*}), 1.23 (dt, 12H, CH_2), 0.90 (dt, 18H, CH_3), 0.02 (s, 3H, H_{ZnMe}) ppm; ^{31}P NMR (162 MHz, C_6D_6): δ = 29.43 ppm. ^{13}C NMR (100.6 MHz, C_6D_6): δ = 113.7 (s, C_{GaCp*}), 110.0 (s, C_{ZnCp*}), 25.6 – 25.4 (m, P(*C*H_2CH$_3$)$_3$), 11.3 (s, C_{GaCp*}), 10.3 (s, C_{ZnCp*}), 8.9 (s, P(CH$_2$*C*H$_3$)$_3$), 6.8 (s, C_{ZnMe}) ppm; IR (cm^{-1}): 2952, 2900, 2884, 2857, 1450, 1419, 1380, 1257, 1141, 1028, 754, 696, 663, 616, 585, 511, 416. Elemental Anal. calcd for $C_{33}H_{63}GaNiP_2Zn_2$: C, 50.75; H, 8.13; Ga, 8.93; Ni, 7.52; P, 7.93; Zn, 16.74; found: C, 50.57; H, 8.24; Ga, 8.79; Ni, 7.34; P, 7.89; Zn, 16.81.

[(H)(SiEt$_3$)Ni(ZnCp*)$_2$(ZnMe)$_2$(AlCp*)]: A solution of $ZnMe_2$ (77 mg, 0.807 mmol, 5.3 eq.) in toluene (5 mL) was added dropwise with a cooled (-50 °C) dropping funnel to a solution of [Ni(AlCp*)$_3$(H)(SiEt$_3$)] (100 mg, 0.151 mmol, 1.0 eq.) in toluene (3 mL) which had been cooled to -50 °C over 15 min. After stirring for 3 h at -50 °C, the mixture was concentrated for 1 h to reach about 50% of the volume (at -50°C). The volatiles were removed *in vacuo* while the mixture was allowed to reach r.t. to obtain a dark green residue. ^{1}H NMR (400 MHz, C_6D_6): δ = 2.18 (s, 30 H, H_{ZnCp*}), 1.76 (s, 15 H, H_{AlCp*}), 1.07 (t, ^3J = 7.8 Hz, 9 H, H_{SiEt3}), 0.70 (q, ^3J = 7.7 Hz, 6 H, H_{SiEt3}), -0.10 (s, 6 H, H_{ZnMe}), -12.0 (s, 1 H, H_{Ni-H}) ppm;. LIFDI MS (toluene): $[M]^+$: 898.56 (calculated: 898.13).

[(PEt_3)Ni($ZnCp^*$)$_2$($ZnMe$)$_2$($AlCp^*$)]: PEt_3 (77 mg, 0.807 mmol, 5.3 eq.) was added to a solution of [Ni($AlCp^*$)$_1$($ZnCp^*$)$_2$($ZnMe$)$_2$(H)($SiEt_3$)] (100 mg, 0.151 mmol, 1.0 eq.) in C_6D_6 and heated to 80 °C for 5 min. The isolation of a pure sample is still under investigation. ^{1}H NMR (400 MHz, C_6D_6): δ = 2.24 (s, 30 H, H_{ZnCp^*}), 1.80 (s, 15 H, H_{AlCp^*}), 1.42 (m, 6 H, H_{PEt3}), 0.80 (m, 9 H, H_{PEt3}), -0.08 (s, 6 H, H_{ZnMe}) ppm; ^{31}P NMR (162 MHz, C_6D_6): δ = 46.4 ppm.

[Ni_2($AlCp^*$)$_5$]: 75 mg [Ni_2(dvds)$_3$] and 110 mg $AlCp^*$ were dissolved in toluene (2 mL) and heated to 75 °C for 15 min. Afterwards volatiles were removed in vacuo. The crude product was dissolved in boiling *n*-hexane (2 mL). Slow cooling to r.t. resulted in a red crystalline precipitate. After one hour, the mixture was cooled to 7 °C and stored in a fridge (7 °C) for several days. The supernatant was removed by Whatman filtration and the red crystalline product was dried *in vacuo*. The obtained product was used for analysis. ^{1}H NMR (400 MHz, C_6D_6): δ = 2.01 (s, 30 H), 1.97 (s, 45H) ppm; ^{13}C NMR (100.6 MHz, C_6D_6): δ = 114.0 (s, C_5Me_5), 112.9 (s, C_5Me_5), 12.27 (s, C_5Me_5), 11.00 (s, C_5Me_5) ppm; LIFDI MS (toluene): $[M]^+$: 926.23 m/z (calculated: 926.37 m/z).

[Ni_4($GaCp^*$)$_4$(EtC≡CEt)$_2$]: A solution of Ni(cod)$_2$ (30 mg) in toluene (1mL) was treated with *3*-hexyne (27 mg). The yellow solution turns deeply red upon addition of the first drops of *3*-hexyne. The resulting mixture was analyzed by liquid injection field desorption ionization mass spectrometry (LIFDI-MS). The reaction mixture was divided into two samples. The first sample was treated with about 1 eq. $GaCp^*$. The mixture was analyzed by LIFDI-MS. The other half of the sample was treated with about 5 eq. $GaCp^*$. This mixture was again divided in two parts. One half was analyzed by LIFDI-MS. The other half was heated to 110 °C for 5 min and subsequently analyzed by LIFDI-MS.

The following reactions were performed by Patricia Heiß during her Master thesis under the supervision of Julius Hornung:

[Ni($ZnCp^*$)($ZnMe$)(PEt_3)$_3$] (1c): [Ni($AlCp^*$)(PEt_3)$_3$] (20 mg, 0.035 mmol, 1.0 eq.) was suspended in toluene (1 mL) and subsequently, $ZnMe_2$ (40 mg, 0.419 mmol, 12 eq.) was added. After stirring for 1 h at r.t., the volatiles were removed *in vacuo*. ^{1}H NMR (400 MHz, C_6D_6): δ = 2.30 (s, 15 H, H_{ZnCp^*}), 1.44 (qd, ^3J = 7.6, ^2J = 2.9 Hz, 18 H, H_{PEt3}), 0.97 (dt, ^3J = 12.6, ^2J = 7.5 Hz, 27 H, H_{PEt3}), 0.03 (s, 3 H, H_{ZnMe}) ppm; ^{31}P NMR (162 MHz, C_6D_6): δ = 12.7 ppm; LIFDI MS (toluene): $[M]^+$: 691.57 (calculated: 692.20).

[Ni($ZnCp^*$)$_2$($ZnMe$)$_2$(PEt_3)$_2$] (2c): Ni($GaCp^*$)$_2$(PEt)$_2$ (246 mg, 0.348 mmol, 1.0 eq.) was suspended in toluene (2 mL) and cooled to -70 °C. A -30 °C pre-cooled solution of $ZnMe_2$ (335 mg, 3.50 mmol, 10 eq.) in toluene (2.5 mL) was added at -70 °C and stirred for 10 min at this temperature. The mixture was slowly warmed to 0 °C and stirred for additional 2 h at 0 °C. The volatiles were removed at 0 °C *in vacuo*

and the oily residue was recrystallized at 90 °C in *n*-hexane (0.8 mL). After slowly cooling to 0 °C, orange crystals could be obtained which were dried *in vacuo*. Yield: 247 mg (0.288 mmol, 83%).^{1}H NMR (400 MHz, C_6D_6): δ = 2.22 (s, 30 H, ArCH_3), 1.23 (qd, ^{3}J = 7.4, ^{2}J = 5.1 Hz, 12 H, CH_2CH$_3$), 0.86 (dt, ^{3}J = 14.9, ^{2}J = 7.5 Hz, 18 H, CH$_2$CH_3), 0.01 (s, 6 H, ZnCH_3) ppm; ^{13}C NMR (101 MHz, C_6D_6): δ = 110.2 (s, C_5Me$_5$), 25.5 – 25.2 (m, P(CH$_2$CH$_3$)$_3$), 10.90 (s, C$_5$*Me*$_5$), 8.12 (s, P(CH$_2$*C*H$_3$)$_3$), 4.77 (s, Zn*Me*) ppm; ^{31}P NMR (162 MHz, C_6D_6): δ = 27.81 ppm; LIFDI MS (toluene): [M]$^{+}$: 856.20 m/z (calculated: 856.11 m/z). Elemental analysis: calc. for $C_{34}H_{66}NiP_2Zn_4$: C, 47.65; H, 7.76; Ni, 6.85; P, 7.23; Zn, 30.51; found: C, 47.13; H, 7.81; Ni, 6.81; P, 7.10; Zn, 28.7. IR (cm^{-1}): 2957, 2895, 2855, 2926, 2817, 2723, 1448, 1416, 1381, 1259, 1097, 1029, 755, 697, 647, 614, 624, 586, 410.

[Ni(ZnCp*)$_3$(ZnMe)$_3$(PEt$_3$)$_1$] (3c): Ni(AlCp*)$_3$(PEt$_3$) (45 mg, 0.07 mmol, 1.0 eq.) was suspended in toluene (1 mL) and ZnMe$_2$ (55 mg, 0.58 mmol, 8.5 eq.) were added as a 1 M solution in toluene. After stirring for 1 d at room temperature, the volatiles were removed *in vacuo* to obtain a brownish solid. ^{1}H NMR (400 MHz, Tol-d$_8$): δ = 2.13 (s, 45 H, C$_5$*H*$_5$), 1.18 – 1.08 (m, 6 H, P(CH_2CH$_3$)$_3$), 0.70 (dt, ^{3}J = 15.2 Hz, ^{2}J = 7.5 Hz, 9 H, P(CH$_2$CH_3)$_3$), -0.05 (s, 9 H, Zn-CH_3) ppm; ^{13}C NMR (101 MHz, Tol-d$_8$): δ = 110.8 (s, C_5Me$_5$), 26.8 (s, P(CH$_2$CH$_3$)$_3$), 10.8 (s, C$_5$*Me*$_5$), 8.05 (s, P(CH$_2$*C*H$_3$)$_3$), -0.01 (s, Zn*Me*) ppm; ^{31}P NMR (162 MHz, Tol-d$_8$): δ = 29.53 ppm; LIFDI MS (toluene): [M]$^{+}$: 1018.5 (calculated: 1019.93 m/z).

The following reactions were performed by Maximilian Muhr during his Master thesis under the supervision of Julius Hornung:

[Ni(GaCp*)(dvds)]: [Ni$_2$(dvds)$_3$] (600 mg, 0.890 mmol) was dissolved in toluene (1 mL) and cooled to -30 °C. A solution of GaCp* (366 mg, 1.78 mmol) in toluene (0.5 mL) was cooled to -30 °C and added. After 10 min at -30 °C the remaining solvent was separated by cannula and the resulting orange precipitate was dried *in vacuo*. Yield: 545 mg (1.21 mmol, 68%). Yellow crystals could be obtained from a toluene solution at -30 °C. ^{1}H NMR (400 MHz, C_6D_6): δ = 3.01 (m, 4H, CH$_2$), 2.69 (m, 2H, CH), 1.84 (s, 15H, GaCp*), 0.57 (s, 6H, Me), -0.05 (s, 6H, Me) ppm; ^{13}C NMR (101 MHz, C_6D_6): δ = 113.8 (s, C$_5$Me$_5$), 55.2 (s, C=C), 47.9 (s,C=C), 9.2 (s, C$_5$Me$_5$), 1.9 (s, CH$_3$), -0.4 (s, CH$_3$) ppm; Elemental Anal. Calc. for $C_{18}H_{33}NiGaSi_2O$: C, 48.0; H, 7.4; Ni, 13.0; Ga, 15.5; Si, 12.5; found: C, 47.7; H, 7.6; Ni, 12.5; Ga, 14.5%; Si, 12.5%; LIFDI MS (toluene): [M]$^{+}$: 451.1 m/z (calculated: 450.05 m/z).

[{Ni$_4$Ga}Cp*$_3$(dvds)$_2$]: Neat [Ni(GaCp*)(dvds)] (200 mg, 0.44 mmol) was heated to 110 °C for 2 h *in vacuo*, resulting in a black crystalline material, which was washed with *n*-hexane (0.5 mL). Yield: 64 mg (0.12 mmol, 47%) of the black solid were obtained, with sufficient crystallinity for single crystal XRD. ^{1}H NMR (250.1 MHz, C_6D_6): δ = 2.30 (s, 30H, ZnCp*), 1.26 (s, 36H, CN*t*-Bu), 0.10 (s, 6H, ZnMe) ppm; ^{13}C

NMR (62.9 MHz, C_6D_6): δ = 108.7, 55.7, 30.6, 11.0 ppm; Elemental Anal. Calc. for $C_{46}H_{81}Ni_4Ga_3Si_4O_2$: C, 45.2; H, 6.7; Ni, 19.2; Ga, 17.1; Si, 9.2; O, 2.6; found: C, 50.1; H, 7.2; N, 5.5%. LIFDI MS (toluene): $[M]^+$: 1224.0 m/z (calculated: 1222.4 m/z);

Crystallographic Data:

	[Ni(GaCp*)$_2$(PEt$_3$)$_2$]	**[Ni(AlCp*)$_2$(PEt$_3$)$_2$]**	**[Ni(AlCp*)$_3$(PEt$_3$)]**
formula	$C_{32}H_{60}Ga_2NiP_2$	$C_{64}H_{120}Al_4Ni_2P_4$	$C_{36}H_{60}Al_3NiP$
M_r [g/mol]	704.87	1238.81	663.44
crystal habit	yellow fragment	Clear yellow fragment	yellow fragment
cryst syst	monoclinic	Monoclinic	orthorhombic
space group	*P 2/n*	*P12/n1*	*P n a 2$_1$*
a [Å]	14.567(8)	14.6150(8)	17.5103(7)
b [Å]	16.615(10)	16.4004(10)	11.9425(5)
c [Å]	29.858(19)	29.7339(19)	18.4956(8)
α [°]	90	90	90
β [°]	90.19(2)	90.234(2)	90
γ [°]	90	90	90
V [Å^3]	7227(7)	7126.9(7)	3867.7(3)
Z	8	4	4
ρ_c [g cm^{-3}]	1.296	1.155	1.139
F(000)	2976	2688	1432
T [K]	100	100	100
μ [mm^{-1}]	2.103	0.702	0.633
data / restraints / parameters	12776 / 532 / 912	14045 / 321 / 827	6841 / 1 / 389
GOF (F^2)	1.036	1.099	1.040
R_1[a], wR_2[b] ($I > 2\sigma(I)$)	0.0291, 0.0561	0.0396, 0.0775	0.0316, 0.0656

[a] $R_1 = \Sigma(||F_o| - |F_c||)/\Sigma|F_o|$; [b] $wR_2 = \{\Sigma[w(F_o^2 - F_c^2)^2]/\Sigma[w(F_o^2)^2]\}^{1/2}$

	[Ni(ZnMe)(ZnCp*)(GaCp*)(PEt$_3$)$_2$]	**[Ni(ZnCp*)$_2$(ZnMe)$_2$(PEt$_3$)$_2$]**
formula	$C_{33}H_{63}GaNiP_2Zn_2$	$C_{34}H_{66}NiP_2Zn_4$
M_r [g/mol]	780.94	857.06
crystal habit	Clear intense yellow block	Yellow- fragment
cryst syst	orthorombic	Tetragonal
space group	*P21212*	*P42212*
a [Å]	17.1356(18)	15.145(2)
b [Å]	18.265(2)	15.145(2)
c [Å]	12.0099(13)	17.343(3)
α [°]	90	90
β [°]	90	90
γ [°]	90	90
V [Å^3]	3758.9(7)	3978.0(15)
Z	4	8
ρ_c [g cm^{-3}]	1.380	1.431
F(000)	1640	1792
T [K]	100	100
μ [mm^{-1}]	2.568	2.942
data / restraints / parameters	6934/ 110 / 413	3784/ 216 / 263
GOF (F^2)	1.085	1.087
R_1[a], wR_2[b] ($I > 2\sigma(I)$)	0.0401, 0.0716	0.0296, 0.0788

[a] $R_1 = \Sigma(||F_o| - |F_c||)/\Sigma|F_o|$; [b] $wR_2 = \{\Sigma[w(F_o^2 - F_c^2)^2]/\Sigma[w(F_o^2)^2]\}^{1/2}$

	$[Ni_2(dvds)_3]$	**$[Ni_2(AlCp^*)_5]$**
formula	$C_{24}H54Ni_2O_3Si_6$	$C_{25}H_{37.50}Al_{2.50}Ni$
M_r [g/mol]	676.63	464.21
crystal habit	Yellow-orange fragment	Dark red fragment
cryst syst	Monoclinic	monoclinic
space group	*P12/c1*	*C12/c1*
a [Å]	6.9926(8)	14.473(9)
b [Å]	10.7321(12)	20.005(13)
c [Å]	23.987(3)	18.784(10)
α [°]	90	90
β [°]	94.064(4)	100.76(2)
γ [°]	90	90
V [Å^3]	1795.6(4)	5343.(6)
Z	2	8
ρ_c [g cm^{-3}]	1.251	1.154
F(000)	724	1984
T [K]	100	100
μ [mm^{-1}]	1.271	0.817
data / restraints / parameters	3678/ 39 / 184	5275/ 1183 / 510
GOF (F^2)	1.085	1.052
R_1[a], wR_2[b] ($I > 2\sigma(I)$)	0.0314, 0.0787	0.0453, 0.1112

[a] $R_1 = \Sigma(||F_o| - |F_c||)/\Sigma|F_o|$; [b] $wR_2 = \{\Sigma[w(F_o^2 - F_c^2)^2]/\Sigma[w(F_o^2)^2]\}^{1/2}$

	[Ni(GaCp*)(dvds)]	**[Ni_2(μ-GaCp*)(μ-GaNiCp*)$_2$(dvds)$_2$]**
formula	$C_{18}H_{33}GaNiOSi_2$	$C_{23}H_{40.5}Ga_{1.5}Ni_2OSi_2$
M_r [g/mol]	450.05	611.23
crystal habit	Yellow-orange fragment	Black fragment
cryst syst	Triclinic	Triclinic
space group	*P-1*	*P-1*
a [Å]	9.5552(10)	12.844(14)
b [Å]	10.9769(12)	13.324(17)
c [Å]	11.8382(13)	20.60(2)
α [°]	64.916(4)	86.12(4)
β [°]	80.903(4)	77.76(3)
γ [°]	72.007(4)	89.64(4)
V [Å^3]	1069.0(2)	3437.(7)
Z	2	4
ρ_c [g cm^{-3}]	1.398	1.181
F(000)	472	1268
T [K]	100	100
μ [mm^{-1}]	2.254	2.325
data / restraints / parameters	4210/ 0 / 217	13046/ 1424 / 939
GOF (F^2)	1.029	1.135
R_1[a], wR_2[b] ($I > 2\sigma(I)$)	0.0216, 0.0548	0.0427, 0.1111

[a] $R_1 = \Sigma(||F_o| - |F_c||)/\Sigma|F_o|$; [b] $wR_2 = \{\Sigma[w(F_o^2 - F_c^2)^2]/\Sigma[w(F_o^2)^2]\}^{1/2}$

VIII References

1. Mayer, K.; Weßing, J.; Fässler, T. F.; Fischer, R. A., *Angew. Chem. Int. Ed.* **2018,** *57*, 14372.
2. Ganesamoorthy, C.; Wessing, J.; Kroll, C.; Seidel, R. W.; Gemel, C.; Fischer, R. A., *Angew. Chem. Int. Ed.* **2014,** *53* (30), 7943-7947.
3. Prinz, J.; Pignedoli, C. A.; Stöckl, Q. S.; Armbrüster, M.; Brune, H.; Gröning, O.; Widmer, R.; Passerone, D., *J. Am. Chem. Soc.* **2014,** *136* (33), 11792-11798.
4. Krajčí, M.; Hafner, J., *J. Phys. Chem. C* **2014,** *118* (23), 12285-12301.
5. Krajčí, M.; Hafner, J., *ChemCatChem* **2016,** *8* (1), 34-48.
6. Tolman, C. A., *J. Am. Chem. Soc.* **1970,** *92* (10), 2956-2965.
7. Tolman, C. A.; Seidel, W. C.; Gosser, L. W., *J. Am. Chem. Soc.* **1974,** *96* (1), 53-60.
8. Steinke, T.; Gemel, C.; Cokoja, M.; Winter, M.; Fischer, R. A., *Angew. Chem. Int. Ed.* **2004,** *43* (17), 2299-2302.
9. v. Wilde, M. P., *Ber. dtsch. Chem. Ges.* **1874,** *7* (1), 352-357.
10. Sabatier, P.; Senderens, J. B., *C. R. Acad. Sci.* **1899,** *128*, 1173.
11. Sabatier, P.; Senderens, J. B., *C. R. Acad. Sci.* **1900,** *131*, 40.
12. Paal, C.; Hartmann, W., *Ber. dtsch. Chem. Ges.* **1909,** *42* (3), 3930-3939.
13. Marvell, E. N.; Li, T., *Synthesis* **1973,** *1973* (08), 457-468.
14. Derrien, M. L., Chapter 18 Selective Hydrogenation Applied to the Refining of Petrochemical Raw Materials Produced by Steam Cracking. In *Studies in Surface Science and Catalysis*, Cerveny, L., Ed. Elsevier: 1986; Vol. 27, pp 613-666.
15. Schbib, N. S.; García, M. A.; Gígola, C. E.; Errazu, A. F., *Ind. Eng. Chem. Res.* **1996,** *35* (5), 1496-1505.
16. Studt, F.; Abild-Pedersen, F.; Bligaard, T.; Sørensen, R. Z.; Christensen, C. H.; Nørskov, J. K., *Science* **2008,** *320* (5881), 1320-1322.
17. Thanh, C. N.; Didillon, B.; Sarrazin, P.; Cameron, C. U.S. Patent 6,054,409. 2000.
18. Sheth, P. A.; Neurock, M.; Smith, C. M., *J. Phys. Chem. B* **2005,** *109*, 12449-12466.
19. Kovnir, K.; Armbrüster, M.; Teschner, D.; Venkov, T. V.; Jentoft, F. C.; Knop-Gericke, A.; Grin, Y.; Schlögl, R., *Sci. Technol. Adv. Mater.* **2007,** *8* (5), 420-427.
20. Armbrüster, M.; Kovnir, K.; Friedrich, M.; Teschner, D.; Wowsnick, G.; Hahne, M.; Gille, P.; Szentmiklósi, L.; Feuerbacher, M.; Heggen, M.; Girgsdies, F.; Rosenthal, D.; Schlögl, R.; Grin, Y., *Nat. Mater.* **2012,** *11* (8), 690-693.
21. Furukawa, S.; Komatsu, T., *ACS Catalysis* **2017,** *7* (1), 735-765.
22. Li, C.; Chen, Y.; Zhang, S.; Zhou, J.; Wang, F.; He, S.; Wei, M.; Evans, D. G.; Duan, X., *ChemCatChem* **2014,** *6* (3), 824-831.
23. Castleman, A. W., *Catal. Lett.* **2011,** *141* (9), 1243-1253.
24. Schwarz, H., *Angew. Chem. Int. Ed.* **2015,** *54* (35), 10090-10100.
25. Hübner, O.; Hornung, J.; Himmel, H.-J., *J. Chem. Phys.* **2015,** *143* (2), 024309.
26. Hebben, N.; Himmel, H.-J.; Eickerling, G.; Herrmann, C.; Reiher, M.; Herz, V.; Presnitz, M.; Scherer, W., *Chem. Eur. J.* **2007,** *13* (36), 10078-10087.
27. Manceron, L.; Hübner, O.; Himmel, H.-J., *Eur. J. Inorg. Chem.* **2009,** *2009* (5), 595-598.
28. Hübner, O.; Himmel, H.-J., *Angew. Chem. Int. Ed.* **2017,** *56* (40), 12340-12343.
29. Hübner, O.; Himmel, H.-J., *Chem. Eur. J.* **2018,** *24* (36), 8941-8961.
30. Heiz, U.; Vanolli, F.; Sanchez, A.; Schneider, W. D., *J. Am. Chem. Soc.* **1998,** *120* (37), 9668-9671.
31. Lim, D.; Hwang, C.; Ganteför, G.; Kim, Y. D., *Phys. Chem. Chem. Phys.* **2010,** *12*, 15172-80.
32. Li, Z. Y.; Young, N. P.; Di Vece, M.; Palomba, S.; Palmer, R. E.; Bleloch, A. L.; Curley, B. C.; Johnston, R. L.; Jiang, J.; Yuan, J., *Nature* **2007,** *451*, 46.
33. Zhou, S.; Li, J.; Schlangen, M.; Schwarz, H., *Acc. Chem. Res.* **2016,** *49* (3), 494-502.
34. Koszinowski, K.; Schröder, D.; Schwarz, H., *J. Am. Chem. Soc.* **2003,** *125*, 3676-3677.

35. Hakkinen, H., *Chemical Society Reviews* **2008,** *37* (9), 1847-1859.
36. Walter, M.; Akola, J.; Lopez-Acevedo, O.; Jadzinsky, P. D.; Calero, G.; Ackerson, C. J.; Whetten, R. L.; Grönbeck, H.; Häkkinen, H., *Proc. Natl. Acad. Sci. U.S.A.* **2008,** *105* (27), 9157-9162.
37. Lopez-Acevedo, O.; Kacprzak, K. A.; Akola, J.; Häkkinen, H., *Nat. Chem.* **2010,** *2*, 329.
38. Sculfort, S.; Braunstein, P., *Chem. Soc. Rev.* **2011,** *40* (5), 2741-2760.
39. Schnöckel, H., *Chem. Rev.* **2010,** *110* (7), 4125-4163.
40. Ecker, A.; Weckert, E.; Schnöckel, H., *Nature* **1997,** *387* (6631), 379-381.
41. Köhnlein, H.; Purath, A.; Klemp, C.; Baum, E.; Krossing, I.; Stösser, G.; Schnöckel, H., *Inorg. Chem.* **2001,** *40* (19), 4830-4838.
42. Schnepf, A.; Schnöckel, H., *Angew. Chem. Int. Ed.* **2001,** *40* (4), 711-715.
43. Schnepf, A.; Schnöckel, H., *Angew. Chem. Int. Ed.* **2002,** *41* (19), 3532-3554.
44. Behrens, M.; Studt, F.; Kasatkin, I.; Kühl, S.; Hävecker, M.; Abild-Pedersen, F.; Zander, S.; Girgsdies, F.; Kurr, P.; Kniep, B.-L.; Tovar, M.; Fischer, R. W.; Nørskov, J. K.; Schlögl, R., *Science* **2012,** *336* (6083), 893-897.
45. Tsai, A. P.; Kameoka, S.; Nozawa, K.; Shimoda, M.; Ishii, Y., *Acc. Chem. Res.* **2017,** *50* (12), 2879-2885.
46. Fischer, R. A.; Weiß, J., *Angew. Chem. Int. Ed.* **1999,** *38*, 2830-2850.
47. Gonzalez-Gallardo, S.; Bollermann, T.; Fischer, R. A.; Murugavel, R., *Chem. Rev.* **2012,** *112* (6), 3136-3170.
48. Freitag, K.; Gemel, C.; Jerabek, P.; Oppel, I. M.; Seidel, R. W.; Frenking, G.; Banh, H.; Dilchert, K.; Fischer, R. A., *Angew. Chem. Int. Ed.* **2015,** *54* (14), 4370-4374.
49. Freitag, K.; Banh, H.; Gemel, C.; Seidel, R. W.; Kahlal, S.; Saillard, J. Y.; Fischer, R. A., *Chem. Commun.* **2014,** *50* (63), 8681-8684.
50. Banh, H.; Hornung, J.; Kratz, T.; Gemel, C.; Pothig, A.; Gam, F.; Kahlal, S.; Saillard, J. Y.; Fischer, R. A., *Chem. Sci.* **2018,** *9* (48), 8906-8913.
51. Kuld, S.; Thorhauge, M.; Falsig, H.; Elkjær, C. F.; Helveg, S.; Chorkendorff, I.; Sehested, J., *Science* **2016,** *352* (6288), 969-974.
52. Nakamura, J.; Fujitani, T.; Kuld, S.; Helveg, S.; Chorkendorff, I.; Sehested, J., *Science* **2017,** *357* (6354), eaan8074.
53. Kattel, S.; Ramírez, P. J.; Chen, J. G.; Rodriguez, J. A.; Liu, P., *Science* **2017,** *355* (6331), 1296-1299.
54. Steinke, T., *Beiträge zur Koordinationschemie der niedervalenten Aluminium, Gallium und Indium-Organyle E Cp* an Übergangsmetallen, Dissertation, Ruhr-Universität Bochum* **2005**.
55. Molon, M.; Gemel, C.; Fischer, R. A., *J. Organomet. Chem.* **2014,** *751*, 573-578.
56. Kempter, A.; Gemel, C.; Cadenbach, T.; Fischer, R. A., *Organometallics* **2007,** *26* (17), 4257-4264.
57. Cadenbach, T.; Bollermann, T.; Gemel, C.; Tombul, M.; Fernandez, I.; Hopffgarten, M. v.; Frenking, G.; Fischer, R. A., *J. Am. Chem. Soc.* **2009,** *131* (44), 16063-16077.
58. Hornung, J.; Weßing, J.; Molon, M.; Dilchert, K.; Gemel, C.; Fischer, R. A., *J. Organomet. Chem.* **2018,** *860*, 78-84.
59. Freitag, K.; Molon, M.; Jerabek, P.; Dilchert, K.; Rösler, C.; Seidel, R. W.; Gemel, C.; Frenking, G.; Fischer, R. A., *Chem. Sci.* **2016,** *7* (10), 6413-6421.
60. Molon, M.; Bollermann, T.; Gemel, C.; Schaumann, J.; Fischer, R. A., *Dalton Trans.* **2011,** *40* (40), 10769-10774.
61. Hornung, J.; Weßing, J.; Jerabek, P.; Gemel, C.; Pöthig, A.; Frenking, G.; Fischer, R. A., *Inorg. Chem.* **2018,** *57* (20), 12657-12664.
62. Dias, P. B.; de Piedade, M. E. M.; Simões, J. A. M., *Coord. Chem. Rev.* **1994,** *135*, 737-807.
63. Dewar, M. J. S., *Bull. Soc. Chim. Fr.* **1951,** *18*, C79.
64. Chatt, J.; Duncanson, L. A., *J. Chem. Soc.* **1953,** (0), 2939-2947.
65. Herges, R.; Papafilippopoulos, A., *Angew. Chem. Int. Ed.* **2001,** *40* (24), 4671-4674.

66. Straub, B. F.; Gollub, C., *Chem. Eur. J.* **2004,** *10* (12), 3081-3090.
67. Molon, M.; Gemel, C.; Jerabek, P.; Trombach, L.; Frenking, G.; Fischer, R. A., *Inorg. Chem.* **2014,** *53* (19), 10403-10411.
68. Molon, M.; Dilchert, K.; Gemel, C.; Seidel, R. W.; Schaumann, J.; Fischer, R. A., *Inorg. Chem.* **2013,** *52* (24), 14275-14283.
69. Hopkins, M. N.; Shimmei, K.; Uttley, K. B.; Bernskoetter, W. H., *Organometallics* **2018,** *37* (20), 3573-3580.
70. Pörschke Klaus, R.; Mynott, R.; Krüger, C.; Romão, M. J., *Z. Naturforsch. B* **1984,** *39* (8), 1076.
71. Pörschke Klaus, R.; Mynott, R.; Angermund, K.; Krüger, C., *Z. Naturforsch. B* **1985,** *40* (2), 199.
72. Frenking, G.; Wichmann, K.; Fröhlich, N.; Loschen, C.; Lein, M.; Frunzke, J.; Rayón, V. c. M., *Coord. Chem. Rev.* **2003,** *238-239*, 55-82.
73. Cadenbach, T.; Bollermann, T.; Gemel, C.; Fernandez, I.; von Hopffgarten, M.; Frenking, G.; Fischer, R. A., *Angew. Chem. Int. Ed.* **2008,** *47* (47), 9150-9154.
74. Kutzelnigg, W., *Angew. Chem. Int. Ed.* **1984,** *23* (4), 272-295.
75. Uddin, J.; Frenking, G., *J. Am. Chem. Soc.* **2001,** *123*, 1683-1693.
76. Molon, M., *Metallatomreiche Koordinationsverbindungen und Cluster: Synthese, Charakterisierung und Funktionalisierung, Dissertation, Ruhr-Universität Bochum* **2013**.
77. Steinborn, D., *Fundamentals of Organometallic Catalysis*. Wiley VCH: Weinheim, 2012; p 27.
78. Tolman, C. A.; Seidel, W. C., *J. Am. Chem. Soc.* **1974,** *96* (9), 2774-2780.
79. Tolman, C. A., *J. Am. Chem. Soc.* **1974,** *96* (9), 2780-2789.
80. Bollermann, T.; Gemel, C.; Fischer, R. A., *Coord. Chem. Rev.* **2012,** *256* (5-8), 537-555.
81. Jutzi, P.; Neumann, B.; Schebaum, L. O.; Stammler, A.; Stammler, H.-G., *Organometallics* **1999,** *18* (21), 4462-4464.
82. Cundy, C. S., *J. Organomet. Chem.* **1974,** *69* (2), 305-310.
83. Resa, I.; Carmona, E.; Gutierrez-Puebla, E.; Monge, A., *Science* **2004,** *305* (5687), 1136-1138.
84. Hursthouse, M. B.; Izod, K. J.; Motevalli, M.; Thornton, P., *Polyhedron* **1994,** *13* (1), 151-153.
85. Buchin, B.; Steinke, T.; Gemel, C.; Cadenbach, T.; Fischer, R. A., *Z. anorg. allg. Chemie* **2005,** *631* (13‐14), 2756-2762.
86. Michalak, A.; Mitoraj, M.; Ziegler, T., *J. Phys. Chem. C* **2008,** *112* (9), 1933-1939.
87. Mitoraj, M. P.; Michalak, A.; Ziegler, T., *J. Chem.Theory Comput.* **2009,** *5* (4), 962-975.
88. Steinke, T.; Cokoja, M.; Gemel, C.; Kempter, A.; Krapp, A.; Frenking, G.; Zenneck, U.; Fischer, R. A., *Angew. Chem. Int. Ed.* **2005,** *44* (19), 2943-2946.
89. Lyaskovskyy, V.; de Bruin, B., *ACS Catal.* **2012,** *2* (2), 270-279.
90. Chen, Z.; Wannere, C. S.; Corminboeuf, C.; Puchta, R.; Schleyer, P. v. R., *Chem. Rev.* **2005,** *105* (10), 3842-3888.
91. Geuenich, D.; Hess, K.; Köhler, F.; Herges, R., *Chem. Rev.* **2005,** *105* (10), 3758-3772.
92. Macchi, P.; Sironi, A., *Coord. Chem. Rev.* **2003,** *238-239*, 383-412.
93. Merino, G.; Vela, A.; Heine, T., *Chem. Rev.* **2005,** *105* (10), 3812-3841.
94. Molon, M.; Gemel, C.; Fischer, R. A., *Eur. J. Inorg. Chem.* **2013,** *2013* (21), 3616-3622.
95. Muetterties, E. L.; Pretzer, W. R.; Thomas, M. G.; Beier, B. F.; Thorn, D. L.; Day, V. W.; Anderson, A. B., *J. Am. Chem. Soc.* **1978,** *100* (7), 2090-2096.
96. Jutzi, P.; Neumann, B.; Reumann, G.; Stammler, H.-G., *Organometallics* **1998,** *17* (7), 1305-1314.
97. Gemel, C.; Steinke, T.; Weiss, D.; Cokoja, M.; Winter, M.; Fischer, R. A., *Organometallics* **2003,** *22* (13), 2705-2710.
98. Steinke, T.; Gemel, C.; Winter, M.; Fischer, R. A., *Chem. Eur. J.* **2005,** *11* (5), 1636-1646.
99. Shoshani, M. M.; Johnson, S. A., *Nat. Chem.* **2017,** *9*, 1282.
100. Bollermann, T.; Schwedler, I.; Molon, M.; Freitag, K.; Gemel, C.; Seidel, R. W.; Fischer, R. A., *Dalton Trans.* **2011,** *40* (46), 12570-12577.
101. Molon, M.; Gemel, C.; Fischer, R. A., *Dalton Trans.* **2014,** *43* (8), 3114-3120.

102. Weßing, J.; Ganesamoorthy, C.; Kahlal, S.; Marchal, R.; Gemel, C.; Cador, O.; Da Silva, A. C. H.; Da Silva, J. L. F.; Saillard, J.-Y.; Fischer, R. A., *Angew. Chem. Int. Ed.* **2018,** *57* (44), 14630-14634.
103. Weiß, D.; Winter, M.; Fischer, R. A.; Yu, C.; Wichmann, K.; Frenking, G., *Chem. Commun.* **2000,** (24), 2495-2496.
104. Ignatyev, I. S.; Schaefer, H. F.; King, R. B.; Brown, S. T., *J. Am. Chem. Soc.* **2000,** *122* (9), 1989-1994.
105. Pacchioni, G.; Rösch, N., *Acc. Chem. Res.* **1995,** *28*, 390-397.
106. Beattie, J. K.; Masters, A. F.; Meyer, J. T., *Polyhedron* **1995,** *14*, 829-868.
107. Garratt, A. P.; Thompson, H. W., *J. Chem. Soc.* **1934**, 1817-1822.
108. Buchin, B.; Gemel, C.; Cadenbach, T.; Fischer, R. A., *Inorg. Chem.* **2006,** *45* (4), 1789-1794.
109. Maciejewski, H.; Marciniec, B.; Kownacki, I., *J. Organomet. Chem.* **2000,** *597* (1), 175-181.
110. Hitchcock, P. B.; Lappert, M. F.; Warhurst, N. J. W., *Angew. Chem. Int. Ed.* **1991,** *30* (4), 438-440.
111. Cotton, F. A.; Troup, J. M., *Dalton Trans.* **1974,** (8), 800-802.
112. Weßing, J.; Ganesamoorthy, C.; Kahlal, S.; Marchal, R.; Gemel, C.; Cador, O.; Da Silva, A. C. H.; Da Silva, J. L. F.; Saillard, J.-Y.; Fischer, R. A., *Angew. Chem. Int. Ed. 0* (0).
113. Schilter, D., *Nat. Rev. Chem.* **2018,** *2* (8), 147-147.
114. Weßing, J. From Intermetallics to Intermetalloid Clusters. Dissertation, Technische Universität München, München, 2018.
115. Shoshani, M. M.; Liu, J.; Johnson, S. A., *Organometallics* **2018,** *37* (1), 116-126.
116. Doerr, M.; Frenking, G., *Zeitschrift für anorganische und allgemeine Chemie* **2002,** *628* (4), 843-850.
117. Krysan, D. J.; Mackenzie, P. B., *J. Org. Chem.* **1990,** *55* (13), 4229-4230.
118. Ganesamoorthy, C.; Loerke, S.; Gemel, C.; Jerabek, P.; Winter, M.; Frenking, G.; Fischer, R. A., *Chem. Commun.* **2013,** *49* (28), 2858-2860.
119. Bogdanović, B.; Kröner, M.; Wilke, G., *Liebigs Ann. Chem.* **1966,** *699* (1), 1-23.
120. Fulmer, G. R.; Miller, A. J. M.; Sherden, N. H.; Gottlieb, H. E.; Nudelman, A.; Stoltz, B. M.; Bercaw, J. E.; Goldberg, K. I., *Organometallics* **2010,** *29* (9), 2176-2179.
121. INC, B. A., *APEX suite of crystallographic software, APEX 3 Version 2015 5.2,* **2015,** *Madison, Wisconsin, USA*.
122. INC, B. A., *SAINT, Version 8.34A and SADABS, Version 2014/5* **2014,** *Madison, Wisconsin, USA*.
123. Sheldrick, G., *Acta Crystallogr. A* **2015,** *71* (1), 3-8.
124. Sheldrick, G., *Acta Crystallogr. C* **2015,** *71* (1), 3-8.
125. Hubschle, C. B.; Sheldrick, G. M.; Dittrich, B., *J. Appl. Crystallogr* **2011,** *44* (6), 1281-1284.
126. Neese, F., *Wiley Interdiscip. Rev. Comput. Mol. Sci.* **2012,** *2* (1), 73-78.
127. Becke, A. D., *Phys. Rev. A* **1988,** *38* (6), 3098-3100.
128. Perdew, J. P., *Phys. Rev. B* **1986,** *33* (12), 8822-8824.
129. Grimme, S.; Antony, J.; Ehrlich, S.; Krieg, H., *J. Chem. Phys.* **2010,** *132* (15), 154104.
130. Grimme, S.; Ehrlich, S.; Goerigk, L., *J. Comput. Chem.* **2011,** *32* (7), 1456-1465.
131. Weigend, F.; Ahlrichs, R., *Phys. Chem. Chem. Phys* **2005,** *7* (18), 3297-3305.
132. Neese, F.; Wennmohs, F.; Hansen, A.; Becker, U., *J. Chem. Phys.* **2009,** *356* (1), 98-109.
133. Glendening, E. D.; Reed, A. E.; Carpenter, J. E.; Weinhold, F., Vol. NBO Version 3.1 Gaussian Inc.
134. Frisch, M. J.; Trucks, G. W.; Schlegel, H. B.; Scuseria, G. E.; Robb, M. A.; Cheeseman, J. R.; Scalmani, G.; Barone, V.; Mennucci, B.; Petersson, G. A.; Nakatsuji, H.; Caricato, M.; Li, X.; Hratchian, H. P.; Izmaylov, A. F.; Bloino, J.; Zheng, G.; Sonnenberg, J. L.; Hada, M.; Ehara, M.; Toyota, K.; Fukuda, R.; Hasegawa, J.; Ishida, M.; Nakajima, T.; Honda, Y.; Kitao, O.; Nakai, H.; Vreven, T.; Montgomery, J. A.; Peralta, J. E.; Ogliaro, F.; Bearpark, M.; Heyd, J. J.; Brothers, E.; Kudin, K. N.; Staroverov, V. N.; Kobayashi, R.; Normand, J.; Raghavachari, K.; Rendell, A.;

Burant, J. C.; Iyengar, S. S.; Tomasi, J.; Cossi, M.; Rega, N.; Millam, J. M.; Klene, M.; Knox, J. E.; Cross, J. B.; Bakken, V.; Adamo, C.; Jaramillo, J.; Gomperts, R.; Stratmann, R. E.; Yazyev, O.; Austin, A. J.; Cammi, R.; Pomelli, C.; Ochterski, J. W.; Martin, R. L.; Morokuma, K.; Zakrzewski, V. G.; Voth, G. A.; Salvador, P.; Dannenberg, J. J.; Dapprich, S.; Daniels, A. D.; Farkas; Foresman, J. B.; Ortiz, J. V.; Cioslowski, J.; Fox, D. J., Wallingford CT, 2009.
135. Lu, T.; Chen, F., *J. Comput. Chem.* **2012,** *33* (5), 580-592.
136. Parafiniuk, M.; Mitoraj, M. P., *J. Mol. Model* **2014,** *20* (6), 2272.
137. Michalak, A.; Mitoraj, M.; Ziegler, T., *J. Phys. Chem. A.* **2008,** *112* (9), 1933-1939.
138. te Velde, G.; Bickelhaupt, F. M.; Baerends, E. J.; Fonseca Guerra, C.; van Gisbergen, S. J. A.; Snijders, J. G.; Ziegler, T., *J. Comput. Chem.* **2001,** *22* (9), 931-967.
139. Snijders, J. G.; Vernooijs, P.; Baerends, E. J., *Atomic Data and Nuclear Data Tables* **1981,** *26* (6), 483-509.
140. Chang, C.; Pelissier, M.; Durand, P., *Phys. Scr.* **1986,** *34* (5), 394.
141. Heully, J. L.; Lindgren, I.; Lindroth, E.; Lundqvist, S.; Martensson-Pendrill, A. M., *J. Phys. B.: At. Mol. Phys.* **1986,** *19* (18), 2799.
142. Snijders, J. G.; Sadlej, A. J., *Chem. Phys. Lett.* **1996,** *252* (1), 51-61.
143. Lenthe, E. v.; Baerends, E. J.; Snijders, J. G., *J. Chem. Phys.* **1993,** *99* (6), 4597-4610.
144. van Lenthe, E.; van Leeuwen, R.; Baerends, E. J.; Snijders, J. G., *Int. J. Quantum Chem.* **1996,** *57* (3), 281-293.

Ⅸ Appendix

Molecular structures of calculated $[Ni(M'R)_n(UHC)_{4-n}]$ complexes

$[Ni(C_2H_x)_3]$:

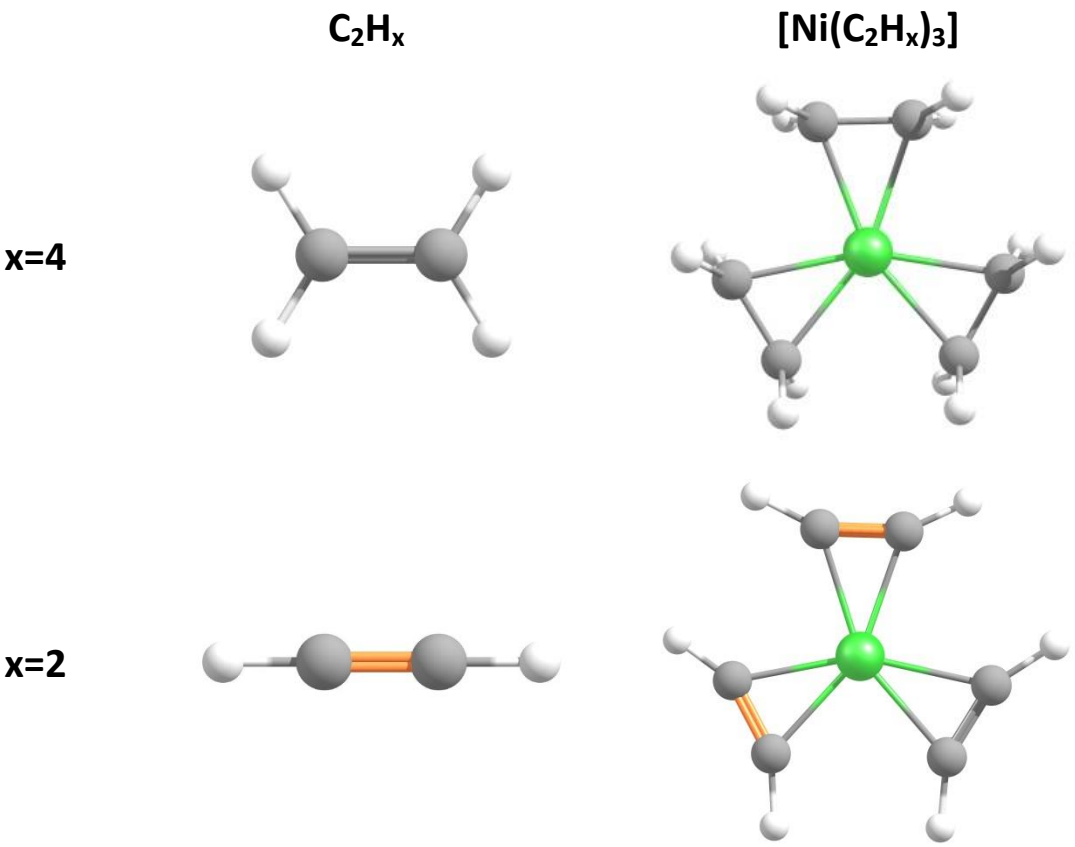

Figure S 1: Optimized Molecular structures (BP86-D3/def2-TZVPP) of C_2H_x and the parent $[Ni(C_2H_x)_3]$ complexes.

Table S 1: Summary of selected structural parameters of optimized C_2H_x and $[Ni(C_2H_x)_3]$ (BP86-D3/def2-TZVPP).

	Free ligands		**$[Ni(C_2H_x)_3]$**	
UHC	C_2H_4	C_2H_2	C_2H_4	C_2H_2
d(CC) [Å]	1.33	1.20	1.39	1.25
d(NiC) [Å]			2.05	1.99

$[Ni(PEt_3)_n(C_2H_x)_{4-n}]$:

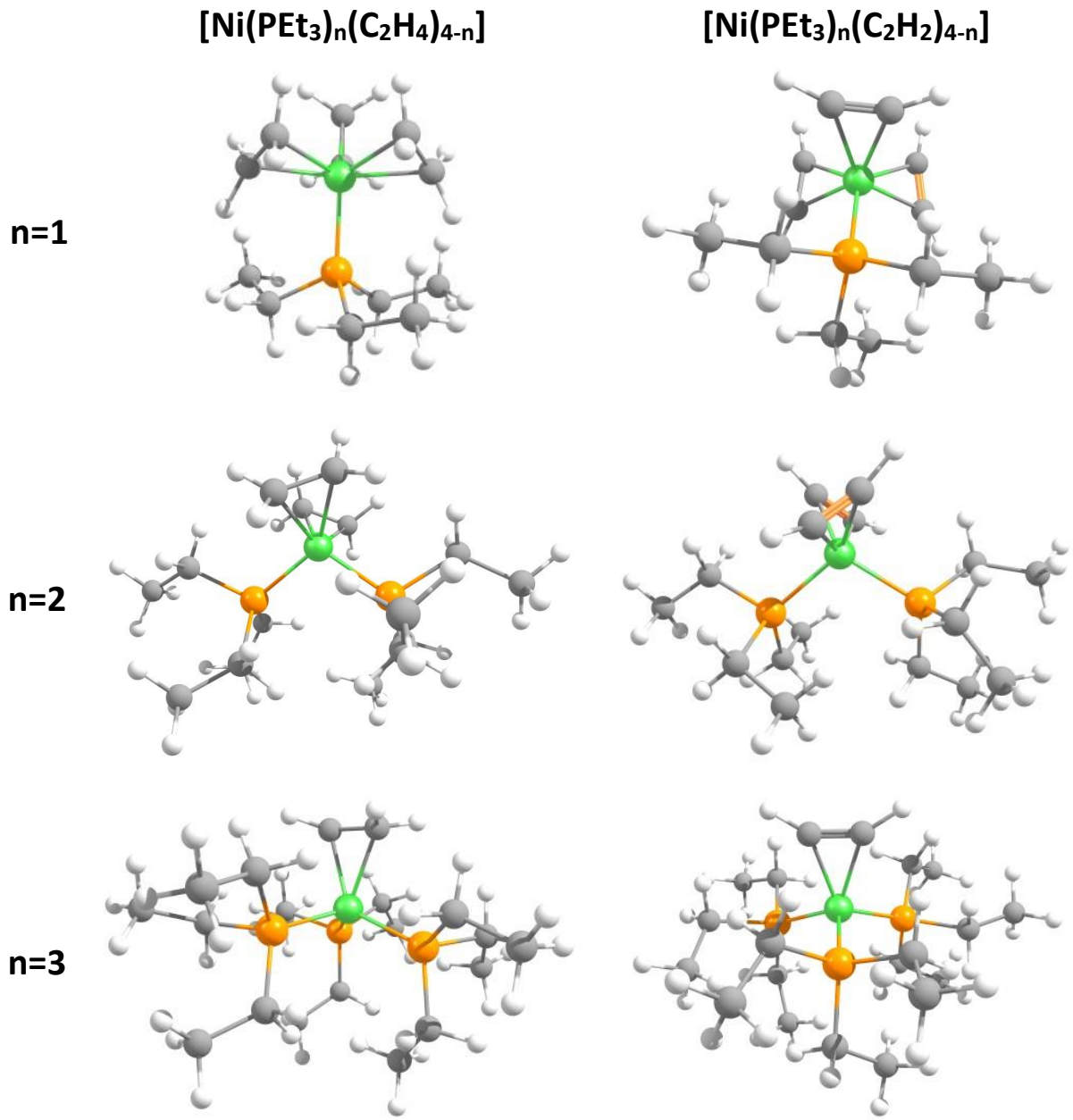

Figure S 2: Optimized Molecular structures (BP86-D3/def2-TZVPP) of $[Ni(PEt_3)_n(C_2H_x)_{4-n}]$.

Table S 2: Summary of selected structural parameters of optimized $[Ni(PEt_3)_n(C_2H_x)_{4-n}]$ (BP86-D3/def2-TZVPP).

	$[Ni(PEt_3)(C_2H_x)_3]$		**$[Ni(PEt_3)_2(C_2H_x)_2]$**		**$[Ni(PEt_3)_3(C_2H_x)]$**	
	C_2H_4	C_2H_2	C_2H_4	C_2H_2	C_2H_4	C_2H_2
d(C-C) [Å]	1.39	1.25	1.40	1.26	1.40	1.27
d(Ni-C) [Å]	2.08 - 2.12	2.02 - 2.10	2.08	1.91 - 2.04	2.06	2.00
d(Ni-P) [Å]	2.21	2.21	2.17	2.21	2.15-2.19	2.15-2.24
d(P-C) [Å]	<3.16	<3.15	<3.09	<3.11	<3.02	<3.06

$[Ni(ZnR)_{2n}(C_2H_x)_{4-n}]$:

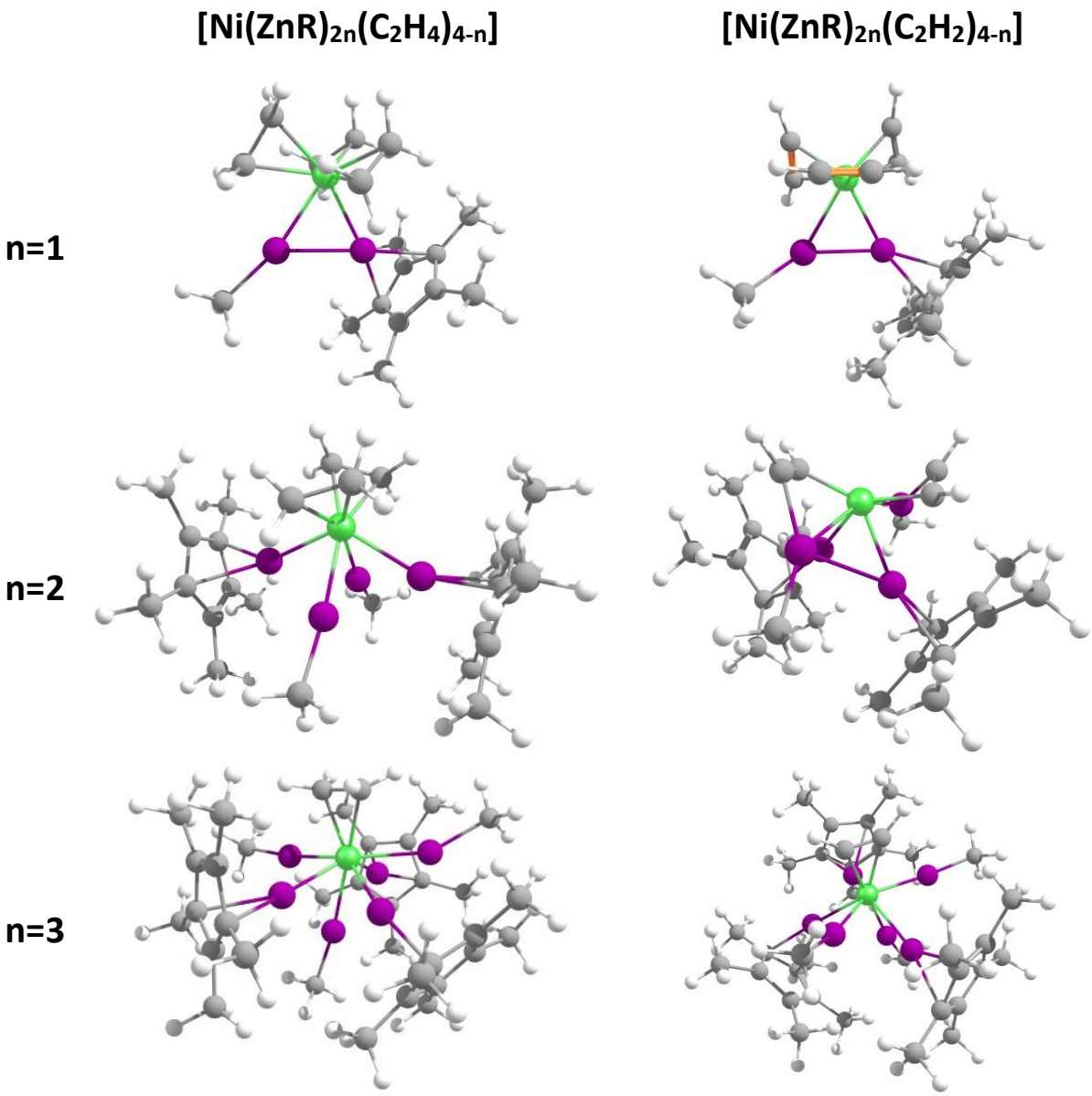

Figure S 3: Optimized Molecular structures (BP86-D3/def2-TZVPP) of $[Ni(ZnCp^*)_n(ZnMe)_n(C_2H_x)_{4-n}]$.

Table S 3: Summary of selected structural parameters of optimized $[Ni(ZnCp^*)_n(ZnMe)_n(C_2H_x)_{4-n}]$ (BP86-D3/def2-TZVPP).

	$[Ni(ZnCp^*)(ZnMe)(C_2H_x)_3]$		**$[Ni(ZnCp^*)_2(ZnMe)_2(C_2H_x)_2]$**		**$[Ni(ZnCp^*)_3(ZnMe)_3(C_2H_x)]$**	
	C_2H_4	C_2H_2	C_2H_4	C_2H_2	C_2H_4	C_2H_2
d(C-C) [Å]	1.40	1.25	1.40	1.34	1.42	1.28
d(Ni-C) [Å]	2.04 - 2.15	1.99 - 2.12	2.08	1.90 - 2.25	2.05	1.99
d(Ni-ZnR) [Å]	2.40	2.41	2.35	2.30 - 2.43	2.33 - 2.38	2.31 - 2.39
d(Zn-C) [Å]	> 2.41	> 2.76	>2.95	2.03	>2.57	>2.55
d(Zn-Zn) [Å]	2.46	2.45	> 2.62	> 2.72	>2.61	>2.59

Ni-Zn bridging output structure of $[Ni(ZnR)_2(C_2H_2)_3]$ (local minimum BP86-D3/def2-TZVPP):

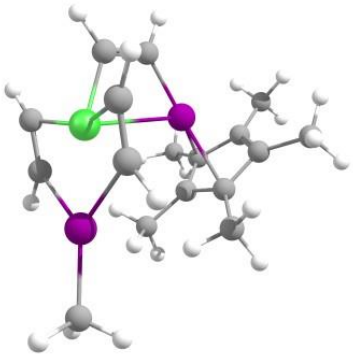

Figure S 4: Calculated structure of $[Ni(ZnCp^*)(ZnMe)(C_2H_2)_3]$ featuring NiZn bridging C_2H_2 coordination.

Table S 4: Structural parameters of $[Ni(ZnCp^*)(ZnMe)(C_2H_2)_3]$ featuring NiZn bridging C_2H_2 coordination.

	$[Ni(ZnCp^*)(ZnMe)(C_2H_2)_3]$	
	Non-bridging	bridging
d(C-C) [Å]	1.25	1.29-1.33
d(Ni-C) [Å]	1.99 - 2.12	1.87-2.75
d(Ni-ZnR) [Å]	2.41	2.38-3.05
d(Zn-C) [Å]	> 2.76	1.93-2.27
d(Zn-Zn) [Å]	2.45	4.20

This structure was obtained when C_2H_2 was put into Ni-Zn bridging coordinations before geometry optimization. Both $[Ni(ZnR)_2(C_2H_2)_3]$ structures are local minima on the potential energy surface. This minimum is about 15kcal/mol more stable. However, the Ni-Zn as well as Zn-Zn distances exceed standard distances.[59] Therefore, this structure was only included in the SI. The values discussed in the manuscript belong to the $[Ni(ZnR)_2(C_2H_2)_3]$ structure with non-bridging C_2H_2 ligands.

[Ni(AlCp*)$_n$(C$_2$H$_x$)$_{4-n}$]:

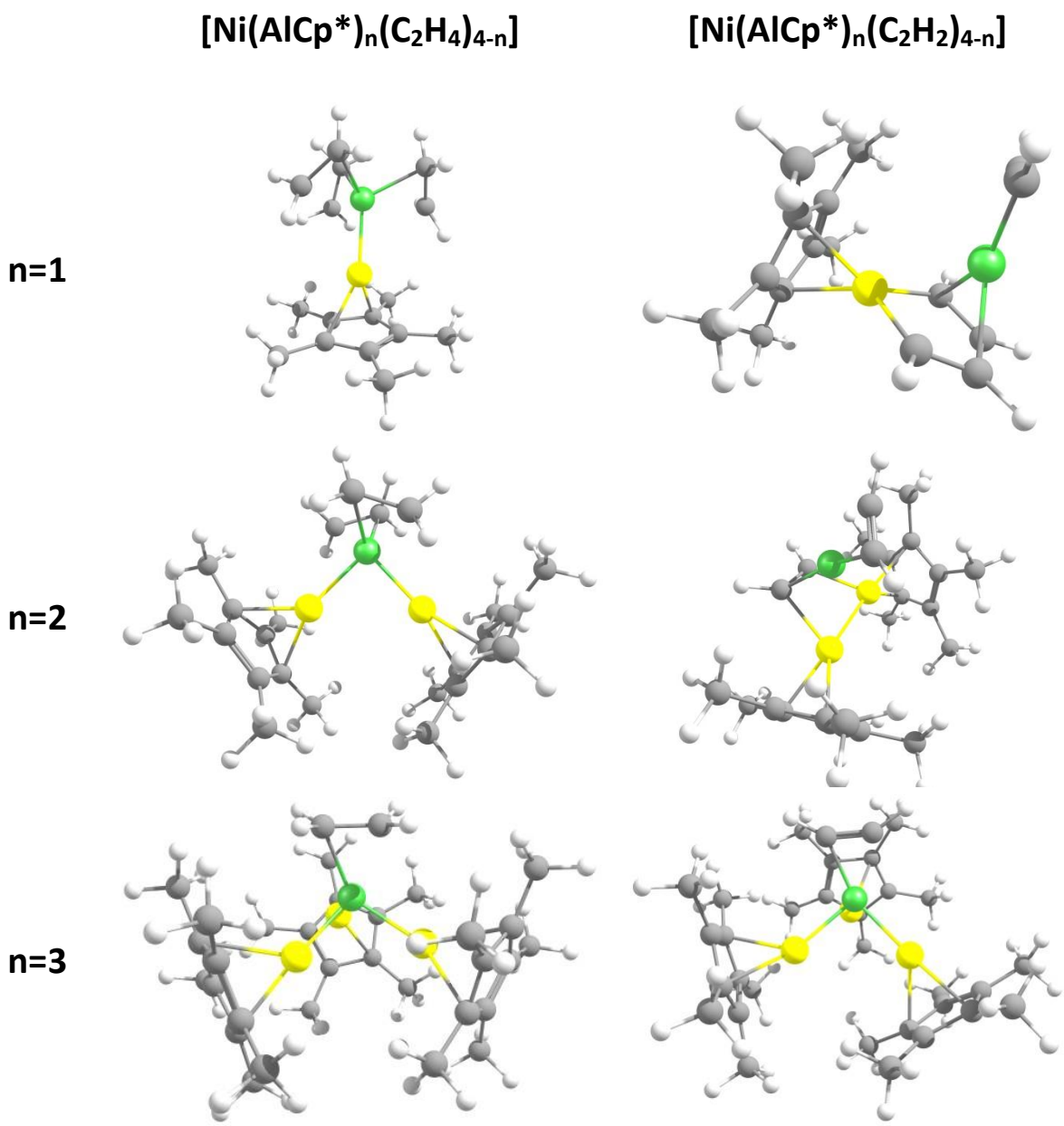

Figure S 5: Optimized Molecular structures (BP86-D3/def2-TZVPP) of [Ni(AlCp*)$_n$(C$_2$H$_x$)$_{4-n}$].

Table S 5: Summary of selected structural parameters of optimized [Ni(AlCp*)$_n$(C$_2$H$_x$)$_{4-n}$] (BP86-D3/def2-TZVPP).

	[Ni(AlCp*)(C$_2$H$_x$)$_3$]		**[Ni(AlCp*)$_2$(C$_2$H$_x$)$_2$]**		**[Ni(AlCp*)$_3$(C$_2$H$_x$)]**	
	C$_2$H$_4$	C$_2$H$_2$	C$_2$H$_4$	C$_2$H$_2$	C$_2$H$_4$	C$_2$H$_2$
d(C-C) [Å]	1.39-1.40	1.28-1.47	1.41	1.27-1.37	1.41	1.27
d(Ni-C) [Å]	2.05-2.17	1.86-2.17	2.05-2.07	1.88-2.24	2.03	1.94
d(Ni-AlCp*) [Å]	2.25	2.48	2.21	2.45-2.60	2.20-2.23	2.22-2.27
d(Al-C) [Å]	> 2.97	1.98	> 3.01	2.04-2.18	> 3.18	> 3.24
d(Al-Al) [Å]			3.12	2.50	3.25	> 3.21

[Ni(GaCp*)$_n$(C$_2$H$_x$)$_{4-n}$]:

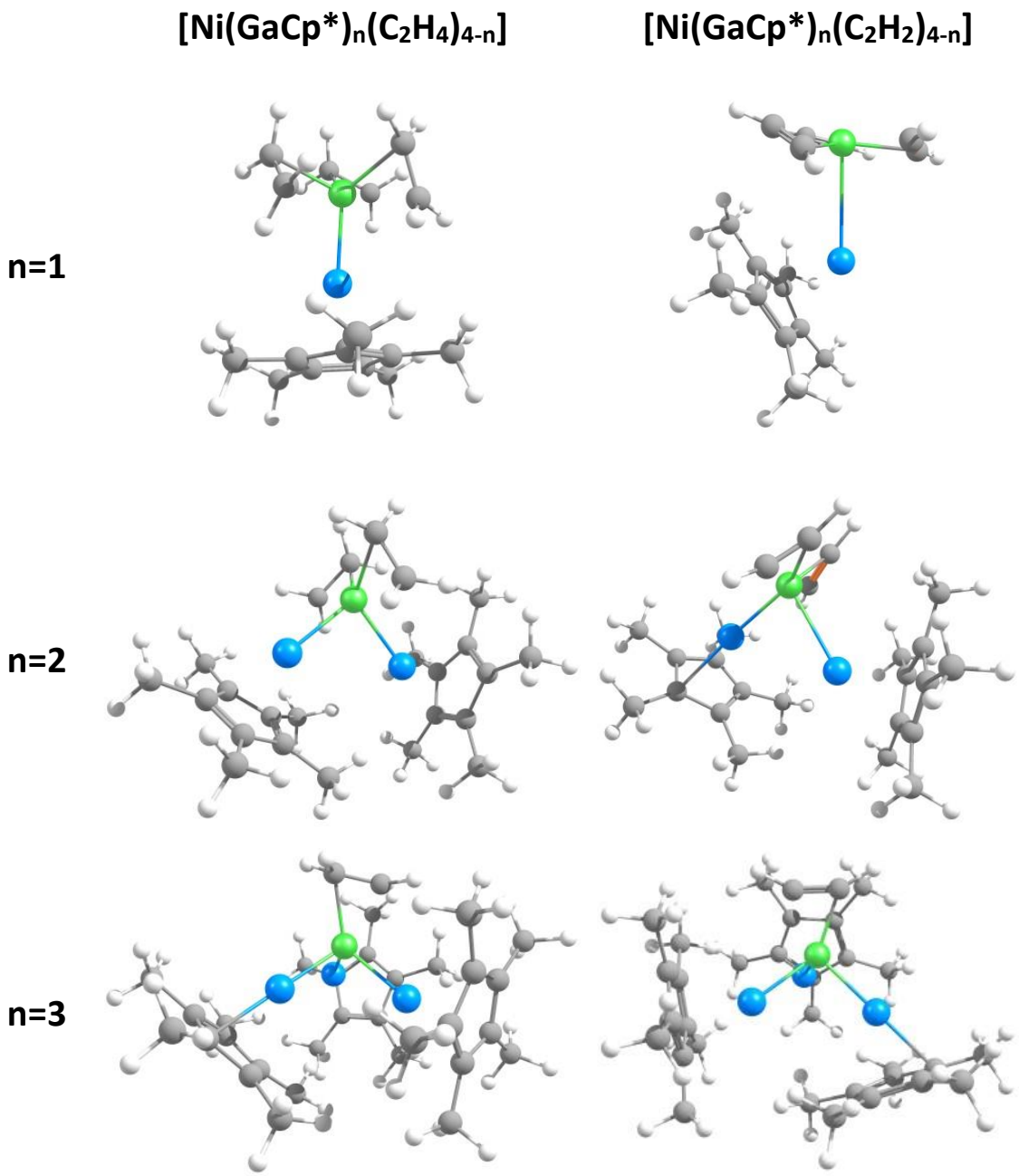

Figure S 6: Optimized Molecular structures (BP86-D3/def2-TZVPP) of [Ni(GaCp*)$_n$(C$_2$H$_x$)$_{4-n}$].

Table S 6: Summary of selected structural parameters of optimized [Ni(AlCp*)$_n$(C$_2$H$_x$)$_{4-n}$] (BP86-D3/def2-TZVPP).

	[Ni(GaCp*)(C$_2$H$_x$)$_3$]		**[Ni(GaCp*)$_2$(C$_2$H$_x$)$_2$]**		**[Ni(GaCp*)$_3$(C$_2$H$_x$)]**	
	C$_2$H$_4$	C$_2$H$_2$	C$_2$H$_4$	C$_2$H$_2$	C$_2$H$_4$	C$_2$H$_2$
d(C-C) [Å]	1.39	1.25	1.40	1.26	1.40	1.27
d(Ni-C) [Å]	2.06-2.14	1.98-2.00	2.02-2.08	1.95-1.97	2.02-2.03	1.93
d(Ni-GaCp*) [Å]	2.37	3.21	2.34-2.37	2.29, 2.70	2.273-2.325	2.28-2.40
d(Ga-C) [Å]	>3.10	>3.58	>3.10	>3.02	>3.10	>3.27
d(Ga-Ga) [Å]			3.39	3.31	>3.39	>3.32

Table S 7: Summary of NBO and WBI results for all compounds. Values in parenthesis refer to $[Ni(PEt_3)_n(C_2H_x)_{4-n}]$. Values without parenthesis refer to $[Ni(ZnCp^*)_n(ZnMe)_n(C_2H_x)_{4-n}]$.

	$[Ni(C_2H_x)_3]$		**$[Ni(L)(C_2H_x)_3]$**		**$[Ni(L)_2(C_2H_x)_2]$**		**$[Ni(L)_3(C_2H_x)]$**			
NBO charges	C_2H_4	C_2H_2	C_2H_4	C_2H_2	C_2H_4	C_2H_2	C_2H_4	C_2H_2	C_2H_4	C_2H_2
Ni			0.19	0.07	-0.74 (-0.30)	-0.74 (-0.40)	-1.65 (-0.61)	-1.15 (-0.68)	-2.52 (-0.96)	-2.44 (-0.99)
Zn					0.94	0.90	0.90 - 0.95	0.95 - 1.08	0.79 - 1.06	0.75 - 1.08
C	-0.39	-0.24	-0.47	-0.25	-0.42 - -0.57 (-0.45)	-0.19 - -0.30 (-0.24)	-0.41 (-0.47)	-0.28 (Ni); -0.64 (Zn) (-0.25 - -0.28)	-0.44 (-0.47)	-0.26 (-0.28)
Wiberg bond index (CC)	2.05	3.00	1.53	2.43	1.49 (1.55)	2.38 - 2.46 (2.45 - 2.50)	1.48 (1.51)	1.93 (2.43)	1.38 (1.48)	2.21 (2.37)

Table S 8: Summary of EDA-NOCV results for all complexes. Values in parenthesis refer to $[Ni(PEt_3)_n(C_2H_x)_{4-n}]$, values without parenthesis refer to $[Ni(ZnCp^*)_n(ZnMe)_n(C_2H_x)_{4-n}]$. The bonding interaction of one C_2H_x fragment with the remaining $[Ni(L)_n(C_2H_x)_{(4-(n+1))}]$ fragment was investigated.

	$[Ni(C_2H_x)_3]$		**$[Ni(L)(C_2H_x)_3]$**		**$[Ni(L)_2(C_2H_x)_2]$**		**$[Ni(L)_3(C_2H_x)]$**	
	C_2H_4	C_2H_2	C_2H_4	C_2H_2	C_2H_4	C_2H_2	C_2H_4	C_2H_2
Total Bonding Energy [kcal/mol]	-47.2	-51.7	-47.5 (-42.9)	-47.4 (-46.4)	-49.4 (-46.8)	-103.8 (-52.4)	-60.3 (-54.2)	-74.3 (-62.2)
Total Pauli Repulsion [kcal/mol]	130.74	134.6	191.8 (146.1)	208.6 (180.8)	177.0 (171.4)	348.3 (181.2)	181.6 (177.1)	197.7 (181.6)
Total Electrostatic Interaction [kcal/mol]	-99.5	-101.58	-132.3 (-103.9)	-140.9 (-126.2)	-123.6 (-122.5)	-215.7 (-126.9)	-128.8 (-126.7)	-137.4 (-128.9)
Total Orbital Interaction [kcal/mol]	-73.2	-80.17	-97.4 (-74.4)	-105.1 (-91.9)	-89.5 (-85.7)	-225.0 (-97.9)	-98.5 (-92.9)	-121.5 (-104.7)
π-type interaction	-41.9	-47.3	-56.3 (-42.1)	-58.5 (-56.6)	-48.8 (-54.9)	(-63.6)	-53.4 (-59.63)	-71.6 (-70.7)
σ_{back}-type interaction	-22.5	-22.0	-28.0 (-21.9)	-31.5 (-24.5)	-27.6 (-20.8)	(-23.08)	-30.3 (-21.26)	-31.1 (-21.5)

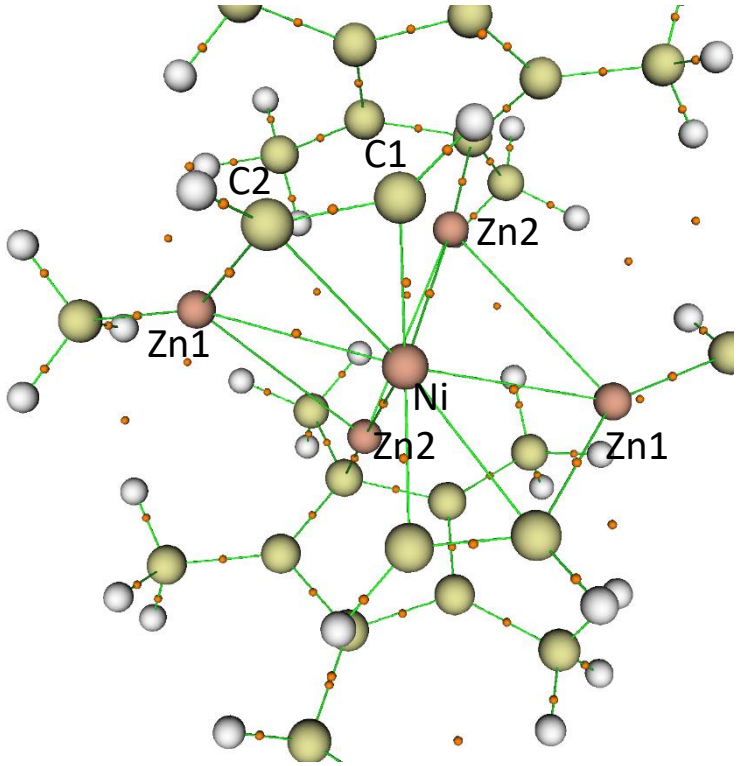

Figure S 7: QTAIM results showing bond paths (green) and bond critical points (orange dots) for $[Ni(ZnR)_4(C_2H_2)_2]$ showing Ni-Zn bonding interactions for all NiZn interactions.

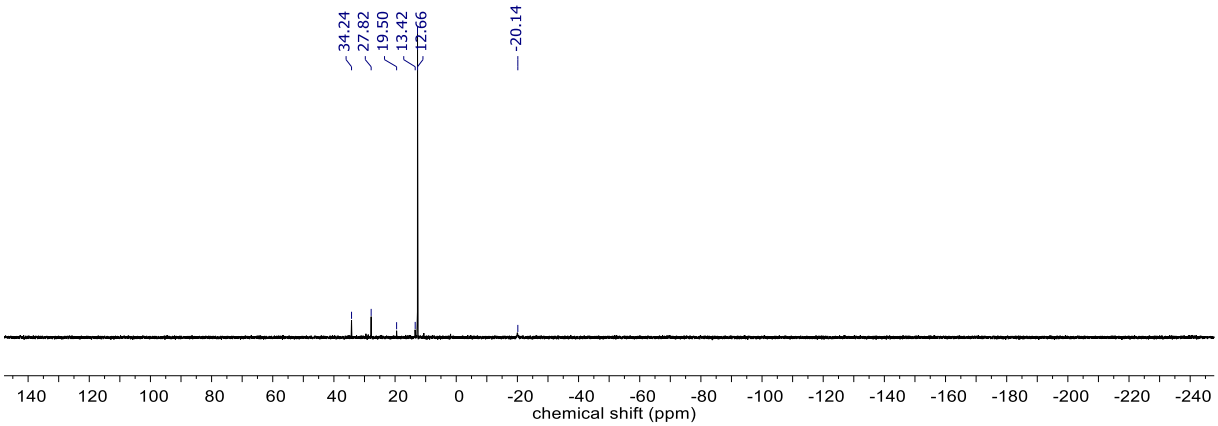

Figure S 8: ^{31}P NMR of impure [Ni(ZnCp*)(ZnMe)(PEt_3)$_3$] in C_6D_6.

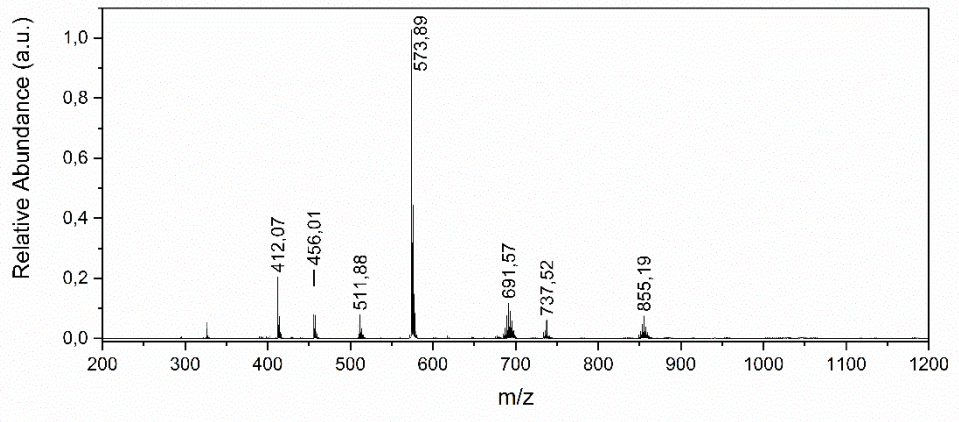

Figure S 9: LIFDI-MS spectrum of impure [Ni(ZnCp*)(ZnMe)(PEt_3)$_3$] (calculated = 694.20 g/mol) in toluene. The intensive peak at 543.9 m/z is the starting material [Ni($AlCp^*$)$_1$(PEt_3)$_3$] (calculated 574.31 g/mol)]. ^{31}P NMR spectroscopy is in accordance to this observation but the relative intensities are reversed.

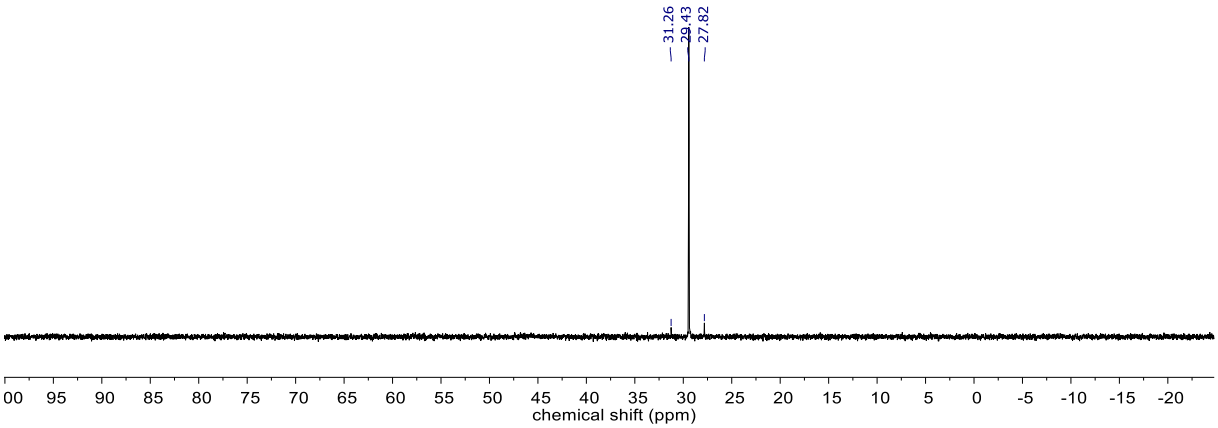

Figure S 10: ^{31}P NMR of [Ni(ZnCp*)(ZnMe)(GaCp*)(PEt_3)$_2$] in C_6D_6.

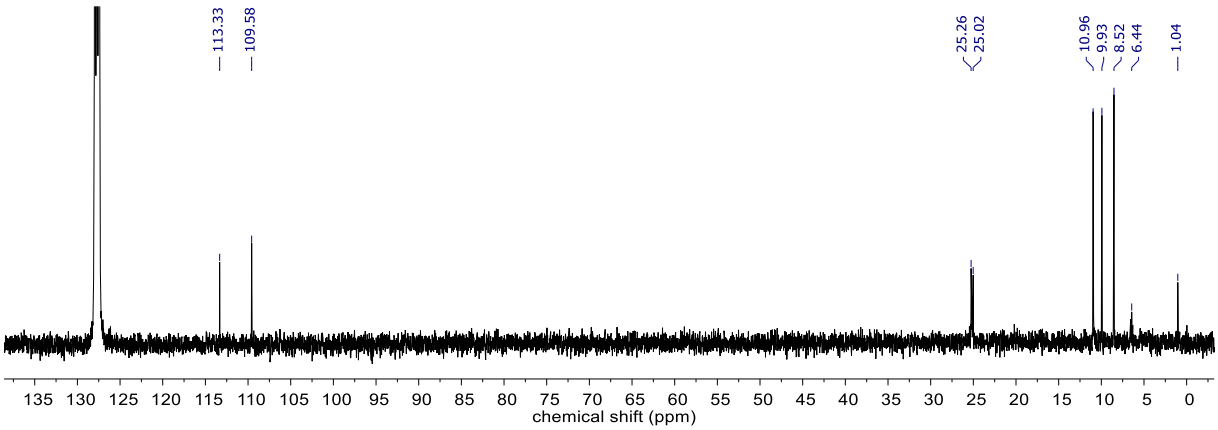

Figure S 11: ^{13}C NMR of [Ni(ZnCp*)(ZnMe)(GaCp*)(PEt_3)$_2$] in C_6D_6.

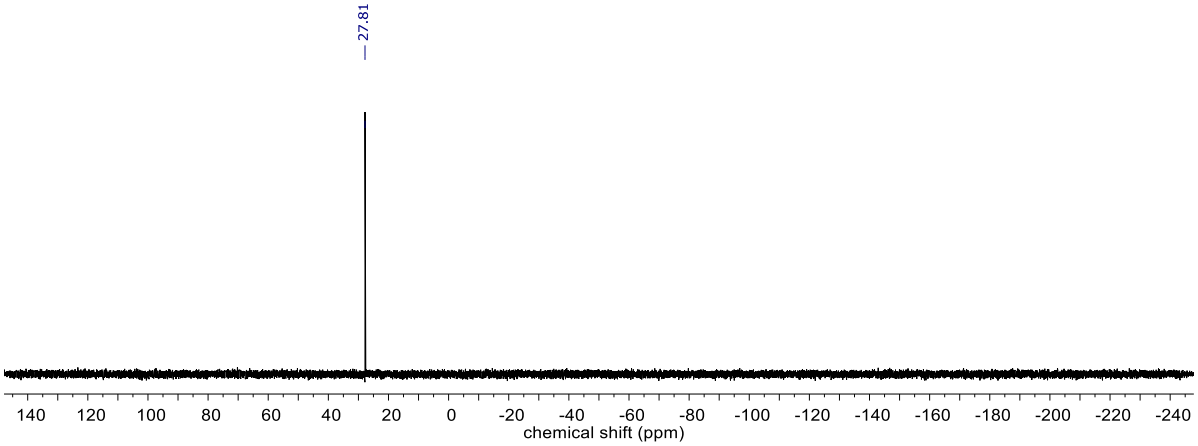

Figure S 12: ^{31}P NMR of [Ni(ZnCp*)$_2$(ZnMe)$_2$(PEt_3)$_2$] in C_6D_6.

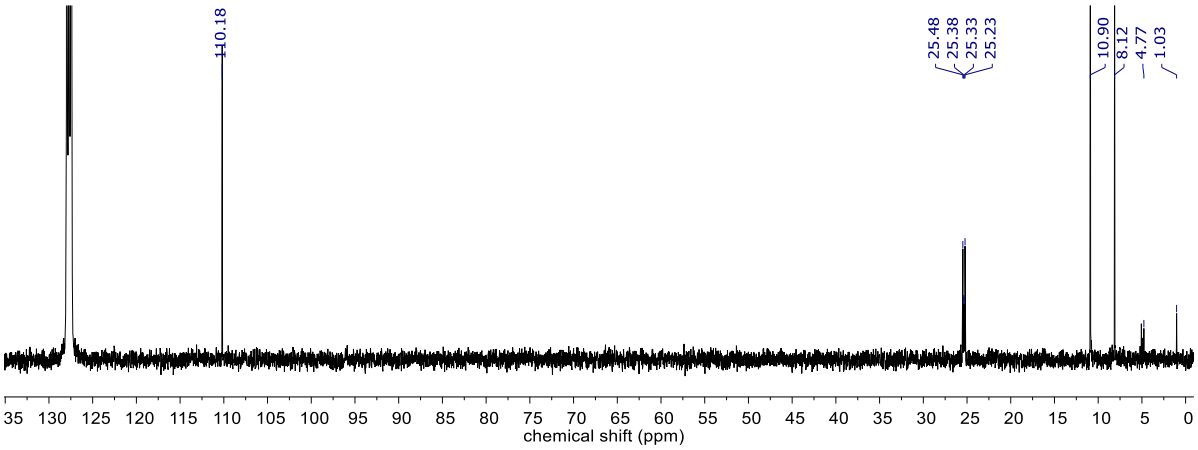

Figure S 13: ^{13}C NMR of [Ni(ZnCp*)$_2$(ZnMe)$_2$(PEt_3)$_2$] in C_6D_6.

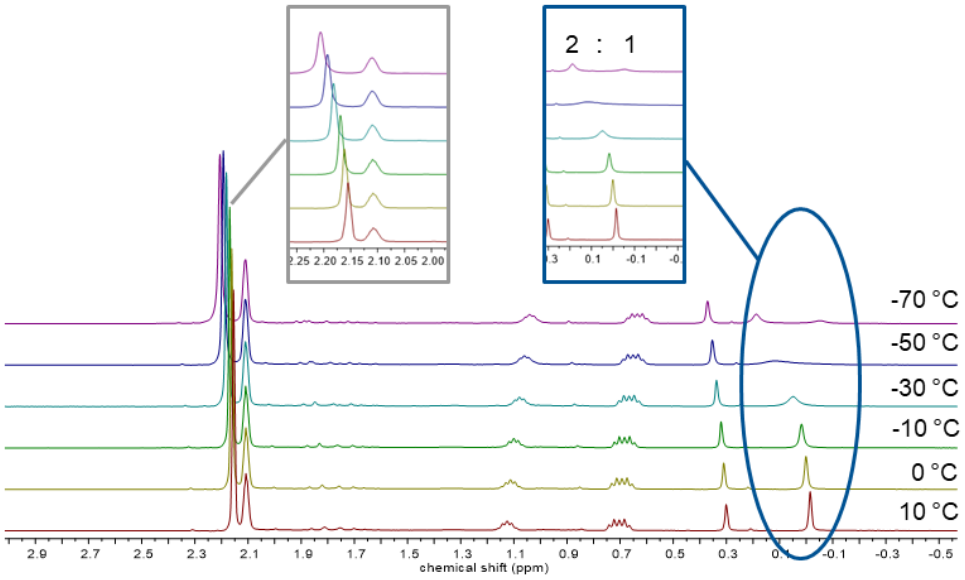

Figure S 14: VT-^{1}H NMR of [Ni(ZnCp*)$_3$(ZnMe)$_3$(PEt$_3$)] in toluene-d$_8$ showing the splitting of the ZnMe groups at low temperatures. This indicates fluxional processes of the ZnR ligands at ambient temperatures resulting in the coalescence of the signals.

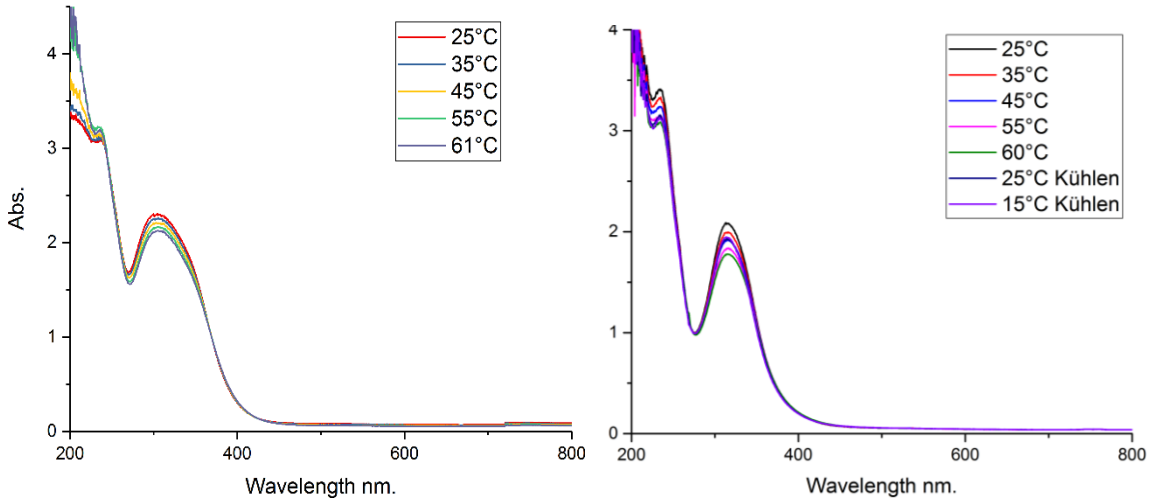

Figure S 15: VT-UV-Vis of [Ni(AlCp*)$_3$(PEt$_3$)] (left) and [Ni(AlCp*)$_4$] (right).

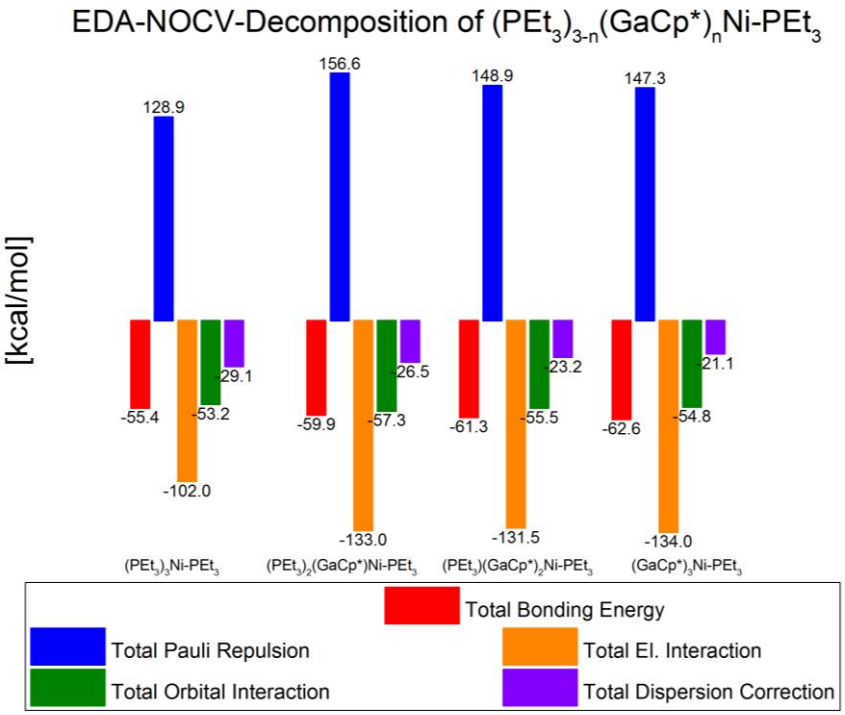

Figure S 16: EDA-NOCV Decomposition investigating the Ni-PEt_3 bonding in heteroleptic NiGaP complexes.

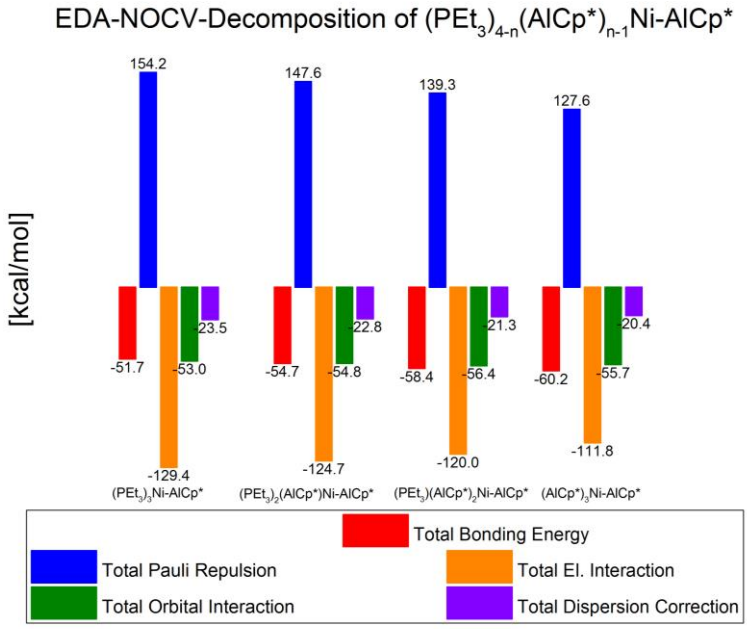

Figure S 17: EDA-NOCV Decomposition investigating the Ni-AlCp* bonding in heteroleptic NiAlP complexes.

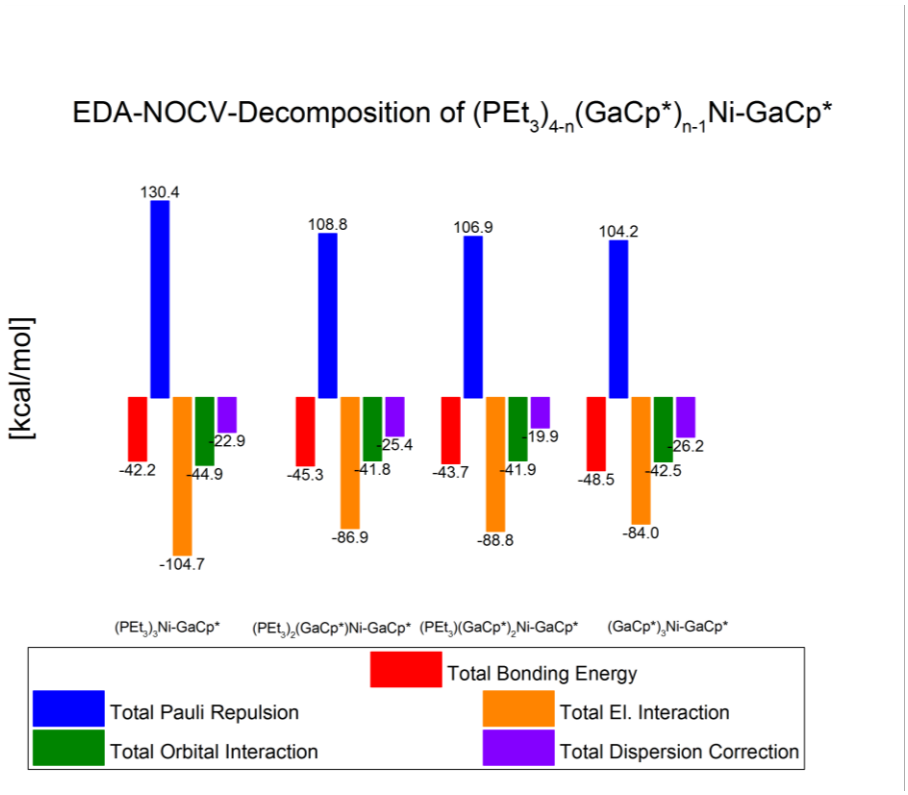

Figure S 18: EDA-NOCV Decomposition investigating the Ni-GaCp* bonding in heteroleptic NiGaP complexes.

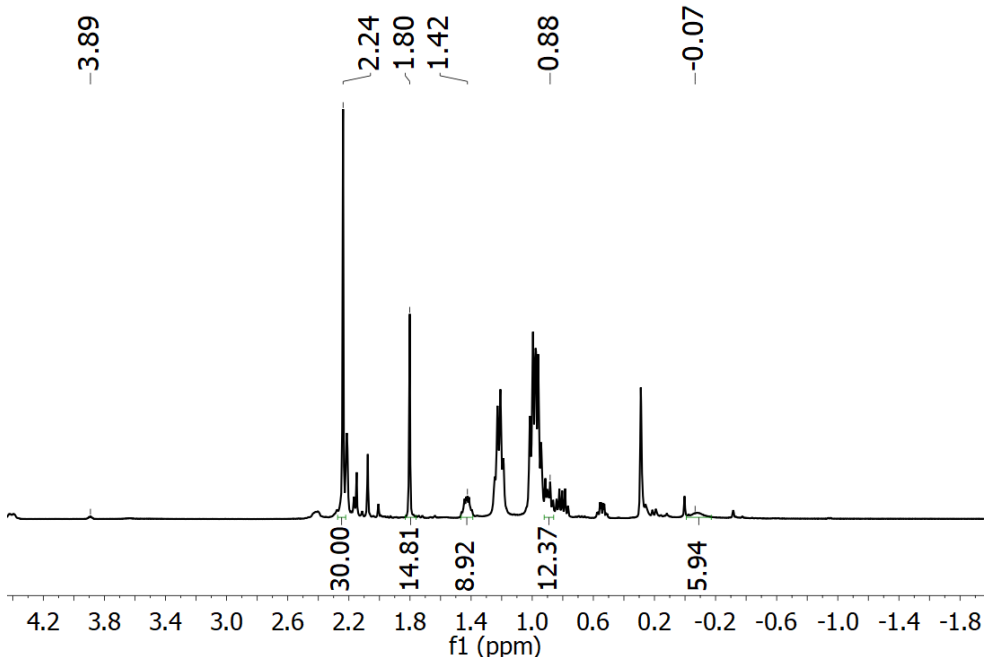

Figure S 19: ^{1}H NMR of the NMR scale reaction of [(H)(SiEt$_3$)Ni(AlCp*)(ZnCp*)$_2$(ZnMe)$_2$] with PEt$_3$, showing the disappearance of the Ni-H signal at -12.0 ppm, the appearance of the H-Si signal (at 3.89 ppm) as a good indication for reductive elimination of H-SiEt$_3$ and new signals for the ZnCp*, AlCp* and ZnMe groups at 2.24, 1.80 and -0.07 ppm respectively and new Ni-PEt$_3$ signals at 1.42 and 0.88 ppm. The two big signals at 1.3 and 0.9 ppm are due to the unwanted formation of [Ni(PEt$_3$)$_4$] (in accordance to the ^{31}P-NMR signals). Taken together, this NMR verifies the reductive elimination of H-SiEt$_3$ from [(H)(SiEt$_3$)Ni(AlCp*)(ZnCp*)$_2$(ZnMe)$_2$] and hints to the formation of [(PEt$_3$)Ni(AlCp*)(ZnCp*)$_2$(ZnMe)$_2$]. However further investigations have to be performed.

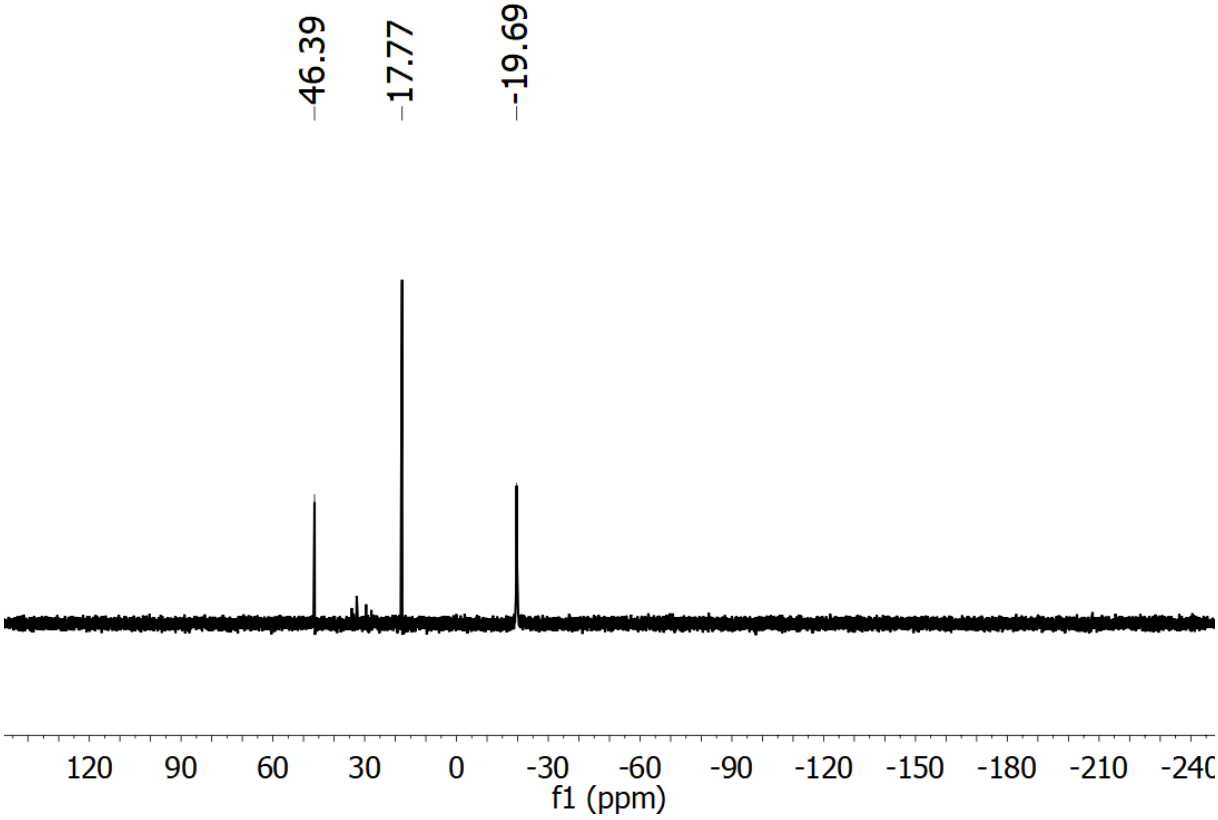

Figure S 20: ^{31}P NMR of the NMR scale reaction of $[(H)(SiEt_3)Ni(AlCp^*)(ZnCp^*)_2(ZnMe)_2]$ with PEt_3 showing the formation of [Ni(PEt3)4] (17.8 ppm) and free phosphine (-19.7 ppm). The peak at 46.4 ppm has not been observed before but is in the range for other $[Ni(M'R)_n(PEt_3)_{4-n}]$ compounds.

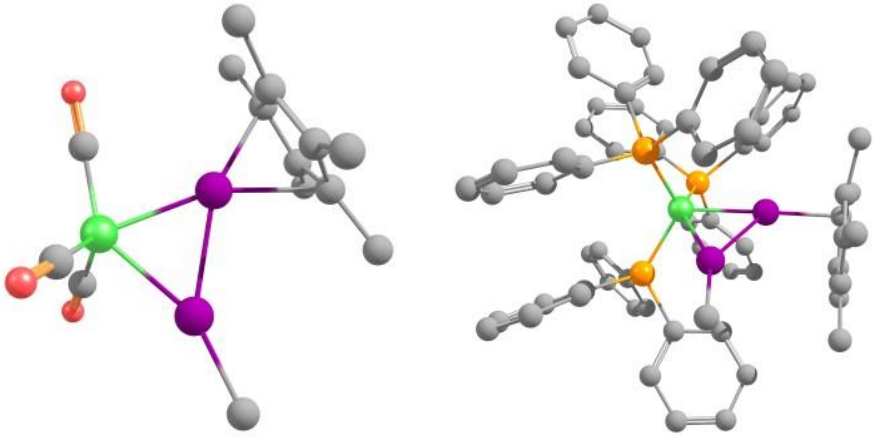

Figure S 21: left: calculated local minimum for [Ni(ZnCp*)(ZnMe)$(CO)_3$] (BP86-D3/def2-TZVPP). Distances in Å: Ni-Zn: 2.39-2.42, Zn-Zn: 2.49, right: calculated structure for [Ni(ZnCp*)(ZnMe)$(PPh_3)_3$] (BP86-D3/def2-TZVPP, local minimum at BP86-D3/def2-SVP). Distances in Å: Ni-Zn: 2.38-2.40, Zn-Zn: 2.48.

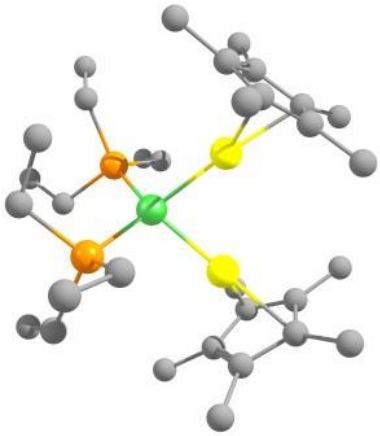

Figure S 22: local minimum structure of $[Ni(AlCp^*)_2(PEt_3)_2]^{2+}$ (BP86-D3/def2-SVP) showing the decrease of the Al-Al distance upon two-electron oxidation. Distances in Å: Ni-Al: 2.23, Ni-P: 2.21, Al-Al: 2.79. For comparison the experimental bond lengths in $[Ni(AlCp^*)_2(PEt_3)_2]$ are: Ni-Al: 2.20, Ni-P: 2.13, Al-Al: 3.37.

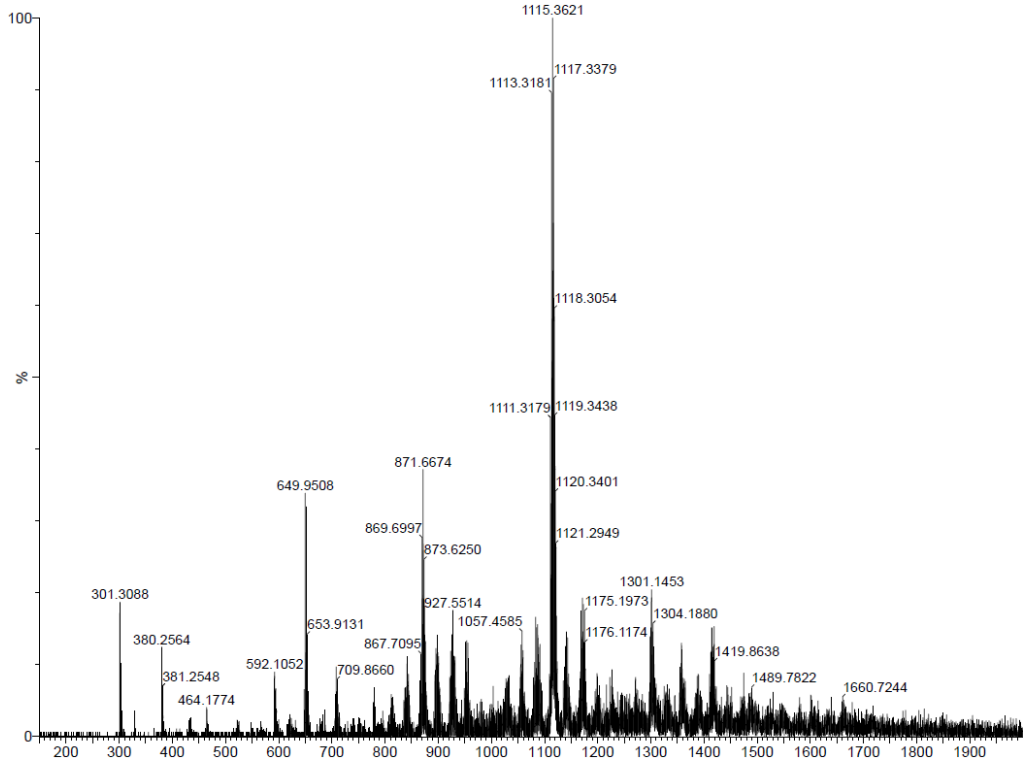

Figure S 23: LIFDI-MS spectrum of the reaction solution of $[Ni_2(dvds)_3]$ with 3 eq. AlCp* in toluene, showing several $[Ni_a(AlCp^*)_b(dvds)_c]$ species. Preliminary assignment: 649 m/z: $[Ni_2(dvds)_2(AlCp^*)]$, 871 m/z: $[Ni_3(AlCp^*)_2(dvds)_2]$, 1015 m/z $[Ni_3(AlCp^*)_4(dvds)]$, 1419 m/z: $[Ni_4(AlCp^*)_5(dvds)_2]$.

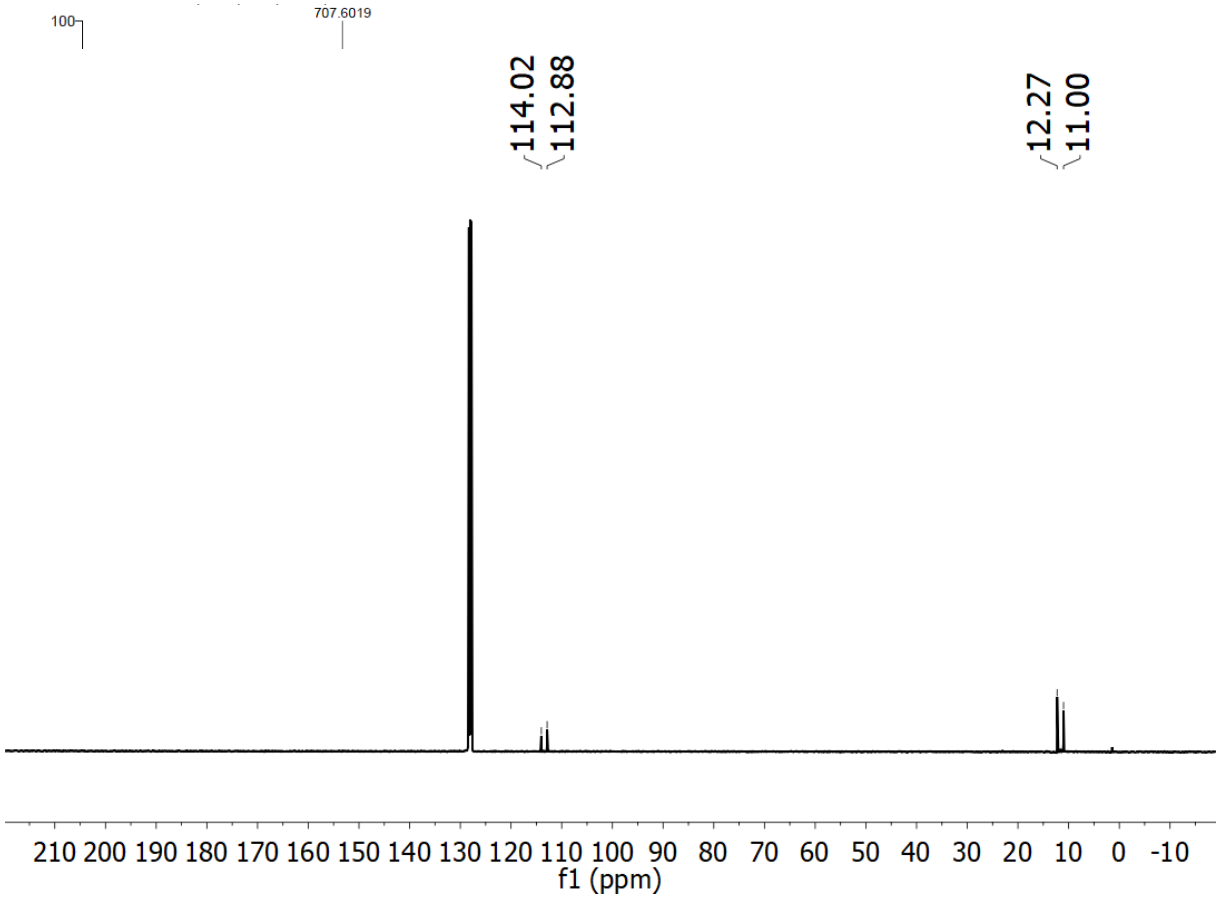

Figure S 26: ^{13}C NMR of the crystalized sample of [Ni2(AlCp*)5] in C_6D_6.

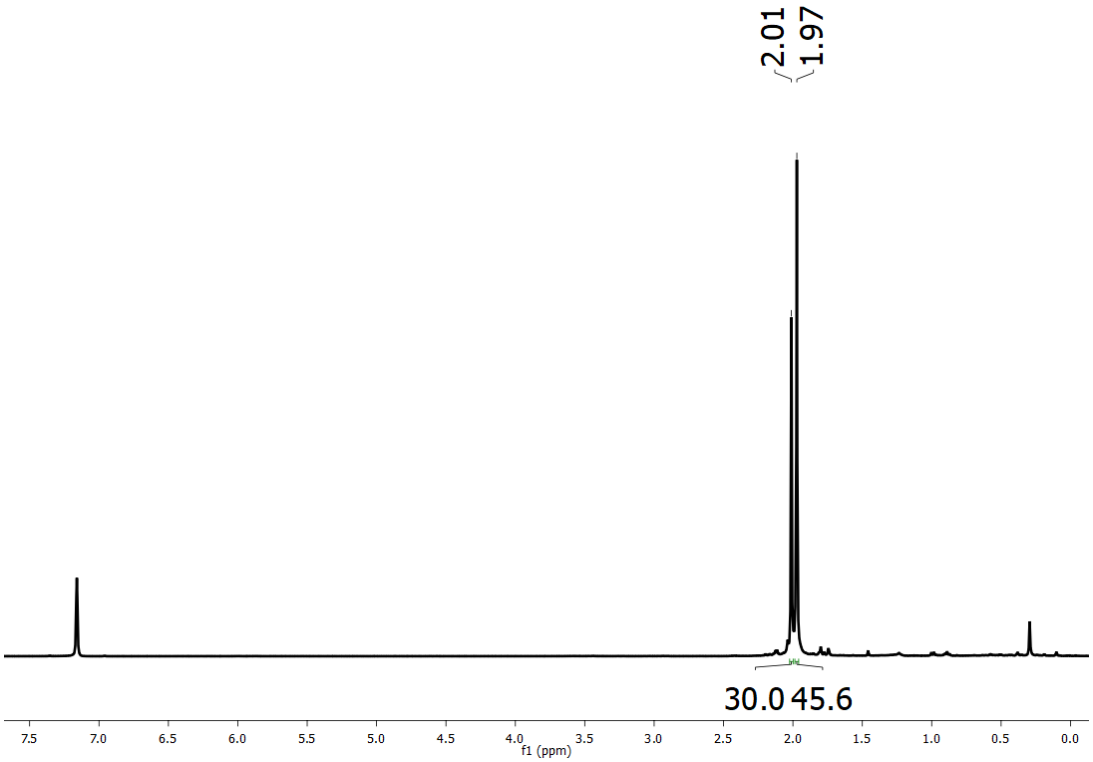

Figure S 24: ^{1}H NMR of the crystalized sample of $[Ni_2(AlCp^*)_5]$ in C_6D_6, showing the two singlets for the distinct AlCp* groups at 2.01 and 1.97 ppm with an integration ratio of 2:3.

	CO	AlMe	AlCp*
HOMO [eV]:	-9.20	-4.76	-4.87
LUMO [eV]:	-2.33	-2.16	-0.84
Gap [eV]:	6.87	2.60	4.03

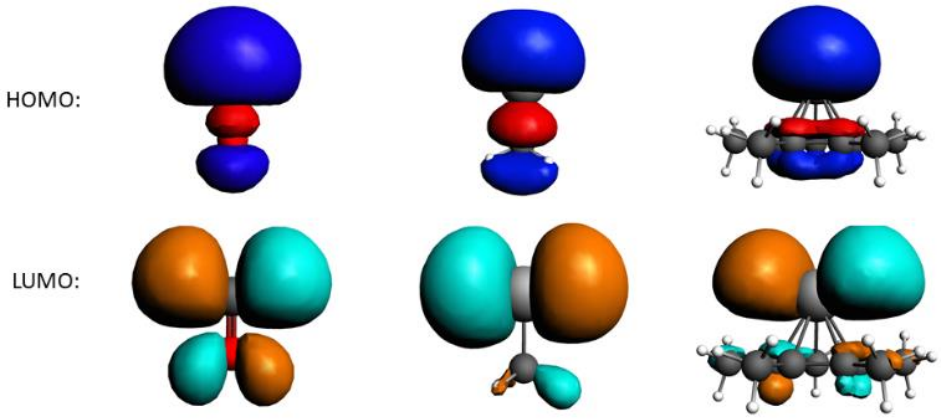

Figure S 28: Comparison of the shape and energy values of the frontier orbitals of CO, AlMe and AlCp*.

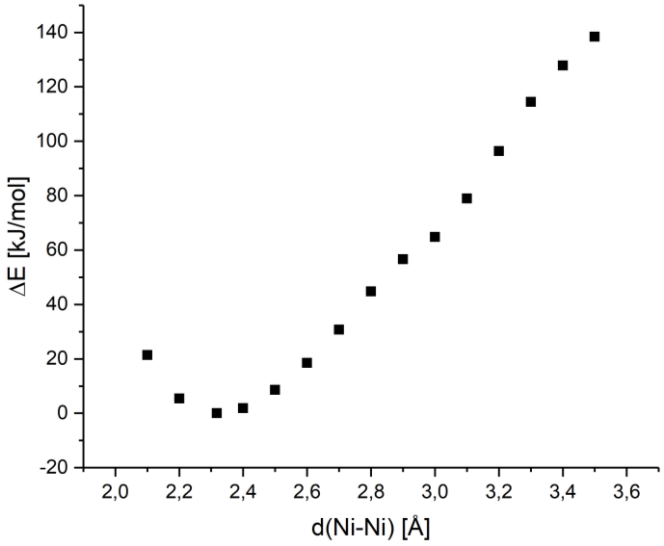

Figure S 27: Constrained Geometry optimizations of $[Ni_2(AlCp^*)_5]$ (BP86-D3(BJ)/def2-TZVPP) with fixed Ni- Ni distances and referenziation of the energy to the global minimum structure.

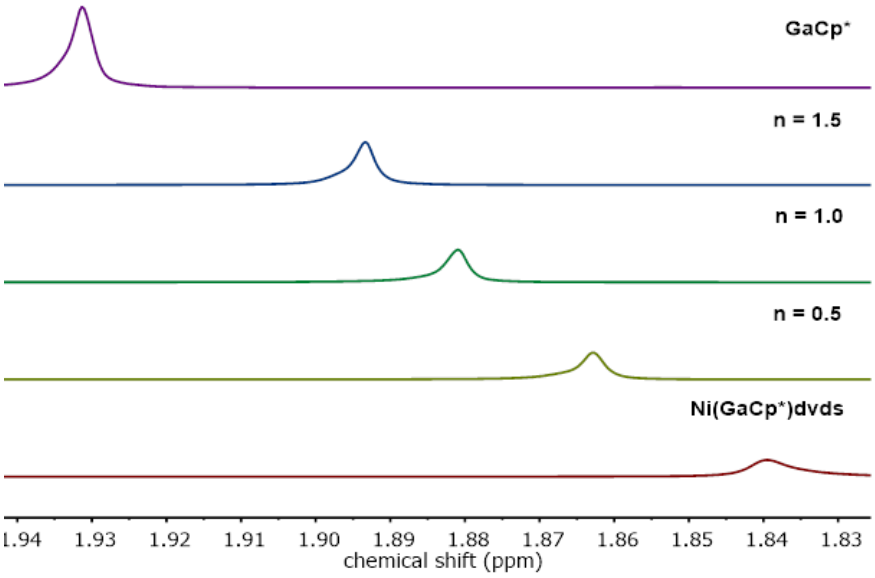

Figure S 29: ^{1}H NMR titration experiment showing the coalesced Cp* signals of GaCp* and [Ni(GaCp*)(dvds)] in C_6D_6.

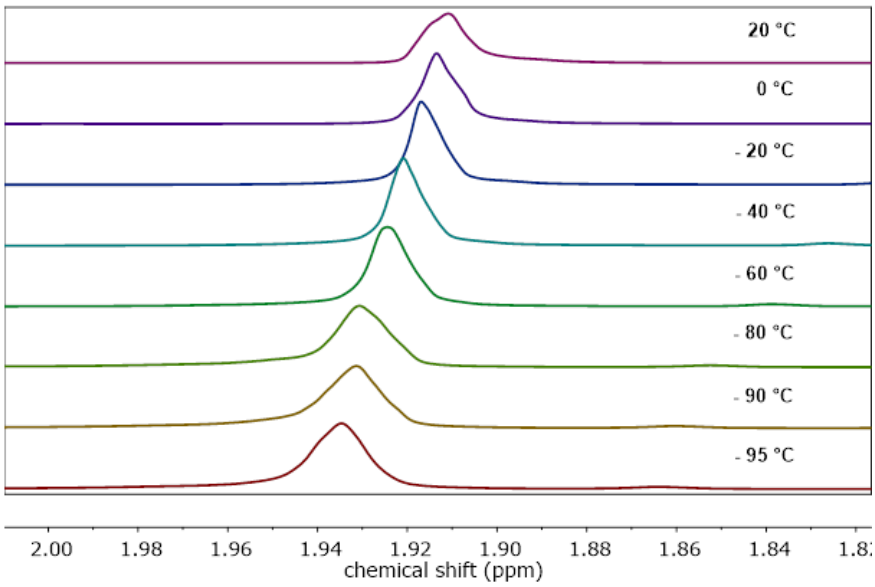

Figure S 30: VT ^{1}H NMR of the coalesced signals of 1 eq. GaCp* and [Ni(GaCp*)(dvds)] in toluene-d_8.

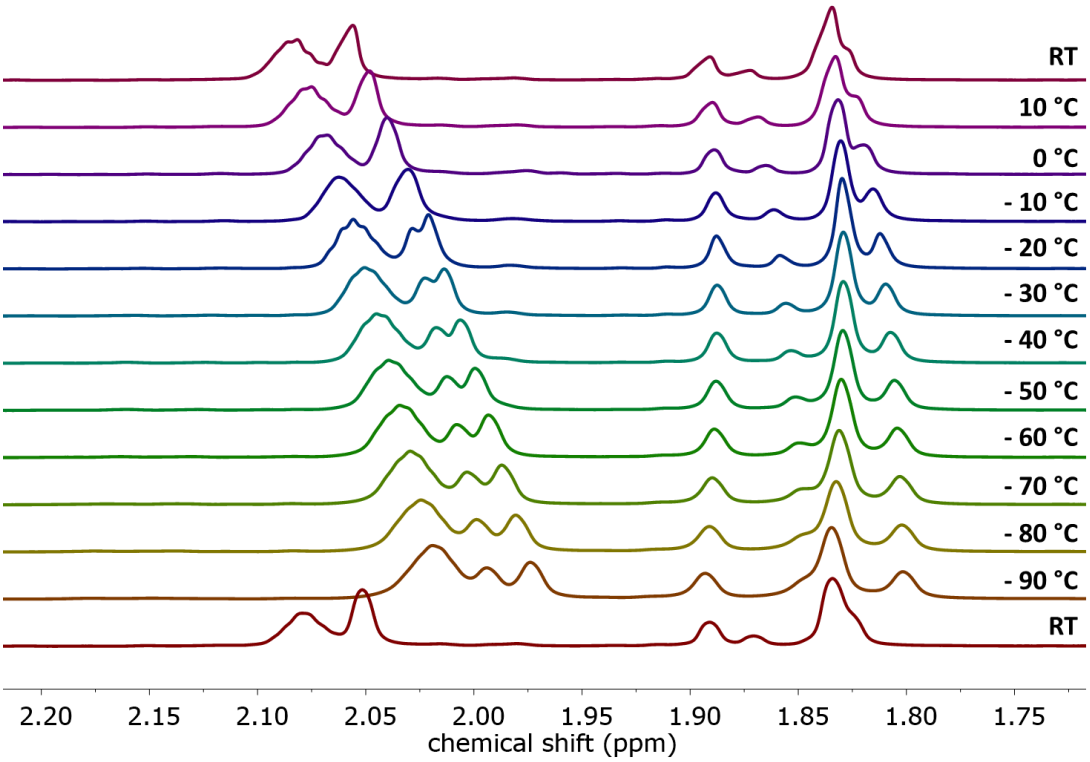

Figure S 31: ^{1}H VT-NMR of [Ni_2(μ-GaCp*)(μ-GaNiCp*)$_2$(dvds)$_2$] showing the splitting of the GaCp* signal at 1.97 ppm and the changing shifts of the NiCp* signals between 1.90 and 1.80 ppm.

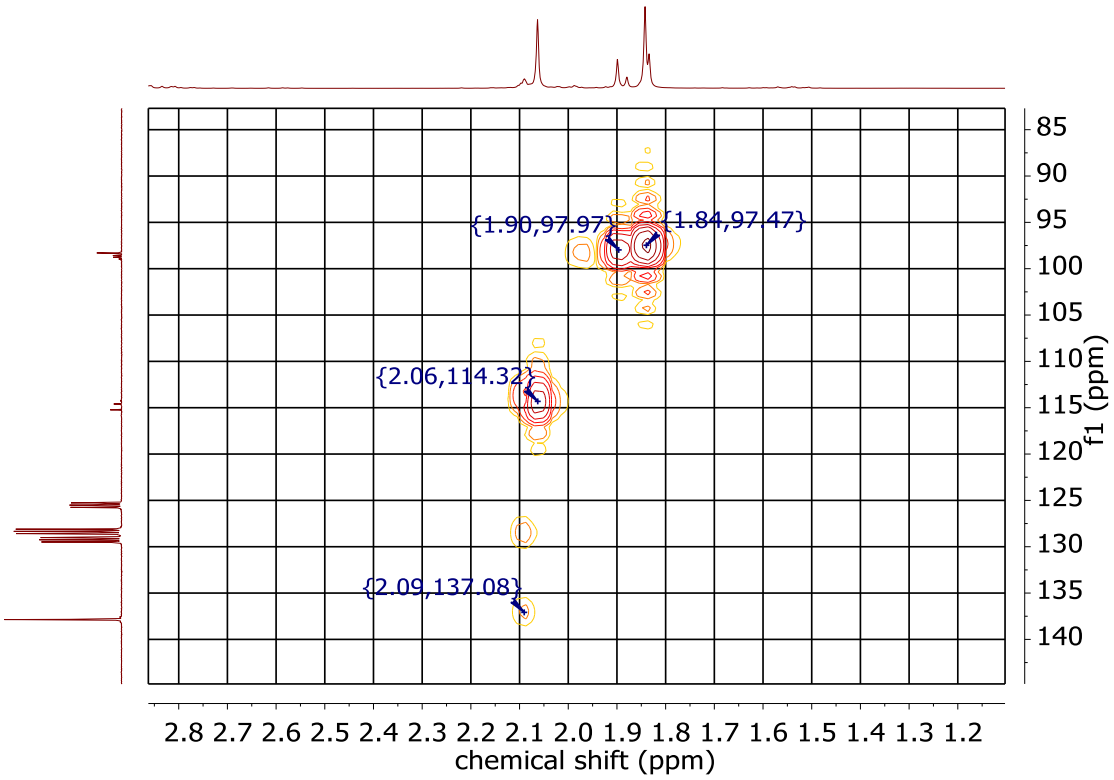

Figure S 32: ^{1}H/^{13}C 2D HMBC NMR experiments of [Ni_2(μ-GaCp*)(μ-GaNiCp*)$_2$(dvds)$_2$] revealing the assignments of GaCp* and NiCp* signals.